UNIVERSIDAD DE GRANADA

Programa de Doctorado en Biomedicina

Centro Pfizer – Universidad de Granada – Junta de Andalucía de Genómica e Investigación Oncológica (GENYO)

Departamento: Medicina Genómica
Genética de enfermedades complejas

Doctoral thesis

Functional mass cytometry for reclassification and precise diagnosis of systemic autoimmune diseases

PhD candidate

Paulina Rybakowska

Thesis supervisors

Dr. Marta Eugenia Alarcón Riquelme

Dr. Concepción Marañón Lizana

CENTRO PFIZER-UNIVERSIDAD DE GRANADA-JUNTA DE ANDALUCÍA DE GENÓMICA E INVESTIGACIÓN ONCOLÓGICA

Editor: Universidad de Granada. Tesis Doctorales
Autor: Paulina Rybakowska
ISBN: 978-84-1117-073-4
URI: http://hdl.handle.net/10481/71169

To patients who suffer from systemic autoimmune diseases

To scientists who struggle with CyTOF

Nikomu z nas życie, zdaje się, bardzo łatwo nie idzie, ale cóż robić, trzeba mieć odwagę i głównie wiarę w siebie, w to, że się jest do czegoś zdolnym i że do tego czegoś dojść potrzeba. A czasem wszystko się pokieruje dobrze, wtedy kiedy najmniej się człowiek tego spodziewa

Maria Skłodowska Curie

(1867 – 1934)

Index

Figure Index

Table Index

Abbreviations

Abs Antibodies
ACPAs Anti-citrullinated protein antibodies
AD Autoimmune disease
ADCC Antibody-dependent cell cytotoxicity
ANA Antinuclear antibodies
anti-dsDNA Anti-double-stranded DNA
AOF Average Overlap Frequency
APCs Antigen presenting cells
APRIL A proliferation inducing ligand
AR Artritis reumatoide
BAFF B cell activating factor
BH-SNE Barnes-Hut stochastic neighbor embedding
BR BAFF-receptor
cDC Conventional dendritic cells
CHB Congenital heart block
CSB Cell Staining Buffer
CTR Controls
CV Coefficient of variation
DA Differential abundance
DAMPs Danger-associated signals
DC Dendritic cells
dcSSC Diffuse cutaneous SSC
DensVM Density-based clustering aided by Support Vector Machine
DMARDs Disease-modifying anti-rheumatic drugs
DMSO Dimethyl sulfoxide
DN Double negative
DS Differential states
dsRNA Double-stranded RNA
EAS Enfermedades autoinmunes sistémicas
ESR Erythrocyte sedimentation rate
ESSDAI Disease activity index
FC Fluorochromes
FC Flow cytometry
Fit-SNE Fast Interpolation-based t-SNE
FSC Forward-scatter
HMGB1 High-mobility group box 1
HLA Human leukocyte antigen
HSNE Hierarchical Stochastic Neighbor Embedding
IBD Inflammatory bowel diseases
IC Immune complexes
IFN Interferon
IMQ Imiquimod
IRF Interferon response factors
ISOMAP isometric feature mapping
JSD Jensen-Shannon divergence
KNN K-nearest-neighborhoods
lcSSC Limited cutaneous SSC
LDG Low-density granulocytes
LDL low-density neutrophils
LES Lupus eritematoso sistémico
LPS Lipopolysaccharides
MAPK Mitogen-activated protein kinases
MC Mass cytometry
MCTD mixed connective tissue disease
MHC Major histocompatibility complex
MS Multiple sclerosis
MSI Median signal intensity
NAS Nonspecific antibody staining
NB Narrow bore sample
NETs Neutrophil extracellular traps
NF-kB Nuclear factor-κB
NK Natural killer
NT Non-treated
One-SENSE One-dimensional soli- expression by non-linear stochastic embedding
PAPS Primary antiphospholipid syndrome
PB Plasmablasts
PBMCs Peripheral blood mononuclear cells
PC Principal components
PC Plasma cells
PCA Principal Component Analysis
pDC Plasmacytoid dendritic cells
PFA Formaldehyde
PMT Photomultiplier tubes
PRR Pattern recognition receptors
RA Rheumatoid arthritis

RBP RNA-binding proteins
RSQ Resiquimod
SADs Systemic autoimmune diseases
SC Spectral cytometry
SJS Sjögren's syndrome
SLE Systemic lupus erythematosus
SOM Self-organizing map
SOP Standard Operating Procedure
SPADE Spanning Tree Progression with Density Normalized Tree
SSC Side-scatter
SSC Systemic sclerosis
SSJ Síndrome de Sjögren
ssRNA Single-stranded RNA
T Treated
TCR T cell antigen receptor
Tfh T follicular helper cells
TLR Toll-like receptors
t-SNE t-stochastic neighbor embedding
UCTD Undifferentiated Connective Tissue Disease
UMAP Uniform Manifold Approximation and Projection

Resumen

Resumen

El lupus eritematoso sistémico (LES), la artritis reumatoide (AR), la esclerosis sistémica (SSC), el síndrome de Sjögren (SSJ), la enfermedad mixta del tejido conectivo (MCTD) y el síndrome antifosfolípido primario (PAPS) se clasifican como enfermedades autoinmunes sistémicas (EAS o SAD en inglés). Estas enfermedades se caracterizan por signos de autoinmunidad que incluyen la producción de autoanticuerpos y el daño a diferentes órganos. Aunque tienen definiciones clínicas y criterios de diagnóstico clínico separados, estas enfermedades son difíciles de diagnosticar de manera diferencial, ya que los pacientes tienen síntomas muy superpuestos y signos clínicos variados, particularmente en las primeras etapas de la enfermedad. Este panorama clínico superpuesto impide el diagnóstico correcto y la administración temprana de fármacos. Si bien durante mucho tiempo se sospechó de la semejanza molecular entre las EAS, la falta de biomarcadores compartidos bien descritos dificulta el tratamiento y el diagnóstico. Por tanto, es necesario realizar estudios moleculares y celulares para clasificar a los pacientes en función del mecanismo fisiopatológico subyacente en una estrategia de medicina personalizada.

Para estudiar la complejidad del sistema inmunológico a nivel de una sola célula, es necesario utilizar tecnologías adecuadas. La citometría de masas (Citometría por tiempo de vuelo, CyTOF, CM) es una técnica de alta dimensión que permite medir más de 50 marcadores en una sola célula. Por lo tanto, es una buena herramienta para realizar estudios de fenotipado profundo rastreando varios tipos de células o niveles de marcadores de activación celular. Sin embargo, para observar los patrones celulares específicos del paciente, es necesario reclutar números importantes de individuos, lo que a menudo involucra a diferentes centros de investigación. Por tanto, es necesario establecer un diseño experimental adecuado. La preservación de sangre completa es una forma atractiva de recolectar muestras de centros ubicados lejos de las instalaciones del centro donde se realiza la CM, sin embargo, hasta ahora no se han validado suficientes protocolos de preservación de sangre para CM. Además, debido a que las muestras adquiridas a través del instrumento CyTOF sufren obstrucción por el material celular así como caída de señal asociada a adquisiciones prolongadas y efectos de lote, se debe tener especial cuidado al analizar los datos cuando se estudian múltiples grupos de muestras. Por lo tanto, es necesario utilizar un flujo de análisis de datos que considere la normalización de datos, el control de calidad y la naturaleza de alta dimensión de los datos de CM. Además, para analizar cientos de muestras, el flujo de análisis debe adaptarse para estudios a gran escala e

idealmente debe automatizarse tanto como sea posible. Sin embargo, hasta ahora, no se ha desarrollado tal flujo de trabajo con esas características.

En esta tesis doctoral hemos estudiado 7 EAS diferentes con el fin de encontrar nuevos biomarcadores que permitan la reclasificación de pacientes según firmas de leucocitos circulan tes. Nuestro objetivo fue realizar un estudio de fenotipado profundo que incluya marcadores funcionales relevantes para las EAS. Como queríamos tener la imagen más completa del sistema inmunológico, decidimos recolectar muestras de sangre completa y usar citometría de masas para analizarlas. Para ello realizamos la recogida de muestras de sangre en diferentes centros ubicados en Granada y Córdoba. Por tanto, tuvimos que establecer un protocolo de criopreservación adecuado para estudios multicéntricos. Como en total se recolectaron más de cien muestras, también establecimos un protocolo experimental que minimiza la variación experimental, y se optimizó un proceso de análisis y control de calidad junto con el preprocesamiento de datos automatizado.

Utilizando estos ajustes, hemos demostrado que los estudios de inmunofenotipificación de alto contenido se pueden realizar con éxito con pequeñas cantidades de sangre fijada / congelada. La fijación inmediata de sangre completa se beneficia de tiempos de manipulación más cortos, lo que evita la muerte celular, especialmente en el compartimento de neutrófilos. Diseñamos un flujo de trabajo experimental que limita la variación experimental y reportamos un flujo de trabajo de curación de datos basado en R que limpia los datos recolectados y corrige los efectos por lotes introducidos durante la preparación y tinción de la muestra. Este flujo está semiautomatizado y optimizado para estudios grandes que involucran fenotipado de sangre humana, junto con marcadores funcionales. Finalmente, demostramos que CM se puede utilizar con éxito para detectar grupos (clusters) de pacientes que tienen patrones inmunes similares, lo que respalda el desarrollo de la medicina personalizada en las EAS. Hemos construido un marco de reclasificación de pacientes utilizando frecuencias celulares y niveles de expresión de marcadores funcionales. Los cuatro grupos de pacientes identificados difieren en la frecuencia y el estado de activación de células mieloides y linfoides. Además, también se caracterizaron por diferentes niveles de citoquinas pro- y antiinflamatorias. Cada grupo contiene una mezcla de diferentes enfermedades, lo que confirma la alta heterogeneidad de cada etiqueta diagnóstica.

Abstract

Abstract

Systemic lupus erythematosus (SLE), rheumatoid arthritis (RA), systemic sclerosis (SSC), Sjögren's syndrome (SJS), mixed connective tissue disease (MCTD) and primary antiphospholipid syndrome (PAPS) are classified as systemic autoimmune diseases (SADs). These diseases are characterized by signs of autoimmunity that include the production of autoantibodies and the damage of different organs. Although having separated clinical definitions and clinical diagnostic criteria, these diseases are difficult to diagnose differentially, as patients have highly overlapping symptoms and varied clinical signs, particularly at early disease stages. This overlapping clinical landscape impedes the correct diagnosis and early drug administration. While molecular resemblance between SADs was suspected for a long time, the lack of well described, shared biomarkers makes treatment and diagnosis difficult. Therefore, molecular and cellular-based studies need to be undertaken to classify the patients based on the physiopathological mechanism underlying the diseases in an strategy of personalized medicine.

In order to study the complexity of the immune system at the single cell level, proper technologies need to be used. Mass cytometry (Cytometry by Time-Of-Flight, CyTOF, MC) is a high-dimensional technique that allows to measure more than 50 markers in one single cell. Thus, it is a good tool to perform deep-phenotyping studies tracking several cell types or levels of cellular activation markers. However, in order to observe patient-specific cellular patterns, significant amounts of individuals need to be recruited, involving often different research centers. Hence a proper experimental design needs to be established. Whole blood preservation seems to be an attractive way to gather samples from centers located far away from MC-core facility, yet not many blood-preservation protocols were validated for MC so far. Additionally, because samples acquired through the CyTOF instrument suffer from cell clogging, signal drop associated to long acquisition and batch effects, special care needs to be taken when analyzing the data when multiple groups of samples are studied. Thus, a data analysis pipeline that considers data normalization, quality control and the high-dimensional nature of MC data needs to be used. Additionally, in order to analyze hundreds of samples the analysis pipeline needs to be adapted for large-scale studies and ideally be automatized as much as possible. However up to now, no such workflow was developed.

In this PhD thesis we studied 7 different SADs in order to find new biomarkers that allow for patient reclassification according to immune cell signatures. We aimed at performing a deep phenotyping study including functional markers relevant for SADs. As we wanted to have the

most complete picture of the immune system we decided to collect whole blood samples and use MC cytometry to analyze them. In order to do this we collected blood samples in different centers located in Granada and Córdoba. Thus, we had to establish a cryopreservation protocol suitable for multicenter studies. As in total more than one hundred samples were collected, we established also an experimental protocol minimizing experimental variation, and a quality control and analysis pipeline was also optimized together with automatized data preprocessing.

Using these settings we have demonstrated that high-content immunophenotyping studies can be successfully performed with small amounts of fixed/frozen blood. Immediate whole blood fixation benefits from shorter manipulation times, hence preventing cell death specially in the neutrophil compartment. We designed an experimental workflow that limits experimental variation and reported an R-based data curation workflow that cleans collected data and corrects the batch effects introduced during the sample preparation and staining. This pipeline is semi-automated and optimized for large studies involving human blood phenotyping, together with functional markers. Finally, we showed that MC can be successfully used to detect groups (clusters) of patients having similar immune landscapes, supporting the personalized medicine development in SADs. So far, we constructed a patient reclassification framework using cell frequencies and expression levels of functional markers. The four detected clusters differed in the frequency and activation state of both myeloid and lymphoid cells. Additionally, they were also characterized by different levels of pro and anti-inflammatory cytokines. Each cluster contained a mixture of different diseases, confirming the high heterogeneity of each diagnosis label.

Introduction

Introduction

1 Systemic autoimmune diseases (SADs)

1.1 Epidemiology of SADs

The most important function of immune system is to recognize foreign antigens and protect the host from infectious agents, and thus, maintain homeostasis. However, when the immune system fails to do so, two major types of disorders can develop. First, immunodeficiency syndromes, when proper response cannot be triggered, and second, the autoimmune disorders when cells fails to distinguish self-antigens from nonself[1]. The second group of disorders are of the interest of this thesis and will be further discussed.

Self-reactivity ranges from low, "physiological" level that is crucial for lymphocyte selection and immune-system homeostasis, to the intermediate level characterized by the presence of circulating autoantibodies and minor tissue infiltrates without clinical symptoms, to pathogenic auto-reactivity associated with immune-system mediated tissue injury[2]. The mechanism involved in switching from physiological to destructive autoimmunity is not fully understood but it is characterized by the breakdown of self-tolerance leading to an adaptive immune response to self-antigens and damage to self-tissues.

On the basis of the tissue involved, autoimmune diseases can be characterized as organ-specific, like multiple sclerosis (MS) or inflammatory bowel diseases (IBD) or systemic disorders also known as connective tissue diseases, where multiple organs are affected[1]. Various disorders can be found in this group being the most common systemic lupus erythematosus (SLE), rheumatoid arthritis (RA) or primary Sjogren's syndrome (SJS), and more rare like systemic sclerosis (SSC), mixed connective tissue disease (MCTD), and primary anti-phospholipid syndrome (PAPS). These multi-organ diseases are highly heterogeneous and associated with substantial morbidity and mortality. They can present classically, which makes the diagnosis simpler or, as they share many common features, patients can show a mixture of the symptoms which makes the diagnosis difficult[3].

SADs are mostly characterized by a gender imbalance, as the female-to-male incidence ratio is above one, being the most marked in SJS 10:1[4] and SLE 9:1[5]. Although both diseases can occur at all ranges of age they are mainly diagnosed between 30 – 50 for SjS[6] and between puberty to menopause for SLE, with an earlier incidence in African American women than in the Caucasian population[7]. For RA and SSC these differences between sexes are less obvious as the

ratio drops to 3:1[8,9]. For SSC the incidence is highest among women in child-bearing age[9] and for RA most women become symptomatic around middle age or at the time of menopause[10]. The incidence rate in PAPS for females and males is the same after excluding patients with SLE and with obstetric antiphospholipid syndrome and its prevalence increases with age[11,12].

The number of people affected by these diseases, the age of onset and the mortality varies considerably between countries. The most complete information comes from European and North American continents and less data is available from Africa, South America, Asia and Oceania, which can also result in an incidence and prevalence underestimation[13]. The incidence rate of SLE can reach 2 – 7.6 and 1 – to 4.9 per 100.000 and year in United States and Europe, respectively with a prevalence reaching 19 – 159 and 28 – 97 per 100.000 in both continents, respectively[5,14–16]. For SJS the incidence in Europe is around 5.3[10] and 3 – 4[6] per 100.000 and year in North America, while for RA it is 9 – 36 and 31 – 45 per 100.000 and year, respectively[17]. In a small study group the incidence of MCTD was estimated at the level of 2 per 100.000 and year[18] and 5 per 100.000 and year for PAPS[12], placing them as the rarest SADs.

Ethnic differences in the prevalence were also reported: for example, SLE is 3 to 4 times more common in non-Caucasian populations especially with African origin. It was shown that these individuals develop the disease at younger age and have a higher risk to suffer more severe manifestations, such as lupus nephritis[5]. Similar results were observed for SSC, as it is more common and more aggressive in African-American than in Caucasian with similar socio-economic status[19]. Additionally, this disease is more common in Australia (23 – 100 000) and North America (27 – 100 000) than in Japan (4 – 100 000) or Europe (15 – 100 000). More interestingly, an increasing prevalence was reported along a North-South gradient in Europe[20].

It is worth to point out that the wide ranges and differences between continents and countries can be due to different study designs and different criteria used to define these disorders, which only emphasizes the difficulty in the diagnosis process of SADs, and also means that the prevalence of these disorders can be much higher than estimated. On the other hand, these differences can point out towards both genetic and environmental factors that trigger the autoimmune response and disease progression.

1.2 Common pathogenesis mechanism of SADs

Dysregulation of both innate and adaptive immune responses plays an important role in the pathogenesis of SADs. Although the autoimmune response affects different tissues in different

SADs, the mechanisms triggering this response seem to be shared between patients. Evidence of common pathogenesis includes alteration in the number and function of blood circulating immune cells, the interferon (IFN) signature in blood and affected tissues, elevated levels of proinflammatory cytokines and the presence of autoantibodies that can be shared between different diseases.

1.2.1 Autoantibodies and the source of autoantigens in SADs

Autoantibodies can target different biological molecules like lipids, proteins or nucleic acids. These antigens can be located both intracellularly, either in the nucleus or cytoplasm, or can be found on the surface of the cells or in the extracellular milieu[21]. The most frequent autoantibody class in SADs is called antinuclear antibodies (ANA) as they mostly recognize the antigens in the nucleus. In this group anti-double-stranded DNA (anti-dsDNA) antibodies (Abs) are present in 43% - 92% of SLE patients and are used as part of the diagnostic criteria, as they have high specificity for this disease. However it should be noticed that they can also be found in the healthy population[22,23], albeit at a lower titer, and in MCTD[24]. Additionally their correlation with disease activity is variable in different studies[25]. As DNA is never present as a pure nucleic acid but rather as a part of nucleosomes, other type of anti-DNA autoantibodies is also observed in SADs. Anti-nucleosome Abs exist in around 60% of patients with SLE, and the probability that the patients with this Abs have SLE is greater than using anti-dsDNA Abs as a marker[25]. Additionally, a positive correlation with disease progression was shown for anti-nucleosome[26,27] Abs. These Abs are also found in some patients with SSC, SS, RA and MCTD, and thus they are not unique for SLE[25]. Anti-histone Abs are also present in SLE and SSC[28], and they can be induced by certain drug treatments, resulting in SLE-like clinical features[29].

The antigens can be post-translationally modified creating the so-called neoantigens. One example is the citrullination of proteins like histones, triggering the induction of Abs against citrullinated proteins (ACPA). The Abs against citrullinated H3 and in general ACPA are seen especially in RA, but patients with SLE[30], SSC[31], SJS and MCTD[32] can also be positive for anti-ACPA. RNA-binding proteins (RBP) are another example of autoantigens and anti-Ro and anti-La Abs occur in SADs, especially in SLE and SJS. In SLE they are associated with disease manifestations of the skin[33] and with cytopenia[34] and in SJS with earlier disease presentation, longer duration and greater severity of glandular symptoms[35]. In both diseases anti-Ro52 Abs are associated with congenital heart block (CHB) in infants of positive mothers[36]. Another example of anti-RBP are anti-Sm and anti-RNP, that are found in SSC, SLE and MCTD[37,38].

The autoantigens sequestered in the intracellular compartments can be exposed to the extracellular milieu upon cell death. In rheumatic diseases programed cell death like apoptosis, and lytic cell death like necrosis, and NETosis, are thought to promote inflammation and lead to a vicious cycle of chronic inflammation, a hallmark of SADs[39].

Upon apoptosis the redistribution of nuclear and cytoplasmic content into membrane blebs and mircoparticles allows antibody opsonization. This opsonized immune complexes can be taken up via Fc receptors resulting in autoantigen presentation, and amplifying the autoimmune response[40]. Furthermore, if excessive apoptosis takes place there is no time for its effective clearance, and thus dying cells can progress into secondary necrosis, resulting in the release of cellular content and danger-associated signals (DAMPs) like high-mobility group box 1 (HMGB1), whose main role is to trigger the inflammatory response through inflammatory cell recruitment[41]. Elevated levels of this protein were reported in various SADs[42]. Apoptosis is also a source of protein modification and can result in histone acetylation[43,44] and methylation[45] being a source of new autoantigens.

The NETosis is a special mechanism of neutrophil cell death in response to microbial[46] but also sterile inflammatory signals like autoantibodies, immune complexes and inflammatory cytokines[47]. DNA released upon NETosis is present in large meshes (NETs) decorated by proteins and cytoplasmic granules[48], and is an important source of autoantigens. The direct role of this cell death was shown for SADs, especially for SLE in the context of kidney involvement, as netting neutrophils were found in the glomeruli and were correlated with enhanced activity indexes in the kidney and elevated autoantibody levels[49]. Higher spontaneous NETosis and low-density neutrophils (LDL) known to be prone to NETosis were also observed in PAPS suggesting a protrombotic potential of the NETs[50]. Similarly to apoptosis, various posttranslational modifications can also occur upon NET release[51] so they can be an additional source of cytoplasmic and nuclear autoantigens in SADs[52]. It was also shown that DNA decorated by cationic peptides like LL-37 is more accessible for plasmacytoid dendritic cells (pDC)[53,54], thus self-DNA can activate intracellular receptors like toll-like receptors (TLR), leading to excessive IFNα production[54].

The autoantigens released constantly by dead cells promote cell activation, as they can directly stimulate pattern recognition receptors (PRR), or can alternatively be recognized by autoantibodies creating immune complexes. These complexes are next phagocytosed through the FcRγ receptor and are able to activate TLR molecules, known to be involved in SADs

pathogenesis. These responses can result in proinflammatory cytokines or autoantibody production, depending on the cells activated. Figure 1 shows how cell death can trigger autoimmune responses.

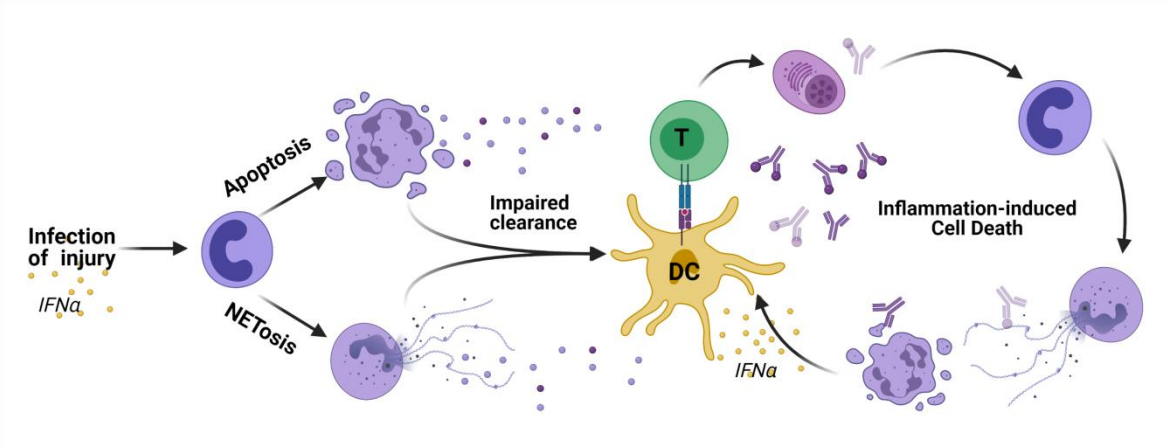

Figure 1 Apoptosis and NETosis as an autoimmune amplification loop in SADs.

For simplicity neutrophils are shown as the initiating source of autoantigens but any dying cell could be a driver in this process. This process requires the impaired clearance of dead cells, activation of DCs and presentation of autoantigens to autoreactive Th cells. Th cells next stimulate B cells to produce autoantibodies that amplify the loop by increasing cell death and DC cell activation. Figure is adapted from Darrah and Andrade, 2013.

1.2.2 Toll-Like-Receptors in SADs

TLR are the best characterized innate immune sensor family that are expressed on both innate immune cells like dendritic cells (DC), monocytes, granulocytes and adaptive immune cells like T and B cells[55]. Every cell type expresses a specific TLR combination. TLRs are located either at the cell surface (TLR1, TLR2, TLR4, TLR5 and TLR6) or intracellularly in the endoplasmic reticulum of resting cells (TLR3, TLR7, TLR8 and TLR9)[56,57]. Based on the PAMPs that they recognize, TLR can be grouped into 3 specificities: lipids and lipopeptides (TLR2/1, TLR2/TLR6 and TLR4), proteins (TLR5) and nucleic acids (TLR3 for double-stranded RNA (dsRNA), TLR7 and TLR8 for single-stranded RNA (ssRNA), TLR9 for unmethylated CpG-rich DNA oligonucleotides)[58,59]. Besides recognition of PAMPS, TLRs are also specialized in recognition of DAMPS released from damaged tissue and apoptotic cells such as heat shock proteins, fatty acids or HMGB1[60]. Their downstream signaling pathways lead to the activation of various transcription factors like nuclear factor-κB (NF-κB), Interferon response factors (IRF) and mitogen-activated protein kinases (MAPK), which induce the transcription of various immune response genes, like chemokines, costimulatory molecules, inflammatory cytokines and type 1 interferons[60]. One of the hallmarks of SADs is the finding of an IFN signature and high levels of proinflammatory cytokines.

The importance of TLR in SADs is reflected in the drugs used as a first line of treatment. Antimalarial drugs like chloroquine and hydroxycholoquine are disease-modifying anti-rheumatic drugs (DMARDS) currently approved for treatment of SLE in all cases[61], RA in mild cases[62], SJS with joint involvement[4] and APS during pregnancy[63]. They were introduced in rheumatic disease treatment since 1940[64]. Back then their mechanism of action was not known, however currently conducted studies gave light on their immunoregulatory and anti-inflammatory effects. These drugs change the pH of endosomes[65] and can directly bind to nucleic acids. Because of this they affect the activation of intracellular TLRs like TLR9[66,67] and TLR7[67,68]. Because they disrupt the function of the lysosomal pathway they also affect the antigen processing and its presentation via MHC class II, and impair the maturation of autophagosomes affecting the process of autophagy[64]. Various inflammatory cytokines are reduced upon treatment with antimalarial drugs in vitro culture, affecting the expression of inflammatory cytokines by PBMC[69] but also more specifically TNFα, IFNα, IL-6 and CCL4 (MIP1-β) in pDCs[70,71]. The reduction of IFNα, TNFα and disease severity was observed in patients with SLE[72]. Also the production of autoantibody is diminished by the drug interference with TLR9 and differentiation of memory B cells into antibody producing plasmablasts[73]. Inhibitors of IRAK4 kinase, a molecule involved in TLR signaling (Figure 2), were shown to be more effective in reducing the production of proinflammatory cytokines than antimalarial drugs[71]. This component is involved in many clinical trials in RA patients[74]. An anti-TLR4 monoclonal antibody is also under investigation in a clinical trial, however recently published results showed no benefits for the treated patients[75].

1.2.3 IFN signature in SADs.

IFNs are functionally related cytokines which have an important role in antiviral response but also in inflammation, cancer and autoimmunity. Three major types of IFNs can be distinguished, type I, II, and III. IFN-I family consists 8 different interferons and among them IFNα and IFNβ are the main members and have shown the strongest implications in SADs[76]. In healthy individuals IFN-I production is initiated upon bacterial or viral infection, however in autoimmune patients' immune complexes coming from dying cells are able to constantly activate immune cells, triggering IFN-I responses and inducing IFN-stimulated genes (ISG)[77]. The main IFN-I producers are pDC, which express the endosomal TLR TLR7 and TLR9, so they can rapidly produce high amount of IFN-I in response to exogenous nucleic acids[78]. Other phagocytes and immune cells are also known to produce it[79]. The level of pDCs in the

circulation in SADs patients is lower than in healthy controls, which is probably due to their migration to the inflamed tissues, as they were found in kidneys and salivary glands of SLE[80] and SJS[81] patients, respectively, although contradictory reports have also been published[82]. The activation of TLR7 and TLR9 in pDCs leads to a signaling cascade involving MyD88 and its interaction with IRAK proteins, triggering the nuclear translocation of NF-κB, IRF5 and IRF7, and the induction of IFN-I and proinflammatroy cytokines (like IL-6, TNF or IL-12)[76], but also to their maturation by upregulation of molecules like class I and II MHC and CD86[83]. IFN-I favors antigen presentation[84] bringing the innate and adaptive immune responses and demonstrating its important role in autoimmunity. The mechanism of IFN-I activation in pDCs can be seen in Figure 2. It is worth noting that pDCs are the current target of diverse therapies in development for cutaneous active lupus patients. A recent clinical trial that used anti-BDCA2 Abs (BIIB059), molecule exclusively expressed on pDCs, met its primary end points[85]. This drug was reported to inhibit the production of pro-inflammatory mediators, including type I interferons and to be more potent in blocking various intracellular TLR response than hydroxychloroquine[86].

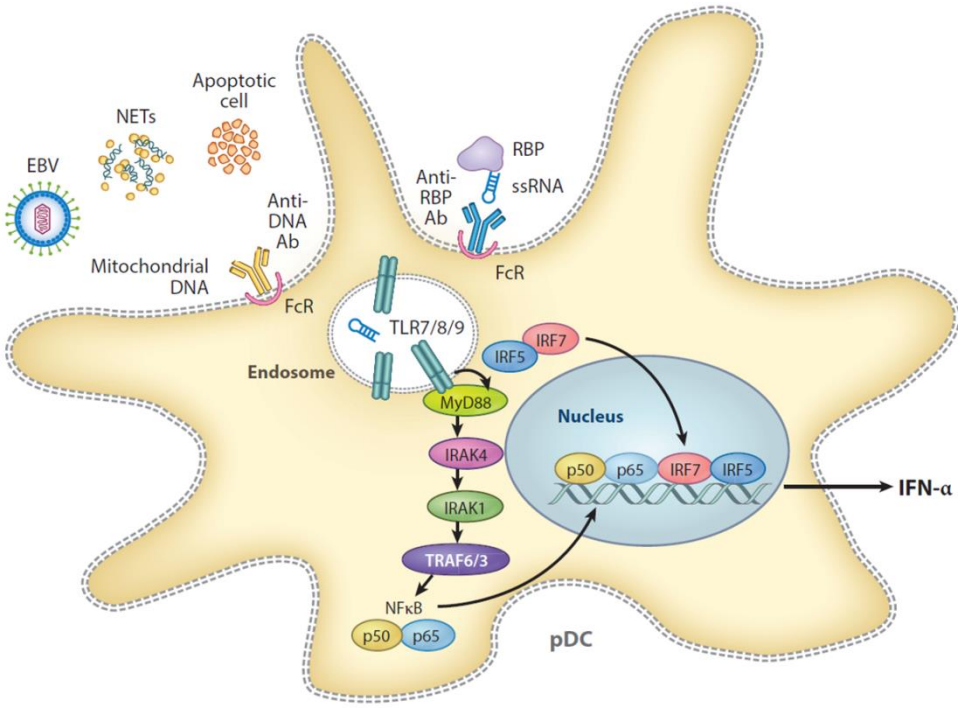

Figure 2 TLR mediated induction of IFNα.

Autoantigens typical for SADs containing nucleic acids are recognized by autoantibodies and internalized via FcR and recognized by intracellular TLRs residing in the endosome. The cascade via Myd88, IRAK4 and 1 and TRAF initiate the translocation of transcription factors like NF-κB and IRF5/7 to the nucleus and triggers transcription of IFNα, although other cytokines can also be produced. Adapted from Crow et al, 2019[87].

Various SADs genetic risk loci involved in either TLR signaling or IFN-I responses have been discovered[88]. These variants are associated with either increased circulating IFN-I activity[89] or with increased ISG expression[90]. Human genetic variants in multiple IRFs are associated with SADs, like IRF5[91–94], IRF7[92,95,96] or IRF8[97,98]. IRF5 is linked with increased circulating IFN-I, which strongly correlates with the presence of anti-RBP or anti-dsDNA antibodies in SLE[99]. Another important pathway affected by IRF5 is connected to B cells, since it is characterized by the production of autoantibodies due to hyperactivity of TLR pathways, leading to anti-immune complex antibody production[100]. Other examples of IFN-related genes are the association of STAT4 with SJS[93], SSC[95,101], RA[102], SLE[92,102], and that of PTPN22 with RA and SLE[103].

Although an IFN signature was found in most of the SADs, a high heterogeneity was also observed. For example SLE patients can be stratified into two groups based on their high or low levels of IFN-I, and a new genetic locus was identified with the first group of patients[104]. SSC[105] and SJS[106] patients with high ANA titer were also characterized by high levels of IFN-I compared with patients with low ANA titer. These findings suggest that although the clinical outcomes of SADs are different, there are subgroups of patients sharing autoantibody profiles and genetic associations involving in TLR and IFN-I pathways.

Although the IFN-I involvement in SAD is well known, the data from clinical trials involving this cytokine are contradictory and do not fulfill the expectations. Two monoclonal Abs directed against IFNα were used in different phase II clinical trials with SLE patients. The rontalizumab (anti-human IFNα antibody)[107] did not meet neither primary nor secondary end points, although the benefits for the patients with low level of IFN signature were observed. On the contrary sifalimumab (anti-human IFNα antibody)[108] met the criteria and its positive outcome was mainly seen in patients with high interferon signature, although clinical benefits were modest compared to placebo group. Another clinical trial[109] involved anifrolumab, a drug that blocks IFNAR receptor and hence has a broader mechanism of action. It showed an improvement in organ-specific disease activity indexes, a decrease in the flare rate and ability to maintain low disease activity for longer times. These benefits were especially seen in the patients with high IFN signature, although the low IFN signature group was underrepresented in this study. In the next two clinical trials TULIP1[110] and TULIP2[111] benefits were seen for the patients again, and the differences were also observed between the groups characterized by high and low levels IFN signature, although the primary endpoint in TUILP1 was not achieved. The benefits from this medication were also found in SSC patients[112], and for SJS a clinical trial using another monoclonal antibody that temporally depletes pDCs is ongoing (NCT02780674).

It should be noticed that clear benefits of the anti-IFN treatment were seen only in around 40-50% of the treated patients, which still leave a significant number of individuals without effective treatment. These studies also show that only particular groups of patients could benefit from these drugs, pointing towards the importance of a proper patient stratification and selection for the clinical trials.

1.2.4 Cytokine signatures in SADs

Besides the elevated levels of type I IFN in the serum of patients, other cytokines were also reported to be elevated in SADs. And many biological treatments or JAK/STAT inhibitors were developed to target them[113,114]. Among the elevated levels of cytokines in the serum and tissue, inflammatory cytokines like IL-6, IFNγ, IL-23/IL-17 and TNFα, as well as anti-inflammatory cytokines (IL-10) were found to be increased and correlated with disease activity.

TNFα is considered as a master proinflammatory cytokine that plays a critical role in autoimmune diseases with chronic inflammation. Besides being rapidly expressed at high levels at the site of inflammation, this cytokine promotes expression of other agents like IL-1, IL-8, IL-6 and IFNγ, enhancing the inflammatory loop[115]. Additionally, the induction of apoptosis by TNFα was also reported in various studies[116,117]. Thus, these findings suggest it has an important role in SADs development.

High levels of TNFα were detected in RA patients[118] and correlated with joint pain[119]. It was also the first SAD that was successfully treated with this agent. Multiple TNF inhibitory (TNFi) molecules have been developed so far, however their outcome depends on their molecular mechanism of action. It was shown that adalimumab, besides biding soluble TNFα, also acts as a TNFα agonist and increases its ability to expand T regulatory cells (Treg), however it can also promote T effector (Teff) expansion[120]. A similar effect was shown for infliximab[121], another TNFi. On the other hand etanercept does not promote Treg expansion and its main effect was attributed to the reduction of Teff cells[120]. These phenomena can explain why significant proportions of patients fail to respond to TNFi treatment, showing exacerbation of the disease[122] or induction of other autoimmune disorders like SLE[123]. Thus, it could be helpful to monitor the moment of treatment initiation, as well as the balance between immune cells like Teff and Treg. It can be important when deciding which anti-TNF agent should be applied. High levels of TNFα was reported in SJS, SLE and SSC, and it was correlated with important pathological factors, like the increase in the expression of autoantigens Ro/SSA and La/SSB[124], downregulation of the expression of water channels in salivary glands[125] or the correlation with

anti-dsDNA Abs[126,127] or IFNα levels in SLE patients[128]. In a small study with SLE patients some improvements were detected upon TNFi treatment, such as a decrease in proteinuria, however multiple secondary effects were also reported[129]. Encouraging results were found in a small study for PAPS[130] resulting in a current ongoing clinical trial (NCT03152058). So far benefits from TNFi treatment were reported for SSC[131,132] and SJS[133,134] patients.

Unfortunately, the high level of non-responders to TNFi, the adverse effects of the treatment, the use of small study groups, and the responses of patients against the drugs encouraged researchers to look for other anti-cytokine therapies that could help to ameliorate or treat the symptoms.

IL-6 is a pleiotropic cytokine which was at first characterized as a B-cell growth factor and later described to be involved in many biological processes including systemic inflammation and fibrosis. It is mainly produced by monocytes and neutrophils upon TLR challenge and has a predominant proinflammatory activity regulating innate and adaptive immune cells[135]. IL-6 acting alone or in combination with other cytokines promotes differentiation of B cells into antibody producing plasma cells[136,137], and additionally induces proliferation and differentiation of T cells into T helper 17 (Th17)[138] and T follicular helper (Tfh)[139] cells, which are known to be involved in autoimmunity. The elevated IL-6 serum levels and the association with disease activity was confirmed in the meta-analysis of SLE[140], and also in studies of RA[141,142] and SSC[143].

Tocilizumab is an antibody that blocks the signaling through the IL-6 receptor. This medication is currently used in RA, as it suppress disease activity, ameliorates joint destruction[144], and is highly effective in early disease development. In a phase I clinical trial for SLE the disease activity scores improved and the level of anti-dsDNA antibody dropped significantly together with the frequency of circulating plasma cells[145,146]. It was also shown to have a positive influence on lung function, a secondary outcome parameter in a clinical trial for SSC[147]. However just recently it failed in the Phase II/III clinical trial for SJS as no difference was observed between treated and placebo[148].

IL-23/IL-17 axis is another important factor in SADs and its blockade gave positive outcomes and has been approved for the treatment of another autoimmune disease, namely psoriasis[149]. IL-23 is a heterodimer composed of two subunits p19 and p40 (the last one is shared with IL-12) and is mainly produced by DC and monocytes/macrophages[150]. The activity of this cytokine is similar to IL-12, increasing IFNγ production by T cells[150], but has also the unique ability to

induce Th17 differentiation[151] and change the balance between Th17/Treg[152,153]. The IL-17 family contains six members from A to F, among which IL-17A is the most studied, and produced mainly by Th17 cells[154]. It can act on neutrophils promoting NETosis[155] and also on B cells triggering autoantibody production[156]. IL-17 accelerates the inflammatory response by inducing the production of IL-6, TNFα and T cells- and neutrophil-attracting chemokines like CCL2 (MCP-1) or CCL7 (MCP-3)[157]. Elevated levels of both cytokines were shown in circulation and in tissues of various SADs patients, correlating with disease activity[158–164]. So far the blockage of the IL-17/IL-23 axis shows poor or moderate efficacy in patients with RA[165], however some promising results were obtained with ustekinumab in a cohort of SLE patients, a monoclonal antibody targeting the IL-23 and IL-12 p40 subunit[166]. Sixty percent of the patients met the end-point criteria, and additionally the risk of new flares was also reduced. The follow-up of these encouraging results is currently ongoing in another clinical trial (NCT03517722).

1.2.5 Cellular blood and tissue abnormalities in SADs.

The high level of cytokines, autoantibodies and the tissue inflammation are provoked by specific immune cells and their interaction with other cells in the tissues. Thus, not only their products are involved in the pathogenesis of SADs but also their particular physiological behavior, function and dysregulation. The high level of autoantibodies present in the circulation of SADs points toward the cells involved in antigen presentation like DC and monocytes, B cell producing the autoantibodies and T cells giving signals to induce those autoantibodies. The association of various gene variants in class II HLA genes including HLA-DQA1, HLA-DQB1, and HLA-DRB1 with multiple SADs was reported and recently reviewed[167], and supports the importance of antigen presentation. Additionally, the NETs produced by granulocytes are potent autoantigen sources and seem to be also important in the vicious cycle of autoimmunity. In general, many immune cells are involved in SADs pathogenesis and some will be discussed below.

Human DC are heterogeneous populations composed by several subsets, like pDC, characterized by the expression of CD123 and BDCA2, two types of conventional DCs (cDC): $CD141^+$ (BDCA3) cDC and $CD1c^+$ (BDCA1) cDC, and inflammatory infDC, generated in the tissue upon differentiation of newly recruited monocytes[168]. As mentioned before, pDCs are the main producers of IFNα and hence play an important role in SADs pathogenesis. Their low circulation level was seen in multiple SADs compared to healthy controls[81,169,170] and it was

recently confirmed in a study where 3 different SADs shared low pDC as a unique common feature[171]. The treatments against pDC described before highlight their importance in SADs.

In the presence of danger signals (DAMPs) cDCs become activated and mature into antigen presenting cells (APCs), increasing the levels of Class I and Class II MHC in their cell surface, and that of chemokine receptors and cytokines and T lymphocyte costimulatory molecules like CD86 and CD80. Depending on the environment, cDCs induce the differentiation of different types of Th and Treg cells, but also promote antibody production by direct interaction with B cells or production of survival factors like B cell activating factor (BAFF) as well as the production of a proliferation inducing ligand (APRIL), involved in B cell differentiation and antibody production[172]. Various studies using flow cytometry (FC) reported decreased frequency of circulating cDCs in the blood of SADs patients, and through histological analysis, the increased numbers in the inflamed tissues[81,173,174]. The accumulation of DAMP signals in the inflamed tissue primes cDCs to release more inflammatory cytokines like IL-12 and IL-23, a phenomenon observed in RA, switching the T cell repertoire towards Th1 and Th17 pathogenic T cells[174]. Additionally, antigen-primed DCs migrate to the lymph nodes where they activate auto-antigen specific T cells and promote autoantibody production by B cells[175]. The local priming of memory T cells can also take place in the tissues in ectopic lymphoid structures[176], leading to B cell activation, local production of autoantibodies[177] and further tissue degeneration.

Monocytes are responsible for phagocytosis and elimination of opsonized microorganisms and apoptotic dead cells through PRR[178] like C1q. which mediates the recognition of various pathogen molecules and plasma proteins[179]. The deficiency of these proteins is correlated with an increased risk of developing RA[180] and SLE[181], owing that proper removal of bacterial and self-proteins can be crucial in preventing the induction of autoantibodies[182]. Human monocytes are constituted by 3 main populations based on the expression levels of CD14 and CD16 markers, although more fine phenotyping was already performed using high-dimensional cytometry techniques[183]. $CD14^{++}CD16^{-}$ monocytes are called classical, and they account for up to 90% of the monocyte compartment; intermediate $CD14^{++}$ $CD16^{+}$, that yield a high level of proinflammatory and anti-inflammatory cytokines like IL-10; and non-classical $CD14^{+/-}CD16^{++}$ with a more mature phenotype and with high migratory and low phagocytic properties, that constitute around 5-10% of the total population[184]. Increased blood frequency of intermediate monocytes was reported in RA and it was shown that these cells promoted a proinflammatory cytokine milieu inducing the generation and maintenance of Th17 cells[185]. Furthermore, it was

reported that a higher number of classical and intermediate monocytes can be used as a predictor of clinical response to methotrexate in RA[186]. In SJS the frequency of monocytes positive for the BAFF-receptor (BR) 3 is higher compared with healthy controls and its expression is correlated with higher expression of IL-6, ANA autoantibodies, and higher disease activity[136]. These results suggest an important role of monocytes in the pathogenesis of autoimmunity. In the blood of SSC patients the absolute count of $CD14^+$ and $CD16^+$ monocytes is elevated compared to CTR and the frequency of $CD16^+$ cells is positively correlated with clinical symptoms like skin severity and pulmonary fibrosis[187]. Additionally, $CD16^+$ monocyte count is higher in diffuse cutaneous SSC (dcSSC) compared to limited cutaneous SSC (lcSSC). However this observation was contradicted in a recently published study where the $CD16^+$ monocytes characterized patients with limited skin involvement while classical monocytes characterized patients with more spread fibrosis[171]. These discrepancies can be due to differences in the analytical approaches and also to the high heterogeneity across SSC patients. Although contradictory, these results show that the severity of tissue involvement in SSC could be predicted based on the frequency of cells circulating in the blood. In another study it was observed that the monocytes from SLE patients have increased expression of CD40L[188] and that this molecule significantly stimulates the production of IgG in SLE but not CTR-derived B cells[189]. Thus, these cells can have a potential role in B cell hyper-reactivity. What is more, monocytes from SLE patients differentiate to cDCs expressing higher levels of CD86, which increases their ability to present autoantigens and trigger autoimmune responses[190].

B cells are multifunctional lymphocytes that contribute to the pathogenesis of SADs via functions like antibody production, antigen presentation, T cell help and cytokine production[191]. The dysregulation of B cells in both periphery and tissue was described in multiple SADs. In SJS one of the most consistent changes in peripheral blood is the reduced number of circulating $CD27^+$ memory B cells[192–194]. It is believed that these cells migrate to or are retained within target organs, as increased number of memory B cells was described in salivary glands of patients[192]. A reduction in memory B cells is also observed in SSC patients; however their low frequency is probably caused by the overexpression of CD95 (Fas) which induces higher sensitivity to Fas-mediated apoptosis[195]. Additionally $CD27^+$ B cells from SSC patients are characterized by higher expression of the costimulatory molecules CD80 and CD86[195], which are crucial for B–T cell interaction. On the other hand increased frequency of memory B cells was observed in the blood of SLE patients[196]. It is known that memory B cells have reduced expression of the FcγRIIb receptor, which lowers their reactivation threshold[197].

They have also lower proliferation rates which makes them less susceptible to the conventional immunosuppressive medication that depend on the cell cycle, becoming easily activated during disease relapse[197]. Additionally, these cells can be rapidly activated in an antigen-independent manner by the combination of TLR agonists with either APRIL, BAFF or IL-21[198]. FcγIIb receptor is crucial in restricted antibody-mediated immune responses and is thought to prevent autoimmunity[191,199]. The mutation in the gene locus of FcRγIIb receptor has been associated with a higher risk of RA and SLE[191], and therapies with an extracellular version of human FcγIIb that works as decoy receptor and prevents immune complex biding to other FcRγ have been developed[200]. Other memory B cells expanded in SLE are $IgD^{-}CD27^{-}$ DN (double negative) B cells, expressing isotype-switched and mutated antibodies, thus having a memory B cell phenotype[201]. The presence of these cells was correlated with anti-dsDNA and anti-RNP autoantibodies. Another study found their positive correlation with proteinuria in patients with lupus nephritis, regardless of disease activity[202]. These cells were further divided in two populations: DN1 ($CXCR5^{+}CD19^{int}$) and DN2 ($CXCR5^{-}CD19^{hi}CD11c^{+}$)**.** The DN2 population is expanded in SLE patients and characterized as pre-plasma cells, that are hyper-responsive to TLR7 stimulation and are predominant in African-American patients with active disease, nephritis and anti RNA, Smith-autoantibodies[203]. These cells are also elevated in RA, and SSC but not in SJS patients[203]. Plasmablasts are increased in the circulation of SJS[204,205], SLE[206] and PAPS[207] patients. Furthermore, genetic analysis revealed that plasmablasts increase in PAPS[207] and SLE patients with APS, is associated with a SNP in TLR7 receptor and with higher IFN-I production[207]. An increased number of circulating plasma cells (PC) was reported in active SLE patients and correlates with higher amounts of autoantibodies. These PC have a mature but not fully differentiated phenotype, inducing their persistence in the circulation[206]. In SJS the increase of PC infiltration was observed within the salivary glands, and the elevated number of plasmablasts (PB) in circulation, and PCs in tissues were correlated with serum IgG levels, disease activity and positivity for autoantibodies[205]. Additionally, these infiltrated plasma cells are characterized by $CD38^{+}CD27^{+}$ marker expression together with a substantial fraction of $CD19^{-}$ cells[205], suggesting a long-lived plasma cell phenotype and function in maintaining the humoral, autoagressive response[208]. An increase of circulating naïve B cells was found in SSC patients and it is believed to compensate for continuous loss of memory B cells due to spontaneous apoptosis as described before[209]. These naïve B cells are characterized by higher expression of CD19, which indicates the presence of persistent B cell activation[210]. On the other hand, a diminished number of these cells was found in SLE patients. The balance of B cell

subpopulations in SLE patients is therefore switched into memory B cells, which, as already antigen experienced cells, have lower activation threshold and are primed for action[211].

The above-mentioned examples show a broad dysregulation of B cells homeostasis in SADs, emphasizing their importance for treatment approaches. Indeed, various B cell-depleting agents are used or studied to treat SADs. Rituximab, an anti-CD20 antibody is currently the drug most frequently used to target B cells and is approved by FDA to treat RA[191]. Despite of the early success in open trials[212–215], it failed to meet the primary endpoints for SJS[216,217] and SLE[218]. It was also shown that SLE treated patients experience flares after the end of the treatment[219]. The flaring patients are characterized by a quick and disproportional repopulation by PB and high levels of autoantibodies[220]. Despite this it is used as an off-label drug to treat SLE patients who did not respond to any other treatment[221], and has also a beneficial outcome for a set of SJS patients[222], emphasizing the need for patient stratification and proper assignment to the clinical trials. Rituximab targets precursors of antibody secreting cells and affects functions like antigen presentation. However due to the lack of CD20 expression on PBs and PCs, it does not directly affect pathogenic antibody generation. Thus, other therapies are being developed. CD19 is expressed on a broader spectrum of B cells including some PBs and PCs (although most of mature and long lived PCs are CD19^{-}[223]), and was also targeted in clinical trials for SLE patients, showing some benefits[224] although the data from a phase II trial (NCT02725515) are still unpublished. BAFF is a key B cell survival cytokine that was observed to be elevated in SADs[225–227]. Humanized anti-BAFF (belimumab) is the only biological drug approved to treat SLE and although it is successfully being used, many patients do not respond to its treatment and its efficiency in patients with renal involvement is still under study[200]. As it was observed that rituximab treatment increases the production of BAFF[228,229] the combination therapy was also tested in SLE patients. However up to now contradictory results were obtained[200], which can be again due to different and heterogeneous cohort groups under study in the different trials. A small phase II clinical trial also showed a positive outcome in SJS with ianalumab, a monoclonal antibody that targets BAFF receptor[230]. B and T cell checkpoints are also of interest, and antagonists disrupting the CD40-CD40L and ICOS-ICOSL interactions important for germinal center and T-B cell interaction were tried in some SADs patients[231–233]. Unfortunately, these trials were terminated due to severe adverse effects[234], lack of efficacy[235] or are still waiting to assess the drug efficacy[200], although some promising results were achieved in a cohort of SjS patients with the anti-CD40 drug[232].

T cells can be divided in two subsets: $CD4^+$ or helper cells, that can differentiate in several T helper subpopulations like Th1, Th2, Th17, Tregs and Tfh; and $CD8^+$ T cells also called cytotoxic T cells (CTL)[236] that can be also subdivided into Tc1, Tc2, Tc9, Tc17, Tcf and Tregs[237] with a similar cytokine repertoire as $CD4^+$ T cells[237]. The involvement of both Th and CTL was reported in SADs.

In general a higher proportion of $CD4^+$ infiltrates is detected in the inflamed glandular tissue of SJS patients[205], supporting the hypothesis that the blood lymphopenia is caused by migration of $CD4^+$ cells into the tissue. A lower amount of $CD4^+$ T cells was also found in the blood of SLE patients [238] and lymphopenia in SLE is associated with a high disease activity index and with renal disease[239]. Furthermore, SLE patients with high disease activity score have elevated levels of $CD4^+$ $CD28^-$ T cells[238], which were also found in patients with RA[240,241] and SSC[242]. These cells are characterized by cytotoxic capacity, expression of natural killer (NK) cell receptors and resistance to apoptosis, they are not anergic but rapidly respond to the stimulation[243]. Because of this they can contribute to disease progression. For a long time it was believed that the bias towards Th1 response was dominant in some SADs[244–246] except SSC, with the bias shifted to Th2 response as shown by an increase of IL-4, IL-6 and IL-13 cytokines in serum and skin[247] and in SJS with severe B cell accumulation in glandular tissue within germinal centers[248]. However, elevated levels of Th2 cytokines were also observed in SLE patients and both Th1 and Th2 – cytokines were correlated with disease activity[249]. Thus, it is currently believed that both Th1 and Th2 cells are involved in SADs pathogenesis. Among the $CD4^+$ Th, Th17 cells are known to be involved in autoimmunity and are also increased in the circulation and in the tissue of SADS patients[159,250–252].

Treg are suppressor cells that inhibit the activation and proliferation of $CD4^+$ Th cells, differentiation of CTL and activation of B cells. The knowledge about Treg population is contradictory in SADs. The main two reasons are the high heterogeneity of the patients but also the lack of consensus on which markers should be used to study these regulatory cells[253], thus different markers are used across the studies and different cell populations are targeted. Both the reduced[254], increased (correlated with disease activity[255]) and non-altered[256] frequency of $CD4^+$ $CD25^{hi}$ $FoxP3^+$ (or $CD25^+CD127^{lo}$ or $CD25^+CD4^+$) cells were reported in the peripheral blood of SLE. The non-altered and decreased expression of this phenotype was demonstrated in the blood of RA[255,257] with affected suppressing function[258]. Their accumulation in synovial fluid and tissues was also described[259,260]. These cells are functional[261] although high level of TNFα inhibits their suppressor behavior[121]. Higher frequency in the

blood was shown for dcSS patients[262] and in SJS patients with high expression of IFN-I[263], although contradictory results were also reported for SSC[264,265]. It was demonstrated that responders to the treatment of anti-TNFα therapy have an increased frequency of peripheral blood Treg[121] and the blockage of IL-6R changes the balance of Th17/Treg favoring Treg and correlates with improved disease activity scores[257]. The abnormalities in the number and frequency of T follicular helper cells (Tfh), other regulatory $CD4^+$ T lymphocytes, were also reported to be altered in SADs[266–268]

$CD8^+$ T cells play a key role in the recognition and removal of cells infected with intracellular pathogens and tumor cells. They kill target cells mainly by releasing granzyme B and perforin, or thorough Fas ligand (FasL), which triggers apoptosis in Fas^+ target cells. They can also produce various cytokines affecting both the innate and adaptive immune system[237]. In the peripheral blood of SADs patients, various irregularities were reported, regarding their phenotype, frequency and function. In SSC an increased proportion of effector ($CD8^+$ $CD45RA^+$ and $CD27^-$) and effector memory ($CD8^+$ $CD45RA^-CD27^-$) cells is found compared to healthy controls[269]. In RA terminally differentiated effector memory $CD45RA^+CD62L^-CD8^+$ T cells are significantly decreased, whereas the central memory $CD45RA^-CD62L^+CD8^+$ population is increased. No difference for naïve and effector memory $CD45RA^-CD62L^-$ $CD8^+$ T was found[270]. Although in a recent study the frequency of effector but not central memory was elevated[271]. It should be noted that different type of markers were used in these two studies, and in the first study only 8 patients were recruited.

A marked activation of $CD8^+$ in peripheral blood of SADs was also reported. In SJS $CD8^+$ T cells show increased expression of HLA-DR and are positively correlated with disease activity[205]. Additionally these cells are positively associated with the damage in the glandular tissue[205]. The increased frequency of effector cells expressing CD69, an early activation marker was also shown in both active and inactive RA patients[272]. Together these results suggest that $CD8^+$ cells might be constantly stimulated by the presence of their cognate antigen[272]. Indeed $CD8^+CD28^-$ cells defined as antigen-specific, oligoclonally expanded, terminally differentiated senescent T cells are increased in SSC[273], SLE[274] and in RA[275]. In SLE they are positively correlated with disease activity[274] and in RA with disease duration, suggesting their important role at early stages of the disease[275]. The infiltration of $CD8^+$ T cells was also reported in the organs affected by SADs, although not to the extent of $CD4^+$ T cells. In SJS, CTLs were observed around apoptotic acinar epithelial cells in the lacrimal gland[276]. The $CD8^+$ signature was also found in the skin of SSC patients and correlated with skin thickness. Immunohistochemical analysis of

skin lesions in dcSS at different disease stages show the predominance of $CD8^+$ T cells in the early stage of the disease and $CD4^+$ at the late stage, suggesting a role of $CD8^+$ T cells in the early stage of the disease. Oligoclonally-expanded $CD8^+$ $CD69^+$ T cells are also found in the synovial fluid of RA patients. These cells are characterized by increased expression of cytotoxic molecules, they induce perforin-mediated histone citrullination and NET formation[277].

Double negative (DN) T cells are another subpopulation of cells that present abnormalities in SADs. Several studies suggest that DN T cells arise from activated, self-reactive T cells that lost their CD8 expression[278–280], but also a CD8-independen origin was reported[281]. These cells are expanded in SLE[282] and SJS[283]. Additionally they induce anti-DNA IgG antibodies as efficiently as $CD4^+$ T cells[280,284] and account for increased production of IL-17 in SLE and SJS[280,283,285]. These cells are also found in the minor salivary gland of SJS patients and are resistant to corticosteroid treatment in the context of IL-17 inhibition[283]. They also infiltrate the kidneys of lupus nephritis patients[282], demonstrating their pathological role in SADs.

T cells can be categorized in two groups based on the type of T cell antigen receptor (TCR) clonally carried by the cell. Thus αβ T cells expressing αβTCR and γδ T cell expressing γδ TCR can be distinguished[286]. γδ T cells are a minor population that constitute around 0.5-5% and 1-5% of T cells in the blood and secondary lymphoid organs[287]. However certain γδ T subsets are found at much higher proportion in epithelial tissues like skin epidermis, the gastrointestinal and reproductive tracks[287]. Human γδ T cells can be classified into three main groups Vδ1 involved in maintaining epithelial tissue integrity; Vδ2 constitutes the majority of blood circulating cells and Vδ3, cells rare in blood but rich in the liver[288]. In contrast to the MHC-I and MHC-II restricted peptide recognition of TCRαβ T cells, γδ T cells recognize unconventional antigens like stress molecules and non-peptide metabolites without MHC restriction[289]. They can bridge innate and adaptive immune responses through their ability to present antigens, and express proinflammatory cytokines, chemokines and cytotoxic molecules[290,291]. A subset expressing FoxP3 transcription factor was also described, and they can also fulfill their regulatory function[292]. Additionally, their role in the control of the production of specific antibodies has been also described[293]. Since they can shape critical functions in innate and adaptive immunity the consequences of their dysregulation were studied in SADs. In SLE, decreased frequency of γδ T cells is found in the blood[294] and is negatively correlated with the disease activity. These cells also produce elevated levels of IFNγ, IL-4, IL-10 and TGFβ[295] and have an activated phenotype as measured by CD69 expression[294]. On the other hand, increased numbers were observed in the cutaneous tissue of SLE patients compared to healthy

controls, and their numbers are higher in active vs inactive patients. Additionally a positive correlation with the disease activity was found [160]. SSC patients positive for anti-Scl-70 Abs and patients with shorter disease duration were characterized by reduced number of γδ T cells[296]. Yet in another study this reduction is only observed on the specific subset of Vδ1 cells, and their higher activation was measured by HLA-DR overexpression. Also elevated infiltration of these cells was observed in the inflamed tissue[297]. Both decreased[298,299] and stable[300] γδ T cell frequency was reported in the peripheral blood of RA, although an increase in synovial fluid infiltration of activated γδ T cells with downregulated CD16 and upregulated HLA-DR was observed[301] and a correlation with tissue inflammation score was also reported[302]. A similar activated phenotype was also observed in the blood of SJS patients[298,303], however no differences in the frequency of γδ T cells were observed between patients and healthy controls.

Many of the therapies applied and tried in SADs are also directed to the T cell functions, like anti-cytokine therapies or treatments directed against CD40 or ICOS interactions. But also additional pathways involving immune check point receptors like CTLA-4/CD28 or PD-1/PD-L have been considered[304].

NK cells are innate lymphoid cells. Although they are derived from lymphoid T progenitors in the bone marrow they lack rearranged antigen receptor genes[305]. They are defined as $CD3^-$ $CD56^+$ mononuclear cells, and can be classified into $CD56^{dim}$, predominantly found in the blood, and $CD56^{bright}$, found mostly in the secondary lymphoid and inflamed tissues[306,307]. $CD56^{dim}$ are more cytotoxic due to their higher expression of inhibitory killer immunoglobulin-like receptors (KIRs), components of cytolytic granules (perforin and granzymes) and FCγIIIA (CD16)[308], which together mediate antibody-dependent cell cytotoxicity (ADCC). The $CD56^{bright}$ cells are characterized by a lower cytotoxic activity[309] and the production of higher quantities of cytokines and chemokines such as IL-10, TNFα, INFγ and GM-CSF[308,309]. Because of this they are characterized as immunoregulatory cells as they can influence innate and adaptive immunity. Both subtypes can also produce MIP1-β, MCP1 and RANTES[310], cytokines important in the pathogenesis of SADs. Decreased absolute NK cell count and frequency was observed in the peripheral blood in multiple SADs[171,311–314]. Additionally in SLE this decrease was associated with disease activity and with severe clinical manifestations like nephritis and thrombocytopenia[313,315]. In SJS an increased ratio of $CD56^{bright}$ NK to $CD56^{dim}$ NK was observed and positively correlated with serum IgG levels, but not with the disease activity index ESSDAI[311]. This imbalance was also observed in SLE patients[311,316], although some other studies

do not support this observation[312,315]. A reduced number of CD56^{bright} cells were also reported in SSC[171,314]. On the other hand, RA patients are characterized by an increased frequency of NK cells in the blood that is inversely correlated with disease activity[317]. This increase is also observed when stratifying SSC patients into dcSSC and lcSSC. dcSSC patients were characterized by higher number of circulating NK cells compared to lcSSC and in both groups they have increased expression of activation markers compared to controls. The cytokine production (IL-5, IL-10, IL-6) was dysregulated in dscSSC but not in lcSSC and both groups presented reduced cytotoxicity compared to controls[318]. Increased infiltration of both NK cell subpopulation was reported in the kidney of patients with lupus nephritis[319], and peripheral blood Ki67^{+} NK cells are significantly correlated with disease activity and nephritis, suggesting an important role of these cells in kidney inflammation[320]. Additionally peripheral CD56^{bright} cells from SLE patients produce more IFNγ in both active and inactive patients, and more TNFα in the active group[315], suggesting their pathological role in the tissue. On the other hand, autoantibodies directed against the KIR receptor were found in SLE, SJS and SSC patients. The anti-KIR^{+} IgG from SLE patients reduced the degranulation and cytotoxicity of NK cells. The presence of these antibodies was correlated with increased disease activity, nephritis and the presence of ANA, suggesting that the reduced and defective function of NK cells may be also a risk factor for developing SADs[321]. Decreased cytotoxicity of circulating NK cells was found in RA[317], SLE[312], and SSC[318] patients, additionally lower level of IFNγ was also produced by NK cells from RA patients[317]. However, the joint infiltrating CD56^{bright} NK cells have high expression of CD69[322], indicating their activated state, although they are perforin^{lo} and do not produce high levels of TNFα and IFNγ[317]. This suggests that other pro-inflammatory mediators secreted by these cells or another associated function can play an important role in SADs pathogenesis. For example it was shown that NK cells accumulated in the inflamed tissue can promote TNFα production by CD14^{+} monocytes[323]. These findings demonstrate an important role of NK cells in SADs, however also emphasize different NK cells roles in different endotypes of the disease.

Neutrophils constitute more than 50% of circulating leucocytes in the blood and are important in the defense against invading microbes. Although they are phenotypically and functionally diverse, due to their short-life time, spontaneous activation after isolation and their terminal and non-proliferative differentiation state in the circulation, makes them resistant to genetic manipulation and difficult to study. Because of this and despite their abundance in the blood they are usually excluded from phenotyping studies and instead peripheral mononuclear cells

(PBMC) are used. This causes a significant loss of information, especially in the context of SADs where neutrophils are known to play an important role.

Neutropenia is found in a great number of SLE patients[324] and in a fraction of SJS[325]. Blood neutrophils in SLE show many abnormalities like impaired phagocytosis and lower activity in C1q-mediated apoptotic cell clearance[326]. Contradictory results were reported for their production of reactive oxygen species (ROS) as both increased and decreased production was found [327,328]. This discrepancy is probably due to differences in the selected study cohorts and again emphasizes the internal heterogeneity of SADs.

Low-density granulocytes (LDG) are a fraction of neutrophils found in the PBMC layer that is characterized as $CD15^{hi}CD14^{lo}CD10^{+}CD16^{+}$[329]. Due to their ability to secrete TNFα, IFNγ and type I IFN[329] they are considered to be proinflammatory, and they are elevated in patients with SLE[330], PAPS[331] and RA[332]. Also, their higher numbers correlates with disease severity and anti-dsDNA antibodies in SLE[333]. LDG from SLE patients were also described as NETosis-prone cells and the kidney and skin of lupus patients are infiltrated by netting neutrophils[49]. As NETs contain citrullinated histones and ACPA antibodies are a hallmark of RA, NETosis was also studied in RA patients and it was shown that neutrophils from RA are characterized by high spontaneous NETosis. The same functional behavior was observed in PAPS[50] and SLE patients[49]. In healthy individuals circulating neutrophils need to be first primed in order to migrate to the tissue and get activated[334]. However, it was observed that neutrophils form RA are already primed for ROS production[335], are characterized by delayed apoptosis[336] and show an activated phenotype[337]. They also have a high chemotactic capacity[338,339] and increased phagocytic activity[340] together with elevated ROS production[335] in response to immune complexes (IC)[341]. These disrupted functions actively participate in the damage of the synovial membrane, mediated by activation through FcγR, causing neutrophil degranulation, release of ROS and cytotoxic agents directly on to the surface or articular cartilage or in synovial fluid[342]. Currently there are no therapies directed against neutrophils of SADs patients, however corticosteroids and non-biological DMARDS such as methotrexate promote neutrophil apoptosis and decrease neutrophil migration and ROS production[343–345]. Anti-TNFα was shown to be effective in down-regulating neutrophil activation by decreasing NF-κB expression and cytokine production[342].

All together it can be seen that various immune cells are involved in the pathogenesis of SADs. However, their functional dysregulation and aberrance in frequency are not disease-specific

and can be present only in a subset of patients and/or shared between different SADs. Figure 3 summarizes the complexity of cells involved in the pathogenesis of SADs.

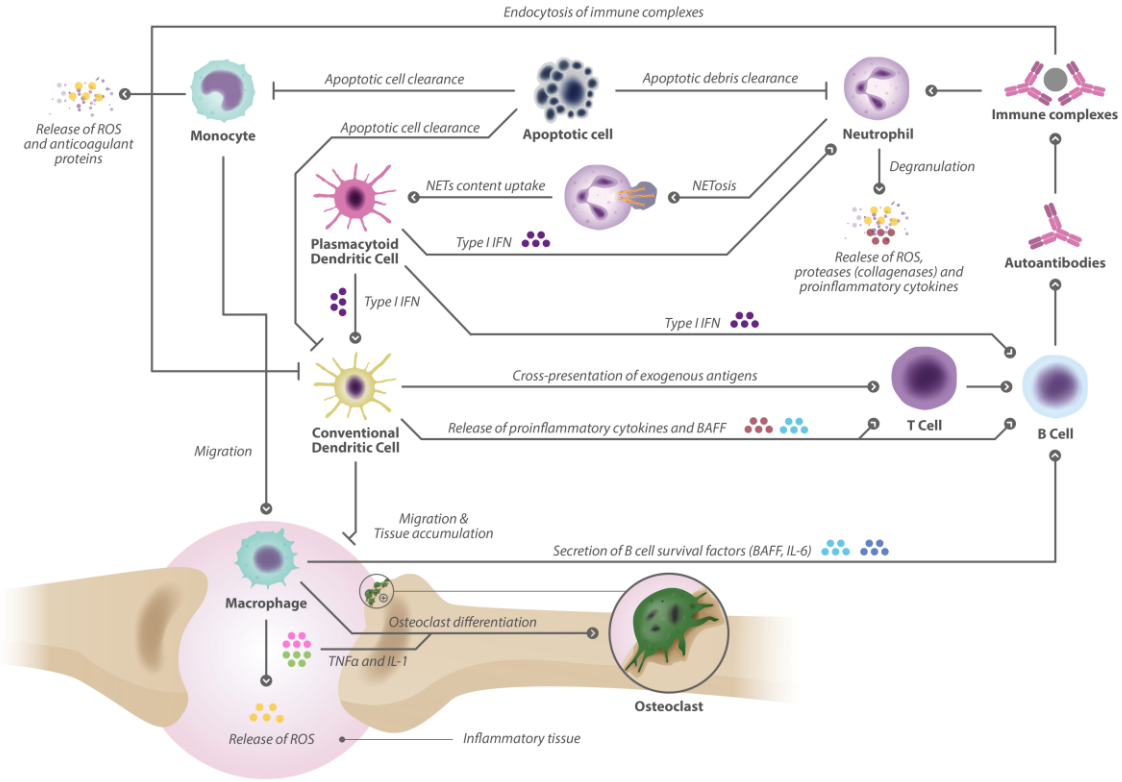

Figure 3 Immune cell involvement in SADs.

Impaired apoptotic cell clearance by phagocytes leads to the accumulation of autoantigens in the tissue. DCs present these self-antigens to autoreactive T and B cells in the presence of proinflammatory cytokines. These trigger the constant secretion of autoantibodies and lead to the accumulation of immune complexes that are next recognized by neutrophils. The neutrophils produce ROS and cytokines and eventually die by NETosis. As described before NETs decorated by autoantigens stimulate pDC triggering IFN-I production. IFN-I activates cDC and B cells, inducing antibody class switching. Peripheral monocytes travel to the tissue and differentiate into macrophages, releasing ROS and mediating the differentiation of pathogenic resident cell type, in this case osteoclast. Taken from Morell et al., 2017[334]

1.3 Difficulties in patient diagnosis and classification

As it could be seen in previous chapters autoimmune rheumatic diseases are characterized by their complex dynamic nature, at the level of clinical symptoms but also at the level of molecular and cellular involvement. Although different diagnostic labels classify patients as separate entities, it could be noticed that patients with different disease labels share many pathological pathways and cellular functions: patients from the same diagnosis group can have totally different cell composition, cellular responses or response to treatment. Although many

advances have been made in the context of therapies, still quite a number of patients are not responsive to the treatment or have strong secondary reactions. This might be due to the high heterogeneity in each clinical entity and the different immunopathological findings will depend on the number and type of patients recruited in a particular study or clinical trial. Another problem is that the diseases develop progressively for many years, and the auto-antibodies or cellular tissue infiltrates can happen long before the clinical symptoms have developed. Early diagnosis is complex as disease clinical manifestations become evident after the damage took place, and currently the autoantibodies used for diagnosis, although they can manifest early, are not disease-specific and can be present in healthy individuals. In general, the time from the disease onset to diagnosis can take many years, leading to late treatment, serious damage, drug irresponsiveness and poor prognosis. Although there are patients with clear clinical picture who are classified easily as a particular SAD, many of them share various clinical features. Patients diagnosed with SLE can develop joint deformities in hands or feet similar to those observed in RA[346] and MCTD patients may present the mosaic of clinical symptoms characteristic for SLE, RA or SSC[347,348]. SLE patients can develop secondary APS or SJS but there are also patients with primary APS and primary SJS without symptoms of SLE[349,350]. Furthermore, some patients never fulfill current clinical criteria for a particular SAD and stays undiagnosed or in the so-called Undifferentiated Connective Tissue Disease (UCTD). These patients can stay undiagnosed for many years and even for a life time[167,351].

The current classification criteria lacks specificity and sensitivity. For example the most recent 2010 ACR-EULAR criteria for RA allows for early diagnosis of the disease, however the risk of false-positive classification is high in the case of patients with osteoarthritis[167]. Additionally the presence of rheumatoid factor and ACPA that are considered for scoring are also present in other SADs and not all the patients are positive for them[352]. Up-to 2019 the world-wide accepted ACR criteria for SLE required at least 4 out of 11 items to be present, which means that patients with a completely different clinical landscape could be equally classified as SLE. In fact, the criteria are biased towards particular forms of disease like cutaneous lesions having 3 items, while neurologic manifestations have only two items, which in addition are not SLE-specific[167]. Recent classification criteria developed with the support of ACR and EULAR improve the reliability and precision. However they also introduced ANA as entry criteria, thus patients without ANA can be missed upon the process of diagnosis and still patients with totally different clinical symptoms will be classified as SLE[353], inducing still a high heterogeneity. Although the most recent ACR-EULAR classification criteria can define SSC patients with

acceptable sensitivity (91%) and specificity (92%)[354] they do not provide any information about the severity of the disease[167], and thus other markers are necessary to distinguish lcSSC from dcSSC and could complement the clinical criteria.

The patient heterogeneity, the lack of disease-specific biomarkers and the significant overlap between the diagnosis complicates, and in consequence, impedes proper assignment of patients to clinical trials and treatments. Due to biomolecular mismatch between patients and treatments many drugs do not give positive outcomes, although properly targeting autoimmune mechanisms. Therefore, they are discarded from further studies which significantly slows down the development of new therapies in SADs.

Due to this, many researchers have attempted to stratify patients based on molecular and cellular criteria rather than on clinical parameters. The stratification was done looking for markers differentiating healthy controls from the disease, within each disease, and also some attempts were already taken to reclassify patients across different SADs. These attempts are the first steps towards personalized medicine in the field of rheumatic diseases.

1.4 SADs stratification attempts

Various technologies like transcriptomics, epigenomics or cytomics were used to stratify SADs and as biological material many studies used blood or blood-derived cells as the easiest and less controversial way to obtain material, but also tissues like skin or synovial fluid were used if a biopsy was available. Both bulk and more specific single cell approaches were also undertaken.

McKiney[355] used the transcriptome of blood isolated $CD8^+$ T cells to stratify SLE patients in two groups that predict their prognosis defined as remission and number of flares. The prognostic gene set is enriched for genes involved in transduction of the IL-7R pathway, TCR signaling and $CD8^+$ effector and central memory T cells. Later, using a pediatric longitudinal cohort and blood transcriptomics, 7 groups of patients were identified with distinct expression modules[356] (set of genes with highly correlated expressed patterns[167]). These modules correspond to five distinct immune signatures in terms of cellular mechanism: lymphoid, plasma cells, neutrophil/myeloid, erythropoiesis and type I IFN. Additionally, the correlation of nephritis with IFN, neutrophil and plasmablast modules was described and patients within these groups had the most severe disease and higher levels of anti-dsDNA Abs. Data from this manuscript was further used for a stratification study together with an additional replication cohort of adult patients[357]. Instead of defining the stratification based on modules, individual genes were

selected based on their correlation with SLEDAI followed by clustering. Three clusters were defined: cluster 1 is a heterogeneous mixture of cluster 2 and 3; cluster 2 shows a clear relationship with IFN-I signature, increased neutrophil levels, low C3 plasma concentration and erythrocyte sedimentation rate (ESR) and negative correlation with lymphocyte levels; cluster 3 is opposite to cluster 2, showing high and low correlation with the level of lymphocytes and neutrophils respectively. Additionally, clusters 1 and 2 are enriched in neutrophils and shows a higher risk to develop proliferative nephritis. Patients from cluster 3 show skin features and antiphospholipid syndrome. Although these clusters are observed in both pediatric and adult cohorts, the separation is less clear in adults. In another study, a single cell approach based on flow cytometry was used to stratify juvenile SLE patients with low disease activity[358]. Four groups were identified, based on total $CD4^+$ and total $CD8^+$T cells, $CD8^+$ effector memory and $CD8^+$ naïve T cells, naïve B cells, unswitched memory B cells, total $CD14^+$ monocytes and invariant NKT cells. $CD8^+$ T cell subsets were the most important populations for the stratification of the patients, and the group with elevated frequency of $CD8^+$ effector memory T cells has higher disease activity and increased enrichment in lupus nephritis. This study again emphasizes an important role of $CD8^+$ T cells in SLE stratification. Unfortunately, in this study PBMCs were used, and hence no conclusion could be drawn for granulocyte populations. Additionally, a limited number of markers (16) split into two antibody panels was used, and therefore a limited number of cell populations was studied.

In RA, 3 subgroups were identified based on transcriptomics information from synovial fluid[359]. Two groups (RA-Ia and RA-Ib) show a high expression of adaptive immunity-related genes, characterized by an increased expression of immunoglobulin genes compared with the patients in the third group (RA-II). RA-Ia and RA-Ib can be distinguished from each other based on the immune-related genes predominant in the first group and the higher expression of complement genes in the second one. Group RA-II is characterized by genes involved in tissue remodeling, suggestive of fibroblast de-differentiation. A recent clinical trial stratified RA patients using RNA sequencing, based on the presence (B cell rich) or absence (B cell poor) of $CD20^+$ B cells in synovial tissue[360]. In this cohort, tocilizumab is more efficacious in B cell poor patients, whereas in patients classified as B cell rich tocilizumab and rituximab are similarly efficacious at modulating B cell function. The authors also demonstrated that RNA sequencing is superior to histology for patient classification. Using mass cytometry (MC) and functional assays Bader identified phosphorylated proteins involved in TNFα signaling that distinguish controls from RA patients, although a small number of samples was used in this study[361].

Two research groups classified the SSC patients using their gene expression profile obtained from skin biopsies. In the smaller sample study, 3 major groups were characterized[362]. The first group contains exclusively dcSSC and is characterized by an increment of genes related to cell proliferation and a decrease in genes of the fatty acid and lipid biosynthesis pathways. The second group contains patients with lcSSC and shows low levels of genes related to inflammation and cell proliferation, while other genes with heterogeneous functions are upregulated. The third group is a mixture of patients with dcSSC and lcSSC that has a significant increase in the expression of genes related to the inflammatory response. In a DNA methylation study CpGs differentially methylated between healthy controls and SSC also revealed the differences between dcSSC and lcSS, as only 5% of the selected CpGs are overlapping between the two groups[363]. In the former study more samples were analyzed, allowing the identification of an additional group of patients characterized by increased inflammatory responses and severity[364]. The IFN signature in the blood was measured by the level of IP-10/CXCL10 and TAC/CXCL11, and it was associated with the severity score in SSC patients[365]. However the signature depends on the clinical subgroups as demonstrated by a later study[366]. Additionally, a strong IFN signature in monocytes was able to distinguish healthy controls from patients with fibrotic SSC[366]. In a study where PBMC were analyzed using MC the alterations in the frequency of monocyte subpopulations allowed to classify patients into 4 different clusters associated with different clinical phenotypes[171]. Additionally one of the identified clusters is enriched in dsSSC, associated with higher expression of chemokines CXCL10 and CXCXL11[171], confirming the IFN signature in this endotype of SSC.

A blood IFN signature measured by SIGLEC1 was reported to be important for SJS patient stratification into those with and without extra-glandular involvement. In another study involving PBMC and MC, 6 populations (pDCs, $CD4^+$ T cells, memory B cells, PB, HLA-DR^+ $CD4^+$ and HLA-DR^+ $CD8^+$ T cells) were identified as the most important cell subsets to predict pSS diagnosis[205]. Disease activity was negatively correlated with $CD4^+$ T cell and memory B cells numbers but positively associated with the frequency of activated $CD4^+$ and $CD8^+$ T cells. Based on these populations, patients are grouped into 5 clusters. Cluster 4 and 5 are characterized by a decreased frequency of $CD4^+$ T and memory B cells, and the highest proportion of activated $CD4^+$ and $CD8^+$ T cells. However, they differ with respect to pDC and plasmablast numbers, being the highest in cluster 4 and 5, respectively. These two clusters have the highest disease activity score. On the other hand, clusters 1 to 3 are all associated with low disease activity but correspond to different subsets of patients. Cluster 3 contain only anti-

SSA^+ patients and shows the highest IgG levels and PB numbers, whereas clusters 1 and 2 identify subsets of patients with less aggressive disease both at the cellular and biological levels. More interestingly, patients from clusters 4 and 5 have more severe infiltration in salivary glands compared to the patients form clusters 1-3. These results indicate that blood phenotyping allows for patient stratification into subsets with distinct disease activity and importantly also for differential immunologic activity within the target tissue.

Several disease-mixed subgroups were identified when two or more diseases were considered. Patients with RA and SLE could be classified into three clusters with specific gene expression signatures in the blood with an overlapping diagnosis composition[367]. Later it was shown that patients with early RA share a gene signature similar to SLE, suggesting common features during the development of the diseases[368]. Sixty two percent of genes differentially expressed between healthy controls and SSC patients are also differentially expressed in SLE patients. These genes are involved in IFN signaling and regulation, JAK-STAT signaling and PAMP recognition. What is more 91% of IFN-inducible genes were shared between SLE and a subset of SSC patients, suggesting a similar disease mechanism. The IFN signature was also found in SJS and in a subset of RA patients associated with disease activity[369]. This highlights the common molecular mechanism among the patients and shows that some individuals with different diagnosis could benefit from the same treatments, e.g. those targeting the IFN pathway. In a meta-analysis study almost 400 genes were shared across SADs (RA, SLE and SJS) and were differentially expressed between SADs and healthy controls. These genes involve cytokine-mediated and IFN-I signaling pathways, inflammatory responses, mitotic cell cycle and apoptosis[369]. In a recent study the use of multiple techniques such as multiplexed cytokine measurements, serological tests and immunophenotyping by FC allowed to detect a proinflammatory group of patients across SADs (SLE, SJS, SSC, RA)[370]. This group is defined by CXCL10, IL-2, IL-6 and TNFα expression, an abnormal B cell distribution, and a $CD8^+$ T cell signature, more severe clinical features and higher levels of autoantibodies. In another study T cells and B cells from SJS, SLE, and patients with secondary SJS associated with SLE had their PBMCs phenotyped using FC[371]. It was shown that all 3 groups of patients share similar immunological disturbances. However, using k-means-based clustering analysis the researchers identified 2 distinct groups of patients that were differentiated by specific T cell populations. It should be noted that in these two studies only T and B cell-specific features were considered, and thus it is possible that other cell-types could bring supplementary information and show other important endotypes. In another study using MC data generated

from SSC, SJS, and SLE blood samples, the authors aimed for patients' group assignment according to the diagnosis labels[171]. However due to some overlap in differential cell frequencies between patients and healthy controls, they did not achieve the goals, which also points toward common mechanisms, at least among some groups of patients. Unfortunately, authors did not use unsupervised analysis to obtain patient classification independently of the diagnosis. Although an extensive panel of antibodies was used, only few manually gated populations were studied and due to the lack of control for batch effects median signal intensities for several markers were not included in the panel, like CD80 or CD38 and, HLA-DR. The measurement was limited to PBMCs thus neutrophils, were again excluded from the analysis.

A study from our group recently proposed a molecular classification of SADs from data coming from the PRECISESADS cohort, involving an unprecedented number of individuals from 7 different SADs (SLE, SSC, RA, SJS, MCTD, PAPS, UCTD) and the data from blood trancriptome and methylome[351]. Four different clusters were defined: 3 pathological clusters named inflammatory, lymphoid and interferon, and one undefined cluster where most healthy controls and patients with lower disease activity score were assigned. Additionally, the inflammatory cluster was characterized by a high neutrophil proportion; the lymphoid cluster by enrichment in T, B, NK and NKT cells; NK enrichment was observed in the undefined cluster and no cellular enrichment was observed for the interferon cluster, mainly because all cells expressed IFN inducible genes. This suggests that cell frequency can also give valuable information about patient assignment to the groups and that neutrophils are also important for patient reclassification. Also, cells beside T cells and B cells should be included.

These results show that patient reclassification can be a valuable tool to find common molecular patterns to group patients and allows for the treatment assignment based on molecular disrupted pathways together with rather than, clinical observations. The above-mentioned studies were a first step towards personalized medicine in SADs. However, some limitations can be also assigned to them. First, quite a lot of studies use bulk cells to obtain cellular information, thus loosing single cell resolution. It is known that besides patient heterogeneity, cellular diversity can play important role in the disease pathophysiology. Small subsets of cells are thought to be important in the pathogenesis of SADs, and hence studying the disruption of immune tolerance and dysregulated pro-inflammatory response at a single cell level presents a great opportunity for rheumatology research[372]. High-throughput single-cell technologies are becoming common approaches in daily research. The impressive

progression in the number of different molecules that can be measured in a single cell changed the way experiments are done and analyzed. FC and MC are great examples of these changes. Starting from the first flow experiments that measured 2-4 markers which were manually gated, the multiplexing capabilities are currently increasing to 30[373] and more than 50[374] parameters in FC and MC, respectively.

The FC and MC studies presented above, although bringing valuable single cell information, also have some limitations. First they are done using a limited number of populations like PBMC, T or B cells, and thus ignore the information from granulocytes, that are known to be involved in SADs. Second, due to the experimental design, the comparison of median signal intensities (MSI) is not applicable because the batch effect introduced in every staining and acquisition is not controlled, and thus precious information about cell functional state is unexploitable. Third, most of them applied FC technology that usually requires the use of multiple antibody panels, therefore not all the marker combinations can be explored. In MC studies, although higher amounts of antibodies were included, not all of them were used when extracting the cell frequency information. In most of the above-mentioned studies manual gating was performed, hence cell diversity was limited to the knowledge of the analyst and high dimensional information was lost. Thus single-cell, high-dimensional and functional studies using flow and mass cytometry can give a new insight in the pathogenesis of SADs, allowing for biomarker discovery but also for patient stratification.

2 Mass cytometry and its application to large scale studies

2.1 Mass cytometry and its comparison to flow cytometry

The general concepts of both FC and MC technologies are similar; antibodies or probes labeled with fluorochromes (FC) or high atomic mass elements (MC) are used to target desired antigens or biomolecules, in order to characterize certain cell properties like cell phenotype, cell cycle[377] or response to stimulation agents via cytokine production, protein phosphorylation[375] or RNA expression[378], among others.

Following the staining, cells are introduced in single-cell suspensions via capillary tubes into the flow cytometer for FC or alternatively into a Cytometry by Time-Of-Flight (CyTOF, Helios) device for MC. The biological information with single cell resolution is obtained via photons or time-of-flight ion's mass-to-charge ratios for FC and MC, respectively, converted into digital values and stored using the same file format called flow cytometry standard (.FCS). Although both technologies are commonly used to measure cell properties, the definition of event is different. In FC every event that emits light and reaches the user-defined threshold will be stored in the FCS file. Both light scatter: forward-scatter (FSC), correlated with cell size and side-scatter (SSC), correlated with cell granularity, together with fluorescence are used to differentiate single cells from noise[379]. In MC the ion clouds that last for more than 10 and less than 150 pushes (spectrum scans) and exceeds the lower convolution threshold are recorded in the FCS file as an event. MC lacks the power of light scatter, and thus cell events are defined using the metals associated with them[380]. Nucleic acid intercalators like Iridium (Ir) or rhodium (Ro) are used to define nucleated cells. For non-nucleated cells antigen specific markers must be used. In FC the light can excite some cell components like flavins, folic acid, retinol, which emit the so called autofluorescence, especially in the green spectrum[381]. This autologous signal is not a problem in MC, since the high atomic mass metals detected are not frequently found within the cells. However, tissue metal contaminations due to medical procedures or environmental exposures were reported[382,383], and should also be considered when deciding which technology to be used, FC or MC.

In both techniques, signal spillover from one channel to another is observed. In FC it is caused by the overlapping emission spectrum of different fluorochromes. In MC it can be due to metal impurities from the metal tags; metal oxidation affecting mainly light lanthanides causes signal spillover to the heavier spectrum of masses; or metal over-abundance when high antibody concentration is used inappropriately and the signal of particular masses cannot be

resolved[384]. In FC the signal cross-talk can be severe and cannot be avoided in multicolor experiments. In MC, maximum spillover does not exceed a small percent and proper panel design can minimize these issues. Inadequate panel design or lack of proper compensation controls, especially in FC, can create false positive events[385]. Additionally, it can introduce spreading errors, an artifact produced by errors in photon counting[386], which can mask low or dim fluorescence positive cells. Spreading errors depend on laser configuration, dye brightness and quality of photomultiplier tubes (PMT). Thus, careful selection of probes and deep understanding of cytometer configuration and its performance are critical in FC[387,388]. For MC, it is also important to be familiar with the instrument performance, as variation in the sensitivity and resolution are observed between different CyTOF devices[389]. During the preparation of the Standard Operating Procedure (SOP) a pilot study including a few samples is strongly recommended, as it can help to fix the protocol limitations[390,391].

Due to higher number of markers that can be used, and lower contamination caused by signal spillover, MC seems to be a more attractive tool to perform high-content immunophenotyping in SADs patients. However, it should be noticed that proper experiment design and analysis pipeline need to be appropriately planned upfront in order to fully take advantage of high-dimensional data, especially when a large number of samples will be analyzed, as it is the case for this thesis.

The acquisition workflow for MC and the differences in the spectrum overlap between FC and MC can be seen in Figure 4 and the typical workflow for the preparation and analysis or muti-parametric FC and MC data is shown in Figure 5.

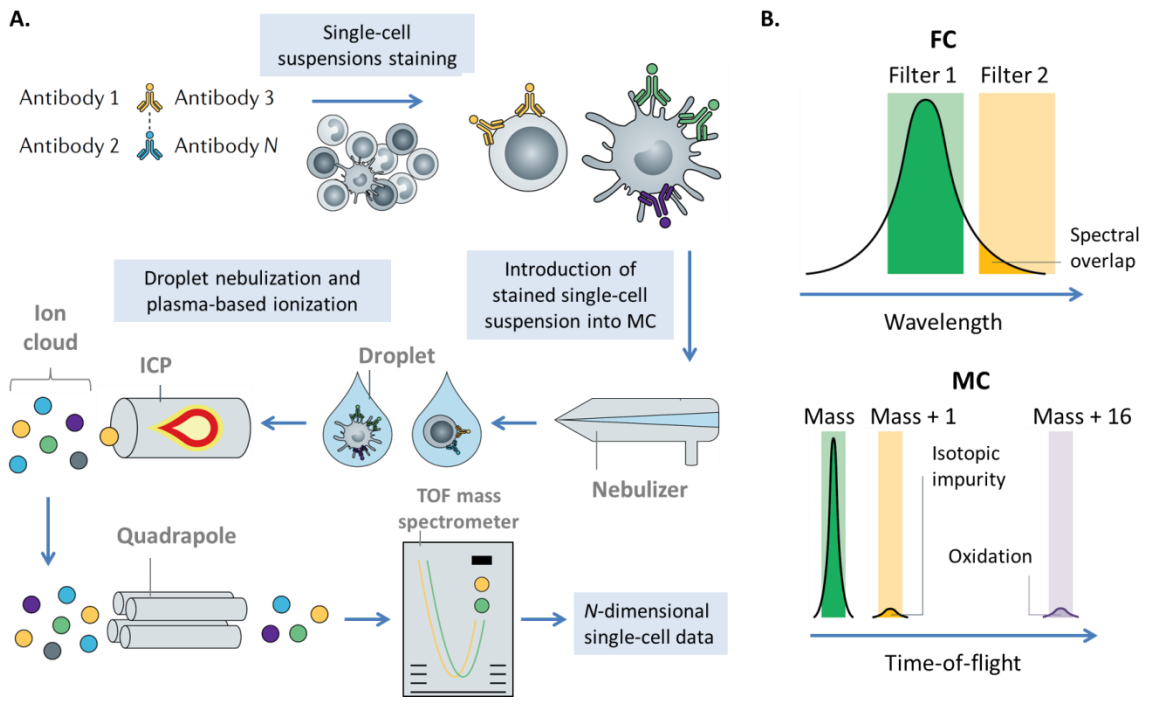

Figure 4 Acquisition workflow for mass cytometry and differences in non-specific signals in FC and MC.

A. A single-cell suspension is incubated with heavy metal-labelled antibodies or other probes of interest. The antibody incubation step can vary depending on the antigens of interest (surface, intracellular, DNA, etc). Next cells are washed and introduced into the CyTOF device. The suspension is nebulized into single cell droplets and introduced through an inductively coupled plasma (ICP). In ICP, droplets are broken down into clouds of elemental ions. Next, low atomic mass ions are removed in a quadrapole, a mass filter. The remaining high mass ions are quantified using an orthogonal time-of-flight (TOF) mass spectrometer. Ion counts are then integrated to quantify the amount of antibodies bound, which is proportional to the marker abundance. Data are further exported to an .fcs file for further analysis. B. In FC (top panel) the major source of non-specific signal is the spectral overlap, caused by broad emission spectra that can be detected in various detectors. In MC, (bottom panel) elemental isotopes conjugated to antibodies have non-overlapping narrow emission spectra and can be easily resolved by TOF. Minor source of overlap (usually <1%) are caused by isotopic impurities that can be detected in Mass+1 channel and oxidation in Mass+16. Adapted from Hartmann and Bendall, 2020[392].

2.2 Obtaining reproducible and high-quality data in MC studies

Preparation of a standard operating protocol (SOP) for sample collection and processing is highly recommended, as it significantly improves data reproducibility[393–395]. For MC, the selection of reagents and their storage is critical to avoid metal contamination events[382,396]. For both FC and MC, it is essential to consider if cells should be stained immediately upon collection or preserved until the recruitment is completed. If all the samples are obtained at once, they can be stained and acquired immediately. However, in large scale studies, or if the cytometer is far from the recruitment center (as it is the case for this thesis), the sample preservation before[397] or after staining[398] should be considered. The goal is to process, stain and acquire as many samples as possible with the same protocol, antibody cocktail, and

instrument settings. Each preservation protocol will affect the sample composition and antigen expression[397,399,400]; hence benefits and drawbacks should be considered in the light of the biological question raised, and should be carefully considered before performing the experiments.

Often, hundreds of samples are included in cytometry studies and are split into multiple experimental groups. This can introduce "batch effects" defined as non-biological differences between them[401]. To minimize this effect, a careful experimental design should ensure the even distribution of biological groups and confounding factors across batches[401]. The antibody labeling and sample staining should be consistent across all the groups, as discrepancies can introduce technical differences in MSI values that can be hard to distinguish from biologically meaningful information. This is why strict control of intra- and inter-group variations should be introduced in the experimental design. To limit intra-batch variation, barcoding (labeling of individual cell samples with unique combinatorial barcodes) and sample pooling before antibody staining is used in MC [402–404]. To minimize inter-batch variation, an aliquoted master-mix of the staining cocktail is recommended to be stored properly and used throughout the project. Both lyophilized and desiccated antibody cocktails were reported[390,399,405] and freezing of the MC cocktail aliquots was also shown to be successful[406]. Unfortunately, even well-prepared SOPs minimize, but do not resolve, the problems with day-to-day reproducibility. Thus, measures allowing estimation and correction of batch effects are needed. The practice of including a reference sample in each barcoded batch is becoming a standard in MC[407]. The reference sample is an aliquot of a bigger volume obtained from one donor at a particular time, aliquoted, and preserved. It carries the information of the technical variability introduced during sample preparation, staining and acquisition, and therefore allows to measure run-to-run variation[407].

In MC, the panel optimization is the most critical step. It requires proper assignment of dim and bright markers depending on the channel sensitivities and their performance in the context of staining index and spillover[373,389,408]. The success of automated methods to resolve cell populations depends more on well-selected markers than on the prevalence of the cells, and thus the probes should be selected carefully[409]. To identify the markers of interest, a recently published antibody staining database can be useful, as it contains staining patterns for 350 antibodies used in fresh and fixed peripheral blood mononuclear cells (PBMCs)[399]. Additionally, antibody titration, done at the same conditions as the final experiment, is essential to ensure proper signal intensity allowing population definition. It should be stressed

that if a population cannot be defined by manual inspection due to sub-optimal amounts of added antibodies, it will not be detected by most clustering algorithms.

Evaluation of antibody staining, titration, and signal spillover is an important but time-consuming process, especially in high dimensional approaches. Fortunately, a recent study showed that clustering algorithms like SPADE (Spanning Tree Progression with Density Normalized Tree)[410] can be used to evaluate the titration of a panel and track the spillover artifacts. Additionally, metrics like Average Overlap Frequency (AOF) can be applied to verify antibody performance by calculating staining distances between the positive and negative populations in bimodal markers, reducing substantially the time required for calculation and plotting of staining indices[411]. This shows that even at the moment of panel optimization, computational approaches can significantly accelerate benchwork and improve data quality. For more details about panel preparation and standardization, readers are directed to the following literature[412–415].

The capillary introduction system in MC suffers from cell clogging, altering the flow rate and signal quality over the time of acquisition. Sample clogs can be caused by specific biological materials starting from “easily” acquired cell lines or PBMC to whole blood or disaggregated tissues (the most prone to clogging). In both FC and MC, the disturbances in the acquisition rate affects signal quality. The higher the speed, the more coincidence events known as doublets are collected, and the more spread of the signal is seen[386]. The maximum recommended acquisition speed for MC is up to 1000 cell/s [416]. It should be noted that the maximum speed depends on the type or cells that are acquired and on the experimental target. If rare cells that constitute 0.01% frequency are of interest flow rate should be lower and well optimized[379].

All these issues need to be addressed when planning large-scale experiments, but also tools that allows data cleaning, quality check and normalization should be included in the post-acquisition analysis pipelines. These tools will be briefly described in the next section.

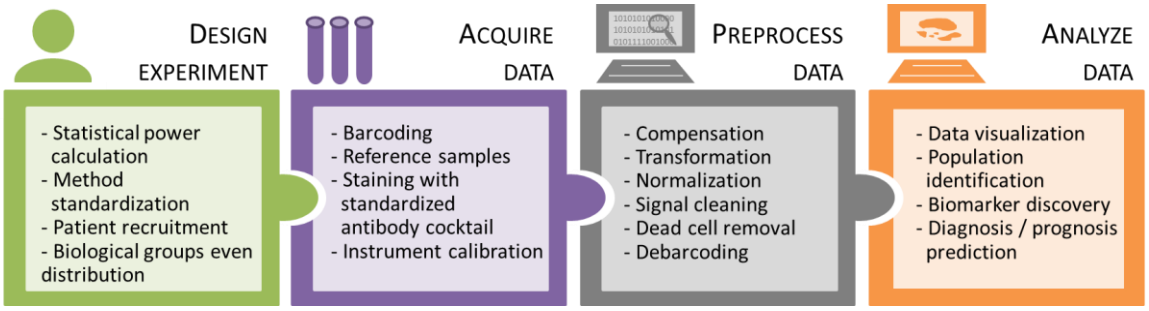

Figure 5 The flow and mass cytometry experimental and data analysis computational workflow.

Adapted from Rybakowska et al., 2020[417]

2.3 Data preprocessing and quality control of MC data

2.3.1 Data transformation

MC raw data are often characterized by skewed distribution with varying ranges of expression. In consequence it can be difficult to distinguish positive and negative populations[418]. As visualization and clustering performance depends on the scale and distribution, it is important to bring the expression peaks as close to a normal distribution as possible[419]. To do so, the expression values are usually transformed using an inverse hyperbolic sine (*arcsinh*) transformation with the cofactor equal to 5[420]. The *arcsinh* conversion behaves similarly to a log transformation at high values, but is approximately linear near zero, and a cofactor controls the width of the linear region. FC data can contain negative values due to the correction of background noise, autofluorescence, and compensation; conversely, MC data contains zero values when no ions are detected and few negative values are introduced due to background subtraction and randomization[420,421]. It should be noted that some of the visualization and clustering tools require transformation to be done upfront, while others perform it as a default. It is important to always check the transformation requirements, as this might affect the downstream analysis.

2.3.2 Signal quality check and cleaning

As mentioned above, the capillary tubes used for sample introduction in MC can clog, resulting in sudden changes in the signal of the detector. Other issues such as unstable flow rate can cause signal shifts and change the mean intensity[422]. These signal disturbances affecting downstream analysis should be identified and removed from the data. Currently, three algorithms can be used to do this: flowAI,[423] that uses change point analysis and allows

automatic or interactive analysis; flowCut[424], that creates summed density measures using mean, median, percentiles, variation, skewness, and removes events based on density curve analysis; and flowClean[425], that tracks the changes in the frequency of artificially created populations, taking advantage of change-point analysis, flagging outliers with unusual ratios of cell populations. The first two methods are fully automated, while flowClean represents a semi-automated approach. In all methods, the signal check is performed for every channel along the time of acquisition. The data are divided into equally sized bins of cell events. For each bin, the models corresponding to each method are calculated and every bin that differs from the rest is flagged in flowClean or alternatively flagged and removed in flowAI and flowCut. Additionally flowAI can remove outliers from the flow rate and dynamic range[423].

Due to their different implementations, the level of stringency differs across methods. Thus the optimal performance will depend on the data and on the parameter settings[422]. It should be noted that all of the methods mentioned above were designed for FC studies and to our knowledge have not been applied to MC data. Due to the differences in the FC and MC data, such as different time resolution (events in FC are acquired faster and at higher concentrations than in MC), negative values in FC versus "zero" values in MC, parameter settings can be different, but up to now no data exists to support this statement. This is an unexplored niche open for further studies.

2.3.3 Data debarcoding and dead cells/debris removal

In order to obtain de-barcoded data, deconvolution of the raw events needs to be performed. The most common way to debarcode MC data is to use a single-cell deconvolution algorithm[426] through user-friendly debarcoding programs or R-based functions that can be used.

Doublets, debris, and dead cells introduce noise into the data, and hence should be removed prior to data analysis as these might affect clustering results. As mentioned before, the definition of event is quite different for FC and MC and hence the gating strategy will differ. For MC, as data are usually acquired with calibration beads[427], they need to be identified using bead-specific channels and removed manually, or automatically using the CATALYST package[428]. The nucleated, intact cells are defined by a balanced intensity for Ir channels, which distinguish them from Ir^{low} debris and Ir^{hi} doublets. In the case of red blood cells, or other non-nucleated particles, this needs to be defined, and the use of specific probes is required. Doublets are a real challenge in MC as FCS and SSC parameters cannot be used. Instead, users should define them based on balanced Ir staining and event length[429] or

Gaussian parameters, such as residual, offset, center, and width[430,431]. It is worth noting that barcoding staining with 3 different isotopes per sample helps to identify and remove doublets[426], thus increasing sample quality.

Among other platforms FlowJo and Cytobank can be used for manual gating, or alternatively data can be imported in an R environment using e.g. flowWorkspace package[432]. If gating is provided for some of the files, semi-supervised gating methods like flowLearn could be used to reproduce the gating strategy for the remaining data[433]. This algorithm employs the gating thresholds provided as an input and transfers them to the rest of the samples using derivative-based density alignments. Packages like flowStats[434], flowDensity[435] or OpenCyto (a framework for constructing automated gating hierarchy) can be useful to build user-defined gating strategies. Although manual inspection is always advised, the automated approach should be considered for projects generating a high number of files.

2.3.4 Staining irregularities, data normalization and removal of batch effects

Inspection of marker expression levels across all batches is an important step of sample quality control. Staining irregularities, such as loss of separation between positive and negative values for a given marker, or significant changes in the signal intensity, must be identified and removed, as they can affect event classification into specific clusters[411]. Recently the AOF algorithm, using cell frequencies to calculate the average of overlapping cells per channel, was applied to more than 2000 files in MC[399]. Based on calculated sample scores and user-defined thresholds, AOF identified problematic marker expression and affected files were discarded prior to analysis. This algorithm might be a good expansion of the quality control pipeline. However, it should be used with caution, since the signal changes could also be due to biological or technical variation. The use of barcoding and reference samples can help to distinguish between these two possibilities, and the introduction of normalization and batch effect correction can help in saving files instead of discarding them. The technical variability can come from day-to-day differences in experimental and instrumental performances. Instrument variation that cannot be controlled by the users (e.g. differences in daily instrument calibration) are identified and corrected by normalization. The variations in the experimental procedure (e.g. slight differences in staining) are identified and removed via a batch effect correction[436]. Both will be discussed below.

The acquisition rate in MC is low, thus sample acquisition time is long. Additionally, a signal drop caused by progressive CyTOF decalibration is frequently observed, especially when big,

barcoded samples are run. Therefore, MC requires special approaches for normalizing the data. In order to correct for it, a bead-based normalization was introduced by Finck et al.,[427] and modified by Fluidigm. The algorithm uses commercially available calibration beads, spiked and acquired together with the sample. Hence, changes in the signal can be tracked through the acquisition time. Next, the beads are identified and the median intensities of the beads are calculated in defined time intervals across all files. Based on the obtained values, the global mean for each bead is calculated and used as a target value. To obtain the transformation factor, a linear model using the global means and interval-specific intensities is calculated. This factor is then applied to all events and interpolated to all markers in the corresponding intervals and files. Although run-to-run machine variation can be corrected, the technical differences introduced upon sample preparation will remain. Therefore, the normalization and batch effect correction play an important role in downstream analysis.

FdaNorm and gaussNorm algorithms were developed to correct the files across the experiments[437]. They both perform density-based normalization per channel using ungated .FCS files. The algorithms assume that each marker has its characteristic number of density peaks called landmarks, which are shared by all samples and can be identified even with some changes in MSI values. During normalization these density peaks are shifted to align the samples. Although algorithms differ in their implementation, they perform similarly in the context of resolution in binary markers like CD3, CD4 or CD8. When using gaussNorm, the number of density peaks needs to be known upfront for each marker, while fdaNorm estimates peaks automatically. Some remarks and an extended version of the fdaNorm algorithm can be found in[438]. In this version the reference file provides information about marker distributions together with gating template, and additional normalization is performed during the gating. The reason for these changes is that the marker densities can differ in distinct populations affecting the normalization process, and the use of a reference sample with gating upon normalization improves the automation process. These methods perform well for automated gating, as the density peak alignment facilitates implementation of reproducible gating hierarchy. However, it requires previous knowledge of the analyzed cells. This can be useful in clinical studies when quantification of known populations in a relatively short time is needed, or for the extraction of cell frequencies identified using binary markers. However, as the intensity of the peaks are shifted, comparison of the MSI cannot be performed, and part of the biological information is lost.

As mentioned before the inclusion of reference samples becomes a useful tool to track batch effects introduced during sample preparation. Recently three methods taking advantage of the introduction of a reference sample became available to researchers, and will be discussed. Shaham et al.,[439] introduced a deep learning approach called BatchEffectRemoval. This approach is based on Maximum Mean Discrepancy (MMD) and Residual Nets, and corrects the distribution of one sample to its corresponding pair, collected at a different time point. Although it can be a good solution when time point experiments are performed, its performance in MSI-sensitive markers is still questionable. CytoNorm[440] and CytofBatchAdjust[441] are two alternatives that use reference samples aliquoted across the batches to obtain batch-specific transformation factors. CytoNorm starts with FlowSOM clustering for each reference file[442]. At the cluster level, quantiles for each marker are computed and the mean quantile distribution is calculated using values from all the reference files. This information is used to calculate the appropriate transformations for each batch and to correct for it. One of the CytoNorm assumptions is that the batch effects are small enough to not impact on the FlowSOM clustering results. In other words, although samples differ at the cluster level, the metaclustering that defines cell populations should be the same across all reference samples. If not, some artifacts can be introduced to the data [441], and therefore a careful and detailed clustering exploration should be performed before normalizing collected batches. On the other hand, CytofBatchAdjust performs the normalization on ungated files, where batches can be scaled to a user-defined percentile, mean, medium or quantile normalization.

Both algorithms have the advantage of preserving the biological information contained in MSI. However, it is important to ensure that the reference sample is prepared using the same protocol as for the studied samples. Therefore, upfront assumption of sample composition needs to be taken into consideration.

2.4 Data analysis and feature extraction

Manual gating not only aims at extracting the important features, but also gives a good insight into data quality, variability, structure or differences between groups of individuals. However manual cell inspection is time-consuming and also limited by a bias towards the previous knowledge of the analyst about the composition of the sample[443]. In high-dimensional data like in MC, the cell abundances and their median marker expressions are typically extracted using clustering or dimensionality reduction. Then the statistical tests are run to associate cell

differential abundance (DA) and differential states (DS) with specific phenotypes and look for biomarkers or perform patient stratification. Both, the currently used dimensional reduction and clustering algorithms will be briefly discussed below.

2.4.1 Dimensional reduction

The goal of the dimensionality reduction methods is to preserve the structure of high-dimensional data in a lower2- or 3-dimensional map, easier to interpret. These methods can be divided into linear and non-linear tools. Linear methods represented by PCA (Principal Component Analysis)[444,445] focus on keeping the maximum variance of the points in the lower space, thus keeping the dissimilar points far from each other[446]. On the other hand the non-linear algorithms like e.g. t-SNE (t-stochastic neighbor embedding)[446] and its derivatives[447–449] keep the similar cells close to each other, therefore focusing on local relationship preservation[446]. Some of the tools like t-SNE and UMAP (Uniform Manifold Approximation and Projection)[450] separate well known populations, giving a nice overview of existing cells. Other methods like ISOMAP (isometric feature mapping)[451,452] or Diffusion Maps[453] visualize differentiation trajectories, as they are able to preserve both local and global distances between cells.

PCA is designed to preserve the features with the highest variability in the principal components (PC). It assumes that the most prominent variation will be explained by the first two to three PCs, making them easily interpretable. As shown by[454,455], due to the linear assumption, PCA cannot separate well populations in the first two PCs, as immune panels are usually designed in the way that each marker brings new and independent information. Nevertheless, PCA as an easily scalable and not-stochastic technique, remains a powerful tool and is widely used in biological and clinical cytometry studies, as shown in[456–458] .

t-SNE is a state-of-the-art visualization method that projects high-dimensional information into easily interpretable 2D maps[446]. t-SNE calculates two similarity matrices based on the distance in the high- and low-dimensional space using pairwise comparison across all the points. Next, in a iterative way the algorithm minimizes the differences between two matrices, which results in the optimized position of each cell in the 2D space[419]. t-SNE pairwise comparison has its pros and cons, on one hand it is a robust and accurate algorithm, and on the other, the more cells are analyzed, the more pairs need to be computed and the increasing computational cost. This limits the use of t-SNE in FC/MC studies where thousands or even millions of events are acquired. To overcome this issue random downsampling (generation of a smaller subset of

cells), is often used, taking the risk of losing rare populations. Therefore, new implementations were developed, aiming at limiting the computational power required to obtain high-resolution data. Among them Barnes-Hut (BH-SNE)[459] reduces the number of pair comparisons by constructing a tree-like structure. This implementation is used in viSNE and published by Amir et al.[454]. HSNE (Hierarchical Stochastic Neighbor Embedding)[447] is a combination of A-tSNE (t-SNE approximation) where, instead of computing precise distances, an approximated k-nearest neighborhood graph is computed and embedded using BH-SNE. Fit-SNE (Fast Interpolation-based t-SNE)[448] uses Fourier interpolation to speed up the convolution step and opt-SNE [449] allows fine-tuning of t-SNE parameters, like the number of iterations, to obtain high resolution maps in a shorter time. It should be noted that t-SNE is stochastic, which means that every new run will give slightly different visualization. Consequently, researchers should perform multiple runs in order to obtain good data representation. Comparison of multiple maps can be only done if the samples were run simultaneously applying the same settings. Jensen-Shannon divergence, a statistical method that measures two probability distributions, can be useful to compare the projection from the same data set as shown before[454,460].

Recently a new visualization tool called UMAP (Uniform Manifold Approximation and Projection) gained attention in the cytometry field. This tool also preserves global distances between cell types, while t-SNE conserves only close neighborhoods[450,461]. For this reason UMAP can recapitulate human hematopoiesis, and is useful for cell continuity visualization[461]. Additionally both UMAP and Fit-SNE can analyze more cells than t-SNE in a shorter time[461]. ISOMAP (isometric mapping)[451] and Diffusion maps[453] also preserve global relatedness and continuity between cells instead of calculating the pairwise Euclidian distance. ISOMAP uses non-linear geodesic distances[462]. Diffusion map introduced by[453], and adapted to single cell studies by[463], constructs diffusion matrices based on random walk probabilities between cells and generate diffusion components DC (known as eigenvectors), that similarly to the PC correspond to the largest coefficients of the data[464,465].

Even though some improvements were made on t-SNE implementation and faster algorithms like UMAP were built, the scalability problem remains. Most of the embedding techniques were first used on transcriptomic data where, in contrast to cytometry, a relatively small number of cells are described by a much larger amount of markers. Although other dimensionality reduction and topology inference algorithms can be used, the lack of good

implementations that enable handling of millions of cells prevents researchers to apply them to big files[466].

Although non-linear dimensionality reduction methods are powerful in projecting phenotypically similar cells, the understanding of the marker contribution to cell segregation can be difficult, as it requires plotting multiple markers in individual maps. In such case, studying marker co-expression is even more challenging as was pointed out[233,458]. One-SENSE (one-dimensional soli-expression by non-linear stochastic embedding) answers to this limitation and proposes 2D assignment of the markers to categories that can be then visualized using a combination of t-SNE map and heatmaps[233]. This method was successfully applied to study T cell and dendritic cell heterogeneity[233,467].

2.4.2 Clustering

Clustering-based algorithms group similar cells and use visualization tools to represent them in a lower dimensional space[443]. When choosing the best clustering method several requirements should be considered, such as the need for downsampling, reproducibility, rare cell detection, and running time. These variables were measured by Weber et al., where several of the currently used cytometry clustering algorithms were compared, identifying FlowSOM as a good trade-off between quality and time[468].

Since its publication, FlowSOM[442] became a widely used clustering algorithm in the field of cytometry[418,469,470]. This algorithm uses a two-step clustering process: a self-organizing map (SOM), and consensus hierarchical clustering. SOM, a type of artificial neural network, contains a grid of nodes where each node represents a point in a multidimensional space. SOM reproduces the data topology by assigning the most similar cells to the same node or its closest neighbors. Increasing the grid size increases the possibility of finding rare populations. However, as shown by Weber et al., the reproducibility of the data can be compromised and artificial splitting of the largest populations can be seen. In the second step, node centers are grouped into metaclusters using a consensus hierarchical clustering, and final cluster labels are obtained. The data can be visualized using a minimal spanning tree, like in SPADE[410], or in a heatmap[418]. Although similar results can be obtained with SPADE and FlowSOM, the two-step clustering in FlowSOM accelerates analysis and evades downsampling, making it a better choice. Unfortunately, the stochasticity problem remains, and unless the seed (starting analysis point) is pre-defined, the comparison between different runs cannot be done. When comparing clustering performance, the F1 score measure tests accuracy using precision, and

recall could be applied[468]. Alternatively the algorithm CytoCompare, which computes the distance between the clusters using marker distribution [471], or the Jaccard coefficient [472] can also be applied.

Multiple tools and workflows implementing FlowSOM have been recently published: EmbedSOM improves data visualization[473]; diffcyt, a new computational framework for differential discovery analyses[420]; Ek'Balam, a hierarchy-based clustering in the Astrolab Cytometry Platform[399]. All these applications emphasize the broad utility of FlowSOM. However as noticed in[474], one of the major drawbacks of this algorithm is the user-defined number of clusters, which limits the capture of population diversity and introduces researcher supervision. Other popular clustering approaches could be used instead, like Phenograph, which uses k-nearest-neighborhoods (KNN) to represent phenotypically similar cells as highly interconnected nodes[475] or X-shift, that also applies KNN with density estimation[476]. Both tools ranked high in benchmark studies, especially for rare population detection[468,477]. They have the ability to predict the number of clusters in a given sample, although they perform poorly in scalability requiring downsampling. Additionally, the fusion of both dimensionality reduction methods using t-SNE and density based clustering was also reported and successfully applied in the immune diversity study of lymphoid compartment using ACCENSE[478], and of the myeloid compartment using DensVM (Density-based clustering aided by Support Vector Machine), which combines density based algorithm with machine learning techniques[452].

2.5 MC in the context of SADs

MC is a powerful high-dimensional technology in single-cell biology. It is becoming an important tool in biomarker discovery research, disease monitoring, and medical diagnostics. As shown in the chapter 1.4. MC can be useful to discover biomarkers, learn about SADs molecular mechanism or event cluster the patients into different groups based on cell frequency or their response to the stimulation. The rapid increase in dimensionality gives an opportunity to understand cell diversity in detail, narrow the research to fine cell populations, and by doing so, enable precision in the development of new therapies and biomarkers. Thus, it is a perfect tool to perform SADs stratification.

However, dimensionality reduction and automated analysis require high-quality data, analytical skills, and powerful algorithms to meaningfully process the multidimensional space. As previously discussed, the design and execution of a good cytometry-based study is not a trivial process. Small details like changes in stocks, pipetting errors, shifts in machine

performance, and improper data preprocessing can significantly contribute to data variation. Controlling for batch effects, although well adopted in transcriptomic data, is still inefficient and not often applied in MC and FC due to different data structures. It should be noted that inclusion of covariates like “batch effect” in the statistical model does not eliminate the bias introduced upon the clustering, and therefore batch effects should be corrected before data analysis, and ideally prevented when preparing the SOP. Many dimensionality reduction and clustering methods are available and they should be combined to verify and confirm results. Hence, high-dimensional analysis can be available to both biologist and bioinformaticians. Since the single-cell high-dimensional era is just starting, it is important to take care when interpreting the data. Careful validation with multiple methods and standard approaches like traditional manual gating should be implemented in the analysis pipelines.

Article: Rybakowska P, Alarcón-Riquelme ME, Marañón C. Key steps and methods in the experimental design and data analysis of highly multi-parametric flow and mass cytometry. Comput Struct Biotechnol J. 2020 Mar 31;18:874-886.

Hypothesis, goals and rationale

Hypothesis, goals and rationale

3 Hypothesis

In the context of the internal heterogeneity and the overlapping mechanisms of the different SADs, together with the difficulties in individual diagnoses, new methods based on the evidence and allowing patient reclassification and stratification need to be established. Precise knowledge on altered immune pathways will allow to reclassify the patients, grouping them into immunologically similar groups that could benefit from the same line of treatment.

Mass cytometry is a systematic, multidimensional approach that allows to study pathological immune responses in patients with SADs. Potentially it can serve as a new diagnostic tool for precise and targeted diagnosis.

4 Goals

The main objective of this study is to develop a basic method in the area of multidimensional cytometry for the stratification and reclassification of patients with SADs. This main objective can be divided into three specific goals:

1. Establish the method for whole blood preservation that allows to perform large-scale, multi-center and retrospective deep immunophenotyping and functional studies.

2. Establish a staining protocol and analysis workflow that allows to minimize the technical variability, perform quality control of the collected data and track and correct for batch effects in large-scale studies.

3. Conduct a deep phenotyping study to compare the SADs patients and perform reclassification using a selected set of cell lineage and functional markers.

5 Rationale

Stabilization of human whole blood samples for multi-center and retrospective immunophenotyping studies

The immune system is crucial for the protection against pathogens and tumors, and is involved in the appearance of autoimmune, inflammatory and allergic diseases. Its monitoring allows to track responses to environmental changes, therapies or disease outcomes. The major components of the immune system commonly measured are leukocyte subsets, but also their cytokine expression and other cell-to-cell communication mediators[472]. These components can be found in blood, the most accessible fluid to researchers and clinicians, and can be measured by the currently available technologies like flow cytometry (FC) and mass cytometry (MC). The outcome can serve as an indicator of the effectiveness of treatments[473], disease progression[453,474], or disease assignment in reclassification studies[164].

In large-scale studies, samples are difficult to obtain and stain in a single day. Frequently, they need to be transported from the collection site to the cytometry site, limiting recruitment centers to those that can guarantee shipping of the blood sample within 24h[384]. Additionally, this short timeframe prevents banking of precious biological samples and their use retrospectively.

To address this issue, it is at times customary to freeze samples until the time of cytometry acquisition. The most common protocols involve whole blood collection followed by peripheral blood mononuclear cell (PBMC) isolation and cell preservation in freezing media containing DMSO[392,475–477]. If responses to stimuli are studied, commonly cells are stimulated after thawing[392,478]. However, as noticed[479] PBMC manipulation and freezing requires experience, larger volumes of biological material, and the use of artificial culture mediums, increasing variation[388]. Additionally, PBMC are not a good representation of blood composition[480]. They are depleted of cells like granulocytes important in anti-microbial, autoimmune and allergic responses [481–486]. Furthermore, the PBMC compartment composition and cellular responses can be affected by the process of PBMC isolation[487,488].

To overcome these limitations several methods were developed for fixing blood cells upon drawing or post-stimulation[453,474,489–491]. These methods require the use of stabilizing solutions containing preservatives such as formaldehyde or methanol. Therefore, detection of fixation-sensitive markers like the chemokine receptors can be seriously affected[394], or changes in

intensity can occur[393]. Nevertheless, main leukocyte subsets can be successfully detected and quantified with adequate selection of probes titrated according to the condition[474,489].

Since previous reports described a limited number of markers for FC and a short time frame in MC, there is a need for a systematic study approaching a broad panel of intracellular and cell surface markers in an easy-to-use protocol facilitating the long term preservation and analysis of whole blood samples. Therefore the goal was to evaluate long-term cell and marker preservation using two whole blood preservation protocols that were previously used to freeze the whole blood[474,489], Phosphoflow Fix and Lyse (BD Biosciences) and Proteomic Stabilizer (Smart Tube). Additionally to MC, data for FC and imaging flow cytometry were also generated.

This part of the results comes from manuscript published in Cytometry Part A and the agreement with the publisher (John Wiley and Sons) was made in order to use the data presented in this article. License number: 5050370654144.

Article: Rybakowska P, Burbano C, Van Gassen S, Varela N, Aguilar-Quesada R, Saeys Y, Alarcón-Riquelme ME, Marañón C. Stabilization of Human Whole Blood Samples for Multicenter and Retrospective Immunophenotyping Studies. Cytometry A. 2021 May;99(5):524-537.

Data processing workflow for large-scale immune monitoring studies by mass cytometry

As mentioned before the CyTOF success is due mainly to its multiparametric capacity, the ease of panel design owing to minimal spill-over issues and the facility to stain multiple samples in one single tube using barcoding approaches[419].

On the other hand, the maximal acquisition capacity of CyTOF devices is limited to 1000 cells/s[410], while a rate of 400 cells/s is recommended to avoid cell aggregation and doublet formation[492,493]. Because of this, it becomes problematic to acquire multiple samples per day, particularly if several tubes of complex tissues like blood or liquid biopsies are acquired to detect rare cell populations. A solution to this is to split the samples in multiple batches and acquire them on different days. Nevertheless, this approach requires an optimized experimental workflow that limits technical variation, including a single antibody cocktail and the inclusion of a reference sample in every batch. In addition, the analysis pipeline should contain tools for normalizing the data and removing experimental and day-to-day detector variation[494].

Although the samples are fixed after staining, they are usually acquired in water in the case of the narrow bore sample injector (NB). Thus, due to the prolonged water exposure and long acquisition times, samples are degraded and lose their tags. To limit the exposure time, samples can be split and acquired in multiple aliquots[495] (as also presented in this manuscript), but still some differences in signal intensity can occur due to variation in detector yield. Furthermore, clogging in the capillary introduction system in cytometry devices alters the flowrate and signal quality over time[416]. . In order to obtain high quality data, fcs files should be screened and cleaned from any abnormalities. Hence, extensive data preprocessing should be included in the analysis pipeline.

Due to the *pros* and *cons* described above, mass cytometry experiments require a special and careful experimental design and an extensive analysis pipeline that allows automatic preprocessing of the data and perform proper quality control, especially when hundreds of files need to be analyzed. Although much effort was put to develop automated gating strategies including clustering and dimensional reduction algorithms[404,442,443,447,468,496] or quantitative analysis[497,498], less was developed in the field of data cleaning and preparation.

Therefore, the goal was to build experimental, preprocessing and quality control workflow that addresses above mentioned issues.

Here we present a semi-automated, R-based, CyTOF analysis pipeline that performs data preprocessing and quality control. It spots and removes potential artifacts introduced during sample preparation and acquisition, like clogs, changes in signal intensities upon acquisition and batch effects, thus improving data quality. This analysis pipeline gathers known tools used in both flow cytometry (FC) and MC and adapts them to large and multibatch MC studies, providing also solutions for data visualization. For data preprocessing, steps like bead-based normalization, debarcoding, file aggregation, and automated gating using Gaussian parameters, DNA and live/dead staining for intact and live cell selection are included. Furthermore, we implement additional quality control steps to remove bad quality events or to identify and correct batch effects using a reference sample. We provide full access to the data set used in this work, so the users can reproduce the data processing and analysis steps. Good data quality starts with a proper sample processing minimizing experimental bias and eliminating bad quality events. Therefore, we also provide the protocol of the experimental setting used to generate the data analyzed in this work and show some important tips and how to scale it up.

This workflow contains all the necessary steps to obtain high quality events in an semi-automated way. Importantly to note, it requires knowledge of basic R language programming. It is especially suited for researchers performing multicenter or retrospective studies involving collection of hundreds of biological samples, but is equally suitable for small-scale studies.

This part of the results comes from manuscript published in Computational and Structural Biotechnology Journal as an open access with author's copyright retained.

Article: Rybakowska P, Van Gassen S, Quintelier K, Saeys Y, Alarcón-Riquelme ME, Marañón C. Data processing workflow for large-scale immune monitoring studies by mass cytometry. Comput Struct Biotechnol J. 2021 May 21;19:3160-3175.

Biomarker discovery and stratification of patients with SADs using mass cytometry

SADs are autoimmune diseases diagnosed based on different clinical and laboratory criteria[345]. Due to their high heterogeneity within each clinical entity and overlapping symptoms, SADs are difficult to diagnose. That is why the time from disease onset to the diagnosis can take many years[499] which leads to poorer prognosis. A fraction of the patients can be classified as MCTD which is still a controversial disease entity[500,501] or even as UCTD, a group that holds patients without a clear clinical picture[499].

The high internal heterogeneity of these diseases and overlaps between them can also be observed at the genetic and molecular levels. The presence of anti-SSA and SSB antibodies was found in SLE and SJS and their genetic association with HLA class II gene DRB1*0301 was reported[502]. Many SADs patients present an IFN-I signature, but patients with low and high level of ISG were reported in SLE, a model for IFN-mediated disease. The cell frequency of a given population can be decreased or increased in different cohorts of the same disease, which can be due to different experimental settings, but also due to different endotypes, emphasizing patients' heterogeneity. When comparing immune cell composition between diseases not many differentially expressed features could be found[365,503], suggesting shared immune cell landscapes between patients with different diseases. Although in these studies only few groups of patients have been compared. Additionally, the current treatments although effective, show high variability in the responses observed and groups of non-

responders are still an issue, suggesting improper molecular fit between the tested drugs and the actual pathogenesis.

In response to these problems molecular-based studies were undertaken to classify the patients based on the biological mechanisms undergoing in their tissues. A recent large-scale study included all 7 SADs discussed in this thesis showed that distinct blood immune signatures across SADs are important for patient reclassification and suggested that the newly identified groups of patients could benefit from a common line of treatment, regardless of their clinical diagnosis[345].

The immune cell landscape using FC or MC was studied within selected SADs[7] and across different diseases[364,365,503]. Biomarkers associated with disease activity or tissue infiltration were identified using these techniques[184,504]. Until now 2 (SJS, SLE)[365] and 3 diseases (SSC, SLE, SJS)[503] were compared together in one study cohort, showing similar molecular mechanism between them, however no further reclassification attempts were undertaken. Additionally, in both experimental groups only PBMCs were considered and no functional markers were measured. In the study of Simon et al., few diseases were compared, but only at the level of B cells and T cells, limiting again the scope of the findings[364].

Keeping in mind the importance of immune cell signatures in previous biomarker discovery or reclassification studies our third goal is to apply MC to perform whole blood deep-phenotyping measuring both cell frequency and the level of functional markers. The goal is to compare patients from multiple SADs, but also reclassify them based on their immunological landscape. We believe that a deeper look into immune composition and immune responses of different SADs can give a better understanding of ongoing mechanisms in each patient and get us closer to the precision medicine in rheumatic diseases.

Materials and methods, results and discussion

Material and methods, results and discussion

6 Stabilization of human whole blood samples for multi-center and retrospective immunophenotyping studies

6.1 Material and methods

6.1.1 Study participants

Whole blood from healthy donors participating in the PRECISESADS study[164] was collected in EDTA vacutainer tubes (BD, Franklin Lakes NJ) and processed within 3 hours after bleeding. All donors signed an informed consent according to the ethical protocol of the Andalusian Biobank and the PRECISESADS project. Samples were recruited at the Andalusian Health System Biobank in Granada node. The protocol of the project was approved by the Ethical Committee of the Hospital "Virgen de la Macarena" according to the Helsinki declaration of 1975, as revised in 2013.

6.1.2 Whole blood processing for FC

Figure 6A shows the sample processing workflow.

Blood samples for FC were split in aliquots. One aliquot of 50 µl (named FRESH condition) was immediately stained using the lyse-wash PRECISESADS protocol as in[384] and acquired within the same day. Aliquots of 450 µl were fixed using Phosphoflow Fix and Lyse buffer (BD Biosciences, referred as BD) or Proteomic Stabilizer buffer (Smart Tube Inc. referred as PROT). For BD, 20 volumes of BD buffer were mixed with blood and incubated for 10 minutes at 37°C. Next cells were pelleted, washed with CST (Cell Staining Buffer, Fluidigm) and the pellets were frozen at -80°C for 1 to 6 months (FROZEN) or stained immediately (FIXED). The pellet was thawed at 37°C (if required), resuspended in 1ml of CST, filtered through 100 µm MACS SmartStrainers (Miltenyi Biotec), pelleted and resuspended in 225 µl of CST. For PROT, 1.4 volume of PROT buffer was mixed with blood and incubated for 10 minutes at RT. Next, blood was directly frozen at -80°C or processed without fixation. After thawing at 4°C on a roller (if required), the sample was diluted 1:1 with Thaw-Lyse buffer (Smart Tube Inc.), filtered and lysed with additional 10 volumes of Thaw-lyse buffer 1X for 10 minutes at RT. Next, cells were pelleted and leukocytes were washed with CST and resuspended in 225 µl of CST. For both buffers an equivalent volume to the FRESH samples was stained. In all 3 protocols cells were incubated with antibodies for 20 minutes at RT using Panel 1 Duraclone tubes (Beckman Coulter, see Table 1) and were acquired on a FACSVerse cytometer (BD Biosciences) previously calibrated

with Rainbow 8-peak beads, as described[384]. Around 50,000 leukocytes per sample were acquired. The results were analyzed using FlowJo 10.0.7 following the gating strategy shown in Figure 7.

Samples for image cytometry were processed as before but were stained with single-color Duraclone tubes for 1 hour at 4°C and 20 μM Hoechst33342 (Merck Life Sciences) for 3 minutes at RT. After washing cells were resuspended in 2% formaldehyde. At least 10,000 nucleated cells were acquired on an ImageStream Mark II imaging flow cytometer (Amnis) using a 60x magnification and low speed. Data analysis was carried out using IDEAS6.2 software (Amnis).

Flow cytometry data were deposited in flowrepository.org[505] using the accession number FR-FCM-Z2NK.

Table 1. Antibody panel used for FC

Antigen	Clone	Fluorochrome	Source	Staining
CD16	3G8	FITC	Beckman Coulter	Surface
CD15	80H5	PE	Beckman Coulter	Surface
CD56	N901	PC5.5	Beckman Coulter	Surface
CD14	RMO52	PC7	Beckman Coulter	Surface
CD19	J4.119	APC	Beckman Coulter	Surface
CD3	UCHT1	APC-AF750	Beckman Coulter	Surface
CD4	13B8.2	PB	Beckman Coulter	Surface
CD8	B9.11	KO	Beckman Coulter	Surface

FITC, fluorescein isothiocyanate; PE, phycoerythrin; PC5.5, Phycoerythrin–Cyanin 5.5;
PC7, Phycoerythrin–Cyanin 7; APC, Allophycocyanin; APC-AF750, Allophycocyanin-Alexa Fluor 750; PB, Pacific Blue; KO, Krome Orange.

6.1.3 Whole blood processing for MC

Figure 6B shows the MC sample processing workflow.

500 μl blood aliquots were incubated for 6h at 37°C at 7% CO_2 with 500 μl of the TLR7/8 ligand resiquimod (R848, Invivogen), 2.5 μg/ml in RPMI (Gibco), in the presence of Protein Transport Inhibitor Cocktail 1X (Thermo Fisher Scientific). The samples were stained immediately (FRESH), or fixed using BD or PROT protocols.

FRESH samples were lysed using BulkLysis buffer (Cytognos), dead cells were stained with 5 μM of cis-diamineplatinum(II) dichloride (Pt, Sigma) for 5 minutes at RT and quenched with CST buffer. Surface staining was performed for 30 minutes at 4°C using an antibody cocktail

diluted in CST followed by fixation step, 30 min RT in Maxpar Fix I buffer (Fluidigm). Next, intracellular cytokine staining for 30 minutes at 4°C in Perm-S buffer (Fluidigm), was performed. The panel of antibodies used can be found in Table 2, Panel A. Next, cells were stained with 5 μM Cell-ID Intercalator-Ir (Iridium, Ir, Fluidigm) in Fix and Perm buffer (Fluidigm) for 20 min at RT, washed with CST, and stored overnight in freshly prepared 2% formaldehyde (Thermo Scientific) until acquisition the following day.

For BD and PROT conditions, after stimulation the samples were stained with 5 μM Pt 5 min at RT, fixed using BD or PROT buffers for the time indicated in each experiment as described above, and frozen. BD and PROT samples were thawed as before and stained after 1 week (n = 7), 1 month (n=9) or 6 months (n=9) as described before. Antibody cocktail was titrated according to the condition (fresh or fixed) and freshly prepared for each experiment. The reference blood sample was stimulated in a big volume and fixed using the PROT protocol. A batch cocktail of titrated antibodies was aliquoted and stored at -80°C as shown[400]. The panel is shown in Table 2, Panel B. Samples were stained as described above. In both panels A and B the probes were obtained in the metal-conjugated format from Fluidigm or were self-conjugated using Maxpar X8 antibody labeling kits (Fluidigm). Around 300,000 cells were acquired on a mass cytometer (HELIOS, Fluidigm) at an event rate of 300-350 cells/second together with EQ Four Element Calibration Beads (Fluidigm). Raw data were normalized using either CyTOF software 6.7 (Fluidigm) for Panel A or normCytof function from *CATALYST*[421] package for Panel B. FlowJo software v10.0 was used to analyze normalized MC data by manual gating. Viable cells were gated as negative for the viability marker Pt and cell percentages were calculated. After noticing some signal instability in the data, we decided to run two selected functions from the *flowAI*[416] package (flow_rate_bin, flow_rate_check) to remove regions with unstable flowrates. To make this function applicable to MC data, we adapted the TIMESTEP to 1 bin per 10 seconds. *flowCut* [506] algorithm was used to remove signal instability with 1000 segments and MaxPercCut to 0.5.

To verify cell yield upon sample fixation and preservation, cell counting was performed using Neubauer chambers for Panel A and Panel B (experiment CYT1 to CYT10) or in a TC20 Automated Cell Counter (Bio-Rad) for Panel B (experiment CYT11 to CYT45).

Mass cytometry data were deposited in flowrepository.org[505] using the accession number FR-FCM-Z2NX for panel A and FR-FCM-Z2NR for panel B.

Table 2. Antibody panel and cell-ID labeling reagents used for MC

Antigen	Clone	Metal	Panel A	Panel B	Source	Staining
CD3	UCHT1	115In		X	ThermoFisher	Surface
CD45	HI30	141Pr		X	Fluidigm	Surface
CD19	HIB19	142Nd	X	X	Fluidigm	Surface
CD123	6H6	143Nd	X	X	Fluidigm	Surface
CD4	RPA-T4	145Nd	X	X	Fluidigm	Surface
IgD	IA6-2	146Nd	X	X	Fluidigm	Surface
CD20	2H7	147Sm		X	Fluidigm	Surface
CD66a/c/e	ASL-32	149Sm	X	X	Fluidigm	Surface
CD14	M5E2	151Eu	X	X	Fluidigm	Surface
CD7	CD7-6B7	153Eu	X	X	Fluidigm	Surface
CD3	UCHT1	154Sm	X		Fluidigm	Surface
CD1c	L161	154Sm		X	Biolegend	Surface
CD45RA	HI100	155Gd	X	X	Fluidigm	Surface
CD27	L128	158Gd	X	X	Fluidigm	Surface
CD11c	Bu15	159Tb	X	X	Fluidigm	Surface
CD38	HIT2	167Er	X	X	Fluidigm	Surface
CD8	SK1	168Er	X	X	Fluidigm	Surface
CD24	ML5	169Tm		X	Fluidigm	Surface
CD141	1A4	173Yb		X	Fluidigm	Surface
HLA-DR	L243	174Yb	X	X	Fluidigm	Surface
CD56	N901	176Yb	X	X	Fluidigm	Surface
CD16	3G8	209Bi	X	X	Fluidigm	Surface
CD45	HI30	89Y	X		Fluidigm	Surface
CD41	HIP8	89Y		X	Fluidigm	Surface
IL-2	MQ1-17H12	144Nd		X	Fluidigm	Intracellular
MIP1B	D21-1351	150Nd	X	X	Fluidigm	Intracellular
TNFα	Mab11	152Sm	X	X	Fluidigm	Intracellular
IL-6	MQ2-13AS	156Gd	X	X	Fluidigm	Intracellular
IFNα	LT27:295	160Gd	X	X	Miltenyi	Intracellular
IL-23p19	23dcdp	161Dy	X	X	Fluidigm	Intracellular
TGFβ	TW4-6H10	163Dy		X	Fluidigm	Intracellular
IFNy	B27	165Ho	X	X	Fluidigm	Intracellular
IL-10	JES3-9D7	166Er	X	X	Fluidigm	Intracellular
IL-12p70	REA123	170Gd	X	X	Miltenyi	Intracellular
GranzymeB	GB11	171Yb	X	X	Fluidigm	Intracellular
MCP1	5D3-F7	175Lu		X	BD Biosciences	Intracellular
Cisplatin		195Pt			Sigma	Viability
Iridium		191Ir/193Ir			Fluidigm	DNA

6.1.4 Data analysis

Statistics and plots were performed using GraphPad Prism 6 or R version 3.6.1 (R Foundation for Statistical Computing, AUT). To compare fixed samples with the fresh condition the Spearman's correlation test was performed using the cell frequencies from fresh and 6 month-frozen samples using the R *stats* package. Bias was calculated using the *BlandAltmanLeh* package. To verify the similarity between fresh and frozen samples the Euclidean distance matrix was calculated using cell frequencies from all fresh and 6 month-frozen samples. Next, the agglomerative hierarchical clustering with average linkage was performed, and the dendrogram was plotted using the *stats* and *dendextend* package. To check sample stability over time, a coefficient of variation (CV) between fixed and frozen samples for FC or all frozen time points for MC were calculated per population using the *goeveg* package and plotted using boxplots with the *ggplot2* package. In the case of the reference sample the CV was plotted using a heatmap from the *pheatmap* package. The frequencies of dead or nonspecific antibody staining (NAS) comparing the FRESH, BD, and PROT protocols were tested using the Wilcoxon paired test or Mann Whitney U test respectively. For unsupervised analysis dimensional reduction was performed on scaled data using UMAP[443] and *uwot* package with default settings. The Jensen-Shannon divergence (JSD) was used to calculate the similarity between pairs of UMAP plots for each individual, as described[447].

6.2 Results

6.2.1 Flow cytometry immunophenotyping after whole blood preservation

In order to assess the quality of whole blood staining in samples preserved for FC, fresh or fixed blood from healthy donors was stained using panel 1 Duraclone tubes (Table 1) designed for the PRECISESADS study[384]. Figure 6A shows the sample processing workflow and Figure 7 gating strategy for the quantification of the main circulating populations for fresh and frozen samples.

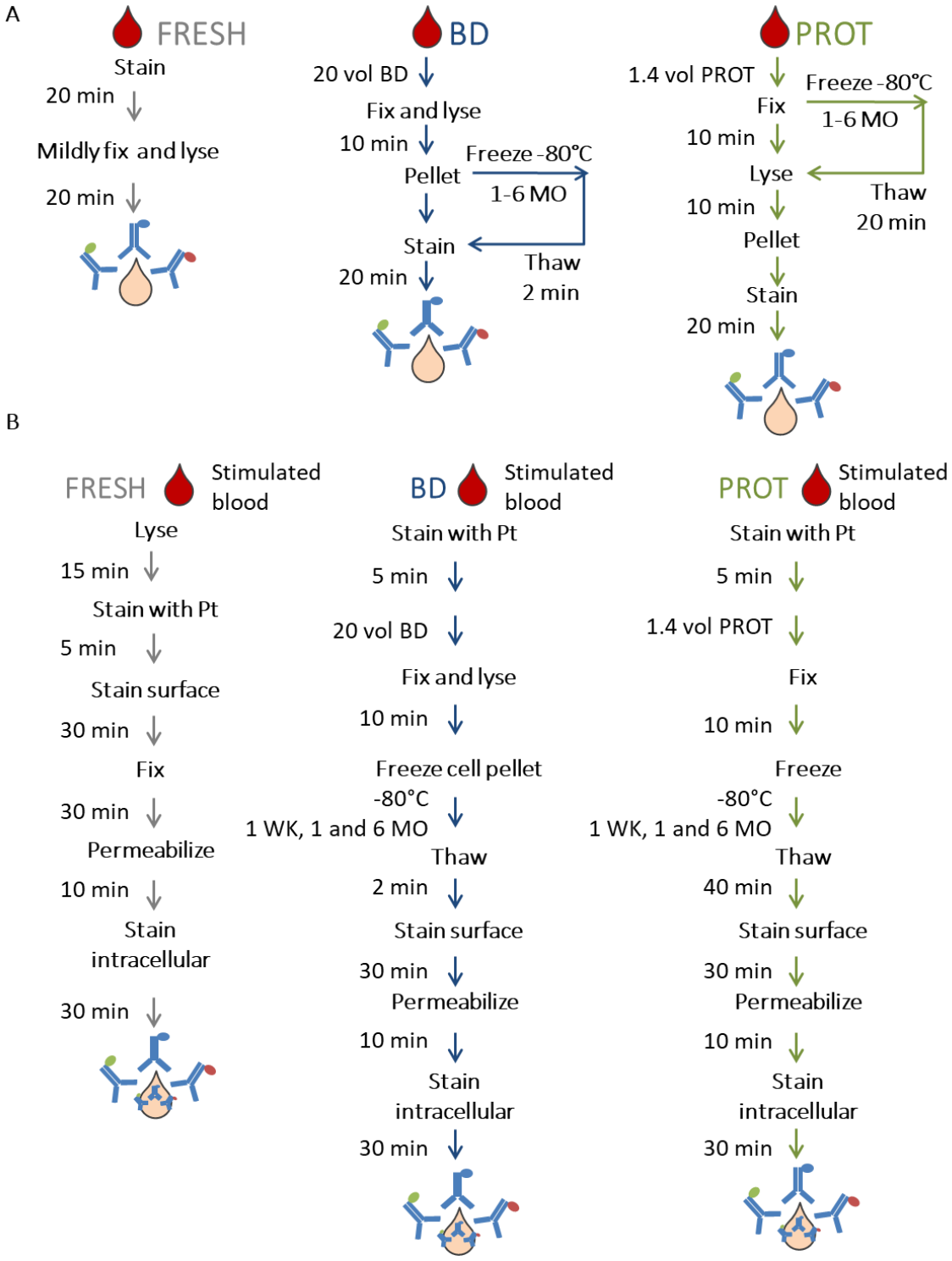

Figure 6 FC and MC study design.

Fresh blood was collected from healthy individuals and processed immediately (FRESH) or alternatively preserved with BD or PROT as detailed in Materials and Methods section. (A) Sample processing for flow cytometry. (B) Sample processing for mass cytometry.

After inspection of the results, overall good quality of the staining allowing for the identification of most circulating populations was observed in frozen samples compared to fresh condition (Figure 7).

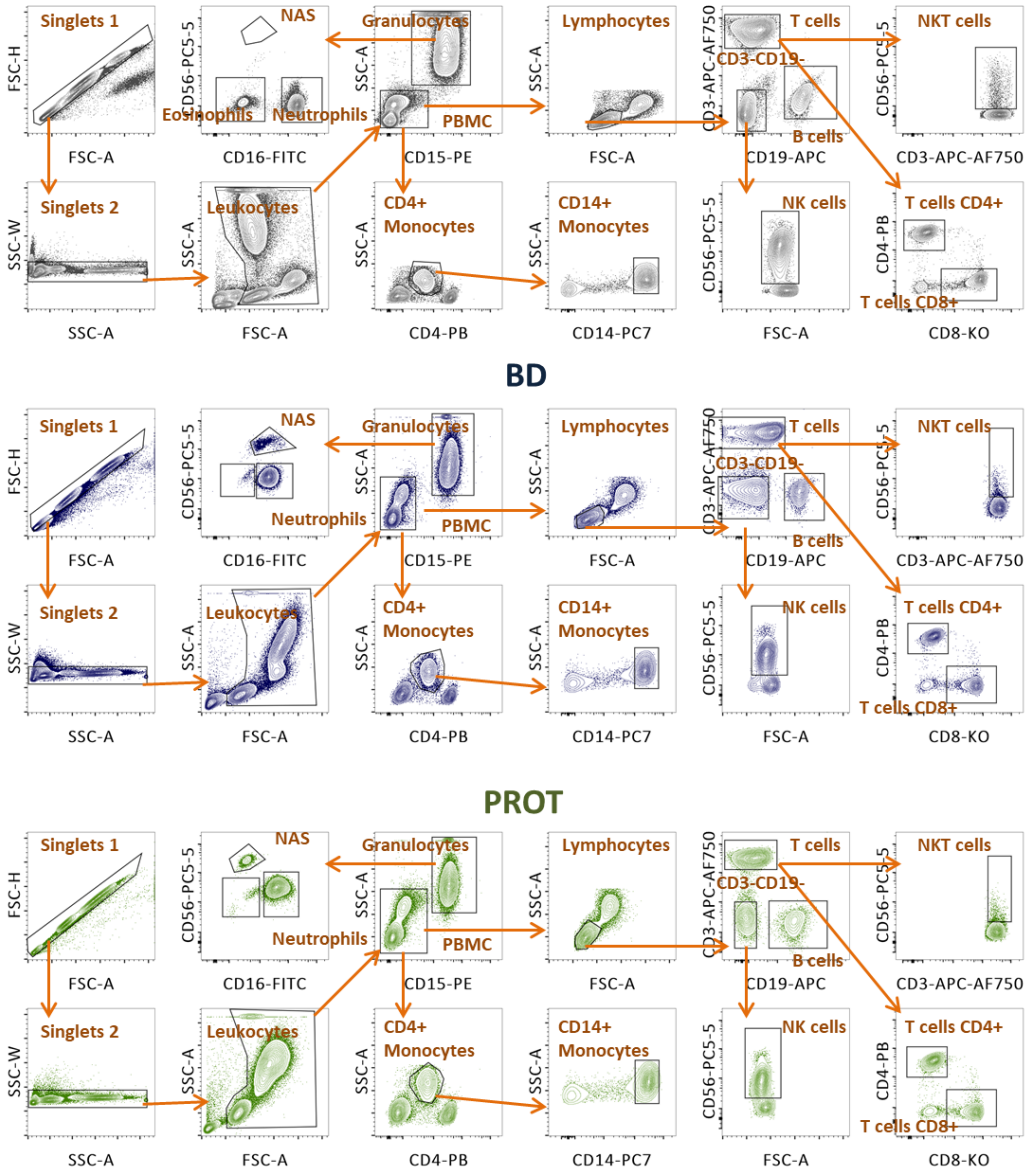

Figure 7 FC gating strategy.

Representative gating strategy for FRESH and 6 month frozen samples stabilized with BD or PROT and stained using the Panel 1 cocktail.

However, some problematic markers were revealed. Although CD56-PC5.5 staining was still detectable, its intensity in positive cells was lower, making the discrimination of positive events difficult (Figure 7 and Figure 8A).

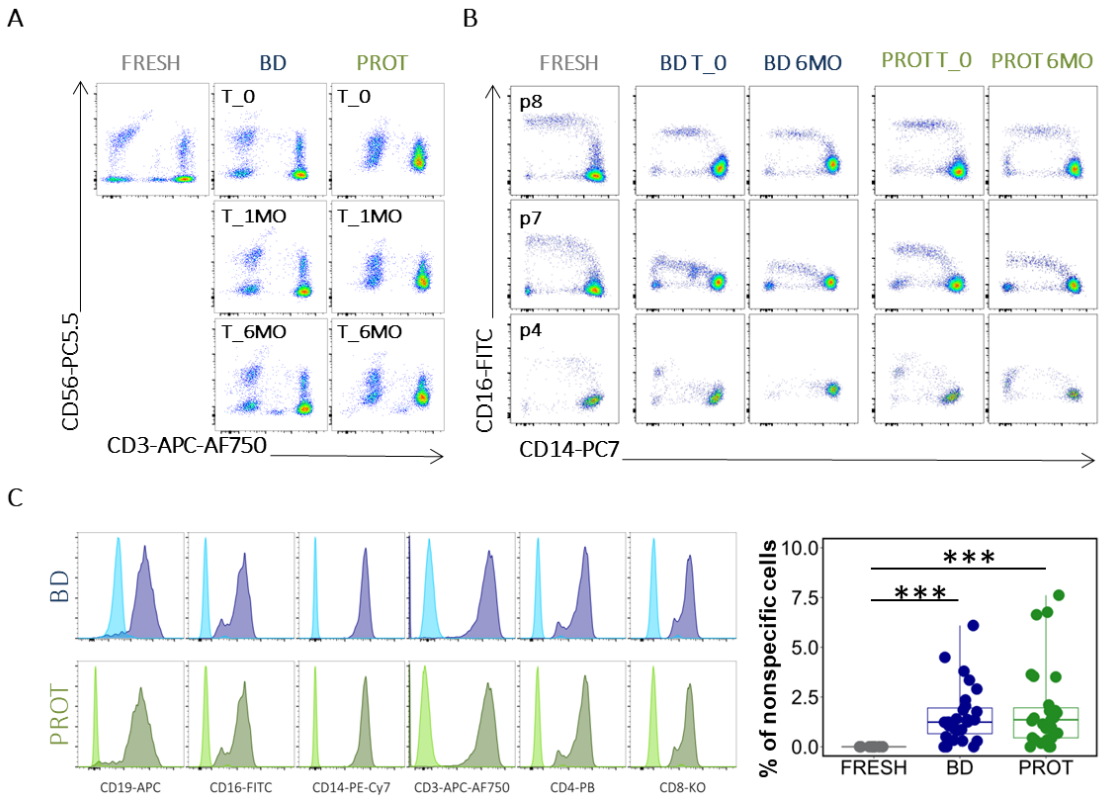

Figure 8 Staining artifacts induced by blood fixation.

(A) Representative staining for NK and NKT cells is shown across FRESH and 3 time points in BD and PROT. (B) Staining for monocyte subpopulations using CD16 and CD14 markers is shown across 3 individuals p8, p7, p4. C. Left panel, representative staining of *NAS* gate with antibodies included in Panel 1. Light color, unstained sample; dark color, stained samples. Right panel, frequency of the *NAS* events in the parental gate in the 3 conditions. Boxes show median and interquartile range, whiskers depict minimum and maximum CVs. Dots represent all collected time points, for 9 individuals. Statistic is calculated using Mann-Whitney test, *0.05, **0.01, ***$p < 0.001$.

The monocyte subset could not be accurately quantified in fixed cells (BD and PROT) due to lowering of the CD16-PC7 signal in some particular donors (Figure 8B). In addition, eosinophils could not be detected in fixed cells using $CD15^{hi}$, $CD16^{low}$, $SSC\text{-}A^{hi}$ gating strategy (Figure 7). $CD15^{hi}$ SSC^{hi} events were positive for multiple markers in both BD and PROT conditions (Figure 8C, left panel) and therefore referred to as nonspecific antibody staining (NAS) (Figure 7), in agreement with previous reports [507]. These cells were not observed in FRESH samples and had similar frequencies in both BD and PROT buffers (Figure 8C). Fixation introduced significant changes in the SSC and FSC parameters compared to the FRESH condition, especially in granulocytes and monocytes (Figure 7, *Leukocyte* gate). Monocytes became lower in FSC, and higher in SSC, while granulocytes became higher in FSC and lower in SSC in agreement with[490,508]. The changes in both monocytes and granulocytes made these two populations

indistinguishable in FSC/SSC plots, although they can still be separated using the fluorescent markers CD14 (Figure 9A) or CD15 (Figure 7). These changes were more marked in PROT than in BD buffer and were independent of the freezing time (data not shown).

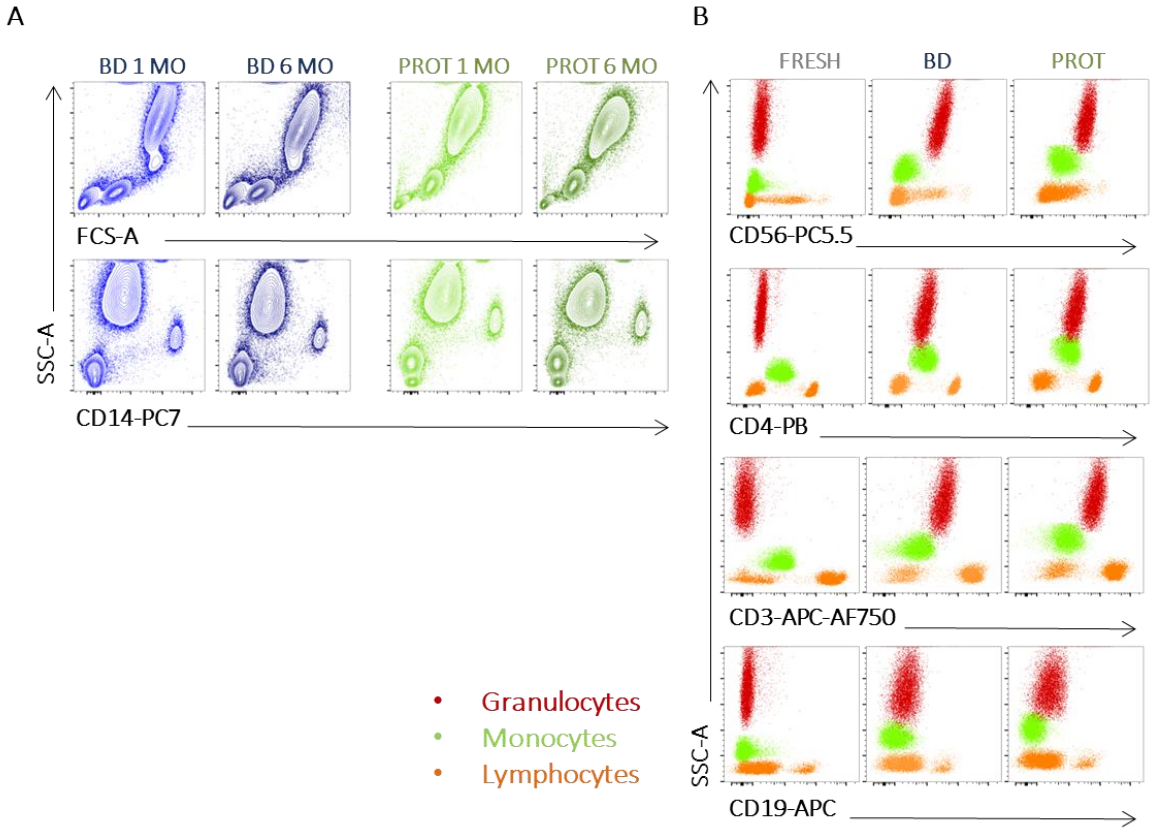

Figure 9 SSC and FCS parameter stability and antibody background in FC after blood preservation.

(A) SSC/FSC and $CD14^{+}$ monocyte visualization after 1 and 6 months of storage in BD (left) and PROT (right). (B) Representative dot plots of 4 markers (CD56, CD4, CD3, CD19) showing higher antibody background in FIXED compared to FRESH samples in different populations. *Leukocytes* gate is shown.

Additionally, careful observation of the staining patterns showed higher nonspecific staining in fixed samples for some markers for granulocytes, particularly in the case of CD3-APC-AF750 (Figure 9B). Cell morphology was well preserved as revealed by imaging cytometry, although some membrane permeability could be observed, mainly in lymphoid cells (Figure 10).

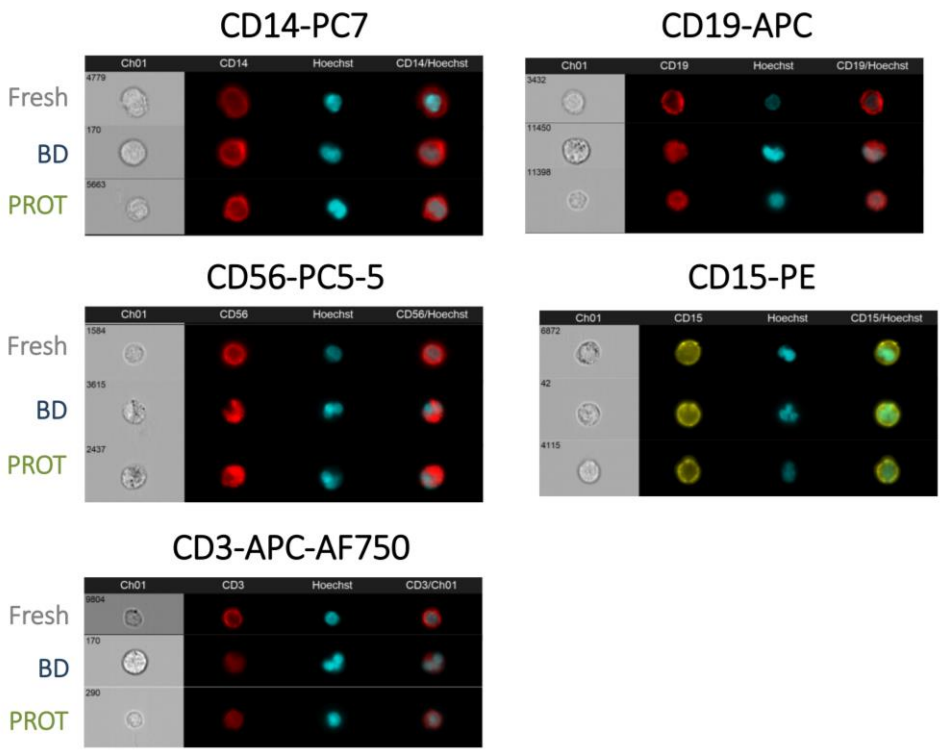

Figure 10 Assessment of preservation of cell morphology by imaging cytometry.

Whole blood samples were stained with single color panel 1 antibodies in FRESH conditions, or alternatively frozen for 1 week in BD or PROT, and analyzed in an image flow cytometer.

In order to assess the reliability of the cell frequency assessment upon sample preservation, the correlation between the proportion of leukocyte populations obtained using FRESH samples and BD or PROT fixed samples frozen for 6 months was studied using the gating strategy shown in Figure 7. Highly correlated ($R \geq 0.8$) results for both buffers were obtained (Figure 11A). Both preservation protocols showed a low bias (Figure 11B). Furthermore, the frequency-based hierarchical clustering analysis grouped samples from the same donor processed with different protocols in 7 out of 9 cases, as shown in Figure 11C.

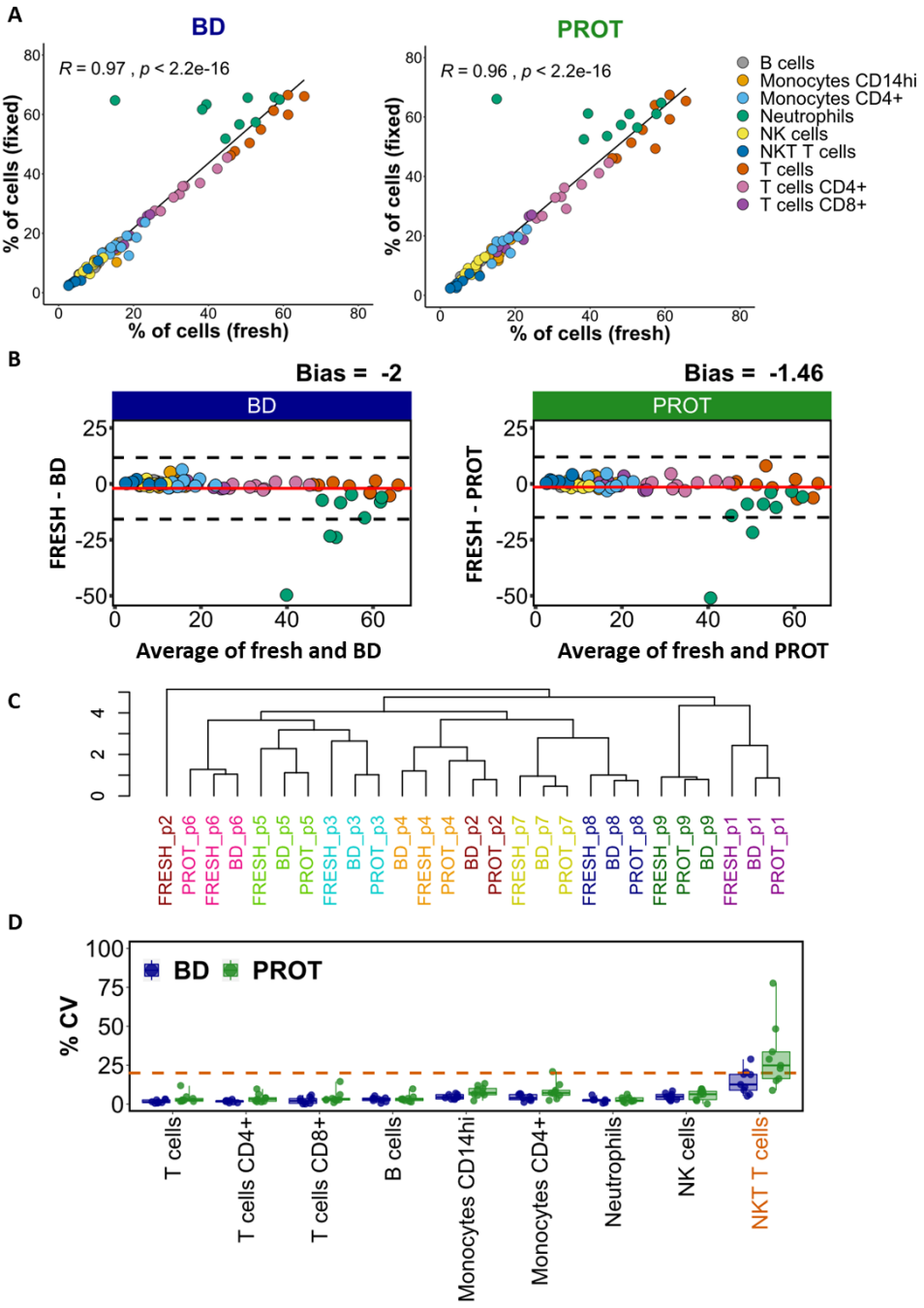

Figure 11 Comparison of cell frequencies of FRESH blood and samples stabilized using BD or PROT in FC.

(A) Spearman's correlation test for leukocyte populations quantified in blood preserved using BD (left panel) and PROT (right panel) buffers against the FRESH condition. Linear regression line is shown in black. For neutrophils, frequencies were estimated using Leukocyte as a parental gate. For the remaining populations, the PBMC parental gate was used, (n = 9). (B) Evaluation of the agreement degree by Bland-Altman test for BD and PROT in the lower and upper panels, respectively. Results are expressed as the difference between fresh and fixed samples with a 95% confidence interval (dotted black lines). Bias is shown with a red solid line. Colored circles indicate cell populations as in A. (C) Agglomerative hierarchical clustering with average linkage of FRESH samples with BD and PROT 6 month frozen samples based on cell frequencies as in A. (D) CVs were estimated for each cell population, within each individual participant using 3 time points (fixed, frozen 1 month, frozen 6 months). Boxes show median and interquartile range, whiskers depict minimum and maximum CVs, and dots represent each individual (blue for BD and green for PROT), n = 9. The orange dotted line represents the 20% CV threshold. The population name is colored in orange whenever more than two samples exceed 20% threshold for at least one buffer.

Overall, the two fixed conditions were slightly more similar to each other compared to the fresh sample (7 out of 9 cases). Additionally, we observed high correlation and low bias in most individual cell populations, although low correlation ($R < 0.5$) values were observed for $CD4^+$ monocytes in BD and neutrophils (Table 3). In neutrophils, low correlation was caused by cell death in 2 out of 9 FRESH samples during the staining, but not in unstained or fixed samples as shown in Figure 12A, upper panel. For this reason sample p2 did not cluster correctly in Figure 11C, as exclusion of the neutrophil population in the analysis caused correct sample assignment (data not shown).

To check the over-time variability of the fixed samples, CVs were estimated for the same populations in each preservation protocol, using three time points: fixed/non-frozen, 1 month and 6 months frozen (Figure 11D). We considered CVs below 20% as good stability, according to the previously published work[509]. Only in the case of NKT cells using PROT CVs were above the 20% limit (population marked in orange), suggesting that both protocols can be used for long-term storage of blood samples for flow cytometry purposes. The NKT cell changes were time-dependent for 3 out of 9 individuals and were significant for fixed and 6 month frozen samples, Figure 12B.

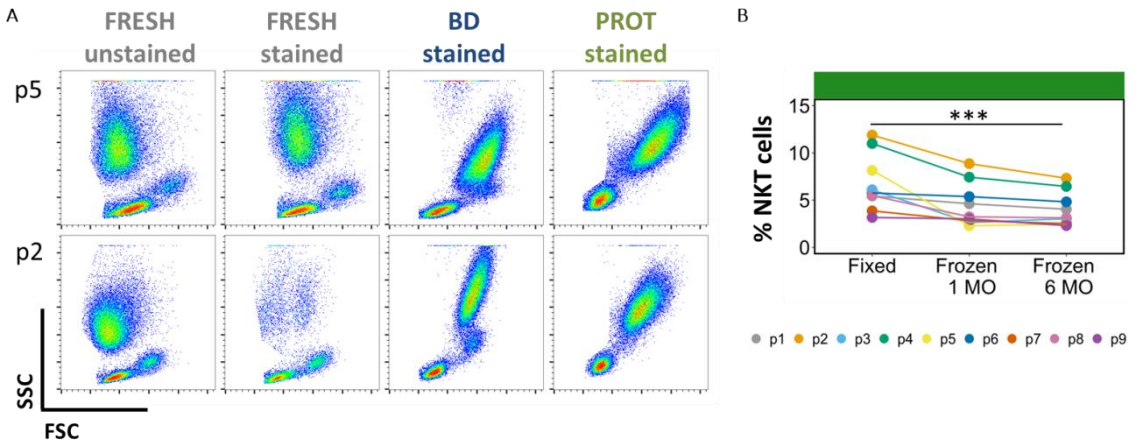

Figure 12 Leukocyte populations affected by blood processing for FC

(A) Dot plot in Leukocytes gate for two representative individuals and 4 conditions. Sample p5 shows correct granulocyte preservation in all conditions, while sample p2 shows granulocyte death in FRESH stained sample but nor in unstained neither in stained fixed samples. (B) The frequency of NKT cells in the PBMC gate measured at three time points, n=9. Statistic is calculated using Wilcoxon paired test, ***$p < 0.001$.

Table 3 Comparison of leukocyte population frequency estimates from fresh and 6-months-frozen samples in FC

Populations	Buffer	Mean ± SD (fresh)	Mean ± SD (frozen)	R	P value	Bias (95% CI)
B cells	BD	9.27 ± 3.51	9.27 ± 3.8	0.98***	4.96E-05	0 (-1.77 to 1.77)
B cells	PROT		9.51 ± 3.78	0.98***	4.96E-05	-0.24 (-1.35 to 0.88)
Monocytes CD14^{hi}	BD	14.22 ± 2.95	13.86 ± 3.24	0.83**	8.27E-03	0.36 (-3.63 to 4.35)
Monocytes CD14^{hi}	PROT		13.24 ± 3.41	0.8*	1.38E-02	0.99 (-3.08 to 5.05)
Monocytes CD4^{+}	BD	16.87 ± 3.69	16.31 ± 3.62	0.58	1.08E-01	0.56 (-4.36 to 5.48)
Monocytes CD4^{+}	PROT		16.68 ± 3.74	0.82*	1.08E-02	0.19 (-4.59 to 4.97)
Neutrophils	BD	50.12 ± 7.25	60.57 ± 5.41	0.57	2.00E-01	-10.45 (-23.34 to 2.44)
Neutrophils	PROT		58.09 ± 4.41	0.89*	1.23E-02	-7.97 (-15.58 to -0.37)
NK cells	BD	8.57 ± 1.93	8.69 ± 1.94	0.88**	3.08E-03	-0.12 (-1.93 to 1.69)
NK cells	PROT		8.97 ± 2.41	0.88**	3.08E-03	-0.41 (-2.35 to 1.54)
NKT T cells	BD	5.19 ± 2.56	4.74 ± 2.78	0.93***	7.50E-04	0.45 (-0.84 to 1.73)
NKT T cells	PROT		5.16 ± 1.79	0.88**	3.08E-03	0.03 (-2.28 to 2.33)
T cells	BD	55.62 ± 6.71	57.14 ± 7.69	0.85**	6.07E-03	-1.52 (-6.05 to 3.01)
T cells	PROT		56.07 ± 8.34	0.78*	1.72E-02	-0.45 (-9.1 to 8.2)
T cells CD4^{+}	BD	34.19 ± 6.46	35.12 ± 5.96	0.98***	4.96E-05	-0.93 (-3.38 to 1.52)
T cells CD4^{+}	PROT		34.09 ± 6.36	0.9**	2.03E-03	0.1 (-4.15 to 4.34)
T cells CD8^{+}	BD	18.02 ± 4.77	18.54 ± 5.62	0.98***	4.96E-05	-0.52 (-2.8 to 1.76)
T cells CD8^{+}	PROT		18.28 ± 5.51	0.95***	3.53E-04	-0.26 (-4.22 to 3.69)

Leucocyte frequencies are shown as average ± standard deviation (SD). The frequencies are relative to live cells for granulocytes and to PBMC for the rest of the populations. Bias is presented as group differences (95% confidence interval) in Bland-Altman tests. Asterisks besides R estimates indicate significance of the Spearman's correlation test. *** $p < 0.001$; **$p < 0.01$; *$p < 0.05$ in Spearman's tests

6.2.2 Mass cytometry immunophenotyping after whole blood preservation

The sample processing workflow is shown in Figure 6B Samples were stained using the 26-plex Panel A (Table 2), together with Ir and Pt for DNA content and viability, respectively. Figure 13 shows the gating strategy used for the analysis of the surface markers for all three protocols.

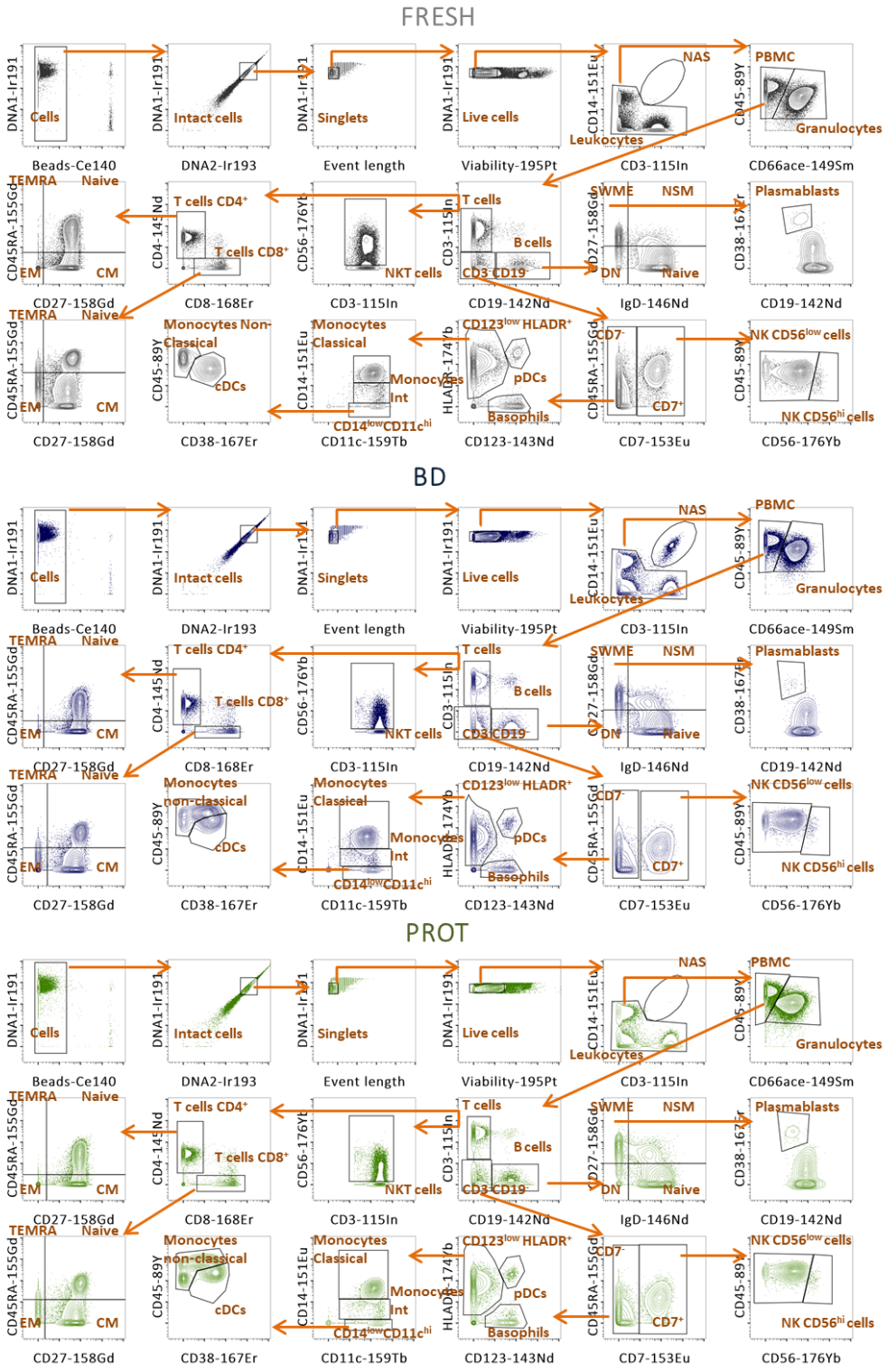

Figure 13 MC gating strategy using surface markers.

Gating strategy for FRESH, and 6 month frozen samples preserved with BD or PROT after staining with Panel A. Beads were excluded and singlet live cells were selected.

In general, both preservation protocols yielded surface staining equivalent to FRESH condition (Figure 13), and a significantly decreased frequency of Pt^+ dead cells in BD and PROT samples was observed, as shown in Figure 14A.

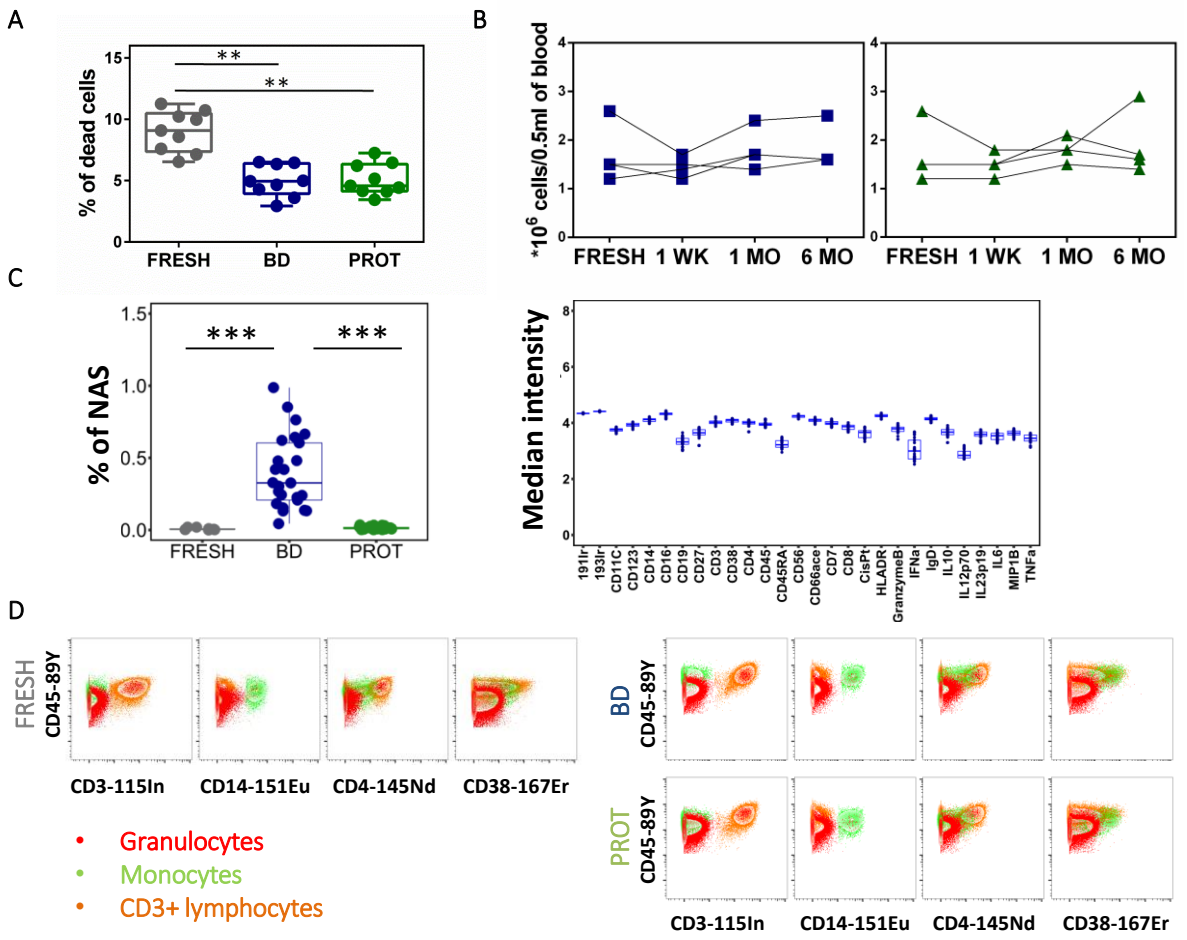

Figure 14 Viability, cell counts, NAS and granulocytes nonspecific staining in preserved blood by MC.

(A) Dead cell frequency (Pt^+ cells) using three protocols (FRESH, BD and PROT, 6 MO) n=9. Results are represented as in Figure 8C. (B) Cell counts after sample preparation for BD and PROT protocols compared with FRESH samples (n=4).(C) Left panel, frequency of cells in the *NAS* gate. Dots represent all collected time points for 9 individuals. Right Panel, arcsine-transformed marker median intensities of cells in the *NAS* gate, using all collected time points for BD protocol. (D) Antibody background comparison of the 3 protocols: FRESH, BD and PROT (6 months frozen samples). Representative dot plots of *live cells* gate are shown. CD3, CD14, CD4 and CD38 are used at the same concentrations in all the conditions. Statistics are calculated using Wilcoxon paired test for panel A and Mann-Whitney test for left panel, C, *0.05, **0.01, ***p < 0.001.

This was probably due to viability staining before RBC lysis in these protocols. Additionally, a comparable cell yields were obtained in FRESH and frozen samples, Figure 14B. MC data does not contain SSC and FSC information, and therefore *NAS* in SSC^{hi} events similar to those seen in FC could not be verified in preserved blood. Instead, highly positive cells for multiple markers

were identified and gated as double positive $CD14^+$ $CD3^+$ events (*NAS* gate, see Figure 13). Similarly to FC, this population was positive for most of the markers, and was present in almost all BD samples, but neither in FRESH nor in PROT samples (Figure 14C). Contrary to FC data, higher staining background for the probes used at the same concentration as in FRESH condition was not observed in granulocytes (Figure 14D).

The frequencies of cell populations calculated by manual gating were compared between FRESH and BD or PROT samples following 6 months of freezing. An overall high correlation for both BD and PROT was observed (Figure 15A). This occurred over a broad range of populations and was not dependent on cell abundance (Table 4), except for some populations (see Figure 16). High correlation values for T cell subsets, granulocytes, dendritic cells and basophils (Table 4) were observed when analyzing a total of 27 separated populations. NK and NKT cells were detected with precision in both BD and PROT conditions (Figure 13 and Table 4). Monocyte subsets were quantified with high correlation for BD and moderate for PROT. B lymphocytes showed high correlation across almost all subsets for the two buffers, with the exception of plasmablasts, which were highly correlated for PROT but not for BD (Table 4). This was due to the loss of many $CD38^{hi}$ cells in the BD samples, although the CD38 signal was not affected (Figure 13), suggesting that plasmablasts are sensitive to the BD preservation protocol, rather than the CD38 antigen itself. The low bias across all leukocyte populations induced by blood preservation indicates that cell estimation was very similar to that of the FRESH condition (Figure 15B and Table 4). Additionally, the frequency-based hierarchical clustering analysis grouped samples from the same donor processed with different protocols, as shown in Figure 15C, with the exception of sample P8 FRESH. As with FC, higher similarity can be seen when comparing fixed conditions and fresh samples, however correct assignment of samples is obtained. To assess the effect of the time of storage, CVs were calculated using three time points: 1 week (7 samples), 1 month and 6 months frozen (9 samples each) for each population. We considered CV above 20% as high variation. Most of the leukocyte frequencies were well preserved along time using both buffers.

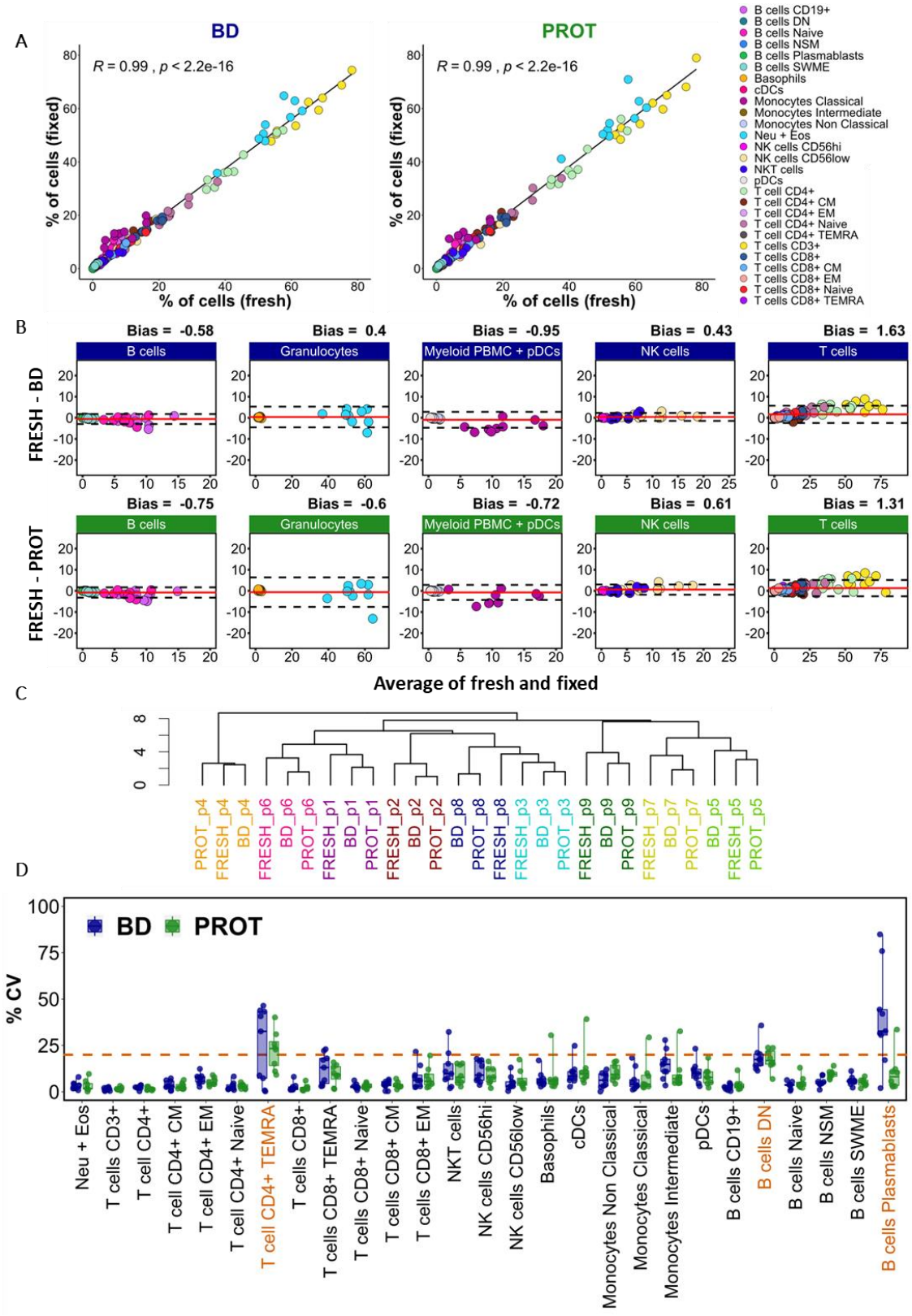

Figure 15 Comparison of cell frequencies of FRESH blood and samples stabilized using BD and PROT buffer in MC.

Granulocyte (neutrophils + eosinophils) frequencies were estimated using Life cells as a parental gate and for the rest of leukocytes PBMC gate was used as a parental gate (n = 9). (A) Spearman's correlation for all leukocyte populations gated as in Figure 13 for BD (left panel) and PROT (right panel) against FRESH condition, with linear

regression (black line). (B) Evaluation of agreement by Bland-Altman test for BD and PROT in upper panel and lower panel, respectively as before. (C) Agglomerative hierarchical clustering with average linkage of FRESH samples with BD and PROT 6 month frozen based on cell frequencies calculated as in A. (D) CVs estimated for each cell population, within each individual donor using 3 frozen time points: 1 week (n=7), 1 month (n=9) and 6 months (n=9). Results are represented as in Figure 11D. One outlier sample from individual p5 in PROT was detected and removed from the analysis.

The only populations that exceeded 20% CV were plasmablasts in BD buffer caused by CD38 expression loss as discussed above, DN B cells and $CD4^+$ TEMRA for both conditions, Figure 15D. These higher CVs were not due to time dependent changes but rather due to known, higher variability in the detection of rare cell populations as shown in Figure 16.

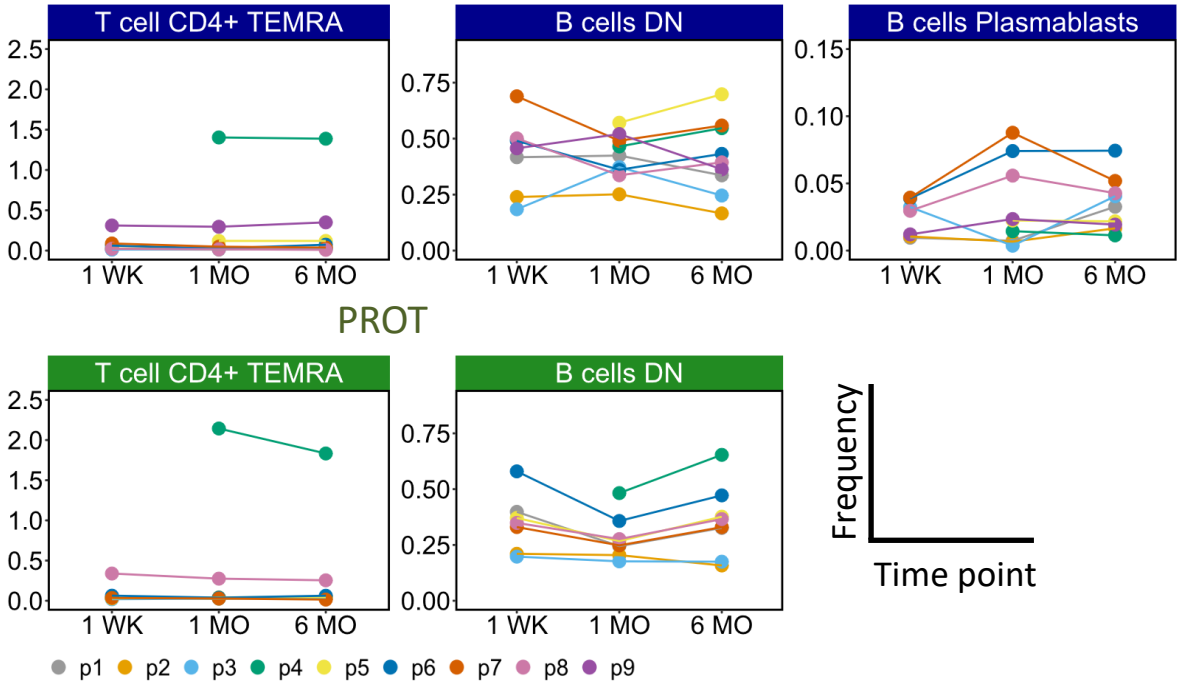

Figure 16 Cell frequency stability across the time for BD and PROT in MC.

A. The frequency of cell populations showing CV>20% was plotted across three time points (1 week, 1 month and 6 months frozen) n=7 for 1 WK, n=9 for 1 MO and 6 MO..

Additionally Jensen-Shannon divergence (JSD) used to quantify similarity between UMAP plots showed high intra-sample similarity, using a threshold of JSD < 0.2 as described before [510] and shown in Figure 17A. Higher JSD was detected for BD in 4 samples when comparing to FRESH or PROT, however these values were still low, and did not exceed JSD>0.29 (Figure 17A). These results suggest that long-term storage is possible and convenient, and gives consistent results for most of the leukocyte populations especially in PROT samples. The representative UMAP plots are shown in Figure 17B

Table 4 Comparison of leukocyte population frequency estimates fresh and 6-months-frozen samples in MC

Populations	Buffer	Mean ± SD (fresh)	Mean ± SD (frozen)	R	P value	Bias (95% CI)
B cells CD19$^+$	BD	8.36 ± 2.8	10.12 ± 2.47	0.72*	3.69E-02	-1.77 (-5.6 to 2.06)
B cells CD19$^+$	PROT		10.6 ± 2.62	0.57	1.21E-01	-2.24 (-5.64 to 1.16)
B cells DN	BD	0.47 ± 0.15	0.42 ± 0.17	0.93***	7.50E-04	0.05 (-0.07 to 0.17)
B cells DN	PROT		0.38 ± 0.17	0.88**	3.08E-03	0.08 (-0.11 to 0.27)
B cells Naive	BD	6.07 ± 2.22	7.2 ± 2.2	0.7*	4.33E-02	-1.13 (-4.4 to 2.14)
B cells Naive	PROT		7.58 ± 2.3	0.73*	3.11E-02	-1.51 (-4.52 to 1.5)
B cells NSM	BD	0.71 ± 0.3	1.06 ± 0.29	0.9**	2.03E-03	-0.35 (-0.76 to 0.06)
B cells NSM	PROT		1.11 ± 0.35	0.83**	8.27E-03	-0.4 (-0.86 to 0.07)
B cells Plasmablasts	BD	0.07 ± 0.04	0.03 ± 0.02	0.38	3.12E-01	0.03 (-0.06 to 0.12)
B cells Plasmablasts	PROT		0.08 ± 0.05	0.93***	7.50E-04	-0.02 (-0.04 to 0.01)
B cells SWME	BD	1.11 ± 0.42	1.45 ± 0.42	0.82*	1.08E-02	-0.34 (-0.69 to 0.01)
B cells SWME	PROT		1.53 ± 0.47	0.95***	3.53E-04	-0.42 (-0.72 to -0.12)
Basophils	BD	2.24 ± 0.61	1.98 ± 0.65	0.95***	3.53E-04	0.26 (-0.29 to 0.81)
Basophils	PROT		2.02 ± 0.7	0.85**	6.07E-03	0.22 (-0.45 to 0.88)
cDCs	BD	0.61 ± 0.16	0.6 ± 0.18	0.87**	4.51E-03	0.02 (-0.18 to 0.22)
cDCs	PROT		0.63 ± 0.25	0.77*	2.14E-02	-0.02 (-0.35 to 0.3)
Monocytes Classical	BD	9.16 ± 4.76	13.23 ± 3.54	0.8*	1.38E-02	-4.07 (-8.92 to 0.78)
Monocytes Classical	PROT		12.33 ± 4.52	0.62	8.57E-02	-3.17 (-9.2 to 2.86)
Monocytes Intermediate	BD	0.78 ± 0.37	1.19 ± 0.47	0.9**	2.03E-03	-0.41 (-0.87 to 0.05)
Monocytes Intermediate	PROT		0.97 ± 0.41	0.65	6.66E-02	-0.19 (-0.74 to 0.35)
Monocytes Non Classical	BD	0.76 ± 0.45	1.03 ± 0.54	0.93***	7.50E-04	-0.27 (-0.61 to 0.06)
Monocytes Non Classical	PROT		0.92 ± 0.46	0.97***	1.65E-04	-0.17 (-0.55 to 0.21)
Neu + Eos	BD	53.91 ± 7.74	53.37 ± 8.91	0.83**	8.27E-03	0.53 (-6.54 to 7.61)
Neu + Eos	PROT		55.31 ± 8.62	0.83**	8.27E-03	-1.41 (-11.28 to 8.46)
NK cells CD56hi	BD	0.43 ± 0.31	0.43 ± 0.29	0.92**	1.31E-03	0 (-0.13 to 0.13)
NK cells CD56hi	PROT		0.42 ± 0.28	0.9**	2.03E-03	0.01 (-0.13 to 0.16)
NK cells CD56low	BD	10.98 ± 4.78	10.15 ± 4.69	0.95***	3.53E-04	0.84 (-1.08 to 2.75)
NK cells CD56low	PROT		9.29 ± 4.29	0.93***	7.50E-04	1.69 (-0.9 to 4.28)
NKT cells	BD	4.17 ± 2.67	3.73 ± 1.65	0.83**	8.27E-03	0.44 (-2.03 to 2.92)
NKT cells	PROT		4.04 ± 2.04	0.82*	1.08E-02	0.13 (-1.97 to 2.23)
pDCs	BD	0.52 ± 0.18	0.56 ± 0.24	0.92**	1.31E-03	-0.03 (-0.22 to 0.16)
pDCs	PROT		0.59 ± 0.27	0.9**	2.03E-03	-0.07 (-0.29 to 0.16)
T cell CD4$^+$	BD	43.06 ± 8.45	38.6 ± 8.22	0.98***	4.96E-05	4.46 (1.33 to 7.59)
T cell CD4$^+$	PROT		39.8 ± 8.96	0.95***	3.53E-04	3.26 (-1.39 to 7.92)

T cell $CD4^+$ CM	BD	15.89 ± 4	15.09 ± 3.45	0.93***	7.50E-04	0.8 (-2.13 to 3.74)
T cell $CD4^+$ CM	PROT		15.07 ± 3.77	0.88**	3.08E-03	0.83 (-2.56 to 4.21)
T cell $CD4^+$ EM	BD	2.9 ± 2.78	2.56 ± 2.7	1***	5.51E-06	0.34 (0.06 to 0.62)
T cell $CD4^+$ EM	PROT		2.52 ± 2.67	1***	5.51E-06	0.38 (0.07 to 0.69)
T cell $CD4^+$ Naive	BD	23.93 ± 7.64	20.72 ± 7.07	0.95***	3.53E-04	3.2 (0.69 to 5.72)
T cell $CD4^+$ Naive	PROT		21.93 ± 7.3	0.95***	3.53E-04	2 (-0.9 to 4.91)
T cell $CD4^+$ TEMRA	BD	0.34 ± 0.62	0.23 ± 0.45	0.75*	2.55E-02	0.11 (-0.25 to 0.47)
T cell $CD4^+$ TEMRA	PROT		0.28 ± 0.59	0.85**	6.07E-03	0.05 (-0.07 to 0.17)
T cells $CD3^+$	BD	64.72 ± 8.84	59.14 ± 9.03	0.98***	4.96E-05	5.58 (1.78 to 9.37)
T cells $CD3^+$	PROT		59.94 ± 9.83	0.97***	1.65E-04	4.78 (-0.88 to 10.45)
T cells $CD8^+$	BD	17.63 ± 3.84	15.91 ± 3.21	0.87**	4.51E-03	1.72 (0.14 to 3.31)
T cells $CD8^+$	PROT		16.1 ± 3.28	0.73*	3.11E-02	1.53 (-0.73 to 3.8)
T cells $CD8^+$ CM	BD	5.79 ± 2.35	5.36 ± 2.15	0.98***	4.96E-05	0.43 (-0.27 to 1.12)
T cells $CD8^+$ CM	PROT		5.31 ± 2.22	0.93***	7.50E-04	0.47 (-0.39 to 1.34)
T cells $CD8^+$ EM	BD	1.27 ± 1.16	1.22 ± 1.13	1***	5.51E-06	0.04 (-0.38 to 0.47)
T cells $CD8^+$ EM	PROT		1.06 ± 0.84	0.98***	4.96E-05	0.21 (-0.62 to 1.03)
T cells $CD8^+$ Naive	BD	9.29 ± 3.54	8.32 ± 2.99	0.98***	4.96E-05	0.97 (-0.28 to 2.22)
T cells $CD8^+$ Naive	PROT		8.7 ± 3.2	0.98***	4.96E-05	0.59 (-0.74 to 1.92)
T cells $CD8^+$ TEMRA	BD	1.29 ± 2.28	1.01 ± 1.74	0.95***	3.53E-04	0.28 (-0.86 to 1.42)
T cells $CD8^+$ TEMRA	PROT		1.03 ± 1.6	0.93***	7.50E-04	0.26 (-1.1 to 1.63)

Leucocytes frequencies are shown as average ± standard deviation (SD). The frequencies are relatives to life cells for Granulocytes and to PBMCs for the rest of the populations. Bias is presented as group differences (95% confidence interval) in Bland-Altman tests. Asterisks besides R estimates indicate significance of the Spearman's correlation test. *** $p < 0.001$; ** $p < 0.01$; * $p < 0.05$ in Spearman's tests

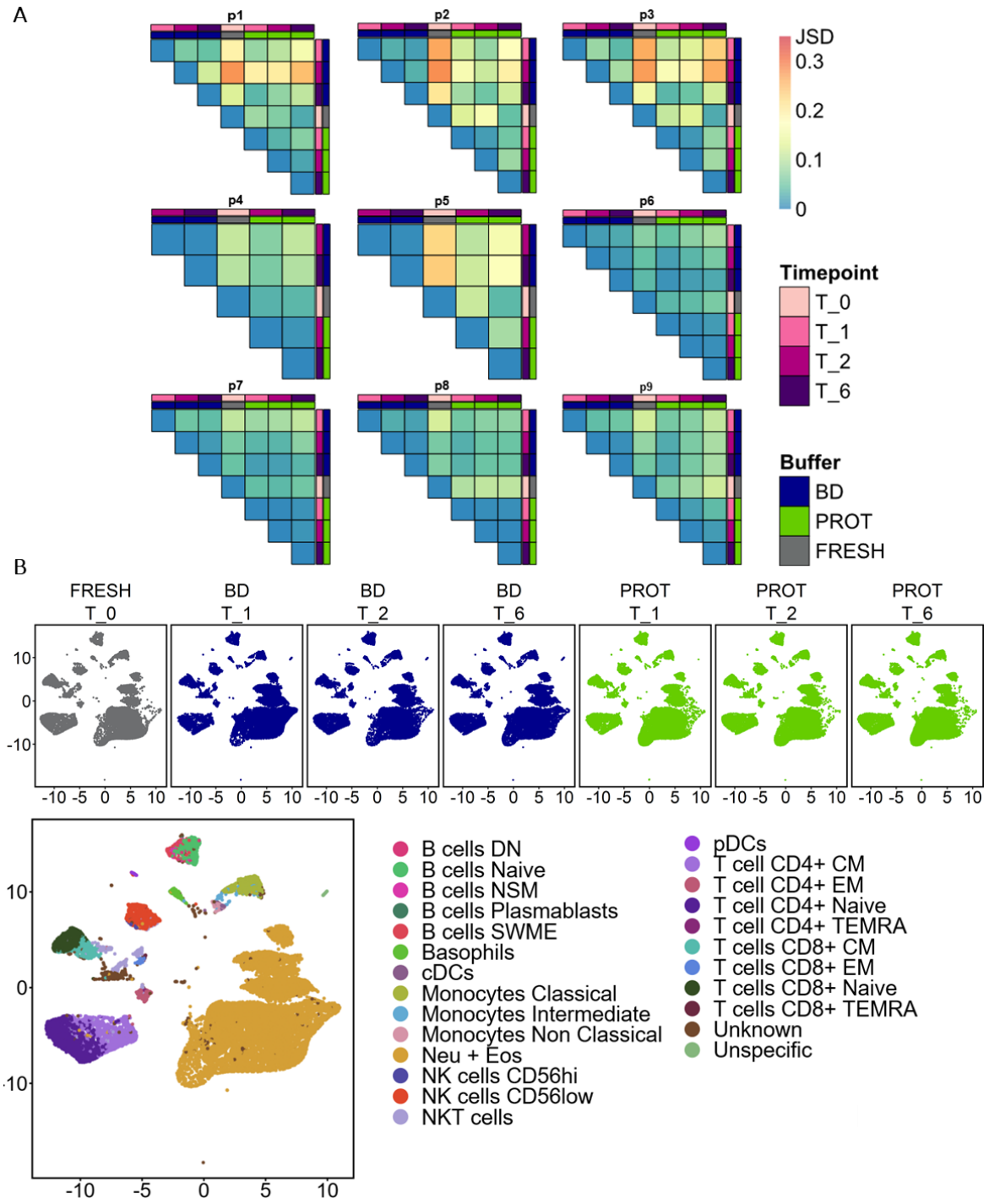

Figure 17 Sample similarity of different time points and protocols.

(A) The similarity of pairs of UMAP plots for each individual using Jensen-Shannon divergence (JSD). Higher JSD values indicate higher dissimilarity between pairwise UMAP plots. (B) Top panel, Representative UMAP analysis (20,000 cell per sample) on *Live cells* population. Bottom panel, manual cell labels.

6.2.3 Intracellular cytokine detection by MC

To test intracellular cytokine detection after blood fixation, we manually gated multiple cytokines across different leukocyte populations in the R848-stimulated blood samples and estimated the frequencies of cytokine-positive cells. All the cytokines that were detected in the fresh samples were also detected in the BD and PROT. Some examples of cytokine detection can be seen in Figure 18.

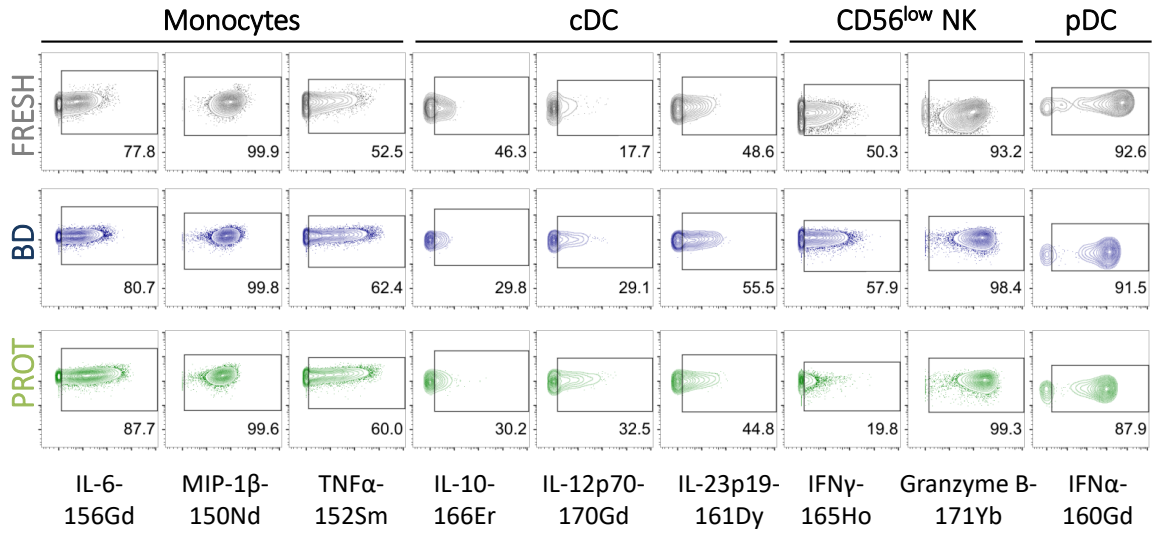

Figure 18 Gating strategy using cytokine markers from Panel A.

The gating strategy is shown for 3 different protocols FRESH, BD and PROT, 6 months frozen. The expression of 9 cytokines is shown across 4 different cell populations expressing them at high levels. Gate boundaries were first setup for FRESH condition for each population, based on the density distribution. Next the same threshold was applied to the corresponding individual and population.

To compare percentages between fresh samples and those with BD or PROT, 6 months frozen, correlation analyses were done. Globally there was good correlation for both buffers (Figure 19A). However, most cytokines were detected with higher frequency in FRESH condition than in fixed and frozen samples as shown in Figure 19B. The correlation and bias analyses for individual populations and cytokines are shown in Table 5.

To see if there are changes in cytokine detection with the time of storage, CVs were estimated using three time points: 1 week, 1 month and 6 month frozen, for each population and cytokine where expression could be detected (Figure 19C). As before, CV above 20% was considered as high variation. Although most of the cytokine frequencies were stable with time (median CV below 20%) using both buffers, we noticed higher variability than in the surface

markers, mostly in the case of BD buffer. Besides IL-23p19 in pDCs we did not observe any time-specific change (Figure 20).

Table 5 Comparison of cytokine-positive frequency estimates derived from fresh and 6-months-frozen samples in MC

Populations	Buffer	Mean ± SD (fresh)	Mean ± SD (frozen)	R	P value	Bias (95% CI)
B cells IL10$^+$	BD	12.3 ± 3.57	8.26 ± 1.17	0.47	2.13E-01	4.04 (-2 to 10.08)
B cells IL10$^+$	PROT		8.86 ± 1.15	0.07	8.80E-01	3.44 (-3.53 to 10.42)
B cells IL6$^+$	BD	23.85 ± 6.72	12.76 ± 2.3	-0.05	9.12E-01	11.1 (-3.44 to 25.64)
B cells IL6$^+$	PROT		16.97 ± 3.53	-0.2	6.13E-01	6.89 (-9.14 to 22.92)
B cells MIP1β$^+$	BD	21.29 ± 4.95	24.7 ± 6.91	0.03	9.48E-01	-3.41 (-18.62 to 11.81)
B cells MIP1β$^+$	PROT		16.31 ± 4.8	0.1	8.10E-01	4.98 (-7.73 to 17.69)
B cells TNFα$^+$	BD	6.18 ± 2.33	4.79 ± 0.91	-0.3	4.37E-01	1.4 (-4.2 to 7)
B cells TNFα$^+$	PROT		5.05 ± 0.84	-0.33	3.85E-01	1.13 (-4.19 to 6.45)
T cells CD4+ GzmB$^+$	BD	22.89 ± 7.23	17.28 ± 7.51	0.77*	2.14E-02	5.61 (-3.21 to 14.42)
T cells CD4+ GzmB$^+$	PROT		60.42 ± 15.64	0	1.00E+00	-37.53 (-70.46 to -4.61)
T cells CD4+ IL6$^+$	BD	15.52 ± 4.13	23.65 ± 4.46	0.35	3.59E-01	-8.13 (-19.57 to 3.31)
T cells CD4+ IL6$^+$	PROT		23.53 ± 4.48	0.32	4.10E-01	-8.01 (-19.07 to 3.06)
NK CD56low GzmB$^+$	BD	94.73 ± 2.52	97.63 ± 1.2	0.75*	2.55E-02	-2.9 (-6.64 to 0.84)
NK CD56low GzmB$^+$	PROT		98.57 ± 0.7	0.2	6.13E-01	-3.84 (-8.51 to 0.84)
NK CD56low IFNy$^+$	BD	52.59 ± 7.63	57.22 ± 11.55	0.3	6.83E-01	-4.63 (-22.13 to 12.87)
NK CD56low IFNy$^+$	PROT		23.2 ± 3.33	-0.3	6.83E-01	29.39 (12.23 to 46.55)
NK CD56low TNFα$^+$	BD	6.14 ± 2.01	7.57 ± 1.32	0.13	7.44E-01	-1.42 (-5.65 to 2.8)
NK CD56low TNFα$^+$	PROT		7.57 ± 1.26	0.57	1.21E-01	-1.42 (-4.93 to 2.08)
T cells CD8+ GzmB$^+$	BD	45.74 ± 11.68	36.66 ± 14.93	0.63	7.60E-02	9.08 (-6.92 to 25.08)
T cells CD8+ GzmB$^+$	PROT		69.23 ± 14.57	0.3	4.37E-01	-23.49 (-51.64 to 4.66)
cDC IL10$^+$	BD	54.56 ± 10.75	29.71 ± 3.78	0.63	7.60E-02	24.85 (9.05 to 40.65)
cDC IL10+	PROT		29.95 ± 4.69	-0.08	8.43E-01	24.61 (3.55 to 45.67)
cDC IL12p70$^+$	BD	25.53 ± 7.48	22.88 ± 3.88	-0.15	7.08E-01	2.64 (-15.19 to 20.47)
cDC IL12p70$^+$	PROT		28.43 ± 7.22	-0.42	2.70E-01	-2.91 (-25.87 to 20.06)
cDC IL23p19$^+$	BD	59.77 ± 9.47	48.15 ± 6.32	-0.13	7.44E-01	11.61 (-11.35 to 34.58)
cDC IL23p19$^+$	PROT		43.04 ± 6.22	0.18	6.44E-01	16.72 (-5.86 to 39.31)
cDC IL6$^+$	BD	71.35 ± 11.73	68.15 ± 6.6	0.63	7.60E-02	3.2 (-13.9 to 20.29)
cDC IL6$^+$	PROT		79.87 ± 5	0.2	6.13E-01	-8.51 (-30.33 to 13.3)
cDC MIP1β$^+$	BD	95.5 ± 4.63	95.47 ± 2	-0.13	7.44E-01	0.03 (-11.1 to 11.16)
cDC MIP1β$^+$	PROT		93.45 ± 2.89	-0.23	5.52E-01	2.05 (-10.08 to 14.18)
cDC TNFα$^+$	BD	80.11 ± 7.11	80.94 ± 2.58	0.33	3.85E-01	-0.83 (-14.57 to 12.9)
cDC TNFα$^+$	PROT		81.14 ± 4.71	0.6	9.68E-02	-1.03 (-16.16 to 14.09)
Mono CD14hi IL10$^+$	BD	77.96 ± 7.13	60.41 ± 6.66	0.62	8.57E-02	17.54 (3.48 to 31.6)
Mono CD14hi IL10$^+$	PROT		59.56 ± 6.88	-0.03	9.48E-01	18.39 (0.18 to 36.6)
Mono CD14hi	BD	15.43 ± 7.34	10.64 ± 2.82	0.72*	3.69E-02	4.79 (-6.69 to 16.27)

IL12p70$^+$						
Mono CD14hi IL12p70$^+$	PROT		12.04 ± 2.67	0.28	4.63E-01	3.39 (-10.15 to 16.93)
Mono CD14hi IL6$^+$	BD	80.45 ± 12.5	80.71 ± 7.21	0.95***	3.53E-04	-0.26 (-14.28 to 13.77)
Mono CD14hi IL6$^+$	PROT		83.77 ± 7.49	0.33	3.85E-01	-3.32 (-24.21 to 17.57)
Mono CD14hi MIP1β$^+$	BD	98.66 ± 3.48	99.64 ± 0.31	-0.12	7.76E-01	-0.98 (-8.04 to 6.09)
Mono CD14hi MIP1β$^+$	PROT		99.02 ± 1.38	-0.08	8.43E-01	-0.36 (-8.26 to 7.54)
Mono CD14hi TNFα$^+$	BD	64.89 ± 15.81	65.06 ± 14.14	0.78*	1.72E-02	-0.18 (-11.31 to 10.95)
Mono CD14hi TNFα$^+$	PROT		62.55 ± 13.36	0.9**	2.03E-03	2.33 (-11.21 to 15.87)
Granulocytes MIP1β$^+$	BD	98.78 ± 0.79	91.02 ± 7.58	0.35	3.59E-01	7.76 (-6.95 to 22.47)
Granulocytes MIP1β$^+$	PROT		85.99 ± 10.82	0.33	3.85E-01	12.79 (-8.29 to 33.87)
NKT cells GzmB$^+$	BD	55.65 ± 23.86	56.51 ± 21.1	1***	5.51E-06	-0.86 (-13.45 to 11.73)
NKT cells GzmB$^+$	PROT		78.03 ± 16.23	0.82*	1.08E-02	-22.38 (-48.53 to 3.77)
NKT cells IFNγ$^+$	BD	25.76 ± 6.01	27.2 ± 8.67	0.1	9.50E-01	-1.43 (-16.24 to 13.37)
NKT cells IFNγ$^+$	PROT		18.59 ± 2.59	0.6	3.50E-01	7.17 (-2.75 to 17.1)
NKT cells MIP1β$^+$	BD	38.35 ± 10.28	54.17 ± 9.2	0.47	2.13E-01	-15.82 (-36.55 to 4.91)
NKT cells MIP1β$^+$	PROT		38.83 ± 8.64	0.32	4.10E-01	-0.48 (-21.64 to 20.68)
NKT cells TNFα$^+$	BD	17.57 ± 3.99	36.95 ± 6.07	0.52	1.62E-01	-19.39 (-29.55 to -9.23)
NKT cells TNFα$^+$	PROT		37.23 ± 5.48	0.42	2.70E-01	-19.67 (-28.86 to -10.47)
pDC GzmB$^+$	BD	86.73 ± 8.33	93.75 ± 3.11	0.5	1.78E-01	-7.02 (-21.86 to 7.82)
pDC GzmB$^+$	PROT		97.54 ± 3.62	0.17	6.78E-01	-10.81 (-29.1 to 7.48)
pDC IFNα$^+$	BD	80.8 ± 10.66	78.94 ± 6.93	0.8*	1.38E-02	1.86 (-11.04 to 14.75)
pDC IFNα$^+$	PROT		76.21 ± 8.61	0.97***	1.65E-04	4.59 (-3.06 to 12.23)
pDC IL23p19$^+$	BD	52.45 ± 14.56	41.93 ± 3.37	-0.43	2.50E-01	10.53 (-21.36 to 42.41)
pDC IL23p19$^+$	PROT		37.96 ± 4.71	-0.68	5.03E-02	14.49 (-20.77 to 49.75)
pDC TNFα$^+$	BD	89.69 ± 5.58	93.76 ± 4.4	0.72*	3.69E-02	-4.07 (-10.61 to 2.48)
pDC TNFα$^+$	PROT		93.4 ± 5.6	0.82*	1.08E-02	-3.7 (-9.44 to 2.04)

Leukocytes producing cytokines frequencies are shown as average ± standard deviation (SD). The frequencies are relative to populations shown in the first column. Bias is presented as group differences (95% confidence interval) in Bland-Altman tests. Asterisks besides R estimates indicate significance of the Spearman's correlation test. *** $p < 0.001$; **$p < 0.01$; *$p < 0.05$ in Spearman's tests

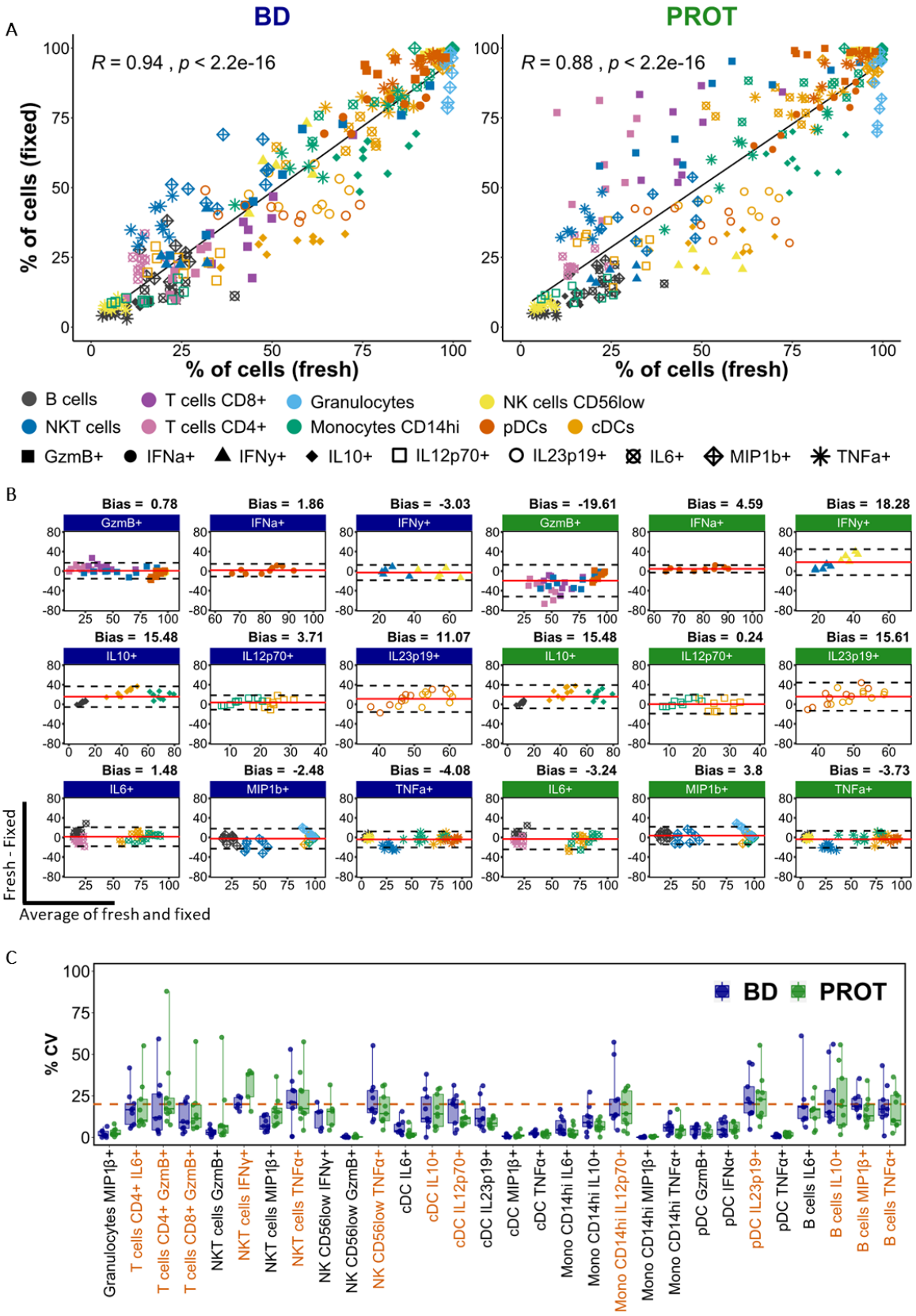

Figure 19 Comparison of cytokine-producing cell frequencies of FRESH blood and samples stabilized using BD and PROT buffers in MC.

Cytokine-positive cell frequencies were quantified using their parental gates. (A) Spearman's correlation test for

cytokine-positive leukocyte populations using BD (left panel) and PROT (right panel) 6 month frozen samples compared to the FRESH condition. Colors indicate populations, and shapes indicate cytokines. Parental gates are the populations, data for 9 individuals are presented. (B) Evaluation of the agreement by Bland-Altman test for BD (left) and PROT (right). The results are expressed as before, n=9 except for IFN (n=5). (C) CVs were estimated for each cytokine and cell populations, within each individual donor as in Fig 4. Data are represented as before.

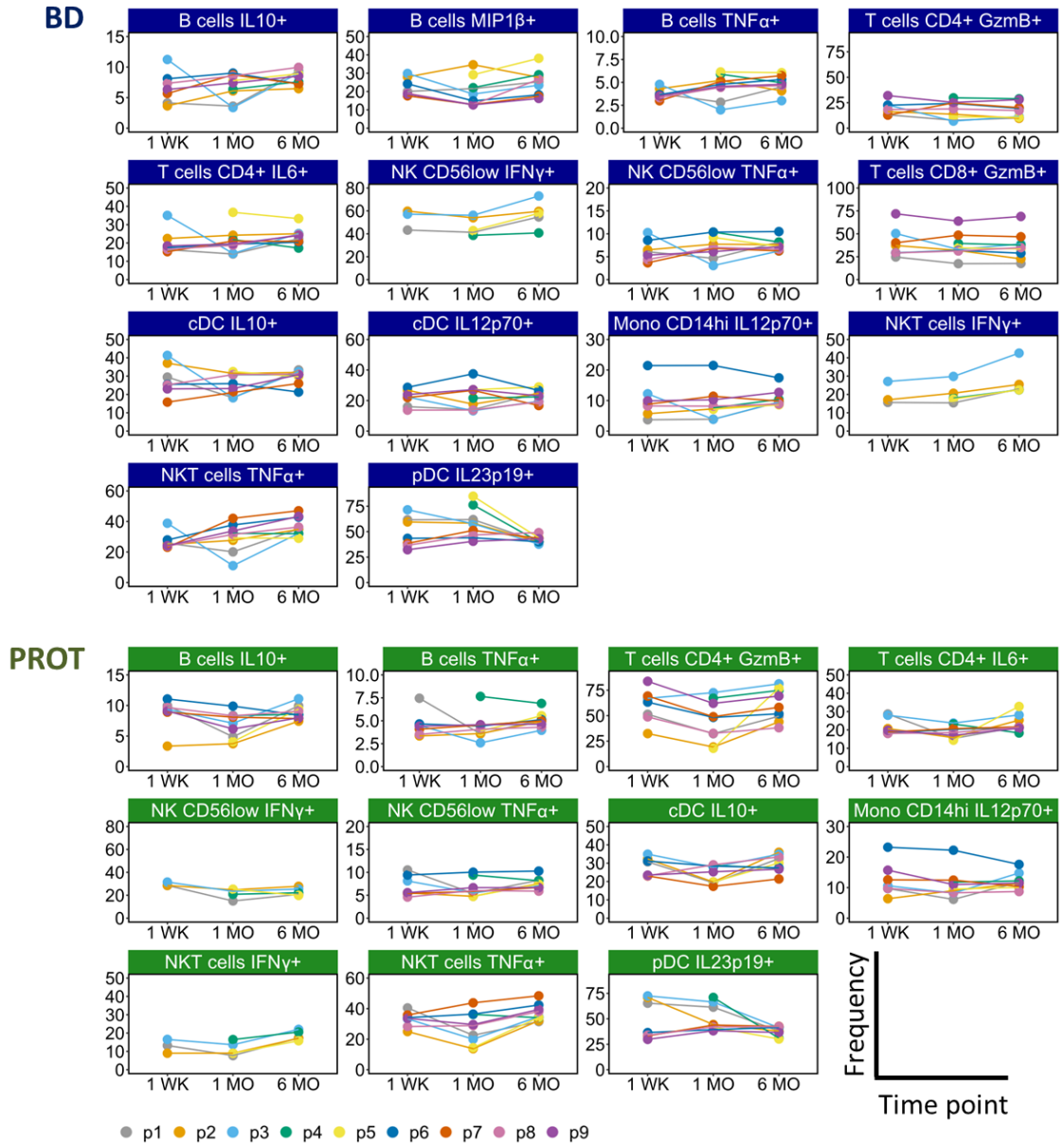

Figure 20 Cytokine-producing cell frequencies along the time for BD and PROT in MC.

The frequency of cytokine-positive cell populations with CV>20% was plotted for three time points as before (1 week, 1 month and 6 months frozen). n=7 for 1 WK, n=9 for 1 MO and 6 MO, n=5 for IFNγ^{+} cells

6.2.4 Long-term stability and inter-assay variability for preserved cells

For MC, both buffers performed comparably well. However, the lack of *NAS*, the ability to detect cells like plasmablasts, better structure preservation in UMAP, and the ease of sample manipulation, led us to choose PROT for further analysis. Therefore, to verify longer times of storage, 45 aliquots of a single donor were fixed and frozen using PROT protocol, and single aliquots were stained regularly using a 34-plex panel that expands both surface and cytokine detection (Table 2, panel B), in combination with Ir and Pt as before. Across the manually gated populations shown in Figure 21 and Figure 22 in the 45 experiments, CVs were estimated together with deviations from the mean values for circulating populations and cytokines (Figure 23, A and B receptively). For most of the populations CV values were below 20%, including low frequent cells such as $CD1c^+$ cDC, pDC and transitional B cells, indicating a remarkably high stability in the long term. The only subsets above 20% CV threshold were $CD4^+$ TEMRA, NKT, plasmablasts and $CD141^+$ cDC (Figure 23A). NKT cell proportions increased with time, and $CD4^+$ TEMRA, plasmablast and $CD141^+$ cDC showed inconsistent values. For cytokines higher than 20% CV was observed for granzyme B production in $CD4^+$ T cells and NKT cells Figure 23B.

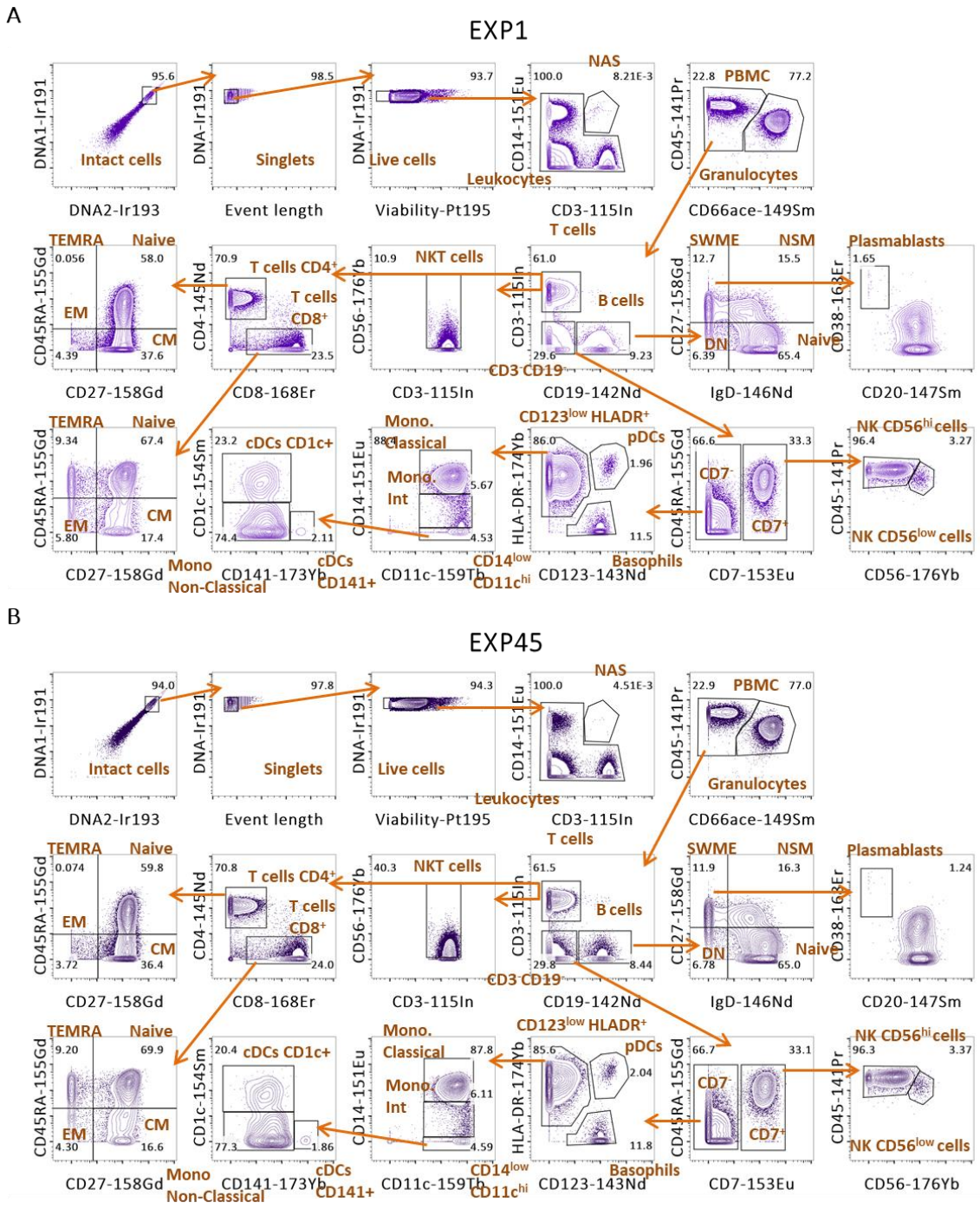

Figure 21 Long-term sample stabilization using PROT in MC and surface markers.

(A) Gating strategy for EXP1 using antibody Panel B (Table 2). (B) Gating strategy for EXP45 (last experiment after 13 months).

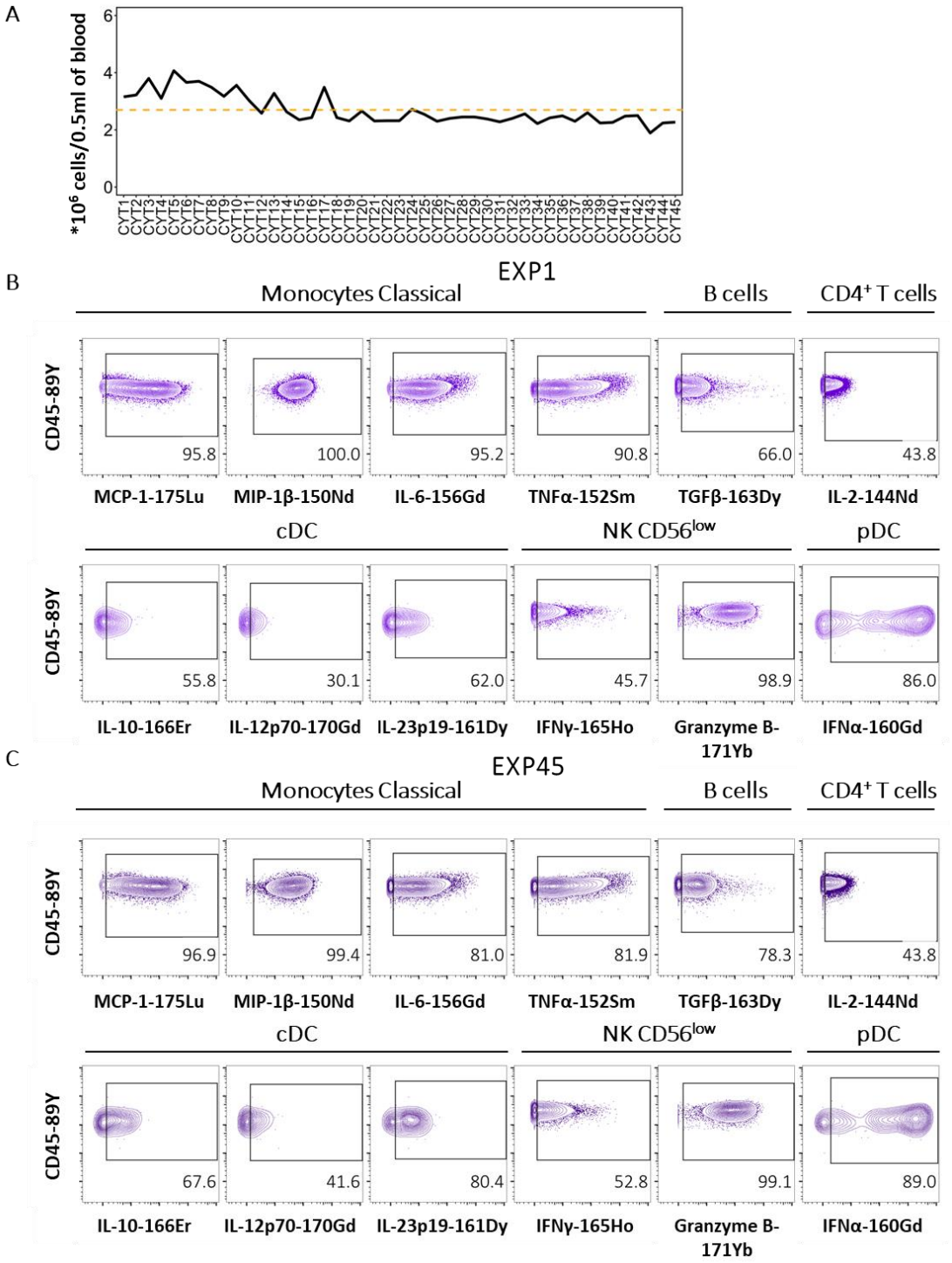

Figure 22 Cytokine detection after long-term sample stabilization using PROT in MC.

(A) Cell counting after thawing and lysis step in 45 consecutive experiments. Dotted orange line represents the mean count for all experiments. Samples from CYT1 to CYT10 were counted manually using a Neubauer chamber, while for the rest a TC20 automated cell counter was used. (B) Gating strategy for EXP1, using antibody Panel B (Table S2). C. Gating strategy for EXP45 (last experiment after 13 months).

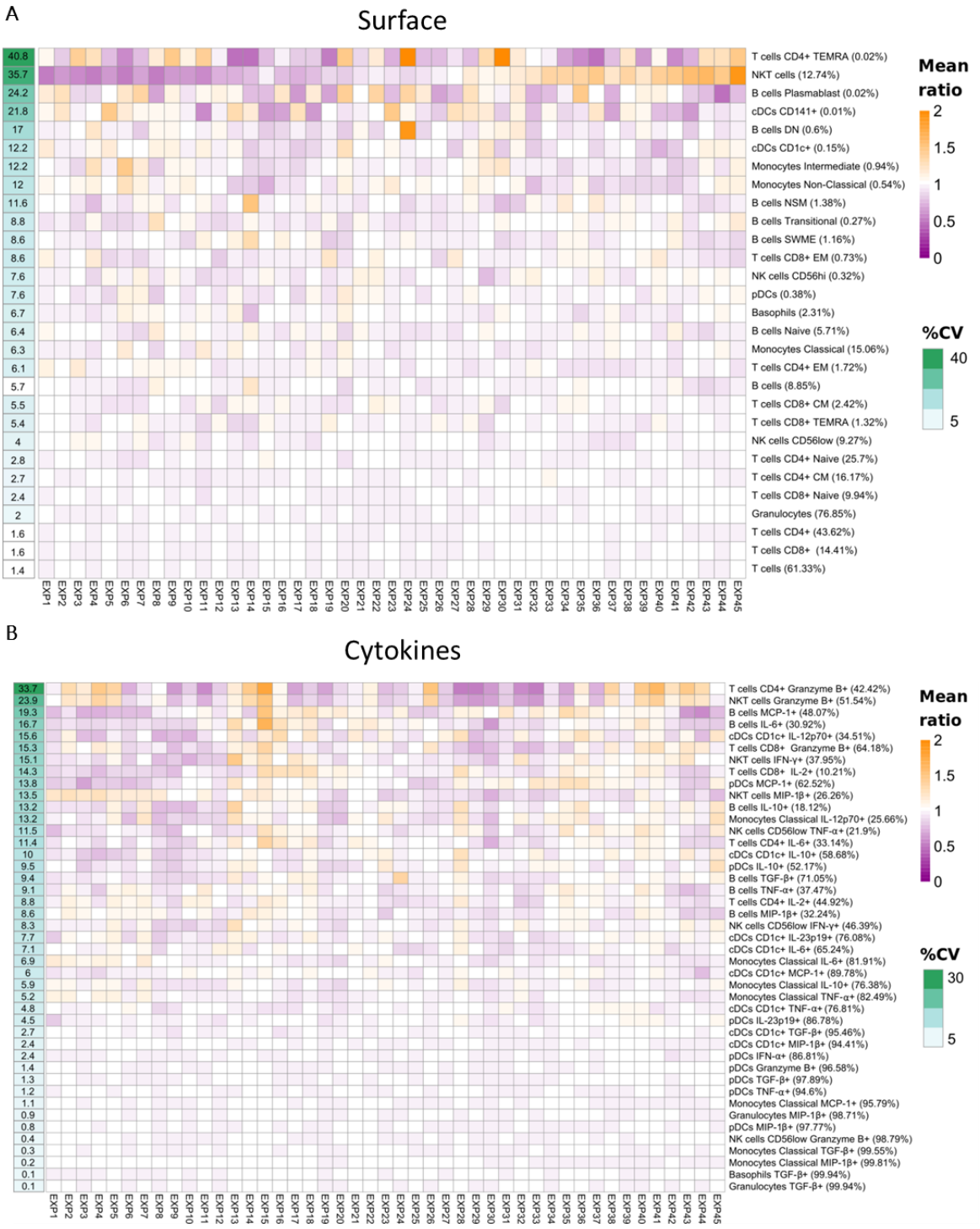

Figure 23 Long-term stabilization of whole blood using PROT buffer assessed by MC.

Forty five experiments (EXP1 – EXP45) were performed periodically for 13 months, using an aliquoted, stimulated blood sample from a single individual, stained with panel B (Table S2). (A) Cell frequencies relative to Live cells for granulocytes and PBMC for the rest of leukocytes were quantified using the gating strategy shown in Figure 21 and plotted as the mean ratio of the frequencies. Values equal to 1 refer to no difference from the mean; 2, double or more positive difference; 0.5, double or more negative difference. CVs were estimated across each row, plotted in green rows and were ordered by decreasing values of the CVs. (B) Cytokine positive cell frequencies were extracted using the gating strategy as shown in Figure 22 and plotted and ordered as in A.

6.3 Discussion

Immune phenotyping and stimulatory immune responses are important parameters in the immune monitoring and biomarker discovery fields. However, due to time-dependent changes in cell composition, blood analysis requires good coordination between recruitment and cytometry centers, where the samples are usually processed. It is even more important when the access to flow or mass cytometry instruments is limited to few research centers or when retrospective studies are performed. The use of whole blood allows a reduction in the volume of sample, a simpler sample manipulation, less variability compared to PBMC isolation and deeper look into immune system, such as granulocytes[480,487,488]. Here we compare the changes and similarities introduced upon whole blood fixation and long-term storage compared to the fresh samples in both FC and MC using an extensive panel of antibodies.

Good correlation, small bias, and correct clustering between fresh and frozen manually gated cell frequencies in both FC and MC indicate correct preservation of sample composition in both protocols tested herein. Additionally, the unsupervised analysis by UMAP and JSD confirmed sample similarity along different time points and conditions in MC. However better results were obtained in PROT indicating that this buffer should be a better choice for deep cell phenotyping studies.

Using both buffers and techniques CVs below 20% were obtained when analyzing all 3 time points for most cell populations, showing good sample stability and low inter-assay variability. However problems in the detection of few particular markers, were observed suggesting antigen sensitivity to fixation, as also reported[394]. Some markers and populations were more affected in one or the other fixation method, and the effect was more marked in FC than in MC. This can be explained by the different composition of the buffers and higher antibody background with fluorescence-based techniques in fixed cells, which limit the proper detection of continually expressed markers. It is possible that sensitive antigens could be still detected through a change in the coupled fluorochrome/metal to the most sensitive channels or by titration of antibodies adapted to sample fixation as it was done in the MC setup. In the case of epitopes that are completely lost during fixation sensitivity, they could be stained before sample fixation, as suggested[507].

An increase in antibody background upon fixation was shown in different studies in both MC and FC studies[394,490] and is also confirmed here. The background was higher in FC than in MC, and was mostly affecting granulocytes. Thus, care needs to be taken when analyzing marker expression in this population. Besides the background, *NAS* in a minor set of cells was observed

in FC for both buffers and MC for BD buffer. This suggests that fluorescence-tagged antibodies are more prone to nonspecific binding, especially when using BD buffer. It has been reported that heparin can help to reduce the nonspecific binding, especially in eosinophils[507].

Although the correlation between fresh and frozen samples was high, more differences in cytokine detection than in surface staining were observed. Most cytokines were better detected in fresh samples, as shown by the positive bias in Bland-Altman plots, but the extent of this effect was different in every cytokine. These discrepancies can be explained by differences in the staining protocols (Figure 6B). In the fresh condition, the cells are fixed after washing the reversible inhibitors of exocytosis, surface staining and red blood lysis, these steps represent around one hour before fixation. Thus, percentages in cytokine-positive cells do not fit perfectly between fresh and fixed samples, probably due to longer exposure times to the stimulus of the fresh samples and the different sensitivity of particular cytokines to brefeldin and monensin[511]. Anyhow, the CV was below 20% for almost all cytokine staining, showing long stability and low inter-assay variability in as small blood volume as 500ul.

The use of a reference sample in MC studies becomes necessary when multiple barcoded batches are run. This reference sample can then be used with confidence to normalize data across multiple runs as shown before[434,512]. Our study provides the way to preserve a reference sample up to 13 months, showing remarkable sample stability in both phenotyping and cytokine studies. Even low abundant cells like $CD1c^+$ cDC, transitional B cells and pDCs, as well as their cytokine responses could be quantified with high confidence in as small volume of blood as 500 ul. The three less abundant cell populations had CVs higher than 20%: NKTs, which increased with time, (suggesting increased nonspecific binding), plasmablasts; and $CD141^+$ cDCs. It is noteworthy that the remarkable stability of the staining was also due to the use of stable and unique batches of antibody cocktails: Duraclone tubes for FC and frozen cocktail aliquots for MC reference samples. CV values are not solely an indication of stating quality, but also represent the variation of antibody cocktail batches. Hence the more effort is put to control of the experimental variables, a better reproducibility of the results will be obtained, as also shown in this manuscript. Additionally, the results demonstrate the need for proper selection of the preservation protocol, depending on the studied markers. In our experience results from different fixation protocols should not be analyzed together, especially when targeting cytokines. Thus, proper experiment design is a key to obtain good reproducibility. In our setting a remarkable sample stability was obtained for over a year, but it is worth mentioning that longer stability up to 3 years was reported[491], suggesting that once

preserved, samples can be stable for a longer time. In this study we used EDTA-tubes, however the protocols should be verified when using different types of anticoagulants, as they can differently affect marker and cell preservation[513–515]. As previous studies using BD[489] and PROT[394] were done using heparinized blood, it is possible that the time of preservation will not be affected by this anti-coagulant.

In summary, we demonstrated that immunophenotyping and cytokine response studies can be successfully performed with small amounts of fixed/frozen blood. Immediate whole blood sample fixation will benefit from shorter manipulation, hence preventing cell death specially in the neutrophil compartment. However, careful selection of suitable buffers and compatible antibodies are absolutely required. Antibody provider websites and databases like[393] can be helpful when building the antibody panels. The samples can be comparable only if they were prepared with the same standardized protocol. The setting presented here allows to perform retrospective studies and is a good solution when Palladium-based sample barcoding is required[419] in combination with a reference sample. Therefore, it brings another important contribution to experimental reproducibility and run-to-run comparability, both in research and clinical studies for phenotyping or cell response monitoring.

7 Data processing workflow for large-scale immune monitoring studies by mass cytometry

7.1 Material and methods

7.1.1 Study participants and whole blood processing

Two human healthy donors were enrolled under a protocol approved by the Ethical Committee of Centro Granada (CEI-Granada) according to the Helsinki declaration of 1975, as revised in 2013. All donors signed an informed consent according to the ethical protocol of the Andalusian Biobank and the PRECISESADS project. The Granada node of the Andalusian Health System Biobank collected whole blood samples in EDTA-K3 vacutainer tubes. Samples were processed following the protocol described[492]. Briefly, 10 ml of blood from two healthy donors was collected using EDTA-K3 vacutainer tubes, and 1.5 ml was diluted 1:1 with RPMI (Gibco) and stimulated with four different Toll-like receptor agonists: R848 (resiquimod, RSQ, 1.25 µg/ml, Invivogen), R837 (imiquimod, IMQ, 2.5 µg/ml, Invivogen), lipopolysaccharide (LPS, 0.05 µg/ml, Invivogen), ODN2006 (CpG, 2 µM, Invivogen) and medium alone (UNS). The stimulations were performed for 6h in the presence of Protein Transport Inhibitor Cocktail 1X (Thermo Fisher Scientific) to prevent intracellular cytokine exocytosis. After stimulation, live/dead staining was performed using cisplatin (CisPt, 5 µM), for 5 min at RT. Blood cells were fixed with 4.2 ml of Proteomic Stabilizer (Smart Tube Inc) and 3 aliquots of 2.4 ml of each stimulation were frozen and kept at -80°C until staining.

The reference sample consisted in 2 ml of whole blood of donor 2 stimulated with RSQ and processed as described above. Four aliquots of 2.4 ml were frozen. The RSQ agonist was chosen as reference stimulation since it induced the expression of all the studied cytokines across multiple cell populations of interest in previous analysis (laboratory data).

7.1.2 Cell staining and sample acquisition on CyTOF/Helios instrument

Fixed blood samples were thawed at 3 different days in batches including all the simulations for both individuals together with an aliquot of the reference sample (see Table 6). In total 11 samples were stained and acquired in each staining batch, and the experiment was repeated for a total of 3 times (Figure 24).

Table 6 Sample metadata

Barcode	ID	Stimulation	Batch
2	p1	RSQ	day1
3		UNS	
4		IMQ	
5		CpG	
6		LPS	
9	p2	RSQ	
10		UNS	
11		IMQ	
12		CpG	
13		LPS	
15	REF	RSQ	
6	p1	RSQ	day2
7		UNS	
8		IMQ	
9		CpG	
10		LPS	
12	p2	RSQ	
13		UNS	
14		IMQ	
15		CpG	
16		LPS	
17	REF	RSQ	
8	p1	RSQ	day3
9		UNS	
10		IMQ	
11		CpG	
12		LPS	
14	p2	RSQ	
15		UNS	
16		IMQ	
17		CpG	
18		LPS	
19	REF	RSQ	

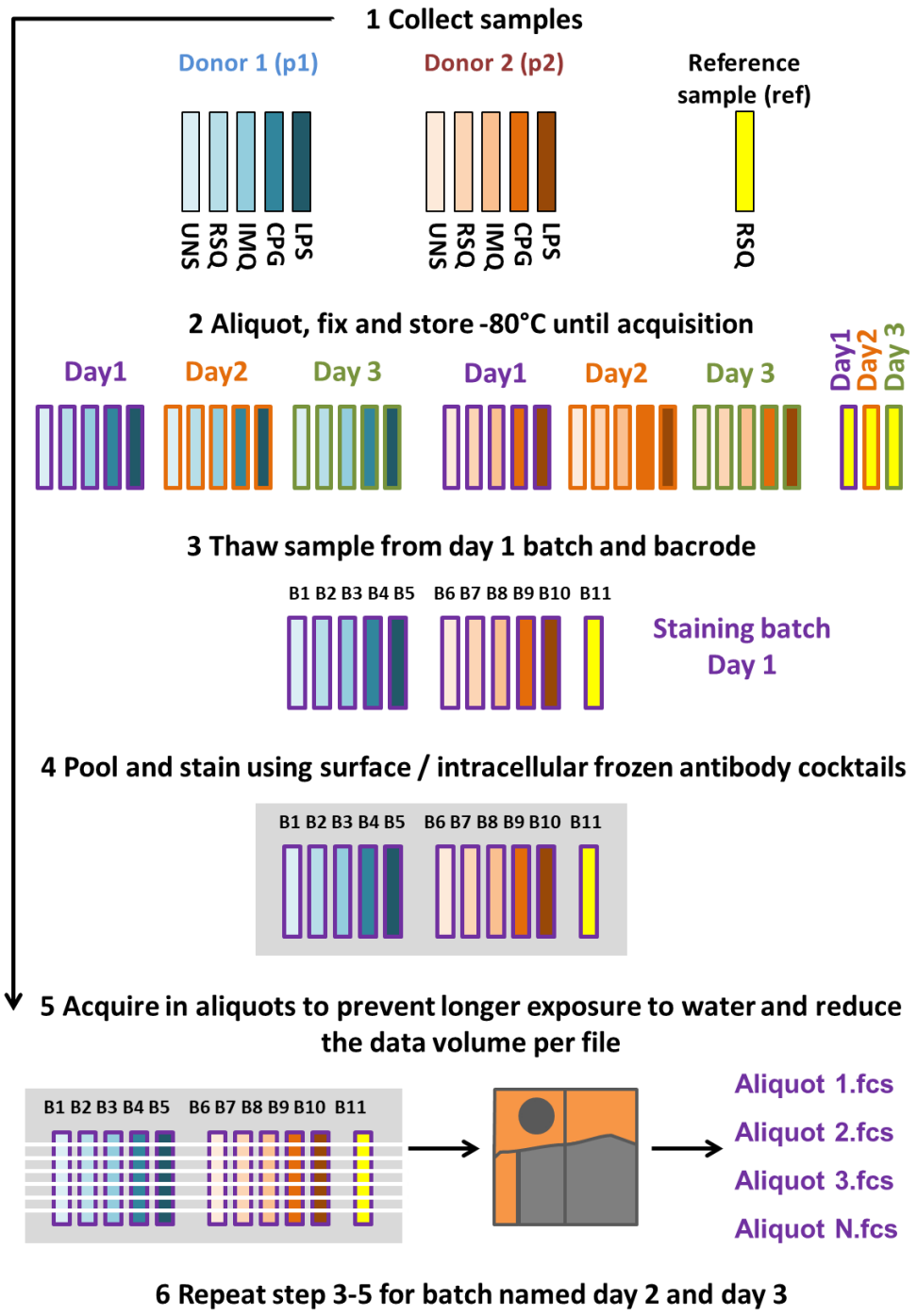

Figure 24 Experimental set up.

(Step 1) Blood from two donors (p1 – shade of blues and p2 – shade of reds) was stimulated with 4 different stimulations agents or left unstimulated. Reference (yellow) sample was stimulated with RSQ. (Step 2) Samples were assigned to three different acquisition batches (day 1, day 2, day 3, marked by different border colors) representing all biological groups, fixed, aliquoted, and stored at -80°C until the time of acquisition. (Step 3) On the 3 consecutive experimental days samples for each batch were thawed (here represented by day1), and barcoded. (Step 4) next were pooled and stained using frozen cocktail of antibody. (Step 5) Barcoded samples were aliquoted (represented by white separation line) and acquired on CyTOF, generating Aliquots.fcs files (Step 6). The staining procedure and acquisition was repeated for two other batches, named day 2 and day 3 on different days.

To minimize experimental variation two frozen antibody cocktails were prepared (for surface and cytokine staining, respectively), aliquoted and stored at -80°C until the day of the staining, as described in[400,492]. Antibody cocktails are shown in Table 7. Most of the antibodies were obtained in a labeled form from Fluidigm. Alternatively, purified antibodies were conjugated using MaxPar Metal-labeling kits (Fluidigm), following the vendor protocol.

Blood samples were thawed as described in [492] and 1.5*10 cells per sample were barcoded. The barcoding was performed using Palladium-based barcoding (Fluidigm, see Table 6) as follows: cells were washed with Barcoding Perm Buffer and stained with the barcode in 500 µl of the same buffer for 20 min at RT, followed by a total of 3 washes with Cell Staining Buffer (CSB, Fluidigm). Samples were then pooled and surface antigens were stained with the surface panel (phenotyping markers, Table 7) in CSB for 30 min at 4°C at a density of $5*10^7$ cells/ml. Afterwards, cells were washed with Perm-S buffer (Fluidigm) and labeled for intracellular cytokines (functional markers, Table 7), for 30 min at 4°C. Next, cells were washed with CSB and stained with Iridium (Ir, 5 µM) for 20 min in Fix and Perm Buffer (Fluidigm), washed with CSB and left overnight (O/N) in 2.75 ml of freshly prepared 2% formaldehyde (PFA) (Thermo Fisher Scientific).

The following day, CyTOF acquisition was performed in aliquots. Briefly, aliquots of 250 µl were washed with CSB, followed by a wash with MiliQ water. The aliquots were resuspended at $8*10^5$/ml in water together with EQ Four Element Calibration Beads (Fluidigm) and acquired in a CyTOF2/Helios device using a NB sample injector. The flow rate was set below 400 events/s and each aliquot was acquired for no longer than 2h. Around 11 aliquots per barcoded batch were acquired.

Table 7 Antibody panel, marker and probe types used in staining and analysis

Antigen	Clone	Metal	Phenotyping markers	Functional markers	Source	Staining
CD3	UCHT1	115In	X		ThermoFisher	Surface
CD45	HI30	141Pr	X		Fluidigm	Surface
CD19	HIB19	142Nd	X		Fluidigm	Surface
CD123	6H6	143Nd	X		Fluidigm	Surface
CD4	RPA-T4	145Nd	X		Fluidigm	Surface
IgD	IA6-2	146Nd	X		Fluidigm	Surface
CD20	2H7	147Sm	X		Fluidigm	Surface
CD66a/c/e	ASL-32	149Sm	X		Fluidigm	Surface
CD14	M5E2	151Eu	X		Fluidigm	Surface
CD7	CD7-6B7	153Eu	X		Fluidigm	Surface
CD3	UCHT1	154Sm	X		Fluidigm	Surface
CD1c	L161	154Sm	X		Biolegend	Surface
CD45RA	HI100	155Gd	X		Fluidigm	Surface
CD27	L128	158Gd	X		Fluidigm	Surface
CD11C	Bu15	159Tb	X		Fluidigm	Surface
CD38	HIT2	167Er	X		Fluidigm	Surface
CD8	SK1	168Er	X		Fluidigm	Surface
CD24	ML5	169Tm	X		Fluidigm	Surface
CD141	1A4	173Yb	X		Fluidigm	Surface
HLA-DR	L243	174Yb	X		Fluidigm	Surface
CD56	N901	176Yb	X		Fluidigm	Surface
CD16	3G8	209Bi	X		Fluidigm	Surface
CD41	HIP8	89Y	X		Fluidigm	Surface
IL-2	MQ1-17H12	144Nd		X	Fluidigm	Intracellular
IL-17	BL168	148Nd		X	Fluidigm	Intracellular
MIP1β	D21-1351	150Nd		X	Fluidigm	Intracellular
TNFα	Mab11	152Sm		X	Fluidigm	Intracellular
IL-6	MQ2-13AS	156Gd		X	Fluidigm	Intracellular
IFNα	LT27:295	160Gd		X	Miltenyi	Intracellular
IL-23p19	23dcdp	161Dy		X	Fluidigm	Intracellular
TGFβ	TW4-6H10	163Dy		X	Fluidigm	Intracellular
IL-10	JES3-9D7	166Er		X	Fluidigm	Intracellular
IL-12p70	REA123	170Gd		X	Miltenyi	Intracellular
GranzymeB	GB11	171Yb		X	Fluidigm	Intracellular
MCP1	5D3-F7	175Lu		X	BD Biosciences	Intracellular
CisPt	-	195Pt	Live/dead cells		Sigma	Intracellular
DNA1	-	191Ir	Nucleated cells		Fluidigm	Intracellular
DNA2	-	193Ir	Nucleated cells		Fluidigm	Intracellular
Bead	-	140Ce	Beads		Fluidigm	-

7.1.3 Data analysis

The fcs files were pre-processed using an in-house R script pipeline built through the assembly of several algorithms. The R script, functions and packages necessary for its installation can be found in github CyTOF_analysis_pipeline (https://github.com/prybakowska/CyTOF_analysis_Pipeline1), and the example fcs files are deposed on flowrepository[505] with the accession id FR-FCM-Z3YR. Additionally, metadata (*meta_data.csv*) and FlowJo gating workspace (*gating_strategy.wsp*) can be found in the

Attachments section in flowrepository experiment, and can be downloaded to reproduce the results.

Fcs fileswere first normalized using the `bead_normalized()` function, which uses `normCytof()` function from the *CATALYST* package[516]. Firstly, a baseline file was generated by the aggregation of 25,000 cells per file using the in-house function `baseline_file()`. This file was further used to compute baseline beads values to which all the files were normalized. The following settings for `normCytof()` were used: *dvs* beads, that were set to be removed post-normalization, *norm_to* was set to the baseline flow frame generated above, transformation was set to FALSE and plot to TRUE. Plots for marker visualization across all normalized files were generated using the `plot_marker_quantiles()` function, which takes advantage of *ggplot2* package[517].

Flow rate examination and signal cleaning were done using `clean_flow_rate()` and `clean_signal()` functions, respectively. For flowrate cleaning we used functions from *flowAI*[416] package with the TIMESTEP adaptation to 1 bin per 10 seconds and alpha set to 0.01. For signal cleaning the *flowcut* package (https://github.com/jmeskas/flowCut) was used with 1000 segments *MaxPercCut* set to 0.5. The parameters *UseOnlyWorstChannels*, *AlwaysClean* and *AllowFlaggedRerun* were set to TRUE.

The outlier detection was done using the wrapper function `file_quality_check()`. This function calls the FlowSOM clustering[496], which serves as an input for the Average Overlap Frequency (AOF) algorithm[405]. The FlowSOM was built using a 10x10 grid and 10 metaclusters. We calculated AOF scores per aliquot and batch using `greedyCytometryAof()` function, with the default parameters from the *cytutils* package (https://github.com/ismms-himc/cytutils), and Scaled and Quality AOF using the formula presented in[393]. Next, we estimated the mean of Quality AOF scores taking into consideration the scores calculated for all the fcs files. We considered as outliers those files with Quality AOF scores > mean + 3 standard deviations (SD). Heatmaps were generated using the *pheatmap* package.

For file debarcoding we applied the `debarcode_files()` function, which uses *CATALYST* debarcoding functions (`assignPrelim()`, `estCutoffs()`, and `plotYields()`), although we introduced the possibility to include minimal separation thresholds.

File aggregation was done using an in-house function called *`aggregate_files()`* and gating for Gaussian parameters and event length were performed using *CyTOFClean* package (https://github.com/JimboMahoney/cytofclean). Additionally, intact and viable cells were

gated using `gate_intact_cells()` and `gate_live_cells()` functions which use *flowDensity* package with `deGate()` function[428]. The parameters depend on the marker to be gated and are discussed below.

CytoNorm package[512] was used to normalize files using a reference sample, and data were normalized without FlowSOM clustering using 5 and 95 percentile and *limit* parameter set to 0 and 8.

The batch effects were visualized using `plot_batch()` function, which performs UMAP dimensional reduction[443], from *uwot* package and *ggplot2.* Prior to dimensional reduction, files were aggregated using 1000 cells per file to reduce data size and speed up the analysis time. The *`umap()`* function was applied with default settings. Additionally `plot_marker_quantiles()` function was used to visualize the differences before and after normalization. Cell population frequencies and MSI of phenotyping and functional markers were extracted using FlowSOM algorithm[496] and used to track batch effects, as well. Briefly, 50,000 cells per file were randomly selected, aggregated and arcsine transformed. FlowSOM was built using default parameters for grid and 35 metaclusters. Phenotyping channels (see Table 7) were used to build the model. Next, cell frequencies and MSI for phenotyping and functional markers were extracted for clusters and metaclusters. Zero-imputation was used for MSI values of clusters without cells as shown before[463]. Only the MSI values with SD > 0.2 per marker and cluster/metacluster were used. The data were further analyzed with UMAP and visualized with *ggplot2* package.

UMAP was also used for data exploration with 5000 cells aggregated per file. To map cell labels on UMAP, the aggregated file was manually gated using FlowJo software (10.0.7). FlowJo workspace was next read in R using *CytoML*[518], *flowWorkspace*[425] and *OpenCyto*[519] packages.

The figures can be reproduced using the data uploaded to FlowRepository and the code is deposited in github, however we noticed some differences when running the script on Linux or Windows operating systems. This was due to the difference in the floating numbers generated after the 14th decimal. The R session information with package versions can be found in Figure 25.

```
R version 4.0.3 (2020-10-10)
Platform: x86_64-pc-linux-gnu (64-bit)
Running under: Ubuntu 18.04.5 LTS

Matrix products: default
BLAS:   /usr/lib/x86_64-linux-gnu/blas/libblas.so.3.7.1
LAPACK: /usr/lib/x86_64-linux-gnu/lapack/liblapack.so.3.7.1

locale:
 [1] LC_CTYPE=en_US.UTF-8       LC_NUMERIC=C               LC_TIME=es_ES.UTF-8        LC_COLLATE=en_US.UTF-8     LC_MONETARY=es_ES.UTF-8
LC_MESSAGES=en_US.UTF-8
 [7] LC_PAPER=es_ES.UTF-8       LC_NAME=C                  LC_ADDRESS=C               LC_TELEPHONE=C
LC_MEASUREMENT=es_ES.UTF-8 LC_IDENTIFICATION=C

attached base packages:
 [1] tcltk     parallel  stats4    stats     graphics  grDevices utils     datasets  methods   base

other attached packages:
 [1] sessioninfo_1.1.1          pals_1.6                   CytoML_2.3.1               ggpubr_0.4.0               RColorBrewer_1.1-2
 [6] forcats_0.5.0              dplyr_1.0.2                purrr_0.3.4                readr_1.3.1                tidyr_1.1.2
[11] tibble_3.0.4               tidyverse_1.3.0            uwot_0.1.8                 Matrix_1.2-18              cytofclean_1.0.2
[16] scales_1.1.1               cowplot_1.1.0              tcltk2_1.2-11              pheatmap_1.0.12            cytutils_0.1.0
[21] devtools_2.3.1             usethis_1.6.1              stringr_1.4.0              flowCut_0.99.27            flowAI_1.18.5
[26] CytoNorm_0.0.5             remotes_2.2.0              ggplot2_3.3.3              FlowSOM_1.20.0             igraph_1.2.5
[31] flowCore_2.2.0             flowDensity_1.22.0         CATALYST_1.12.2            SingleCellExperiment_1.10.1
SummarizedExperiment_1.18.2
[36] DelayedArray_0.14.1        matrixStats_0.57.0         Biobase_2.50.0             GenomicRanges_1.40.0       GenomeInfoDb_1.24.2
[41] IRanges_2.22.2             S4Vectors_0.28.1           BiocGenerics_0.36.0        FlowRepositoryR_1.20.0

loaded via a namespace (and not attached):
  [1] flowWorkspace_4.2.0        knitr_1.29                 irlba_2.3.3                multcomp_1.4-13            data.table_1.13.6
  [6] RCurl_1.98-1.2             generics_0.1.0             callr_3.5.1                TH.data_1.0-10             xml2_1.3.2
 [11] lubridate_1.7.9            assertthat_0.2.1           viridis_0.5.1              xfun_0.16                  hms_0.5.3
 [16] evaluate_0.14              fansi_0.4.1                caTools_1.18.0             dbplyr_1.4.4               readxl_1.3.1
 [21] Rgraphviz_2.34.0           DBI_1.1.0                  ellipsis_0.3.1             ggcyto_1.18.0              backports_1.1.9
 [26] cytolib_2.2.0              RcppParallel_5.0.2         RSEIS_3.9-3                vctrs_0.3.6                GEOmap_2.4-4
 [31] Cairo_1.5-12.2             abind_1.4-5                withr_2.3.0                aws.signature_0.6.0        RPMG_2.2-3
 [36] prettyunits_1.1.1          cluster_2.1.0              splancs_2.01-40            dotCall64_1.0-0            crayon_1.3.4
 [41] drc_3.0-1                  pkgconfig_2.0.3            vipor_0.4.5                pkgload_1.1.0              changepoint_2.2.2
 [46] rlang_0.4.10               lifecycle_0.2.0            sandwich_2.5-1             modelr_0.1.8               rsvd_1.0.3
 [51] dichromat_2.0-0            cellranger_1.1.0           rprojroot_2.0.2            graph_1.68.0               carData_3.0-4
 [56] zoo_1.8-8                  reprex_0.3.0               base64enc_0.1-3            beeswarm_0.2.3             ggridges_0.5.2
 [61] GlobalOptions_0.1.2        processx_3.4.5             png_0.1-7                  viridisLite_0.3.0          rjson_0.2.20
 [66] bitops_1.0-6               ConsensusClusterPlus_1.52.0 KernSmooth_2.23-17        spam_2.5-1                 blob_1.2.1
 [71] DelayedMatrixStats_1.10.1  shape_1.4.4                jpeg_0.1-8.1               rstatix_0.6.0              ggsignif_0.6.0
 [76] aws.s3_0.3.21              memoise_1.1.0              magrittr_2.0.1             plyr_1.8.6                 hexbin_1.28.1
 [81] gplots_3.0.4               gdata_2.18.0               zlibbioc_1.36.0            compiler_4.0.3             RFOC_3.4-6
 [86] plotrix_3.7-8              clue_0.3-58                cli_2.2.0                  XVector_0.28.0             ncdfFlow_2.36.0
 [91] ps_1.5.0                   MASS_7.3-53                tidyselect_1.1.0           stringi_1.4.6              RProtoBufLib_2.2.0
 [96] yaml_2.2.1                 BiocSingular_1.4.0         latticeExtra_0.6-29        ggrepel_0.8.2              grid_4.0.3
[101] tools_4.0.3                rio_0.5.16                 circlize_0.4.10            rstudioapi_0.13            foreign_0.8-80
[106] gridExtra_2.3              MBA_0.0-9                  Rtsne_0.15                 digest_0.6.27              BiocManager_1.30.10
[111] rgeos_0.5-3                Rcpp_1.0.5                 car_3.0-9                  broom_0.7.1                httr_1.4.2
[116] IDPmisc_1.1.20             ComplexHeatmap_2.4.3       colorspace_2.0-0           rvest_0.3.6                XML_3.99-0.5
[121] fs_1.5.0                   splines_4.0.3              fields_10.3                RBGL_1.66.0                scater_1.16.2
[126] sp_1.4-2                   mapproj_1.2.7              jsonlite_1.7.2             testthat_3.0.1             R6_2.5.0
[131] pillar_1.4.7               htmltools_0.5.0            nnls_1.4                   glue_1.4.2                 BiocParallel_1.22.0
[136] BiocNeighbors_1.6.0        class_7.3-17               codetools_0.2-16           maps_3.3.0                 pkgbuild_1.2.0
[141] tsne_0.1-3                 mvtnorm_1.1-1              lattice_0.20-41            flowViz_1.54.0             curl_4.3
[146] ggbeeswarm_0.6.0           Rwave_2.4-8                gtools_3.8.2               zip_2.1.1                  openxlsx_4.1.5
[151] survival_3.2-3             rmarkdown_2.3              desc_1.2.0                 munsell_0.5.0              e1071_1.7-3
[156] GetoptLong_1.0.2           GenomeInfoDbData_1.2.3     haven_2.3.1                reshape2_1.4.4             gtable_0.3.0
```

Figure 25 R session information

The figure represents packages used in the workflow.

7.2 Results and discussion

7.2.1 Analysis workflow

The analysis pipeline presented herein includes all the major steps necessary to process and clean collected data. However, it should be noted that although the presented tools significantly improve data quality, they cannot fully fix the improper design of the experiments, according to the rule *garbage-in, garbage-out*. We emphasize the importance of well-designed experiments and therefore we also present the experimental workflow (Figure 24) and protocol (Table 8), used to generate the fcs files for this manuscript.

Table 8 Protocol for high quality data preparation

Before starting the protocol	Staining and acquisition protocol
1. Calculate the number of samples that will be analyzed and the number of batches that will be acquired on CyTOF Comment: Estimate the number of samples required to prove or reject the hypothesis 2. Prepare all the reagent needed for the whole protocol using a limited number of lots. Aliquot those reagent requiring freezing. Comment: As the reagent expiration date might be a problem, check batch-to batch equivalence. 3. Design the antibody panel, conjugate antibodies if necessary, check cellular epitopes resistance to fixation if necessary, titrate each probe using the same experimental conditions[520] Comment: Titrate the antibody using a fixed number of cells, this way it will be easily scalable to experiments involving barcoding 4. Prepare a single big batch of antibody cocktails, stimulation agents and reference sample, aliquot and freeze at -80°C, as described [400,492] Comment: at least one extra aliquot should always be prepared. In the case of multicenter studies we recommend preparing all reagents in one central laboratory and ship them on dry ice to the rest of the centers 5. To limit experimental variability use barcoding when multiple samples are run in one batch Comments: Different barcoded approaches can be used [396,398,419,521,522]. Titrate barcoding reagent according to the number of cells used for staining 6. Design each acquisition batch ensuring even distribution of biological groups Comments: If multiple patient groups or culturing conditions are studied, each batch should contain a representation of each group, including healthy controls	1. Thaw selected blood samples assigned to the staining batch as described[492] a. Count cells b. Aliquot equal number of cells for each sample, in this protocol $1.5*10^6$ cells/sample 2. Barcode samples, in this protocol with palladium based barcoding a. Wash with Barcoding Perm buffer (BPB) b. Stain with barcoding reagent resuspended in 500 µl of BPB, 20 min RT c. Wash with CSB d. Pool all the samples in a single tube 3. Stain surface antigens with previously thawed surface antibody cocktail a. Resuspend cells at $5*10^7$ cells/ml with surface cocktail b. Incubate for 30 min 4°C 4. Stain intracellular antigens with previously thawed functional antibody cocktail a. Wash with Perm-S buffer b. Resuspend cells at $5*10^7$ cells/ml with the intracellular cocktail c. Incubate for 30 min 4°C 5. Stain DNA with Iridium solution a. Wash with CSB b. Incubate 20 min RT with 5 µM Ir in Fix and Perm buffer 6. Store in 2% PFA O/N a. Wash with CSB b. Resuspend in freshly prepared 2% PFA at $6*10^6$ cells/ml 7. Acquire on CyTOF2/Helios instrument in aliquots (if cells are acquired in water,or if reduction of data size is of interest) a. Take an aliquot of 250 µl b. Wash with CSB c. Wash with acquisition solution (AS) d. Resuspend at $8*10^5$/ml in AS e. Acquire in CyTOF2/Helios. Adjust the flow rate to the AS and the type of cells

The example data set used in this work contains whole blood samples collected from two individuals (p1 and p2). EDTA-K3 blood from each donor was stimulated with 4 different stimuli (RSQ, IMQ, LPS, CpG) or left unstimulated, as described in methods section. In total 10 samples (5 per donor) were aliquoted in triplicates, fixed and frozen to generate 3 staining batches. Every batch included 10 stimulated samples plus the reference sample, and was barcoded, resulting in 11 samples per staining and acquisition (Figure 24). After pooling the barcoded samples, they were stained with a cocktail of antibodies recognizing surface markers,

permeabilized and stained with an cocktail of antibodies recognizing intracellular cytokines (see Table 7). The samples were acquired the following day, as described above. Therefore, in total 3 acquisition batches were analyzed (day 1 to day 3). This experimental workflow can be scaled up for multibarcoded, multibatch and multicenter studies (Figure 26). Each barcoded experiment was acquired in aliquots, and 11-12 fcs files were generated each day using an NB sample injector.

For data curation we built an R-based pipeline. Although R studio and basic programming skills are required, we will point out which steps can be performed with standalone or user-friendly programs. The data analysis workflow can be seen in Figure 27.The pipeline starts with the aliquots collected for each acquisition batch. In total, this example data set contains 35 aliquots obtained in 3 acquisition batches (12 aliquots for day1, 12 aliquots for day2, 11 aliquots for day3). These aliquots are not aggregated until step 5 (Figure 27), as one-by-one file processing is more beneficial in the context of algorithms and computer capacity. However, if data are acquired in one big aliquot using a wide bore injector (WB), or in the case of FC or spectral cytometry (SC) experiments, and the computer resources are limited, the data can be split upfront into aliquots to generate a set of smaller files. The function to do this is provided and is called `split_big_flowFrames`. Alternatively they can be analyzed as a single big fcs file.

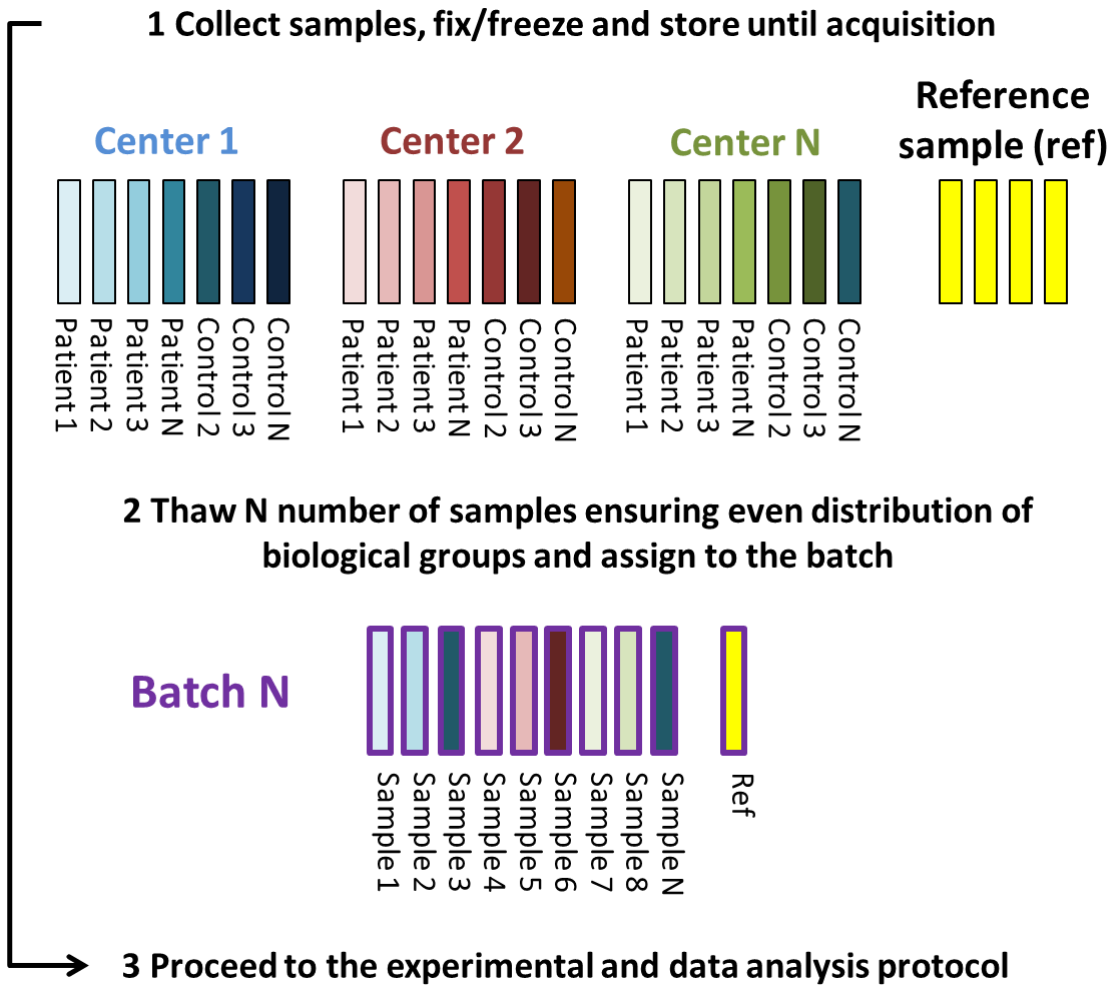

Figure 26 Experimental workflow proposed for big-scale multicenter, retrospective studies

(Step 1) Collection of samples at different centers (represented by different colors), fixation and freezing. Preparation of N reference sample aliquots equal to the number of batches to be acquired. (Step 2) Sample assignation to the staining batches ensuring even distribution of biological groups, here represented by patient and controls from each center, together with an aliquot of the reference sample. (Step 3) Experimental and data analysis workflow should be followed as a next step (Step 5, Figure 1).

As a first step, a bead-based normalization is performed, followed by flow rate and signal cleaning. Next, the bad quality aliquots are detected and removed from the data set. Cleaned files are then debarcoded, resulting in generation of 11 (# barcodes) x 35 files and at this point files from the same barcode and experimental day are aggregated. The gating of the fcs files is performed to remove doublets and dead cells and afterwards batch effect detection and normalization using the reference sample is performed. The data are further explored using dimensional reduction methods. To build this pipeline we gather already published algorithms and put them in the sequential order, that we believe is optimal for CyTOF data curation. We have also modified some steps to adjust these tools for CyTOF data or to improve their performance. These modifications will be highlighted along the workflow and some of them will be illustrated in the figures. We also provide wrapper functions for an easier use of the code. The workflow steps are prepared for CyTOF data, however as it is built in blocks, some of them can be skipped or adapted to FC or SC data. This will be also highlighted along the manuscript.

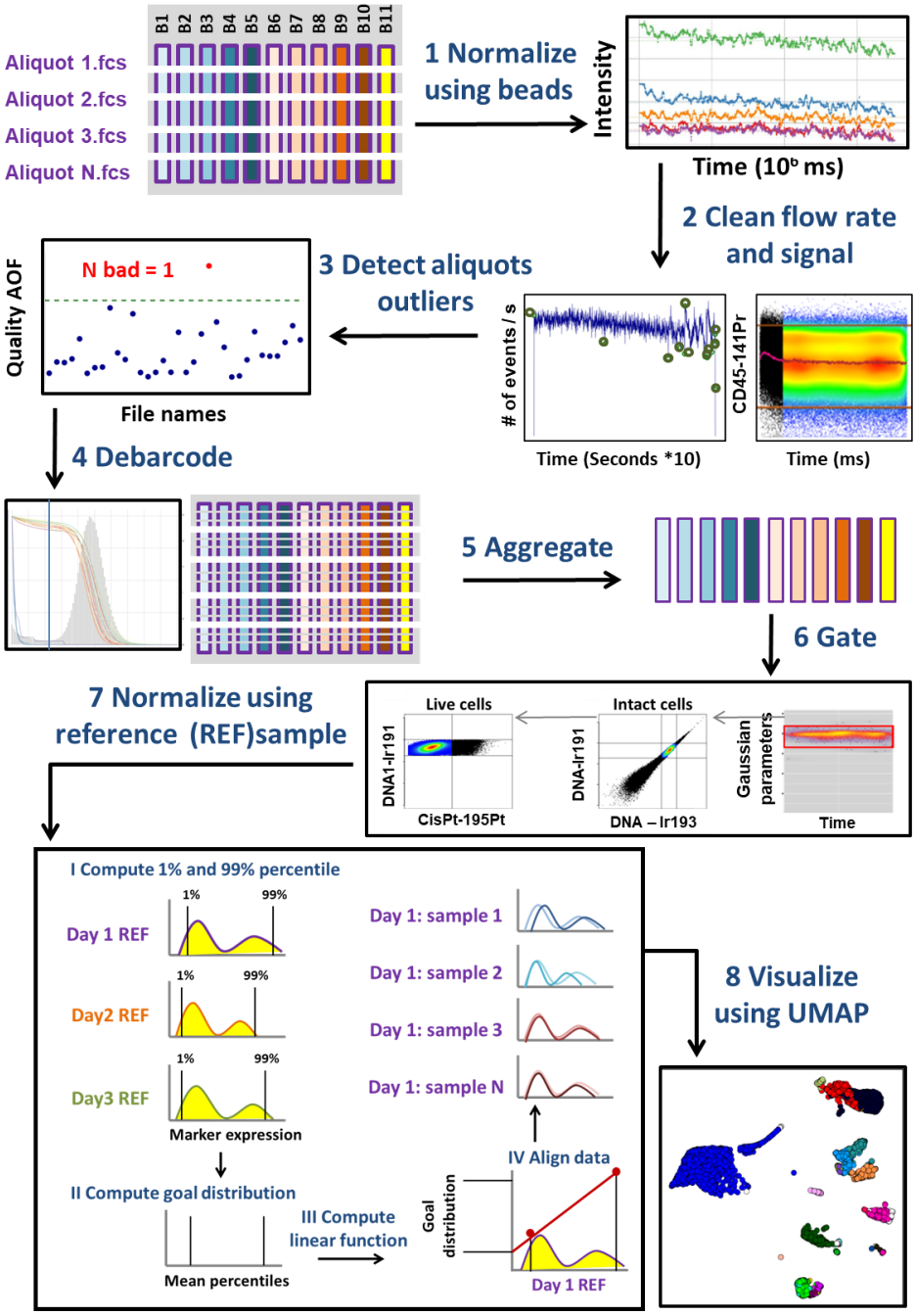

Figure 27 Computational pipeline.

Each barcoded batch was acquired in aliquots resulting in multiple .fcs files obtained from each experiment. Therefore, in this figure fcs files are called "Aliquot.fcs". We represent aliquots as 1…N for clarity. The colored rectangles indicate the aliquots together with their origin and are numbered with barcodes (B) from B1-B11 (as shown in Figure 24). The blue shade comes from p1 sample, red shades from p2 and yellow rectangle represents the reference sample. The purple border of each rectangle denotes Day 1 of the experiment. Each aliquot is processed individually until the aggregation step. The steps from 1 – 8 represent the blocks used in the R pipeline. First, bead normalization (Step 1), followed by flow rate and signal cleaning (Step 2) are performed. Next, the aliquot outliers are detected by calculating the Quality score and files with high score are discarded from further analysis (Step 3). Files are then debarcoded (Step 4) and aggregated (Step 5). Gating of Gaussian parameters and intact, live cells is performed (Step 6) and files are normalized using the reference samples collected in each batch (Step 7). In the data exploration (Step 8) cell populations are visualized using UMAP dimensionality reduction.

7.2.2 Bead-based normalization

The first step of data preprocessing is the bead-based normalization, performed for all collected aliquots. This step uses the signal of the EQ four element calibration beads acquired together with the sample [523] and the *CATALYST* package[516].

In the *CATALYST* package the function `normCytof` allows for the selection of the parameter *norm_to,* that requires an fcs file as an input. This file will be used as a baseline hence the rest of the files will be normalized according to its values. The selection of baseline file is important for proper data normalization and can be difficult when hundreds of files needs to be normalized to the same intensities. Therefore, in this pipeline we propose to aggregate all the collected fcs files in order to obtain the mean bead intensities across experimental aliquots and batches, as shown in Figure 28A. To avoid the generation of a big object, we used `baseline_file` function that first aggregated 25,000 randomly selected events per aliquot to obtain at least 200 beads per fcs file (the number of aggregated cells is user-defined). Next, using this aggregated file we created a baseline file for which bead mean intensities were calculated and used for aliquot normalization. In this way all the files were normalized to the global mean of the aggregated file, Figure 28A.

As an outcome, normalized files with suffix *beadNorm.fcs* were generated in a new subfolder called *BeadNorm*. The diagnostic plots for one aliquot were plotted in Figure 28B,C. Beads were gated as negative for Ir and highly positive for the bead channels 140Ce, 151Eu, 153Eu, 165Ho, 175Lu (Figure 28B). These events were further used for the estimation of the beads-derived normalization factor that will be applied to the channels selected by the users. The bead gate area can be adjusted by changing parameter *trim*, however for our samples the default parameter was good enough, as it properly gated all the necessary events. As shown in Figure 28C, normalized bead intensities became higher and more stable along the acquisition time.

Another important and novel step that we introduced is the verification of the behavior of the cell markers after bead-based normalization. This possibility is provided using the `plot_marker_quantiles()` function, giving a good insight of the homogeneity of the aliquots and the batch effects present in the data. Thus, to have an insight into normalization quality and its artifacts we recommend to plot all the markers that were chosen to be normalized and verify their expression before and after normalization as shown in Figure 28D for CD45RA. For this marker a slight signal decrease with the time of acquisition was observed, which was corrected by bead-based normalization. No significant differences were observed

between different acquisition days for this particular marker. This part of the code does not include a user-friendly interface, although data could be also normalized using the *premessa* package (https://github.com/ParkerICI/premessa/). It should be noted that this option is not automatic, and hence the user will need to define bead gates manually.

In FC, the data are not usually acquired with spike-in beads, and thus this step is not useful for FC users. However, the advantage of using Rainbow 8-peak beads (acquired just before samples acquisition) was recently published[524] in the context of day-to-day instrument variation correction for PRECISESADS[164] project. Therefore, this step could be introduced here and be beneficial for FC data quality. Alternatively the package *flowBeads* could be also used[525,526].

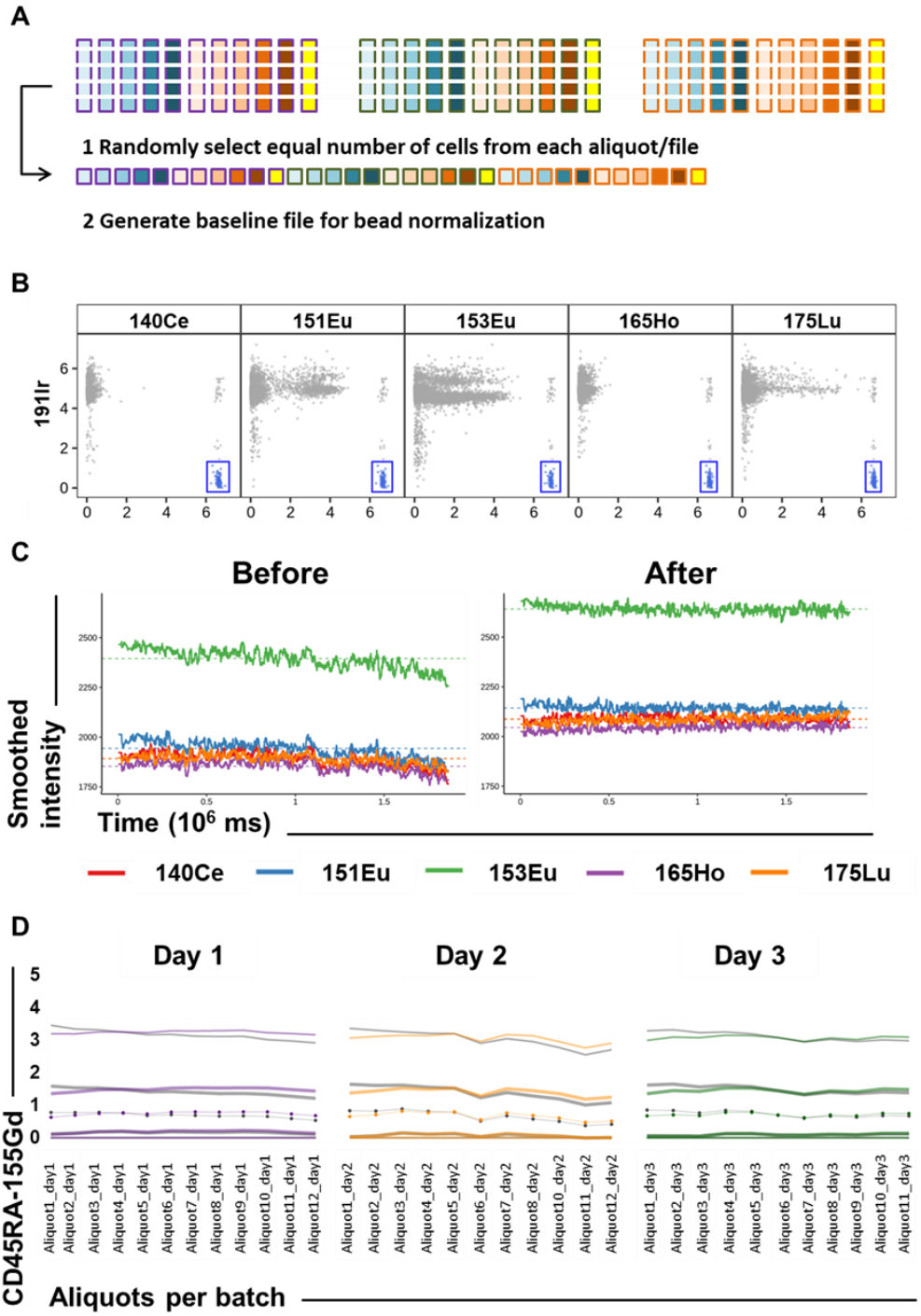

Figure 28 Bead-based normalization

(A) Randomly selected cells from each aliquot and each experimental day are aggregated to generate baseline files. Files are then normalized to the mean intensities of baseline file. (B) Dot plots generated using *CATALYST* package for one representative aliquot with arcsine transformed DNA channel (191Ir) on y-axis versus all bead channels (x-axis). The beads in the gated blue region are used for normalization. (C) Smoothed bead intensities in their positive channels along the time of acquisition for one representative aliquot. "Before" (left) and "After" (right) normalization data are plotted. (D) All aliquots are plotted for each acquisition day for CD45RA-155RA. The lines represent percentiles, circles represent median values, while thicker lines represent 25 and 75 percentiles. The thinner lines represent the 1 and 99 percentiles. Grey lines represent the percentiles before normalization, and colored lines after normalization.

7.2.3 Flow rate and signal cleaning

Sample acquisition using CyTOF instruments can suffer from clogs or sudden changes in the flow rate, which affects the quality of the data. Therefore, it is important to detect and clean these abnormalities. To do this we used two algorithms: *flowAI*[416] to spot flow rate irregularities and *flowCut*[417] to track signal instability. Since these two packages were initially created to clean FC data, this step can be also applied to fluorescence data with their default parameters.

The functions from these packages were adapted to the nature of the MC data and were written to wrapper functions `clean_flow_rate()` and `clean_signal()` for *flowAI* and *flowCut* respectively, although the user can still modify the original parameters.

The time resolution is different for FC/SC and MC data, thus, we modified the *TIMESTEP* parameter of *flowAI* to 1 bin per 10 seconds. As the acquired files contained high number of events per file (around 700,000) we also increased the *Segment* parameter (the number of events per bin) from 500 to 1,000 in *flowCut* setting. In this way we could spot bigger changes in the mean but still analyze sufficient number of segments to obtain a good statistic. The settings of these parameters are sensitive to the file size (number of events collected), and should be adjusted according to the user needs. If less cells were acquired per file, less events should be analyzed per segment. The same is applied for the removal of small or big changes in the mean signal, the bigger the segment the bigger mean changes can be removed. Thus, this parameter is data-specific and should be carefully adjusted in the case of barcoded or big fcs files. We also increased the *MaxPercCut* (the maximum percentage of cells to be removed) from 0.3 to 0.5 in order to ensure that most of the bad quality events will be removed. This parameter setting depends on the quality of the data but also on the number of events that users can tolerate to loose, and therefore it should be adjusted carefully. We set the parameter *UseOnlyWorstChannel*, and *AllowFlaggedRerun* to TRUE. This is because in the multiparametric MC data bad quality events in some channels can be missed when taking into consideration the statistic across all the channels (as it is the case in *flowCut*). To be stricter in the cleaning, we enabled this parameter. As it can occur that some other channel will have signals severely affected and won't get cleaned when a predefined channel is selected, we allow the algorithm to re-run the cleaning after the first bad quality events are removed. The setting of these parameters will depend on the data quality and the number of markers used. We also forced the algorithm to always clean the data, by setting *AlwaysClean* parameter to TRUE, as we did not observe any excessive cleaning in high-quality files; instead some small

signal disturbances were efficiently cleaned. We did not observe any benefits in changing other parameters, and therefore the rest of them were set as default. These tools were firstly created for FC studies, thus same reasoning about the parameter setting can also be applied to high-dimensional FC data. If FC or SC data are run the *data_type* parameter should be changed to "FC". This will automatically switch algorithms parameters to the original FC-optimal setting.

This step generated a new folder called *Cleaned,* containing clean files with suffix *cleaned.fcs*. Additionally, two subfolders were created called *FlowRateCleaning* and *SignalCleaning* having 1 plot per file for both flow rate and signal cleaning, as shown in Figure 29. These plots are convenient to check the quality of the signal across the markers and flow rate, and also the level of the cleaning achieved. Therefore, we recommend verifying if all the low-quality events are removed from the data, and to re-adjust the parameters when required. Example plots for flow rate and signal cleaning in one sample aliquot are shown in Figure 29A and 3B. It can be observed that the anomalies occurred just at the beginning of the acquisition, when probably the flowrate was still unstable, and also at the end of the acquisition when more fluctuation typically occurs. This can be a sign of some cell clogging, sample degradation or the tube getting empty. As can be seen in Figure 29B, overall a good quality signal was observed even in the worst channel (CD66ace). The indices removed at the end of the signal correspond with the flow rate abnormalities, confirming some problems at the end of the aliquot acquisition.

flowAI can be run in a user-friendly mode, and therefore no programming skills are required. On the other hand, *flowCut* can only be used through R language. Alternatively, *flowAI* can be used as a signal cleaning tool, however in our experience it is too stringent for MC data because it removes too many acceptable events (data not shown).

It can be argued that some events can be removed from the data due to their original properties. However, cells acquired either in MC or in FC/SC are homogenously distributed in the sample and thus across the "Time" parameter during acquisition. As those algorithms divide data into bins, and each bin represent the mixture of all cells, it is highly unlikely that some specific type of cells will be removed from the file.

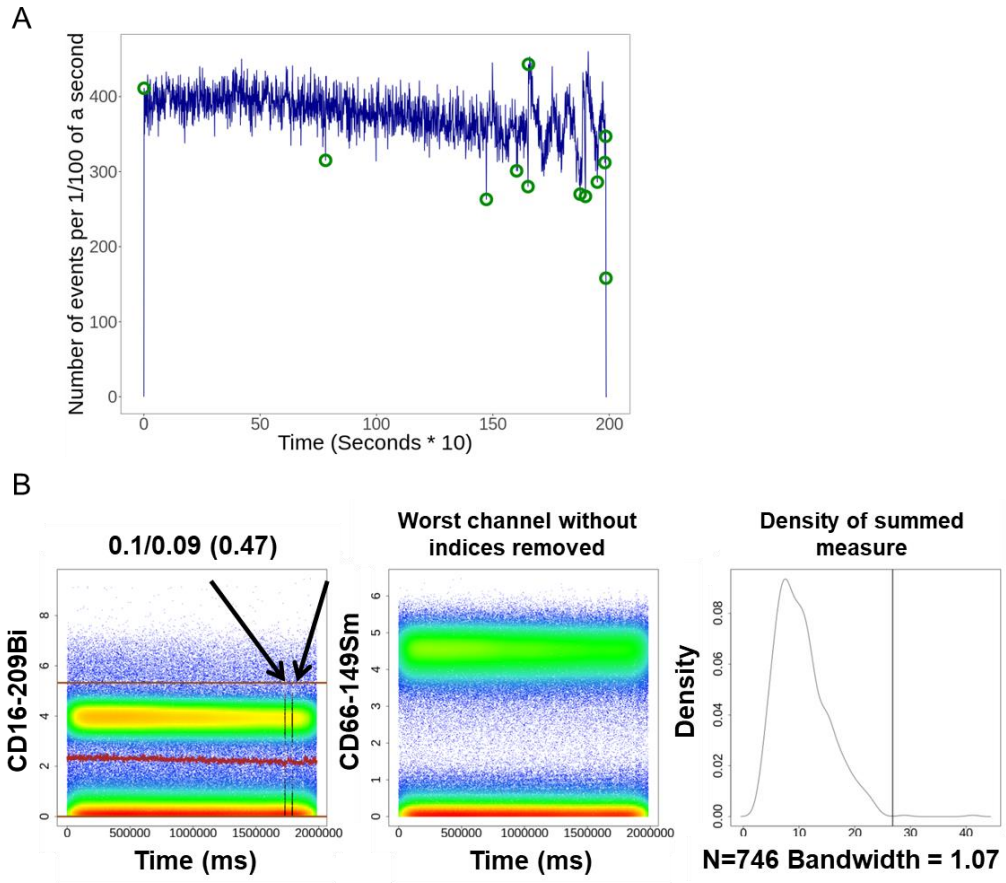

Figure 29 Flow rate and signal cleaning

(A) Flow rate of one representative aliquot using *flowAI*. The x-axis represents the time of acquisition in seconds and the y-axis the number of events acquired per 1/100 second. The green circles indicate the outliers that were detected by the *flowAI* algorithm and removed from further analysis. (B) Signal cleaning for the aliquot shown in A using *flowCut*. The first two dot plots on the x-axis represents the time of acquisition in milliseconds (ms) and the y-axis the arcsine transformed intensity for cleaned CD16-209Bi and CD66ace-149Sm detected as the worst channel. For CD16 plots, the arrows indicate the indices removed from the analysis, and the numbers above the plots the mean change before and after cleaning and the maximum mean change for this aliquot. On the right panel, histogram representing the summed measures of mean, median, several percentiles, skewness, and variation of the flow signal, parameters used by the *flowCut* algorithm. The vertical line represents the threshold for event removal.

7.2.4 Aliquot outlier detection

As mentioned before, in order to obtain a sufficient number of high-quality events during long acquisitions, barcoded data are acquired in aliquots. For this reason, sudden changes in detector sensitivity or problems with instruments like unexpected shut-down can happen, requiring additional tuning. Thus, it is advisable to verify the quality and channel intensities of the different aliquots acquired in each acquisition batch. To do this, we took advantage of AOF algorithms[405] that detect potential staining problems[393].

It is recommended to use AOF algorithm on gated or clustered events as input. In order to allow for automated quality check, we used FlowSOM[496] algorithm (Figure 30) to cluster the cells.

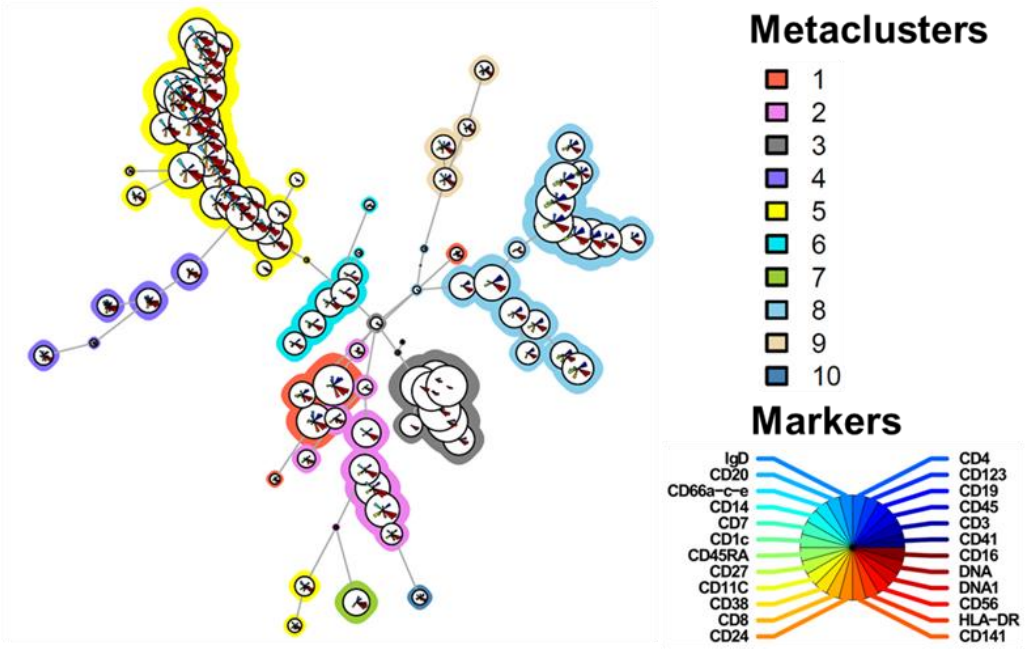

Figure 30 FlowSOM clustering

FlowSOM tree is represented by star charts. In each chart the mean expression of selected phenotyping markers is shown, the height of each part indicates the intensity of the marker. 10 metaclusters are denoted by background colors as shown in the legend on the right.

Upon clustering (using the phenotyping markers shown in Table 7), the AOF scores were calculated for each marker and scaled to obtain Scaled AOF scores as illustrated in Figure 31A and described in[393]. These scores were summed for each aliquot, and the Quality AOF score was obtained for each fcs file as shown in Figure 31B. To detect outlier aliquots the mean for all the Quality AOF scores was calculated per all files. The files with Quality AOF score > mean + 3SD were considered as outliers and removed from further analysis.

If the data were acquired as single big barcoded samples we recommend to divide this file into segments and calculate the AOF and Quality score for each segment in order to spot signal decrease issues. If the user decides not to split the data, we advise to carefully inspect the files with high quality scores and markers with high AOF score across time. It can happen that upon

the long acquisition only a portion of the data is affected, thus some good quality part of the data can be used for further analysis, as shown before [393].

In this setting we use AOF to detect abnormalities in the aliquots. All the aliquot files have exactly the same cell distribution, and thus removing one outlier aliquot from the data does not remove any specific cell subpopulation. However, this algorithm can also be used to spot staining discrepancies (missing antibodies, lower staining index) across samples from different individuals or acquisition batches[405], and in this case the results should be carefully checked to make sure that the observed low quality scores are due to technical problems and not to sample-specific or cell-specific phenotypes. We also focused on phenotyping markers and not functional, cytokine markers, as the performance of this algorithm is optimal when using bimodal markers. By doing so we assumed that if some phenotyping markers are affected and sample was scored high, most of the markers will have poor resolution and will be difficult to analyze. For FlowSOM we used a small number of metaclusters (N=10) in order to detect and validate the marker expression in the main leucocyte populations, across homogenous aliquots. We reasoned that the less metaclusters, the less aliquot-specific clustering will occur, thus all the cells will be assigned to the same metacluster and the AOF calculation will be performed exactly for the same group of cells. FlowSOM parameters can be adjusted according to the sample diversity and user needs. To verify the quality of clustering, it can be useful to plot the FlowSOM tree, as shown in Figure 30. The range of the SD in the definition of the threshold can also be adjusted by the users, if necessary. We choose FlowSOM as a clustering method as it is the fastest and most accurate algorithm[461], however users are free to choose their own clustering algorithm to partition the data using the `greedyCytometryAOF()` function from *cytutils* package and next calculating scores with functions `scaled_aof_scores()` and `file_outlier_detecion()` from our pipeline.

This pipeline block is only available as R code. FC/SC data can also be analyzed, however, the arcsine transformation should be changed to a cofactor of 150 in the function `fsom_aof` and *aof_scoring*.

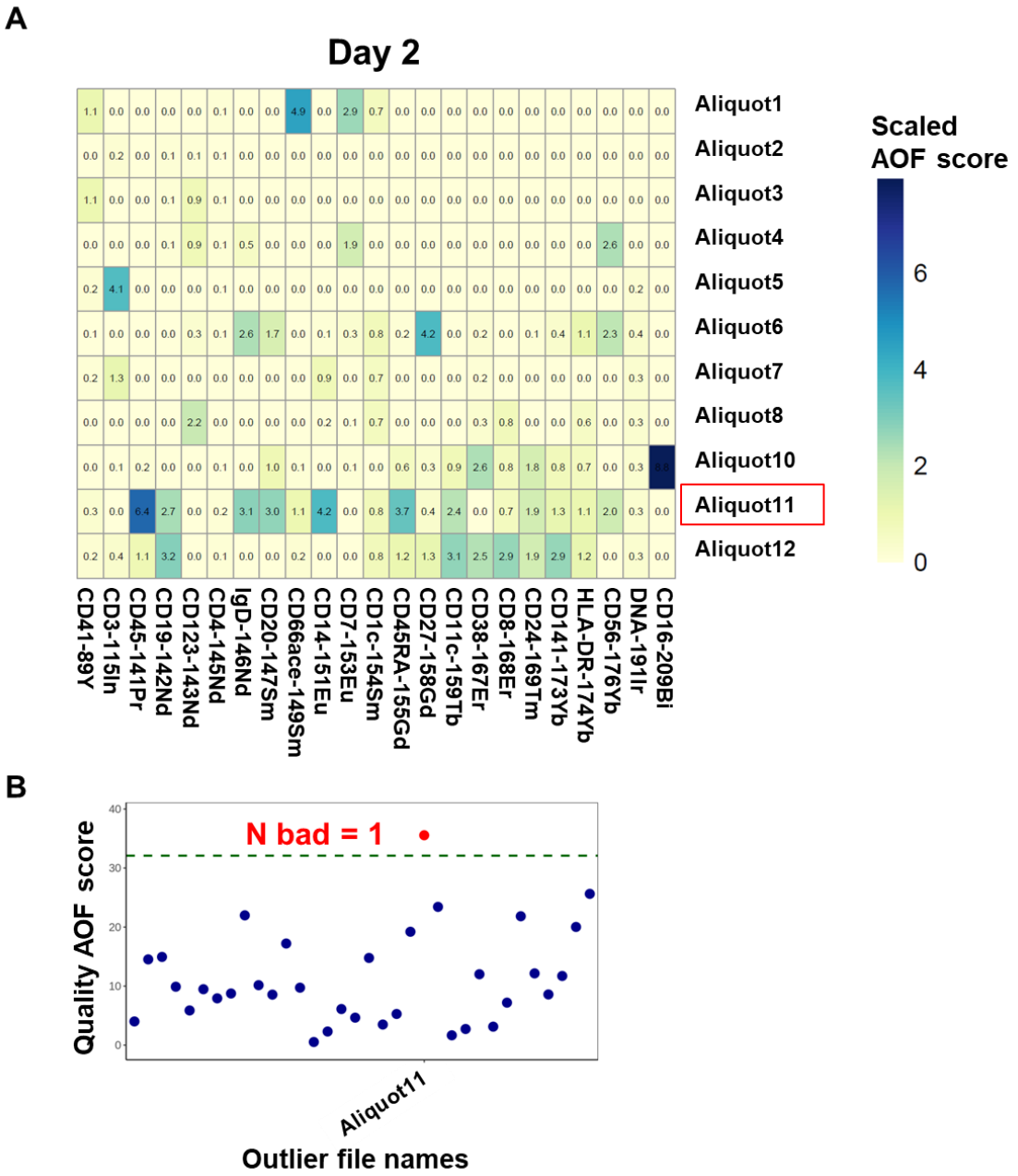

Figure 31 Oulieres detection

(A) Heatmap representation of Scaled AOF scores for each surface marker across all the aliquots collected on day 2. (B) Outliers detection. On the x-axis the file names marked as an outlier (aliquot 11 from day 2) and on the y-axis Quality AOF scores. The green dotted line represents the threshold for outlier definition. Dots represent scores for each aliquot, red dot is a file above the threshold.

7.2.5 File debarcoding

The samples included in this data set were barcoded with eleven different palladium-based barcodes. Therefore, in order to recover the individual sample information, we performed a data debarcoding step, using debarcoding functions from *CATALYST* package with the automated separation threshold identification setting. The generated files were stored in a

new subfolder called *Debarcoded* with the suffix *debarcoded.fcs*. Additionally, we introduced a minimal separation cutoff of 0.18, which ensured a safe separation threshold for files with unclear barcode distribution. File names with detected threshold values lower than 0.18 can be stored in an RDS file called *files_with_lower_debarcoding_threshold.RDS* if the parameter *less_than_th* is set to TRUE. The minimal separation threshold can be modified if necessary.

To verify the quality of debarcoding two plots were generated for every debarcoded sample using *CATALYST* package, as shown in Figure 32. The visualization of the separation between events positive or negative for the different Pd isotopes (see Figure 32A) is key to assess the correct sample assignation during debarcoding. The second plot allows the monitoring of the yield and cell count obtained with the chosen minimal separation cutoff (Figure 32B). We recommend reviewing all the plots generated upon debarcoding especially if the file names are stored in the *.RDS* file due to the assignation of separation threshold below to the minimum established.

In this protocol we used a 6-choose-3 scheme, resulting in maximum of 20 barcodes, and for the purpose of this work presentation we used 11 barcodes. However other approaches could also be taken, like 7-choose-3 (35 barcodes), CD45-based cadmium barcoding scheme recently offered by Fluidigm or the combination of commercial barcoding with monocisplatin isotopes (60 or even more barcodes)[521]. The parameter *bc_key* that defines the barcoding scheme would need to be re-designed by the users and adjusted to new isotopes. It should be noted that Zunder-based algorithm used in *CATALYST* package will correctly deconvolute the data if positive and negative populations are present, thus barcoding with serial dilution of amine reactive fluorescence dyes commonly used in FC multiplexing won't work in this case. For the FC/SC users we recommend to deconvolute the data by manual gating or using *flowClust* algorithm as previously described[527].

In our experience when using the barcoded approach presented here some barcode intensity problems can be noticed when dead cells and debris were present in excess (data not shown), a fact also observed before[396]. As reported[528], small polymer-palladium conjugates have high affinity to dead cells. Furthermore, a high amount of debris capture barcoding reagents and reduce the amount of complexes able to stain the cells of interest[419]. It is noteworthy that labeling with this barcoding reagent is sensitive to the number of cells, thus titration with the exact cell number is required. Accordingly, if a large amount of debris is present in the sample a reduction of the total amount of cells is recommended[419], alternatively if a lot of cells are available samples can be cleaned by a dead cell removal kit before barcoding. Additionally, the

use of saponin-based reagents requires sample fixation, which could be problematic when live cells are studied using fixation-sensitive markers. Alternatively, palladium barcoding using surface markers can also be considered[396,398,522]. In case of low separation between barcoded samples, manual gating could also be performed, alternatively clustering with cluster number equal to barcode number could also be tested[393].

A user-friendly application for debarcoding is provided by Fluidigm as a part of CyTOF software. However, it should be noted that this software estimates the separation threshold for all the files after aggregation, in contrast to the method proposed in this workflow. This global threshold is not always correct for all the samples and can lead to precious event loss. Additionally, it is only dedicated to palladium as barcoding channels cannot be manually defined. Instead the *premessa* package (https://github.com/ParkerICI/premessa/) could be used which allows the definition of barcodes in a user-friendly interface.

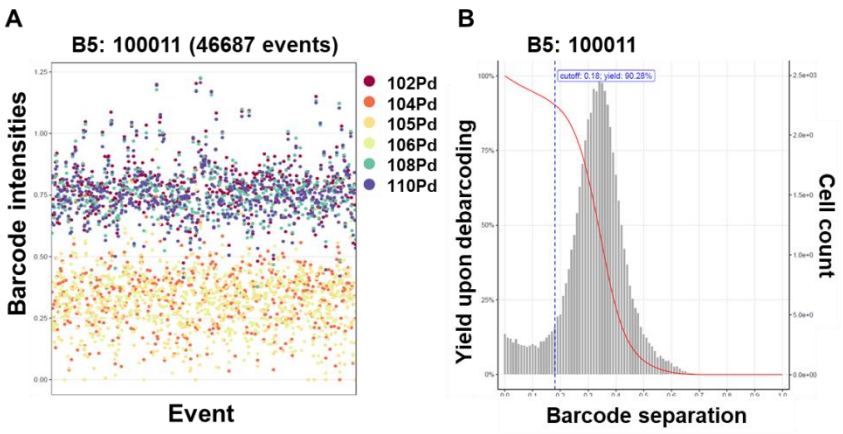

Figure 32 Debarcoding quality plots.

(A) All cell events assigned to barcode B5 (100011) are shown, with each cell event represented as a dot. The intensities for each palladium isotype are displayed on the y-axis with different colors. Each event is plotted on the x-axis. (B) Distribution of the events by separation distance (grey histogram) and the cell yield (red line) are displayed as a function of the separation threshold. The vertical, blue dotted line represents the cutoff for the separation threshold. The data for one representative aliquot is shown.

7.2.6 File aggregation

We performed file aggregation of the debarcoded aliquot files using an in-house function called `aggregate_files()`. To do this, the names of the files containing metadata (barcoding identity and staining batch) need to be provided as shown in the Table 6. The resulting aggregated files were stored in a folder called *Aggregated* and they contained the

sample-specific names provided in the metadata. If files were barcoded and acquired as one big aliquot (for example while using the WB injector or in FC or SC) and the computer power resources are limited we recommend to split them into smaller fcs files, preprocess, and then aggregate after the debarcoding step, as shown in this workflow. If the data do not require aggregation this part of the code can be skipped.

7.2.7 Cell gating

The aggregated files contained a mixture of events including dead cells, debris and doublets, which should be removed from further analysis. To do this we took advantage of *CyTOFClean* package (https://github.com/JimboMahoney/cytofclean) and *flowDensity*[428].

CyTOFClean is a user friendly R package that excludes doublets using event length and 4 Gaussian parameters: Center, Offset, Residual and Width (see Figure 33**A**), as described in[529]. Using the *flowDensity* package, the gating of intact cells is also provided with `gate_intact_cells()` function, and is based on the expression of DNA1 and DNA2 marker. Additionally the live/dead cells gating was applied by calling the `gate_live_cells()` function. Both gating strategies are shown in Figure 33**B**. In this example CisPt and ^{195}Pt channels were used to detect dead cells, but users can change these parameters accordingly to the live/dead marker chosen. This part of the code does not have graphical user interface (GUI) implementation, however the fcs files can be analyzed using standard softwares as FlowJo, and the resulting files could be exported to R. Alternatively, the packages *flowWorkspace*, *CytoML* and *openCyto* can be used to import the gating settings into R[425]. As an output *CC_gated.fcs* files and control plots were generated for each file in the *Gated* folder.

It is important to know that *CyTOFClean* is a closed GUI app and therefore no parameter can be adjusted without changing the application code. Inversely, all the parameters can be adjusted for *flowDensity*-based gating. The parameters that we modified for the analysis of this example dataset were *upper* and *use.upper* that defines which lower or upper inflection points of the density curve are analyzed and also *alpha* and *tinypeak.removal*, that specifies the significance of the change in the slope being detected and the inclusion/removal of tiny peaks in the density distribution respectively. The change in *alpha* parameter will affect the tightness of the gate, thus can be useful if less strict gate for the Ir channels is necessary.

In this workflow we introduced the common gating strategy used for nucleated cells stained with Ir. However, the gating strategy could change depending on the type of cells acquired and

the antibody panel configuration. This statement especially applies to the parameter "Event length" and "Ir" channels. The event length of each cell depends on the amount of metal that the cell is loaded with, thus the non-nucleated cells with only one probe have lower event length than nucleated cells with high number of probes directed to them. *CyTOFClean* package uses a density function to apply the cutoff for both event length and Gaussian parameters, thus it will gate on the cells where the majority of events are located as recommended for these gates[422] and rather undergate than overgate. Therefore it is suitable for NB and WB injectors despite the known differences in the event length[530]. Additionally, it introduces the thresholds 10 and 50 to exclude events below and upon these values respectively, if bad quality files are provided. Most of the cells are typically located in between these values, unless some contamination or low metal content cells are present, so the users should verify the event length of the cells of interest before the gating. In the case of non-nucleated cell analysis, the gating strategy for intact and live/dead cells should be changed and re-designed to fit the users' needs. The gating presented here is especially useful for human leukocytes stained with Ir, however could also be applied to other type of cells like mouse splenocytes.

The gating using "Event length" and Gaussian parameters will remove the doublets caused by fusion of ion clouds. However, the true cell aggregates will still remain in the fcs files. Barcoding with more than 2 probes per sample improves the quality of the data and helps to remove cellular aggregates when cells are coming from different barcoded samples. Unfortunately, aggregates within the same sample won't be cleaned, neither will be debris. Thus, to deal with this we use "Intact cell" gate to remove Ir^{low} events (debris) and Ir^{hi} events (aggregates). Cells late in the S, G_2 and M phases of the cycle can fall in the region of Ir^{hi} cells, due to their higher DNA content [531] and thus this algorithm can result in undesired cycling single cell removal. To avoid it we use a less strict gate at the upper part of Ir intensity. The use of markers specific to cell cycle in the antibody cocktail and automated clustering could also be helpful[531]. When using a less strict gate, care needs to be taken when analyzing the data, as some cell aggregates can still persist in the data and could be spotted upon gating or clustering, together with marker expression analysis. This gating is specific for MC data, and thus FC/SC users would need to apply their own gating strategy at this point. A good example of how to do it using R is published[532]. As mentioned before, as an alternative manual gating can be done using programs like FlowJo or FCS Express and then the population of interest can be imported into R. However, this can be time–consuming, especially when hundreds of files are processed. It is also known that manual analysis can be biased[533], and hence it is faster and

more robust to use automated approaches. Nevertheless, we recommend to always revise the quality of the obtained gating and optimize the parameters if necessary and possible.

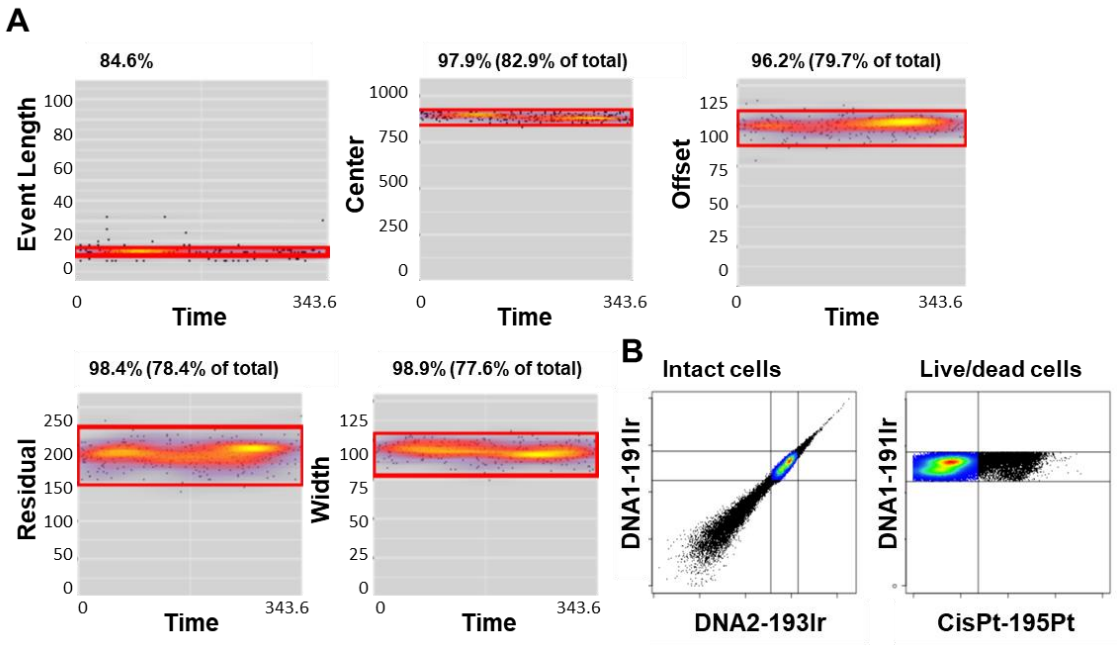

Figure 33 Cell gating. One representative file is shown.

(A) Doublet exclusion with *CleanCyTOF* package. "Event length" and Gaussian parameters ("Center", "Offset", "Residual", "Width") are represented on the y-axis against "Time" on the x-axis. Events that fall outside of the red gate are discarded form further analysis. (B) Gating for intact cells and live/dead cells using DNA and CisPt parameters and *flowDensity* package. The black events are removed from further analysis.

7.2.8 Batch normalization using the reference samples

Although bead-based normalization helps to normalize different acquisition batches, it uses the information of a limited set of channels. The correction factor is calculated using 5 bead channels and then extrapolated to the rest of the markers, hence there is a risk that some markers and cell specific changes are not precisely corrected. Even more, normalization using beads does not consider the experimental variation introduced during sample staining or manipulation (batch effects). Therefore, normalization with a reference sample that is present upon sample preparation and spans the whole spectrum of the channels used, is advisable. Because of this, as a last step in the preprocessing and quality control pipeline, we performed batch normalization using the *CytoNorm* package[512].

In contrast to *CytoNorm* default setting, instead of using quantile normalization (parameter *quantileValues* = 101) we computed 5% and 95% percentiles across the reference samples for

each marker and obtained the marker-specific goal distributions using the function `QuantileNorm.train()`. This was because quantiles normalization introduced artifacts (data not shown), as previously reported[434]. In our experience this setting was good enough for the correction needed, although in some particular cases the distribution of the signal won't be modelled sufficiently if only two quantiles are used. In this case the users can change *quantileValues* parameter accordingly. Additionally, the normalization was performed on unclustered data, as clustering can be biased by the variation potentially introduced in the raw data. If a big batch effect is observed upfront in the markers used for clustering, improper cluster assignation can also introduce artifacts. We set the parameter *limit* to 0-8, as recommended by the authors, to avoid the introduction of extreme values, like negative values that are normally absent in MC data. We normalized our data to the "mean" marker quantiles of reference sample, using *goal* parameter. However, this can be changed by the users and data can be normalized to one of the batch values or to specific quantile values. The goal distributions obtained in the first step were then used for marker-specific batch normalization using the function `QuantileNorm.normalize()` The scheme of the normalization process can be seen in Figure 27, step 7 and Figure 34A.

As output, fcs files with the new prefix *Norm* were generated together with several diagnostic plots. These files were stored in the new subfolder *CytofNormed*. An example of generated plots are shown in Figure 34 for the marker CD4 for the three days of acquisition. A shift in the 95% peak position can be seen especially on day 1. The mean for each intensity peak was estimated using data from the 3 days. This mean is called a goal distribution and was used to obtain normalized data distribution as shown Figure 34A. Furthermore, we provide a plot showing the expression of CD4 across samples by day of acquisition (Figure 34B). A downshift of the 95% percentile colored line can be seen for day 1 when compared to the 95% grey line (normalized). In contrast, a slight upshift can be noticed for day 2 and 3, giving comparable median intensities after normalization when looking for all 3 days. These correspond with the shifts seen for the density peaks. In the same way the plots for IL-6 are shown in Figure 35A, as an example for a functional marker normalization.

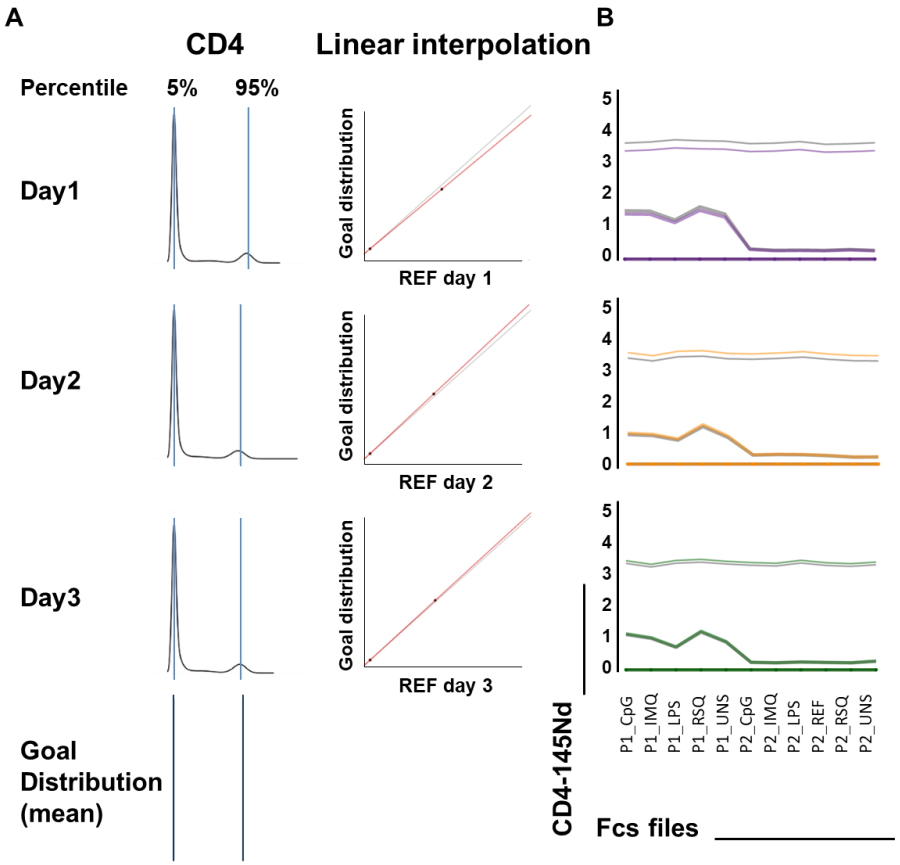

Figure 34 Normalization based on reference samples.

(A) Distribution of the CD4 marker for the reference sample on each staining day. Left panel, the 5% and 95% percentiles are represented by the blue vertical lines and the computed means for 3 experimental days are represented below in dark blue lines (goal distribution). Right panel, the linear function that transforms the result is represented with a red line and the grey line represents the identity function. If the red line is below the grey one, the values in the batch are decreased, and vice versa. (B) CD4 expression in the individual samples acquired in the three staining days is represented as in Figure 28D, 99% and 75% percentile lines can be seen. The rest of the quantiles have 0 values and thus are located at point 0 on the y-axis.

Batch effects are commonly monitored using dimensionality reduction methods, which allow the visualization of the cell distribution in each file in a single plot. In our pipeline we also provide the possibility to run UMAP dimensional reduction[443] as shown in Figure 35B. It can be appreciated that the cells from day1 were unevenly distributed before normalization, however the homogeneity of the cell distribution was improved after normalization and cells become uniformly mixed between acquisition days. The same can be observed when cell frequencies for clusters or metaclusters were extracted using FlowSOM algorithm, followed by dimensional reduction analysis, see Figure 35C and D respectively. It can be noticed that the batch effect is stronger at the cluster than at the metacluster levels, thus if researchers want to perform sample comparison in more detail, special care needs to be taken for batch effect adjustment.

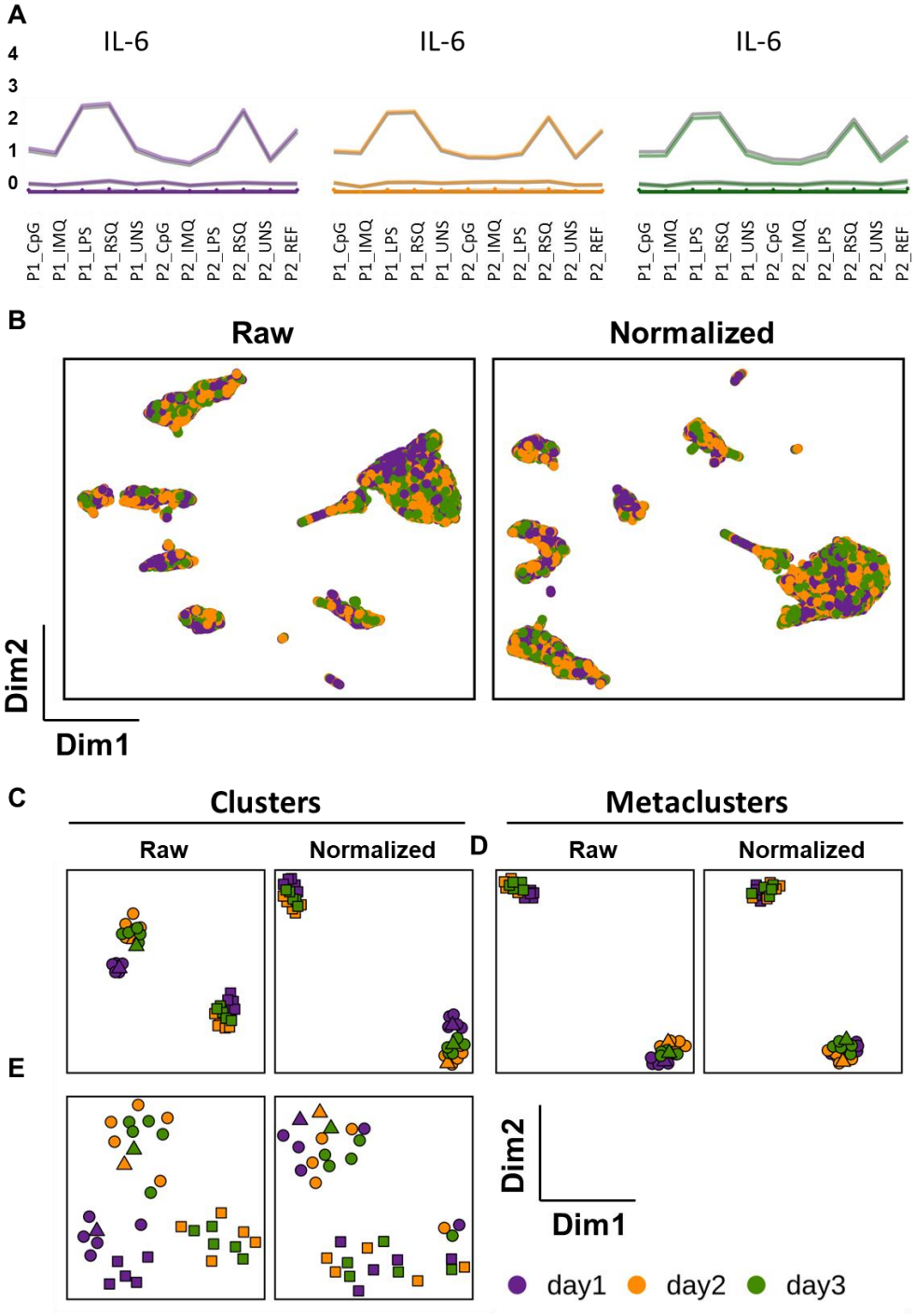

Figure 35 Batch effect representation.

(A) IL-6 expression in the individual samples acquired in the three staining days is represented as in Figure 34B, 99% and 75% percentile lines are shown. The rest of the quantiles have 0 values and thus are located at point 0 on the y-axis. (B) Scatter dot plots representing two dimensions from UMAP analysis. UMAP was built on aggregated files (1,000 cells from each fcs file) using default parameters and phenotyping markers (Table 7). Data are shown before (Raw) and after normalization (Normalized) with the reference sample. Cells are colored according to the staining day. (C, D) Dimensional reduction analysis with UMAP using cell frequencies extracted from FlowSOM analysis for clusters (C) or metacluster (D). (E) UMAP analysis using MSI of all markers extracted per FlowSOM cluster. (C,D,E) data were represented using scatter dot plot where x and y-axis represents 1st and 2nd dimension of UMAP and are colored as in B.

In general, no strong batch effect was observed in UMAP or cell frequency analysis where only phenotyping markers were used. To take a deeper look into functional markers and features more sensitive to batch effect, like marker intensities, we extracted median marker intensities (MSI) per cluster and metacluster and visualized sample distribution by dimensional reduction, Figure 36A (all the markers), B (functional markers) and Figure 35E. In Figure 36A it can be appreciated that the day 1 samples were differentiated from the rest, including the reference sample, but upon normalization they got intermixed with the corresponding donor samples. The references also got into close proximity. In this experiment, the blood was treated with 5 different conditions, hence sample grouping in accordance to the stimulation and not only to donor is expected. In panel B, grouping according to the donor and to the stimulation was observed after the normalization, but not before. These results showed that MSI is more sensitive to the experimental variation and it can be tracked and corrected when reference samples are included.

These results underscore that batch effect correction is a necessary step when multiple batches are acquired, even in well-controlled experiments, and especially when fine phenotyping and MSI values are of interest. In this example we used a reference sample that was always barcoded and stained along with other samples, but spike-in cells could also be used[401]. However, it should be noted that spike-in cells should be treated with the same experimental protocol and should be stained with one specific channel or antibody to allow for their identification, thus the sacrifice of one channel should be taken into consideration. If this solution is considered, additional gating step would need to be performed to identify and split the reference file. The reference sample is not commonly used in FC or SC, however this normalization could be also applied to fluorescence data and should improve the quality of the data in high-scale and longitudinal studies. The transformation cofactor should be changed in the *transformList* parameter and the *limit* should be set to default settings or adjusted to FC/SC data.

The *CytoNorm* function can be used as a plugin in FlowJo, as well as UMAP. Alternatively tSNE[439] can also be used for data exploration and detection of batch effects using platforms like Cytosplore [534]. The values for quantiles can be adjusted if necessary and FlowSOM clustering could also be introduced when no strong batch effect on phenotyping markers is observed. The extraction of cell population frequencies and MSI is a good way to track the differences between acquisition batches. In this example we used FlowSOM clustering, but any other tool or manual gating can be used. FlowSOM clustering can be used in FlowJo as a plugin.

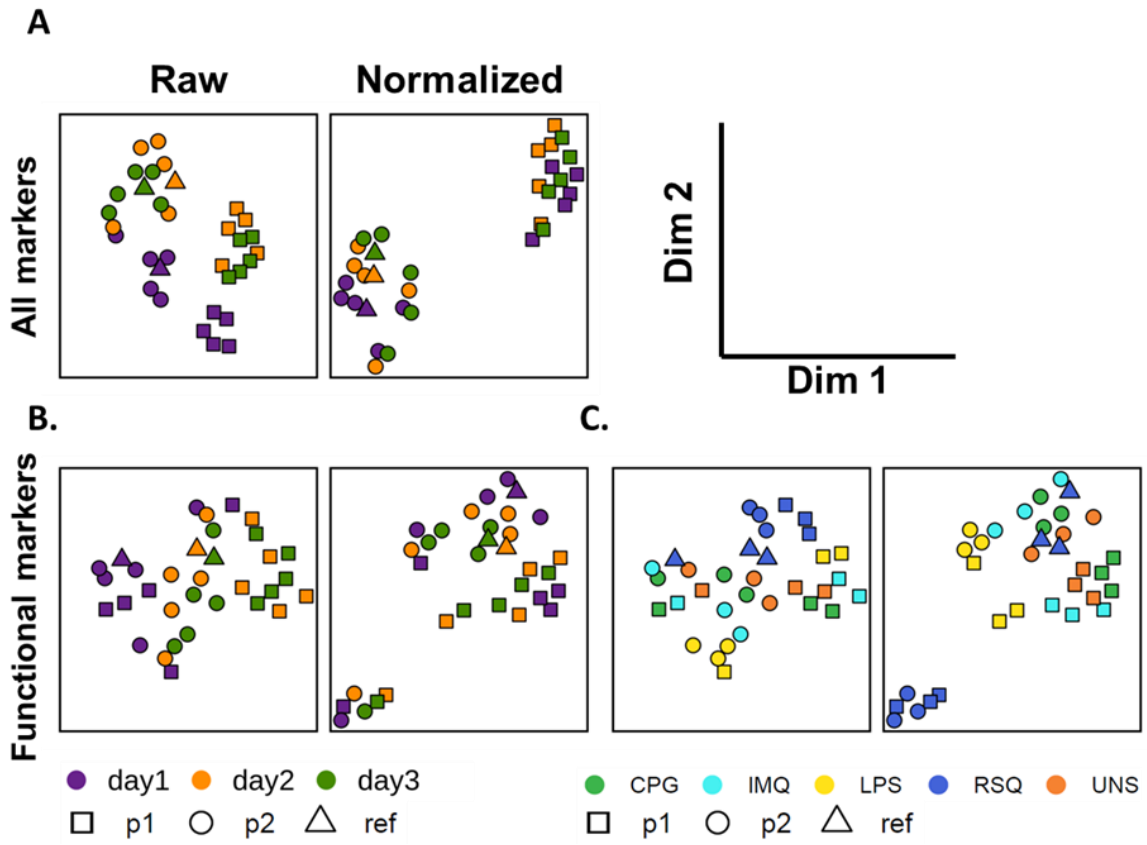

Figure 36 Batch effect visualization using MSI values.

Data were clustered using FlowSOM and MSI for each phenotyping and functional markers were extracted across all metaclusters. Next, dimensional reduction using UMAP was performed to verify sample distribution and data were represented as in Figure 35. (A) MSI for all the markers, (B, C) MSI for functional markers colored either by the day of acquisition or by the stimulation, respectively. Samples are colored by staining batch (A) and (B) or by stimulation (C). Donors are represented with shapes.

7.2.9 Data exploration

Finally, we explored the cleaned and normalized data using a dimensional reduction method. In this example we choose UMAP due to its good performance and ability to handle a large number of events in a relatively short time[454]. To speed up the analysis we aggregated 5000 cells per fcs file and performed a dimensional reduction using the phenotyping markers as input (see Table 7). In total 165,000 cells were used for the analysis. This allowed us to track marker expression across the studied individuals as shown in Figure 37A and to map them to the manually-gated populations as shown in Figure 37B.

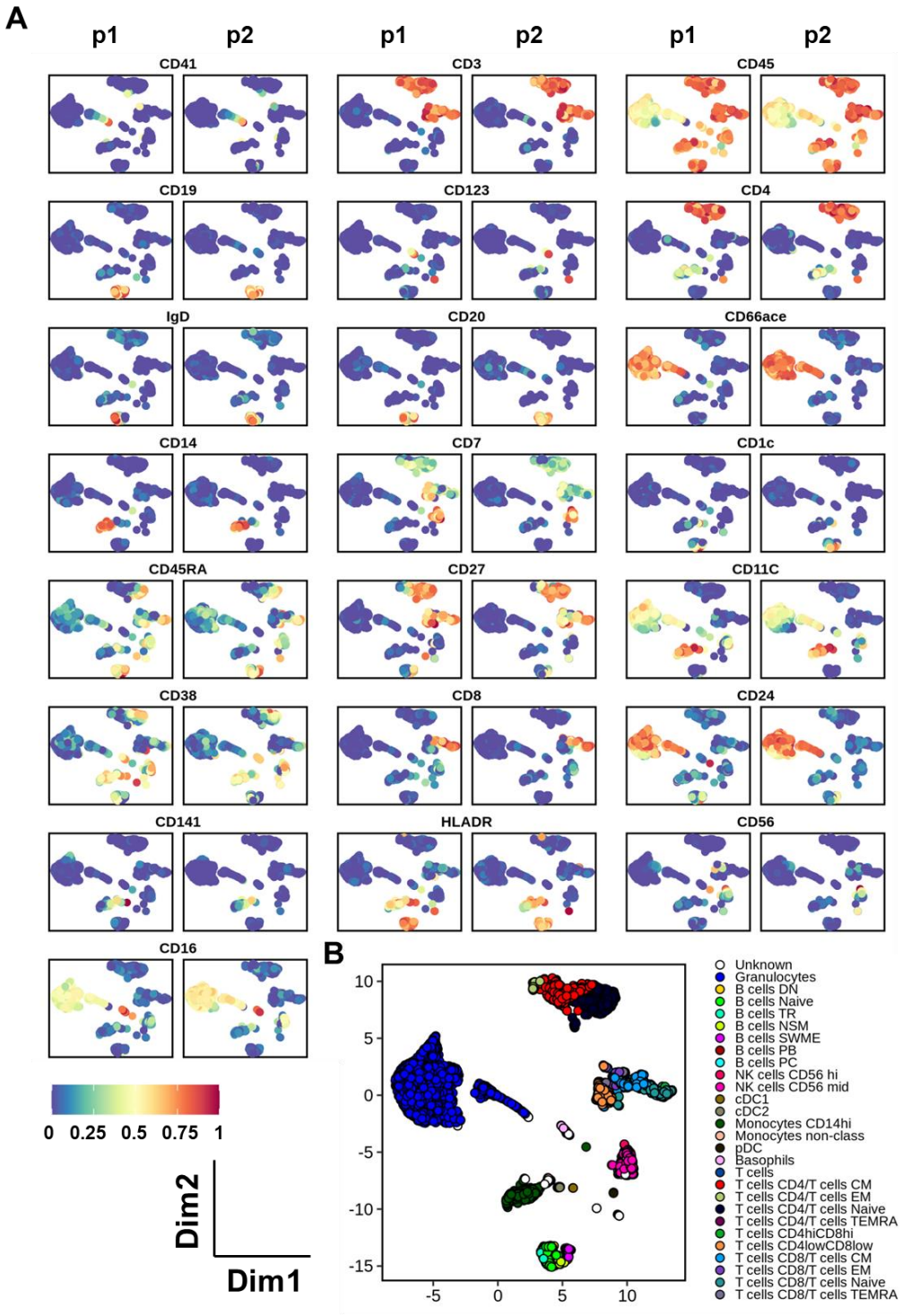

Figure 37 Data exploration by dimensional reduction using UMAP.

(A) UMAP was built on aggregated files (1000 cells from each file) using default parameters and phenotyping markers (Table 7). For the visualization purpose marker expression was 0-1 normalized. The expression of the phenotyping markers is shown in each plot for two individuals stimulated with RSQ on day 1. (B) UMAP colored by manual labels obtained upon gating as shown in Figure 38.

The manual gating strategy used can be found in Figure 38. Due to this approach we could explore the differences in sample frequencies (Figure 39A) and MSI expression of cytokine markers (B, C). In panel A the density of the different populations can be visualized, suggesting differences in the frequency of different populations between p1 and p2. Additionally, differences in the cytokine expression could be detected. For instance, after RSQ stimulation MIP1β was more expressed in p2, and the expression was restricted to monocytes and pDC and moderately to $CD16^{+}CD66ace^{+}$ granulocytes (Figure 39A). TNFα was expressed in pDC and some subsets of the monocyte compartment, and the intensity of TNFα was higher in pDC than in monocytes for p1, while this ratio was inversed in p2 (Figure 39B).

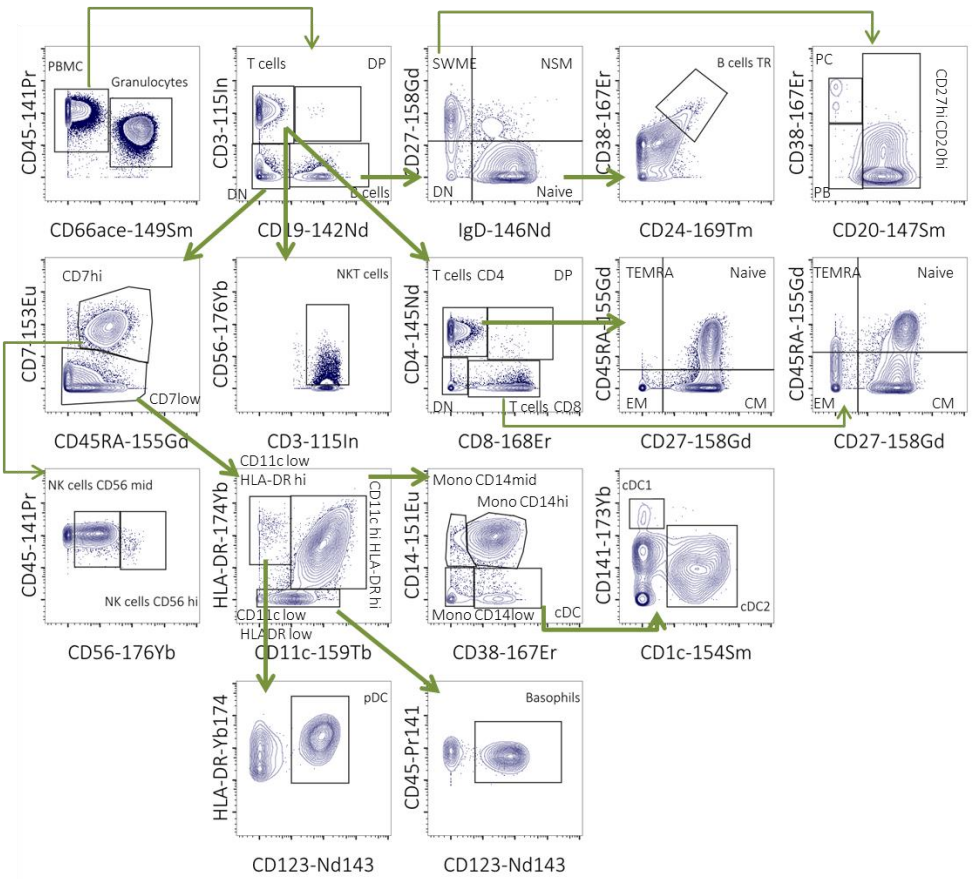

Figure 38 Gating strategy to obtain manual labels for UMAP analysis.

The manual labels were obtained using the aggregated file used for UMAP analysis. SWME – switched memory B cells, PC – Plasma cells, PB – Plasmablast, DP – double positive, DN – double negative, TR – Transitional B cells, TEMRA – Terminally differentiated T cells, CM – Central memory, EM – Effector memory, Mono – monocytes.

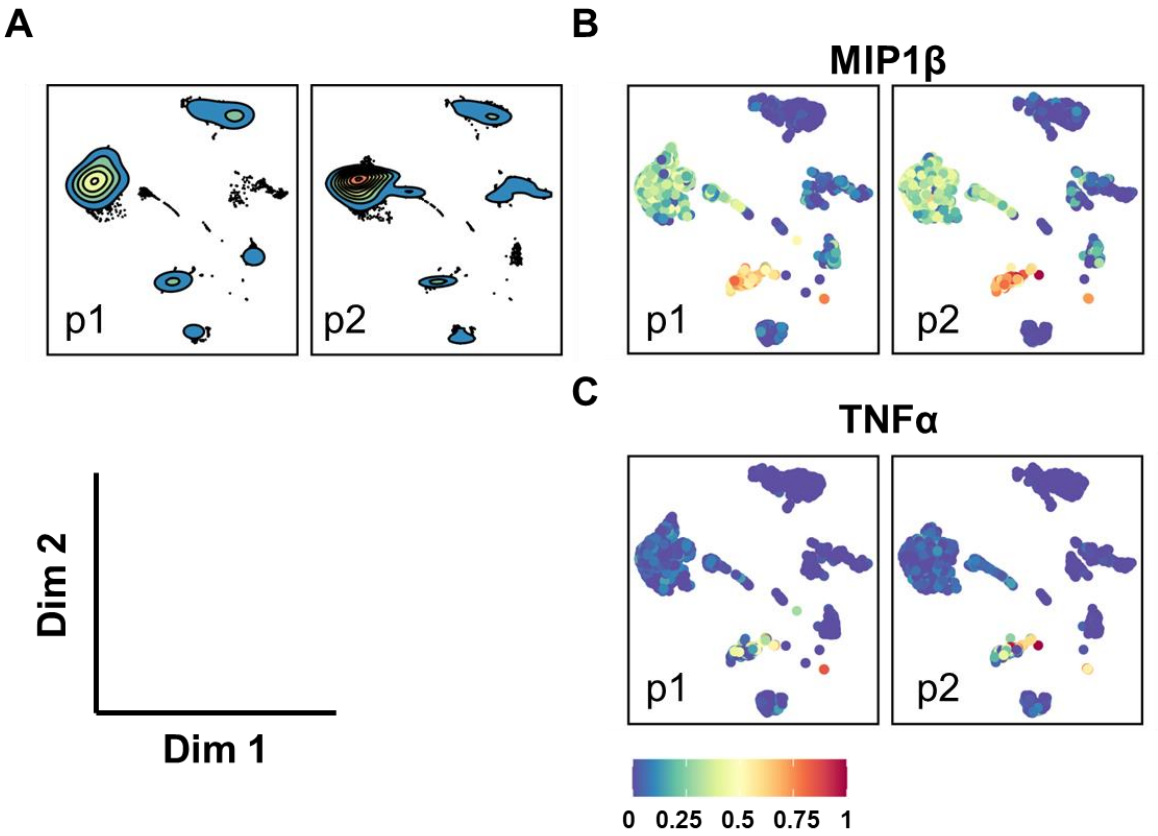

Figure 39 Data exploration by dimensional reduction using UMAP.

One thousand cells per file were aggregated. The UMAP was built with default parameters using phenotyping markers and scale set to TRUE. Samples stimulated with RSQ are visualized for 2 donors on day 1. (A) Equal number of cells are visualized by density plot for donors p1 and p2. (B, C) Dot plot showing 0-1 normalized, arcsine transformed expression of the cytokines MIP1β (B) and TNFα (C) for p1 and p2.

This basic data exploration can already give an insight into the internal diversity of the samples and give a first idea of the individual differences, although further analysis should be performed to verify the hypothesis generated before the experiments and upon data exploration. Data analysis and interpretation is dependent on the biological question raised, as was already discussed in different publications[497,534].

7.2.10 Preconditions, limitations and conclusions

Here we report an R-based data curation workflow that cleans collected data and correct the experimental variation introduced during the sample preparation and staining. This pipeline is semi-automated and optimized for large studies involving human blood phenotyping together with functional markers. To our knowledge this is the first data preprocessing pipeline that

gathers and optimizes all the tools necessary for the processing of MC data. It is especially useful for multibatch studies and can be also applied to multicenter settings. Since our experimental setting uses fixed and frozen whole blood samples, this pipeline is useful for retrospective multicenter studies, as discussed in[492]. The example data set and the code are provided to the users, thus each step can be reproduced. Although the data set provided here is limited in size, it is big enough to show the advantage and usefulness of each tool.

The analysis is performed in R environment without a user-friendly interface (except for part of the gating), thus basic programming skills are necessary and knowledge of R environment is mandatory. Although the workflow is presented as a script, we gathered all the tools into easy-to-use functions with detailed descriptions, thus we believe that inexperienced R users will be able to follow the steps and analyze their own data.

The function parameters are optimized for cellular studies, especially whole blood immune phenotyping studies by MC, but different samples such as bone marrow aspirates, PBMC or mouse splenocytes, can also be analyzed. This might require parameter adjustment that can be performed by the users. As in our gating strategy we are using the Ir parameter to detect genomic DNA, only nucleated cells are analyzed. For the batch correction it is mandatory to use the same reference sample stained and acquired on each experimental batch together with the samples. Otherwise the normalization proposed in this manuscript cannot be achieved and precious information contained in MSI should not be analyzed. This pipeline is specifically dedicated to mass cytometry data, however, some steps can also be used for FC and SC experiments with the adjustment suggested along this script. Some tools can be sensitive to the size of the fcs files processed, therefore we recommend to acquire data in aliquots, especially when the acquisition is performed in low ionic environments like water, or split them just before the preprocessing. This pipeline gives some insight about data exploration, but does not fully cover deep data analysis. The final interpretation of the data will depend on the question raised in every individual project.

8 Biomarker discovery and stratification of patients with SADs using mass cytometry

8.1 Material and methods

8.1.1 Study participants

Eligible patients were aged 18 or older and diagnosed as having one of the following SADs: SLE, SJS, SSC, RA, MCTD, PAPS, UCTD and CTR. Individuals were recruited in four recruitment centers (Reumatología and Enfermedades Sistémicas Services at the Hospital Universitario San Cecilio, Granada; Andalusian Health System Biobank, Granada; Reumatología Service at Hospital Universitario Reina Sofia, Córdoba). Each patient was diagnosed according to the prevailing international classification or diagnosis criteria established for each of the SADs[12–17]. As criteria for UCTD we considered patients with clinical features of SADs, but not fulfilling any of the diseases clinical criteria for RA, SSC, SJS, SLE, PAPS or MCTD, as previously described[18], or having any other SADs criteria for at least 2 years, with presence of antinuclear antibodies (ANA) ≥ 1:160 with or without other specific autoantibodies. Patients fulfilling 3 out of 11 SLE classification criteria and patients with early systemic sclerosis[19] were not classified as UCTD.

The main exclusion criteria were with high doses of immuno-suppressants 3 months prior to recruitment, cyclophosphamide or belimumab in the past 6 months or pregnancy. Eligible CTRs were matched on the projected and expected profile of patients in terms of age. All donors signed an informed consent according to the ethical protocol of the Andalusian Biobank and the PRECISESADS project. Exclusion and inclusion criteria are detailed in Table 9. Diagnosis distribution across centers, demographic information and prescriptions are given in Table 10.

Table 9 Main inclusion and exclusion criteria

Inclusion criteria	Exclusion criteria
For all patients	For all patients
- Male or female, aged ≥ 18 years with no upper limit - Diagnosed according the prevailing criteria for one of the following autoimmune diseases • Rheumatoid arthritis (RA) • Scleroderma or systemic sclerosis (SSC) • Primary Sjögren's syndrome (SJS) • Systemic lupus erythematosus (SLE) • Primary antiphospholipid syndrome (PAPS) • Mixed connective tissue disease (MCTD) • Patients with undifferentiated connective tissue disease (UCTD) for over 1 year and that do not fulfill the diagnosis of any of the above diseases. - Informed consent signed	- Neonatal lupus - Drug-induced lupus - Severe nephrotic syndrome with proteinuria ≥ 3,5 g/day - Patients with stable doses of steroids >15 mg/day for the last 3 months or with IV corticosteroids in the last 3 months - Patients under immunosuppressant treatment in the last 3 months prior to recruitment and patients with combined therapy using two or more immunosuppressants • Methotrexate ≥25mg/week • Azathioprine ≥2.5mg/kg/day • Cyclosporine A > 3mg/kg/day • Mycophenolate Mofetil > 2gr/day - Treatment with cyclophosphamide (any dose or route of administration) or belimumab in the past 6 months - Patients under depletative therapy such as rituximab in the last year - Chronic HBV or HCV infection - Patients who fulfil more than one clinical diagnostic criteria For controls - Individuals under chronic medication - Individuals suffering from any inflammatory autoimmune, allergic or infectious condition, and with a history of autoimmune disease, particularly thyroid disease or other diseases that may modify cellular profiles in blood.

Table 10 Cohort Demography, treatment and sample processing center distribution

	CTR (N = 22)	MCTD (N = 6)	PAPS (N = 4)	RA (N =15)	SJS (N = 23)	SLE (N = 24)	SSC (N = 19)	UCTD (N = 13)
Age (years)	46±7	45±12	40±17	63±10	56±10	44±16	59±15	59±16
Female, n (%)	22 (100)	5 (83)	2 (50)	10 (67)	20 (87)	18 (75)	18 (95)	12 (92)
SAD duration (years)		8.4±7.1	9.4±8.8	4.4±4.4	7.7±6.8	6.7±6.4	9.1±10.4	2.9±1.9
Treatments, n (%)								
Antimalarials, n (%)		2 (33)	1 (25)	8 (53)	9 (39)	18 (75)	2 (11)	6 (46)
Immunosuppressants, n (%)		3 (50)	0 (0)	10 (67)	3 (13)	1 (4)	3 (16)	0 (0)
Steroids, n (%)		3 (50)	0 (0)	11 (73)	6 (26)	10 (42)	5 (26)	4 (31)
Antibiotics, n (%)		0 (0)	0 (0)	0 (0)	0 (0)	1 (4)	3 (16)	0 (0)
Center: COR GRA	 0 22	 3 3	 0 4	 13 2	 8 15	 12 12	 13 6	 11 2

8.1.2 Sample processing for MC

Samples were processed in two research centers in Granada (GENYO, GRA) and Córdoba (IMIBIC, COR), following the SOP prepared for the PRECISESADS project and described before[20]. Briefly, 10 ml of blood from healthy donors and patients was collected using EDTA-K3 vacutainer tubes. For MC deep-phenotyping study 500 µl of blood was stained with live/dead reagent (CisPt, 5µM) for 5 min, RT. Blood cells were fixed for 10 min with 700µl of proteomic stabilizer (PROT, SmartTube) and frozen at -80°C until staining. For cytokine/chemokine detection, 250µl of blood was diluted 1:1 with RPMI (Gibco) and stimulated with four different TLR receptor agonists as described in section 7.1.1: Resiquimod (RSQ), (1.25 µg/ml, Invivogen), Imiquimod (IMQ) (2.5 µg/ml, Invivogen), LPS (0.05 µg/ml, Invivogen), CpG (2 µM, Invivogen) and medium alone (UNS) for 24h. Next, samples were spun 800g for 5 min, 4°C and the supernatants (diluted plasma) were collected and stored frozen at -80°C. Sample processing workflow can be found in Figure 40. Frozen samples from Córdoba were transported on dry ice to GENYO for further processing and MC acquisition.

The reference sample for MC consisted in 6 ml of whole blood from a single donor and processed as before: blood was stained with CisPt and fixed with 7.2 ml of PROT. Aliquots of 1.2 ml were stored at -80°C until the time of staining.

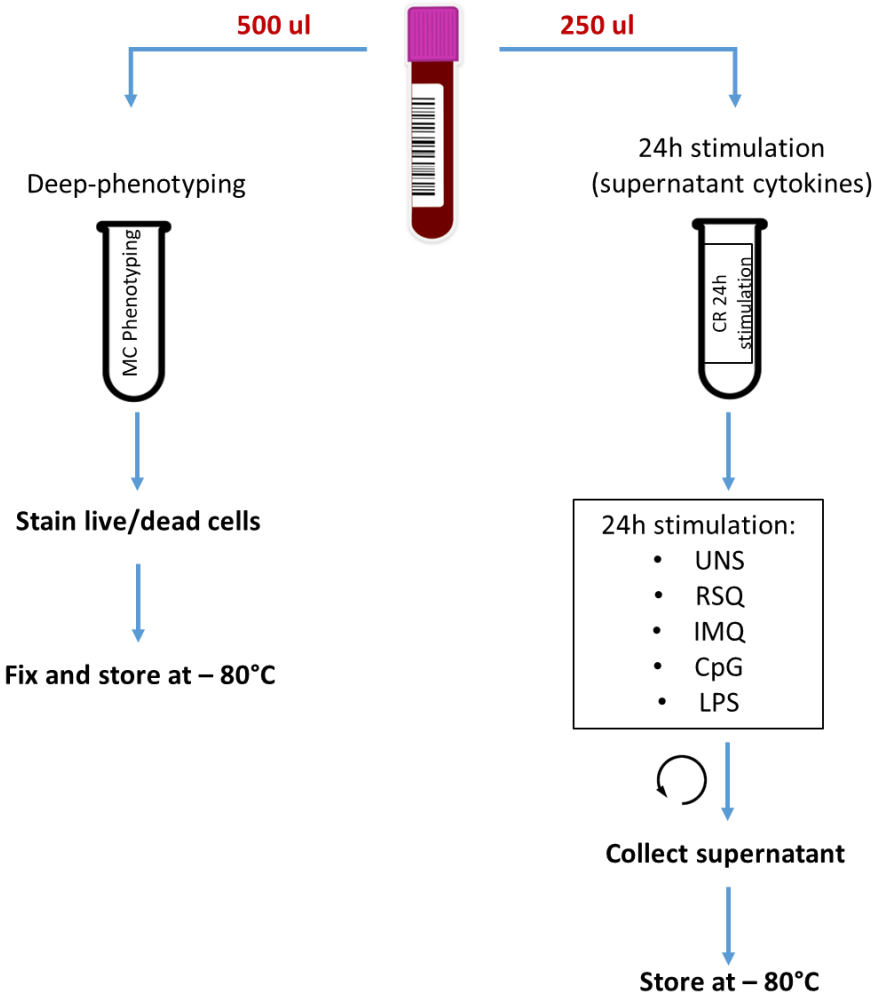

Figure 40 Whole blood processing workflow for MC and Luminex study

8.1.3 Sampling, staining, acquisition in MC

Samples were assigned to 9 experimental batches with even distribution of biological groups. Each batch consisted of 15 samples + 1 reference sample. To minimize experimental variation a frozen antibody cocktail was prepared (see Table 11), aliquoted and stored at -80°C until the moment of staining, as described[21]. Most of the antibodies were obtained in a labeled form from Fluidigm. Alternatively, purified antibodies were conjugated using MaxPar Metal-labeling kits (Fluidigm), following the vendor protocol.

Blood samples were thawed as described in section 6.1.2 and processed as described in section 6.1.3 and Table 8. Briefly, $1.5*10^6$ cells/sample were used for the barcoding step. The barcoding was performed using the Cell-ID 20-Plex Pd Barcoding Kit (Fluidigm) as follows: cells were washed with Barcoding Perm Buffer and stained with the barcode in 500 µl of the same

buffer for 20 min at RT, followed by a total of 3 washes with Cell Staining Buffer (CSB, Fluidigm). Samples were then pooled and surface antigens were stained with the antibody cocktail in CSB, for 30 min at 4°C, and at a density of $5*10^7$ cells/ml. Afterwards, cells were washed with CSB and the cells were stained with Iridium (Ir, 5 µM) for 20 min in Fix and Perm Buffer (Fluidigm), washed with CSB and left overnight (O/N) in 4 ml of freshly prepared 2% formaldehyde (PFA) (Thermo Fisher Scientific).

The following day the CyTOF acquisition was performed in aliquots to avoid prolonged cell exposure to water. Briefly, aliquots of 250 µl were washed with CSB, followed by a wash with MiliQ water. The aliquots were resuspended at $8*10^5$/ml in MiliQ water together with EQ Four Element Calibration Beads (Fluidigm) and acquired in a CyTOF2/Helios device using a NB sample injector. The flow rate was set below 400 events/s and each aliquot was acquired for no longer than 2h.

Table 11 Antibody cocktail for high-content immunophenotyping

Antigen	Clone	Metal	Source	Staining
CD41	HIP8	89Y	Fluidigm	Clustering
CD3	UCHT1	115In	ThermoFisher	Clustering
CD45	HI30	141Pr	Fluidigm	Clustering
CD19	HIB19	142Nd	Fluidigm	Clustering
CD123	6H6	143Nd	Fluidigm	Clustering
CD15	W6D3	144Nd	Fluidigm	Clustering
CD4	RPA-T4	145Nd	Fluidigm	Clustering
IgD	IA6-2	146Nd	Fluidigm	Clustering
CD20	2H7	147Sm	Fluidigm	Clustering
PD-L1	29E.2A3	148Nd	Fluidigm	Functional
CD127	A019D5	149Sm	Fluidigm	Clustering
CD43	84-3c1	150Nd	Fluidigm	Clustering
CD14	M5E2	151Eu	Fluidigm	Clustering
TCRγδ	11F2	152Sm	Fluidigm	Clustering
CD7	CD7-6B7	153Eu	Fluidigm	Clustering
CD1c	L161	154Sm	Biolegend	Clustering
BAFF-R	11C1	155Gd	Fluidigm	Functional
CD86	IT2.2	156Gd	Fluidigm	Clustering / Functional
CD27	L128	158Gd	Fluidigm	Clustering
CD11c	Bu15	159Tb	Fluidigm	Clustering
CD28	CD28.2	160Gd	Fluidigm	Clustering / Functional
CTLA-4	14D3	161Dy	Fluidigm	Functional
CD69	FN50	162Dy	Fluidigm	Functional
CD95	DX2	164Dy	Fluidigm	Clustering / Functional
CD40	5C3	165Ho	Fluidigm	Functional
CD24	ML5	166Er	Fluidigm	Clustering
CD38	HIT2	167Er	Fluidigm	Clustering / Functional
CD8	SK1	168Er	Fluidigm	Clustering
CD25	2A3	169Tm	Fluidigm	Clustering / Functional
CD45RA	HI100	170Gd	Fluidigm	Clustering
CD57	HCD57	172Yb	Fluidigm	Clustering
CD141	1A4	173Yb	Fluidigm	Clustering
HLA-DR	L243	174Yb	Fluidigm	Clustering / Functional
PD-1	EH12.2H7	175Lu	Fluidigm	Clustering / Functional
CD56	N901	176Yb	Fluidigm	Clustering
CD16	3G8	209Bi	Fluidigm	Clustering
CisPt	Live/dead cells	195Pt	Sigma	Intracellular
DNA1	Nucleated cells	191Ir	Fluidigm	Intracellular
DNA2	Nucleated cells	193Ir	Fluidigm	Intracellular
Bead	Beads	140Ce	Fluidigm	-

8.1.4 Mass cytometry data preprocessing and quality control

Data were preprocessed and cleaned as described in chapter 7 and Figure 24. As neutrophils constitute around 50% of blood we decided to split granulocytes and PBMCs and perform feature extraction and differential analysis, independently. The separation was done using the ratio computed for the markers CD15 and CD45. Cells with CD15/CD45 ratio < 1 were considered as PBMC and cells with ratio ≥ 1 as granulocytes. Representative gating is shown in Figure 41. It should be noted that although basophils are granulocytes, due to their low CD15

expression, they are analyzed in the PBMC compartment. Batch effect detection was performed as described in section 7.2.8 and feature extraction was done as described in section 8.1.5 for both granulocytes and PBMC.

8.1.5 Cell population identification and feature extraction

As mentioned above we split PBMC and granulocytes and performed automated gating for PBMC and granulocyte populations separately.

FlowSOM[22], one of the best performing automated gating techniques, was used to identify PBMC populations. In order to capture all populations of interest, including rare cell subtypes of dendritic cells, a grid of 20 x 20 was used to obtain 400 clusters[23], which where next grouped into 45 metaclusters, using hierarchical consensus clustering. The number of metaclusters was selected based on visual inspection. The markers used for the clustering can be found in Table 12. To construct the FlowSOM tree, an aggregated file was created by randomly subsetting 25,000 cells from each fcs file, generating a file with $3{,}375*10^6$ cells in total. To check the quality of the clustering, the aggregated file was manually gated using FlowJo 10.0.7 and the F1-measure and weighted purity scores were calculated as described[24]. The manual labels for each metacluster were assigned using the cell population representing the majority of the cells included in a particular metacluster. Each individual file was then mapped to the aggregated FlowSOM and cell frequencies and median signal intensities (MSI) for functional markers (see Table 11) were calculated for each metacluster. Total PBMC were used as a reference population to calculate cell population frequencies. The metaclusters with less than 50 cells in all the fcs files were removed from further analysis. Similarly, MSI with low variability (SD < 0.2) and/or low expression (arcsine transformed MSI < 1) were also removed. Additionally, CD28, CD69 and PD-L1 markers were excluded from the MSI analysis, since they generated a strong batch effect on PBMC despite file normalization. FlowSOM clustering was performed using an R-based implementation and was visualized using the aggregated file. Heatmaps showing MSI calculated for each metacluster, FlowSOM trees colored by mean intensity of clustering markers or by manual labels were used for clustering visualization. Additionally a UMAP analysis[25] was performed using a random subset of 5,000 cells per file, and MSI or metacluster frequencies, were represented on two-dimensional maps using *ggplot2* package. For UMAP and heatmap analysis *uwot* and *pheatmap* packages were used, respectively.

To identify cell subsets in the granulocyte compartment, PhenoGraph[26], another well performing clustering algorithm[27], was used. The data were first aggregated taking 2,500 cells per fcs file, building an fcs file with 337,500 cells in total. Next, clustering was run on the aggregated file with the parameter k (defining the number of the nearest neighbors), set to 100 as described before[28]. The markers used for the clustering can be found in Table 12. Only markers with high variability, selected by visual inspection were selected for clustering analysis. Cell frequencies and MSI for functional markers (see Table 11) were extracted per cluster and file. Total number of granulocytes was used as the reference population to quantify cluster frequencies. MSI imputation and removal was performed as described above, with the exception for CD28, CD69 and PD-L1 markers, as we did not observe strong batch effect for these markers in granulocytes. Data was visualized using heatmaps and two-dimensional (2D) maps from UMAP analysis, as described before.

Table 12 Clustering markers

	Clustering markers
PBMC	CD3, CD4, CD43, CD7, CD127, CD27, CD28, CD45RA, CD11c, CD38, HLA-DR, CD8, CD57, CD24, IgD, CD19, CD20, TCRyd, CD14, PD-1, CD1c, CD141, CD56, CD123, CD25
Granulocytes	CD41, PD-1, PD-L1, CD86, CD11c, CD95, CD24

8.1.6 Multiplexed cytokine and chemokine quantification

Cytokines and chemokines were analyzed in the supernatants of stimulated blood samples. Forty five analytes were measured using Human XL Cytokine Discovery Premixed Kit (R&D System) and a Luminex 200 device. Samples were thawed on the day of the experiment and diluted 1:2 with calibration diluent. The assay was performed following the steps recommended by the manufacturer but half volume of the reagents was used and diluted supernatant was incubated with the beads O/N at 4°C. At least 50 beads were acquired for each analyte. The concentration of each protein was calculated using the corresponding standard curves and Bio-Plex Manager v6.0 software. The standard curves were created using 4 or 5-parametere logistic curve fit and were expressed as pg/ml. For visualization purposes the expression was log2-transformed. The beads with less than 25 counts were removed from the analysis of this sample. Cytokines for which no expression was detected in 90% of the samples were removed from further analysis (IL-17A, IL-3, IL-7, IL-4, IL-5). The imputation for

out-of-range values (OOR) was performed as follows: for high detection range the maximum value for each stimulation was calculated and 50% of the signal was added; for data in the low detection range the minimum value for each stimulation was calculated and 50% of the signal was subtracted. In this thesis, only data from UNS condition were used for further analysis.

8.1.7 Statistical analysis

The differences in cell frequencies were first explored by UMAP analysis and 2D density plots using *ggplot2* package. Equal number of cells per disease were randomly selected from aggregated file and plotted. For the MSI analysis 10,000 cells were plotted per diagnosis. The outliers were identified in every group using Grubbs' test and were removed from further analysis. Next, a differential analysis across all diseases and controls was performed using Kruskal-Wallis (K-W) statistical test followed by Dunn analysis. To account for multiple comparisons Dunn test was corrected using the FDR method. For the visualization, only the significant features for K-W were represented by heatmap or violin plots. For heatmap, visualization median expression for each selected feature was calculated and represented as a z-score scaled data. Agglomerative hierarchical clustering was performed using ward.D2 linkage and *pheatmap* package.

To select features for patient clustering, Mann-Whitney (M-W) test was performed comparing controls (CTR) and all autoimmune disease (AD) patients, using both frequency and MSI features from PBMC and granulocytes data. The features with p-values ≤ 0.05 were selected for further analysis. To verify the association of the features with medication, M-W test was performed between treated (T), non-treated (NT) and healthy control (CTR), correction for multiple testing was applied as described before. For reclassification study, K-means clustering was performed using *stats* package from R with 4 centers and 1000 iterations. Spearman correlation parameters were calculated to check the relation of the selected features. The cluster differences in cytokine production were calculated by K-W test, followed by Dunn test, as described above, CTRs were excluded from this analysis.

K-W and M-W analysis were performed using *rstatix* package, correlation analysis was run using the R *stats* package and Grubb's test for outlier detection was done using *outliers* package. Plotting was done using *pheatmap* and *ggplot2* packages. All analyses were performed in R.

8.2 Results

8.2.1 Granulocytes, PBMC separation and batch effect

First, the granulocyte fraction, consisting in neutrophils and eosinophils, was separated from PBMCs using the CD15/CD45 ratio, as described in methods (Figure 41)..

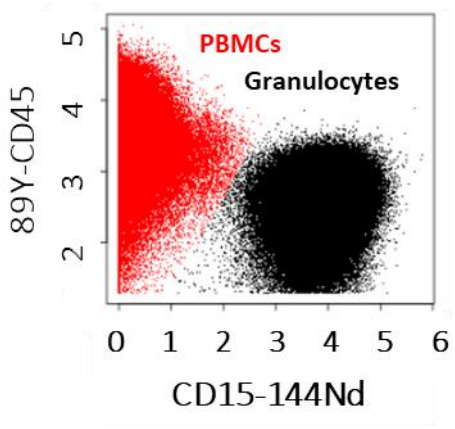

Figure 41 Gating strategy for PBMC and granulocytes (neutrophils + eosinophils separation).

Granulocytes and PBMC were separated using the ratio calculated for CD15/CD45 expression. PBMC are presented in red and granulocytes in black.

We next investigated the batch effect introduced in the data before and after the normalization with the reference sample. As data were acquired in 9 staining/acquisition batches, we tracked the batch effect across these batches called RUN. Additionally, as blood was processed in two different centers, sample distribution across centers (COR, GRA) was also visualized. Additionally we checked the batch- and center- specific effects at both, cell frequency level and MSI of the functional markers, across clusters and metaclusters in granulocytes and PBMC.

We saw strong batch effects introduced specially in PBMC, which was caused by RUN1 and RUN2 experiments, at the frequency and MSI levels, Figure 42. This effect was stronger at the cluster than metacluster level, Figure 42A. At the cluster level all light and dark blue circles (representing the individuals from RUN1 and 2 respectively), as well as squares (representing reference samples) were grouped together and were clearly separated from the rest of RUNs. This effect decreased after normalization, although still some slight separation between reference sample could be observed for the clusters. At the metacluster level nice distribution of all the colors and closer grouping of reference samples was observed after the normalization. Similar situation was seen when MSI of functional markers (Table 11) were analyzed, (Figure 42B). The batch effect level was not center-dependent, as it can be seen in the Figure 42 (right panel), even distribution of samples across the centers was observed. In general, a significant improvement was observed after data normalization, leading to removal of the batch effect, specially at the metacluster for both, frequency and MSI.

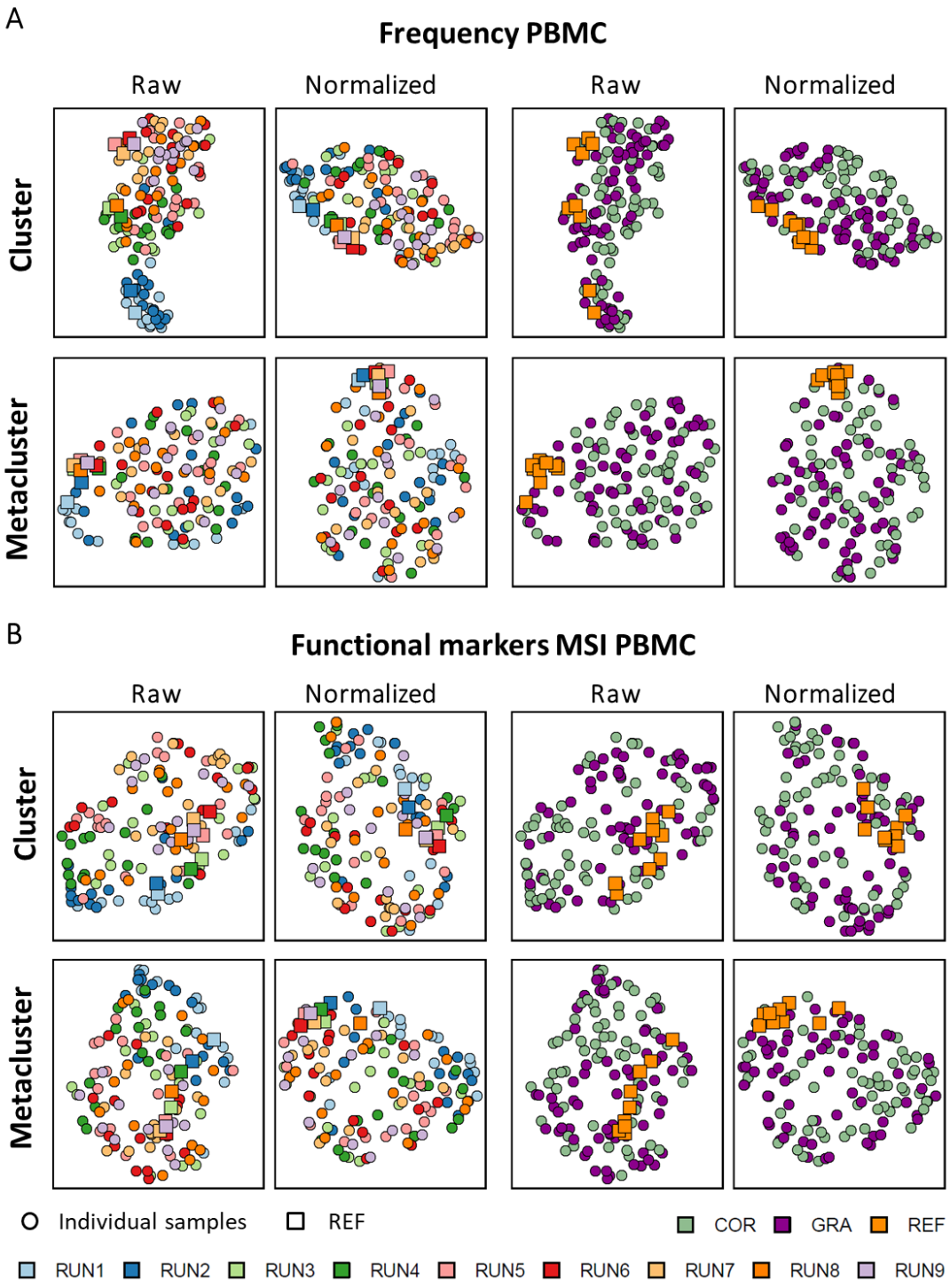

Figure 42 Batch effect before and after the normalization for PBMC.

Data were clustered using FlowSOM and cell frequency (A) and MSI for functional markers (B) were extracted for clusters and metaclusters. Next UMAP dimensional reduction was performed to verify sample distribution. Data are represented before the normalization (Raw) or after the normalization using reference sample (Normalized). Samples from all the individuals are presented by circles and reference samples are represented by squares. Additionally, samples are colored by RUNs (left panels) or by centers (right panels) and reference sample.

On the other hand, in granulocytes a strong batch effect was observed for RUN 1, 7, and 8 at the cluster level (Figure 43A) and additionally for RUN5 in MSI of functional markers (Figure 43B). This effect was significantly improved after data normalization. Reference samples grouped together and samples from the same RUN spread around other samples. There was no center-specific batch effect observed.

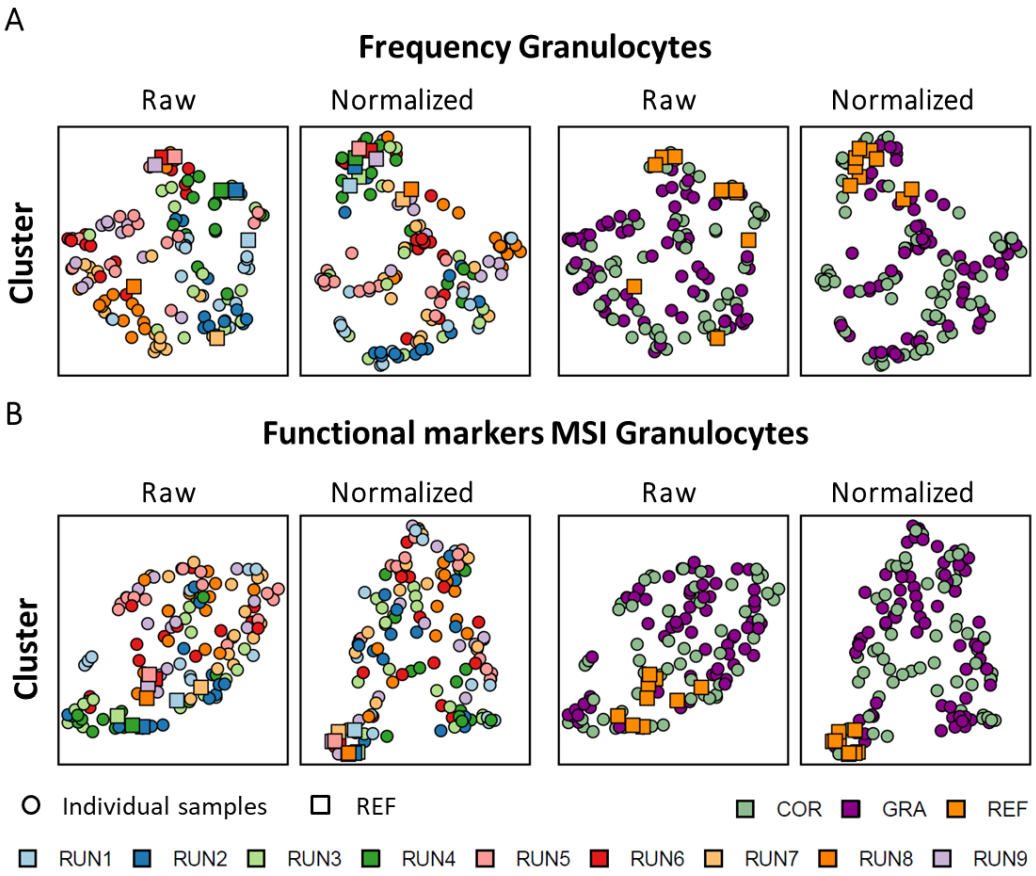

Figure 43 Batch effect before and after normalization for granulocytes.

Data were clustered using PhenoGraph and cell frequency (A) and functional marker MSIs (B) were extracted for clusters. Next UMAP dimensional reduction was performed to verify sample distribution. Data are represented before and after the normalization. Data are represented as in Figure 42.

8.2.2 PBMC landscape in SADs

As mentioned before, PBMCs and granulocytes were separated from each other. In this section we will focus on the PBMC compartment and mostly, the metacluster analysis will be presented. We clustered the data using FlowSOM as described in the methods, the results of the clustering can be found in Figure 44.

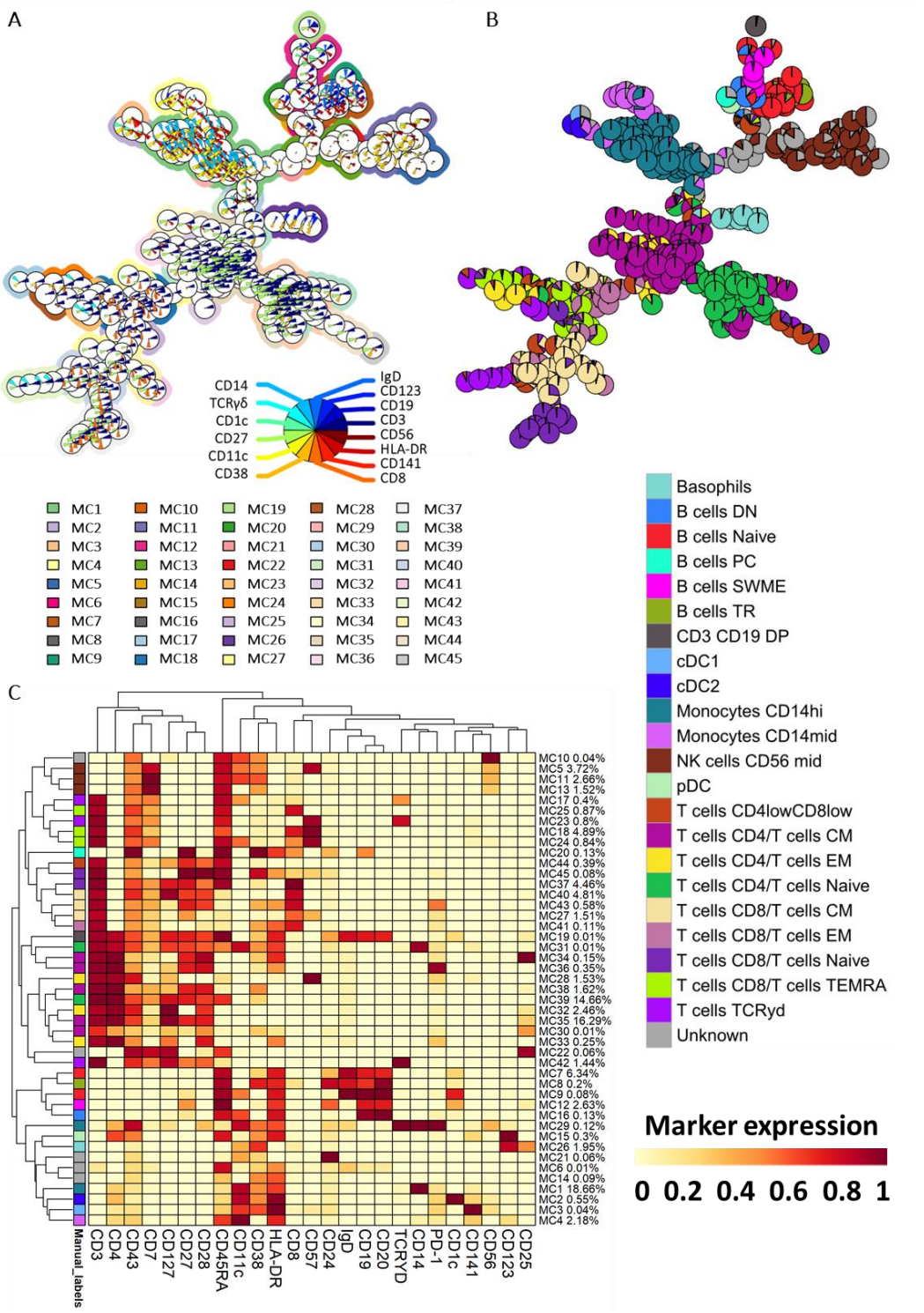

Figure 44 FlowSOM Clustering for PBMC data.

(A) FlowSOM tree was built on an aggregated file using 400 clusters, represented by the tree nodes. In each node the mean expression of a set of the clustering markers is represented using star charts, the height of each part indicates the intensity, the color assigned to each marker is represented in the legend. For the clarity of the figure, only a selected set of clustering markers is shown. The clustering markers are fully represented in C. 45 metaclusters are denoted by the background colors, shown below the tree. (B) Manual labels overlaid on FlowSOM tree. Pie charts indicate the percentage of the cells represented by the node falling in the manual gates. A different color is assigned to each label and the manual annotation can be found in C. (C) Heatmap representing median intensities for clustering markers across the 45 FlowSOM metaclusters shown in A. The color intensity in the heatmap represents the median of the arcsinh, 0-1 transformed marker expression of the cells included in the

metacluster in the aggregated file. The colors assigned to the metaclusters correspond to the manual labels assigned by manual gating and are the same through all the figures corresponding to PBMC analysis. The relative size of each metacluster is indicated in the row names of the heatmap. The dendrograms represent the hierarchical clustering using Euclidian distance and average linkage.

To facilitate metacluster interpretation, we performed the manual gating shown in Figure 45, and obtained manual labels for each metacluster. As described in the methods, the manual label for each metacluster was selected based on the majority of cells represented in this particular metacluster, although some mixture of cells could still be observed, as presented in Figure 44B.

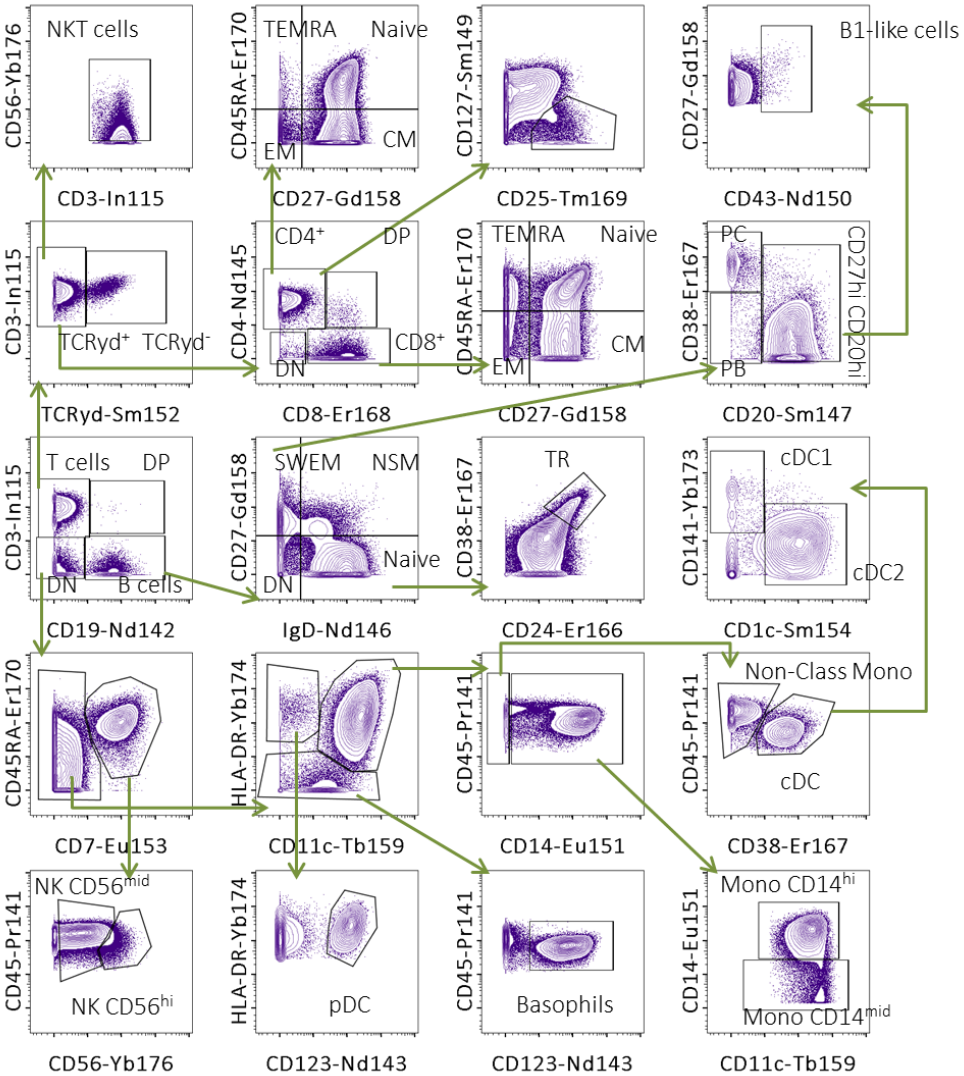

Figure 45 Manual gating of aggregated file.

The aggregated file was manually gated to obtain cluster and metacluster labels for FlowSom tree.

To verify the quality of the clustering we calculated weighted purity and F1 scores for clusters or metaclusters compared with the manual labels as shown previously[24]. Overall the purity scores were 0.9 and 0.83 for clusters and metaclusters, respectively with the F1 score measure between manual gating and FlowSOM metaclusters being equal to 0.79 (0.88 for precision and 0.80 for recall)

These results show a good correspondence between metaclusters identified by FlowSOM and the gold standard manual gating of known populations, and are confirmed in the Figure 44C, where the MSI of each metacluster is represented together with the manual label. It can be clearly seen that the canonical marker expressions in metaclusters correspond well with manually-defined cell populations. It is worth mentioning that some *Unknown* metaclusters were also identified, which are mostly low frequency events not assigned during the manual gating process. We also visualized the data using UMAP analysis and 2D maps and confirmed a good correspondence between the automated methods and manual gating, as shown in Figure 46A and B. The FlowSOM and gating annotation was consisted with expression of canonical markers (Figure 46A) and UMAP visualization (Figure 46B). All together this result indicates a good clustering performance and proper identification of well-known cell populations using an automated approach, FlowSOM.

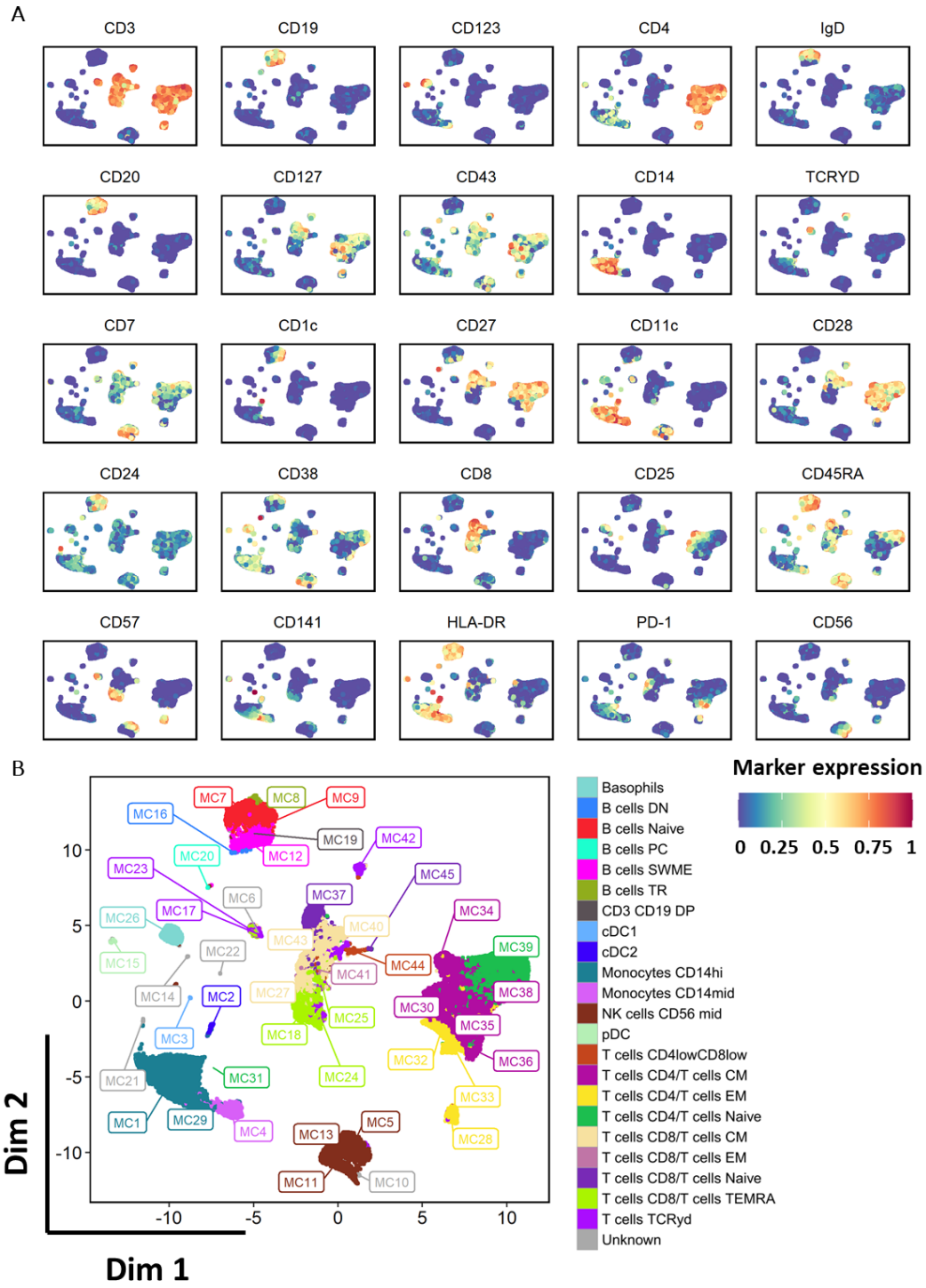

Figure 46 UMAP visualization.

For each individual, 5,000 cells were randomly selected to build an aggregated file. UMAP was built using the aggregated file and arcsine-transformed expression of clustering markers in the PBMC compartment. (A) Cells are colored according to the expression level of the clustering markers, the expression is 0 – 1 transformed. 50,000 randomly selected cells are used for the visualization. (B) The same UMAP representation as in A showing the metaclusters obtained from FlowSOM clustering colored by manual labels as in the legend.

8.2.3 Differential analysis in PBMC

As a first approach, we explored the differences in the relative frequency and expression of functional markers of the different PBMC metaclusters in relation with the diagnosis. The exploratory analysis using UMAP and density plots showed evident differences in the cell distribution across different diagnoses (Figure 47A). Differences in the MSI of several functional markers were also observed, and some of them are represented in Figure 47B.

To get a deeper look into the alterations between patient groups we performed K-W analysis followed by a Dunn *post-hoc* test for both metacluster frequencies, Figure 48 and MSI features, Figure 49. For the cell frequency in the PBMC compartment, we have detected 14 differentially expressed cell populations in different cell compartments, of which 12 have significant results in the *post-hoc* analysis (Figure 48). Only 8 populations were characterized as statistically different between SADs, among them 5 differed between SADs but could not differentiate SADs from CTR, suggesting that they could be of use after initial classification of an individual as an autoimmune patient. Three metaclusters were statistically different between the CTR and patients and also differentiated some diseases. Cells expressed at different level only between SADs were represented by MC8 (TR B cells), MC20 (PC), MC44 ($CD4^{low}CD8^{low}$ T cells), MC45 ($CD8^{+}$ naïve T cells) and MC28 ($CD4^{+}$ EM T cells) and contained different subpopulations of T and B cells. These MCs were mostly decreased in RA compared to either SJS, SLE and SSC. Additionally, they have usually lower frequency compared to the CTR group, although no statistical differences were detected. This may suggest that the T and B cell compartments are more informative when comparing different SADs, although it is not enough to separate sick individuals from healthy population and RA patients from diseases such as UCTD and MCTD. It should be noticed that 3 populations were downregulated in RA compared to SLE (MC8, MC44, MC45) and 2 when compared to SJS (MC8, MC45). These populations were overlapping between SLE and SJS, indicating their higher discriminative power when diagnostic doubts concerns RA and SJS or SLE diseases. Cells that showed differences between CTR but also separated some SADs belonged to the myeloid (MC3, cDC1) and lymphoid compartments (MC37, MC12, $CD8^{+}$ Naïve T cells, SWME B cells respectively) and in principle were characterized by their higher frequency in CTR than in SJS. An interesting metacluster MC37, represented by $CD8^{+}$ Naïve T cells, showed decreased level for multiple SADs (RA, SJS, UCTD) when compared to CTR and SLE, but no difference was observed between SLE and healthy population nor SSC, PAPS, thus these cells could not be treated as an SLE biomarker. In the SADs/CTR comparison 4 populations were different and did not show

further alterations between the diseases. These populations were mostly decreased in SADs: MC11, ($CD56^{mid}$ NK cells), MC15 (pDCs) and MC42 (γδT cells) and one population MC1 ($CD14^{hi}$) was increased in SLE, although having lower HLA-DR expression when compared to either CTR or SSC and UCTD patients.

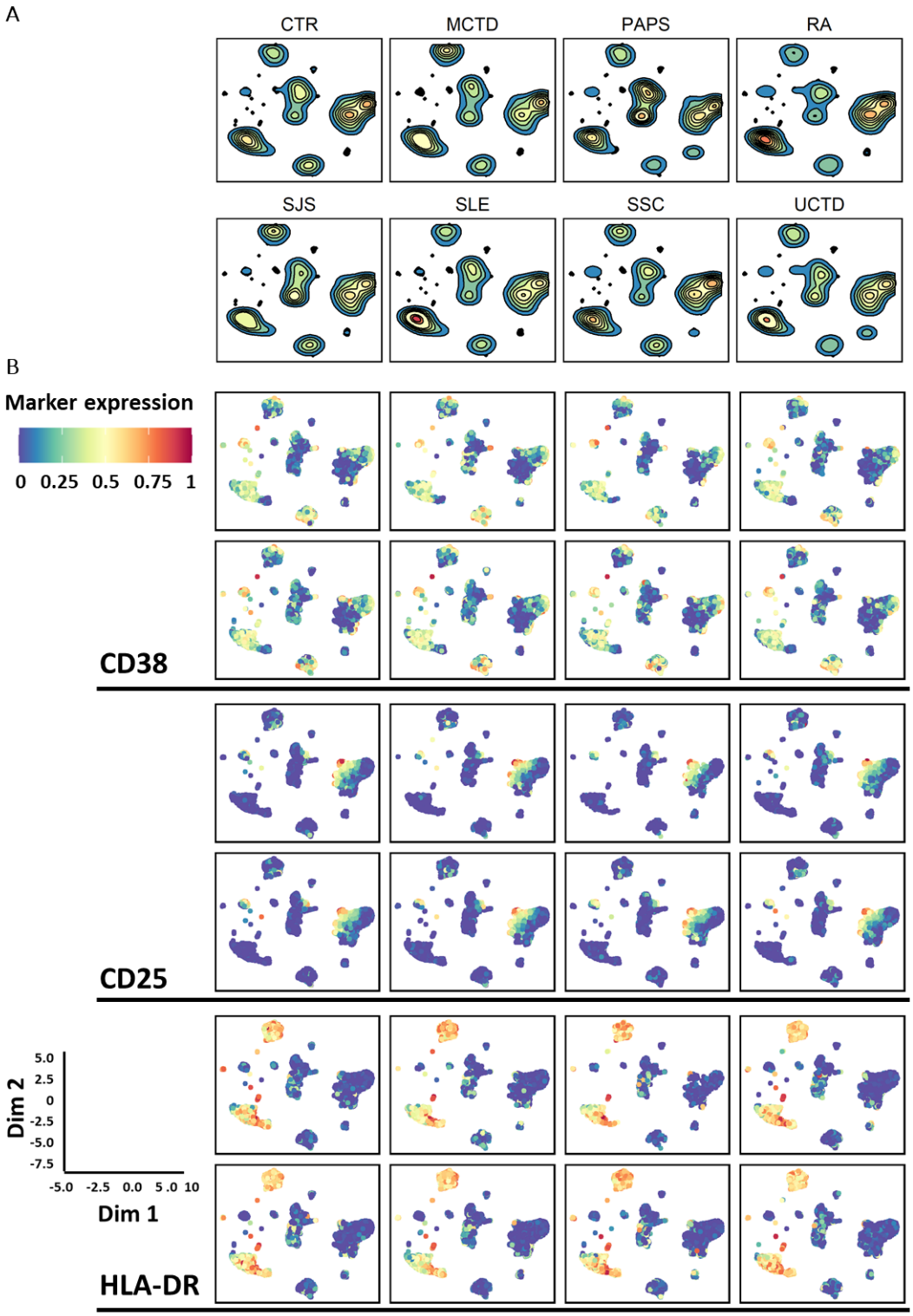

Figure 47 Cell frequency and MSI exploration in PBMC.

UMAP was generated as described above and represented across different groups of patients using density plots (A) or dot plots (B). For the density plot, equal number of randomly selected cells (10,000 per diagnosis) from each disease are represented, and for the dot plots 50,000 cells are drawn. (A) Differences in the cell population distribution are observed across different group of patients. The redder the color the denser the region is. (B) The diagnosis labels are represented as in A. Cells are colored according to the expression level of the functional makers CD38, HLA-DR and CD25. For plotting purposes, the expression is 0 – 1 transformed.

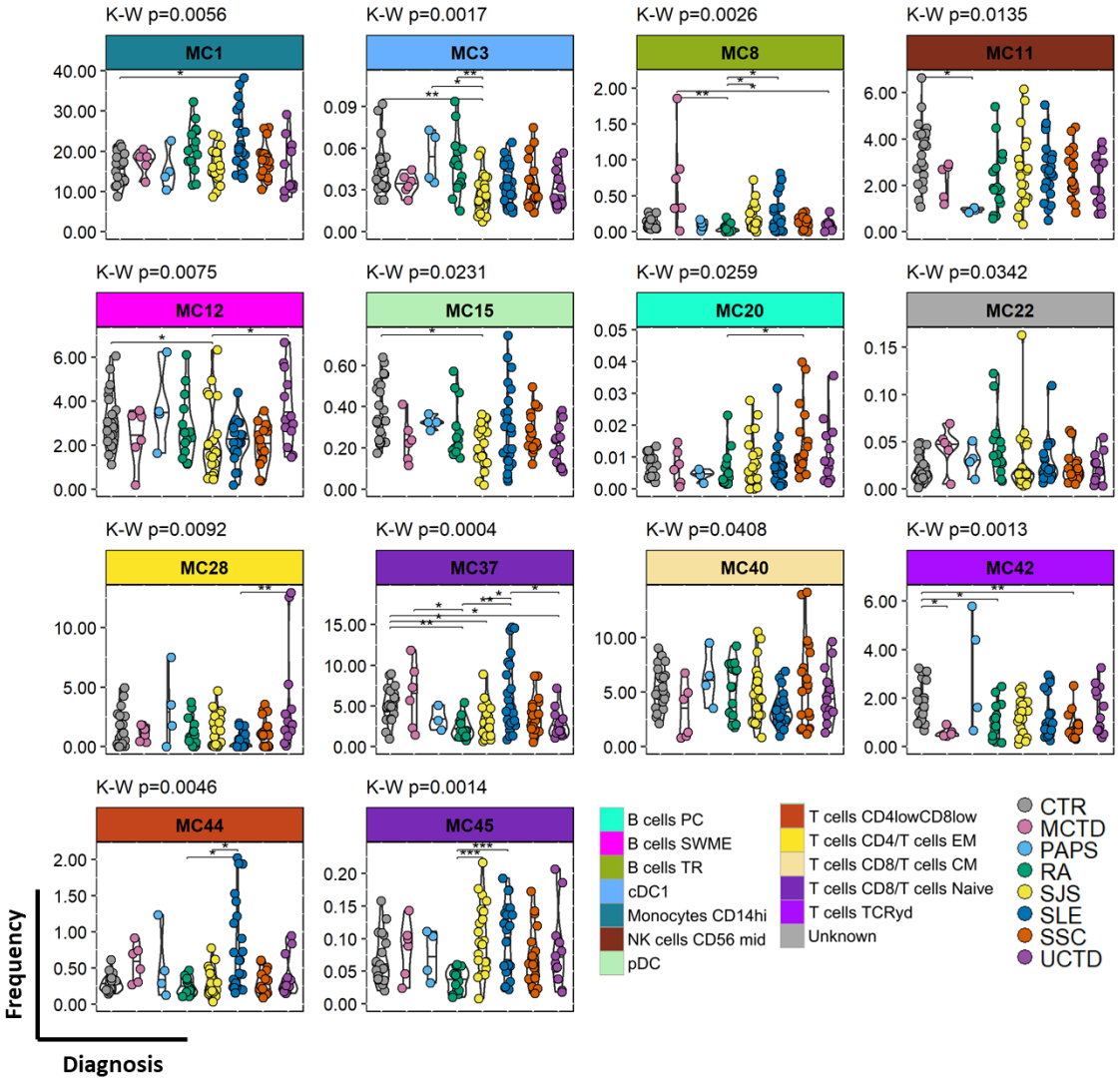

Figure 48 Differential analysis based on PBMC metacluster frequencies.

Cell frequencies were quantified for each metacluster as described in methods. Differential analysis was performed using K-W followed by a Dunn test. The K-W p-values can be found above each plot and the Dunn test statistical intervals are shown on the plots. p-values for the Dunn test were adjusted using the false discovery rate (FDR) method to account for multiple comparisons. Only metaclusters with p-value ≤ 0.05 for K-W are shown. Each plot is colored by the manual label of the metacluster and each dot in the plot represents an individual, colored by diagnosis. *p < 0.05, **p < 0.01, ***p < 0.001 in Dunn test.

Next, we verified the differences in the MSI of the functional markers shown in Table 11 in different metaclusters between the different disease labels. We identified 5 different markers being statistically different between groups in several metaclusters (Figure 49). For instance, CTLA-4 was differentially expressed in MC45 ($CD8^+$ Naïve T cell compartment). UCTD and SJS were characterized by higher expression of this marker when compared to CTR. Additionally UCTD had higher expression when compared to MCTD, RA and SLE patients but not to SJS, and SJS had higher expression than MCTD. For CD95 marker although K-W analysis shows

differences in MC16 and MC32, the only significance for Dunn test was obtained for MC32 ($CD4^+$ EM T cells) and SLE showed higher expression than UCTD patients.

Multiple differences were observed in the expression of the CD38 marker across various cell populations. In MC5, MC11 and MC13 (NK T cell compartment) the lowest expression was observed in RA, and this reached significance compared to multiple diseases: MCTD, SJS, SLE and SSC. Also differences between MCTD and CTR were observed in MC13, showing higher CD38 expression in MCTD. In MC7 (naïve B cells) again the lower expression was observed for RA and UCTD, reaching the statistical significance when compared to CTR, MCTD, SJS, SLE and SSC. No differences were observed comparing groups with higher CD38 expression. MCTD had the highest expression of CD38 in MC3 (cDC1) and MC15 (pDC), reaching statistical significance for comparison with RA for MC3 and RA, CTR and UCTD for MC15. Additionally, UCTD and RA had lower CD38 expression in MC15 compared to SJS patients. Differential CD38 expression was also found in MC34, MC39 ($CD4^+$ T cells) and in MC41, MC43, MC45 ($CD8^+$ T cells). Although all the patient groups (besides PAPS) had high expression of CD38 in MC34 ($CD4^+$ CM T cells) compared to CTR, only comparison for SSC reached statistical significance. In MC41 ($CD8^+$ EM T cell) the biggest change in CD38 expression was observed for SJS and RA in MC43 ($CD8^+$ CM T cells) for SJS when compared to RA and CTR. Significant differences could also be seen for MCTD and SLE compared to RA, with RA patients having lower CD38 expression.

Higher expression of CD25 in MC26 (basophils) was found in RA and SJS when compared to CTR. Differential expression for HLA-DR was found mostly in MC1 ($CD14^{hi}$ monocytes), MC2, MC3 (cDC1 and cDC2 respectively) and also in MC34 ($CD4^+$ CM T cells). The lowest expression was observed for SLE when compared to CTR, SSC and UCTD in MC1 or to RA for MC2. Aditionally, SLE was characterized by lower HLA-DR expression in MC34 ($CD4^+$ CM T cells) when compared to RA, SSC and CTR, as well as for SJS when compared to CTR.

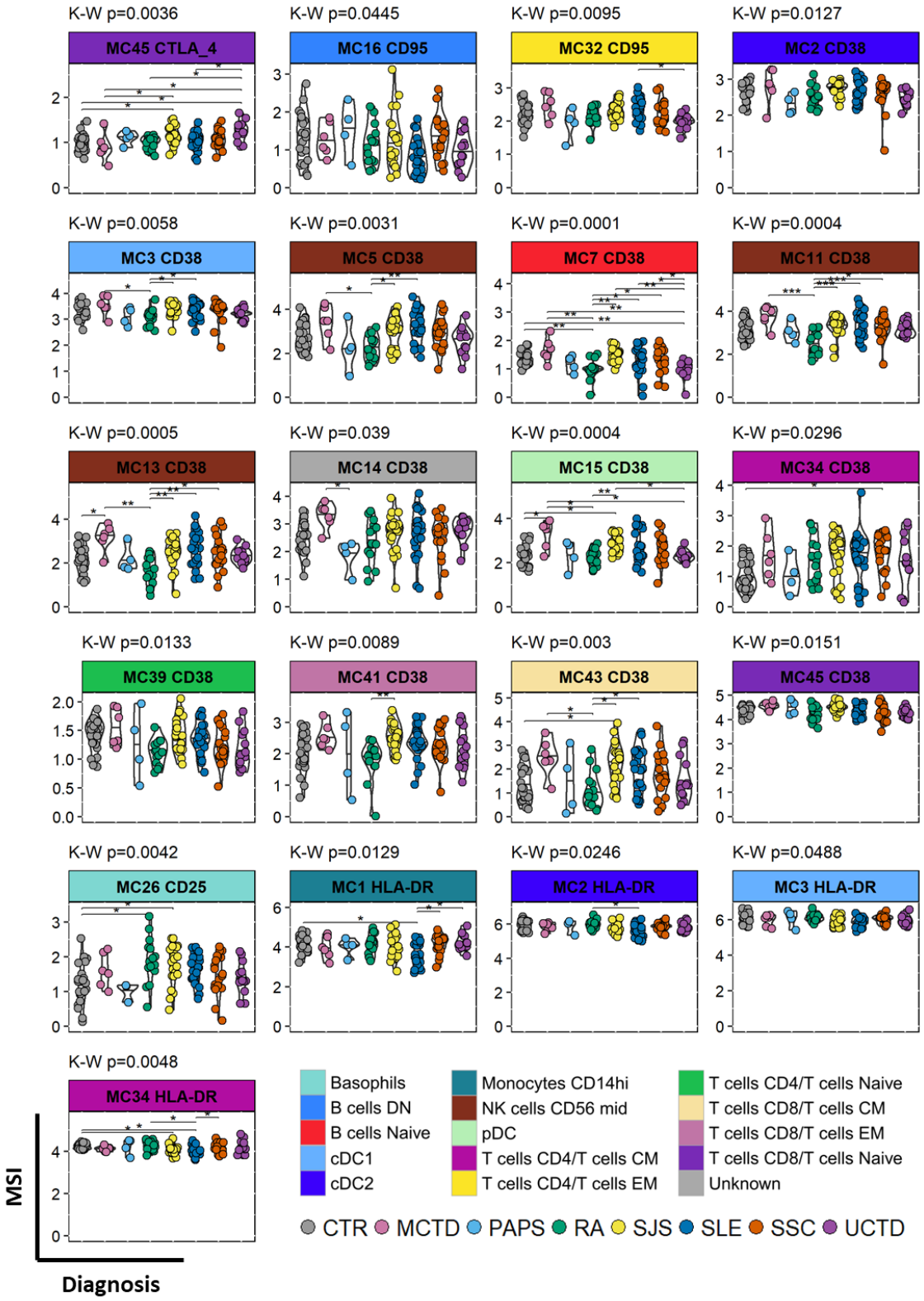

Figure 49 Differential analysis based on PBMC metacluster MSI.

MSI of functional markers were quantified for each metacluster and the data are represented as in Figure 48.

In total 35 features were identified as statistically significant by K-W and summarized in Figure 50 using median expression per group of diagnosis and hierarchical clustering analysis. Three main groups were found. Group 1 gathered together MCTD, SJS and SLE patients. Within this group SJS and SLE patients were more related to each other as already described[7] than to MCTD. This group was characterized by general higher CD38 expression, being the strongest in MCTD, and lower HLA-DR expression compared to other two clusters. The second group was composed by CTR and PAPS and the third one contained RA, SSC and UCTD, showing more similarity between SSC and UCTD than RA. The features of group 2 and 3 were almost completely opposite to Group 1, as they were characterized by low expression of CD38, being the lowest in RA, and higher expression of HLA-DR. They could be distinguished from each other based on the monocyte (MC1) frequency and expression of CD25 and CD38 in MC26 (basophils) and MC34 ($CD4^+$ CM T cells), respectively.

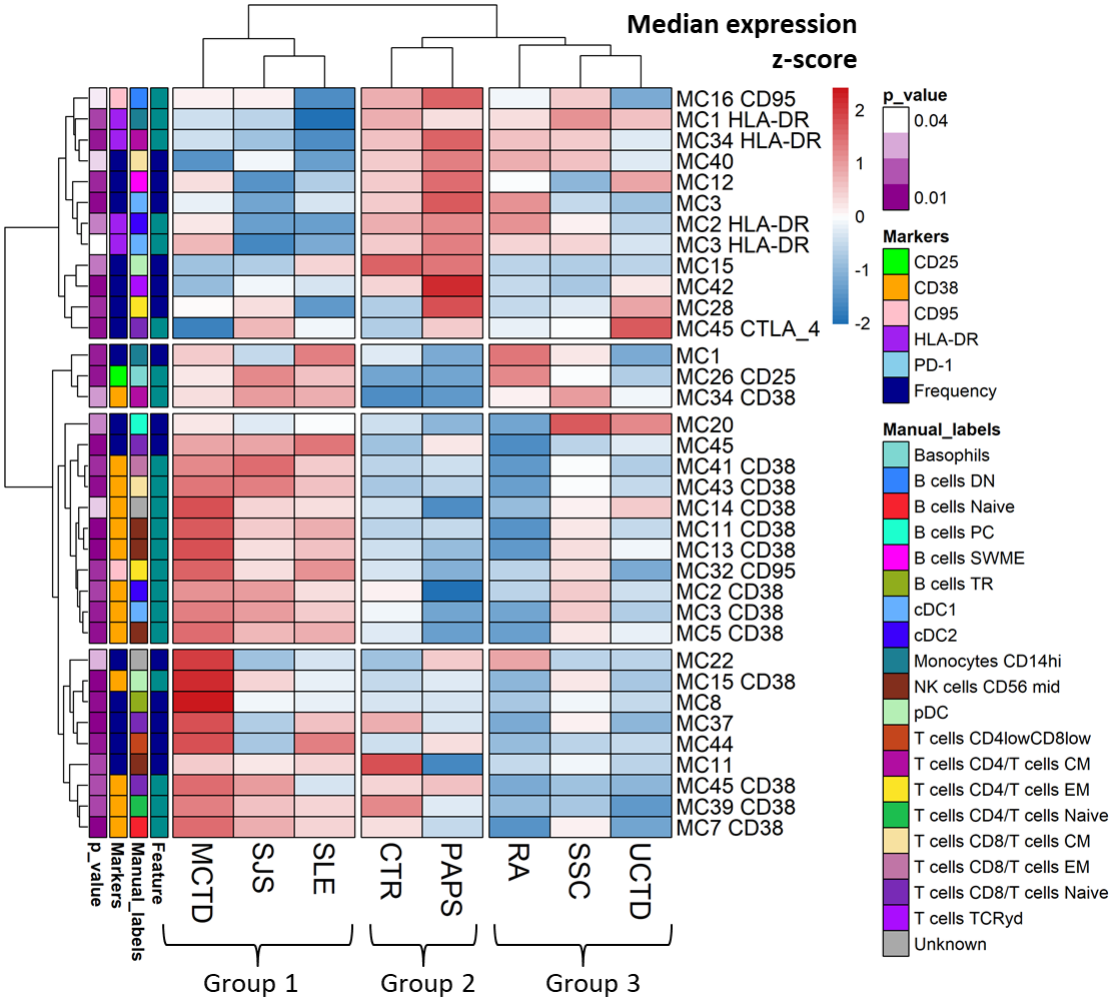

Figure 50 Hierarchical clustering of diseases using K-W selected features.

Features with significant values in the K-W test (shown in Figure 48 and Figure 49) were selected for clustering analysis. The median for each feature was calculated for each disease label. Color scale represents the z-score. Hierarchical clustering with Euclidian distance and ward.2D linkage was performed, and three groups of diseases and four groups of features were identified.

8.2.4 Granulocyte landscape in SADs

We clustered the data using PhenoGraph as described in the methods section, and the results of the clustering can be found in Figure 51. Panel B and C showed markers selected for the clustering analysis. In contrast to PBMC these markers are not canonical neither for neutrophils nor eosinophils, and thus we did not perform manual gating. Although CD15 is a canonical marker for granulocytes, because we used it to separate granulocytes from PBMC we did not include it in granulocytes clustering.

PhenoGraph identified 17 different clusters (CL), that can be seen in Figure 51A and B. Based on the median marker expression of functional markers 3 main groups could be distinguished

mainly based on PD-1 and CD11c (Figure 51B). The first group represented CL that were PD-1^{low} and $CD11c^{low}$. Within these cells four different subsets were identified and differed mainly in CD24 and CD95 expression. CL3 and CL11 were $CD95^{hi}$ and $CD24^{hi}$, but they differed in CD86 and CD11c expression. And CL6 and 10 were low for CD95 and CD24 expression and could be separated using expression level of PD-L1 marker. Next, the PD-1^{hi} group contained three clusters with $CD11c^{hi}$ and two with $CD11c^{low}$ cells. $CD11c^{hi}$ clusters could be distinguished based on CD95, CD86, PD-L1 and PD-1 expression (CL15, CL8 and CL14), while $CD11c^{low}$ clusters based on the difference in PD-1 expression (CL5 and CL7). The last group contained mostly PD-1^{low} cells, besides CL16 that still had higher expression of PD-1. CL17 and CL4 were high in PD-L1, CD86 and CD11c, and could be distinguished based on differences in CD95 levels. On the other hand, CL9 and CL2 were low in PD-L1 and CD86, and also could be distinguished based on CD95 and PD-1 levels. CL1 and C13 had medium level of PD-L1 and CD86 markers and were lower in CD11c expression. They could be discriminated based on PD-1 expression. In this group, cells characterized by the high expression of CD41, a canonical marker for platelets, were also found and grouped in CL12. These cells were separated from the rest of granulocytes as show with UMAP analysis, Figure 51A, B, and are considered as platelet-contamination[29], therefore they were removed from further analysis. In our setting we observed loss of CD16 marker (as shown in section 6.2.1), thus we could not separate the eosinophils from neutrophils. Eosinophils are $CD11c^{-}$ thus they could be included in the CL5, CL6, CL7 and CL11, however up to know we were not sure if they were preserved upon fixation.

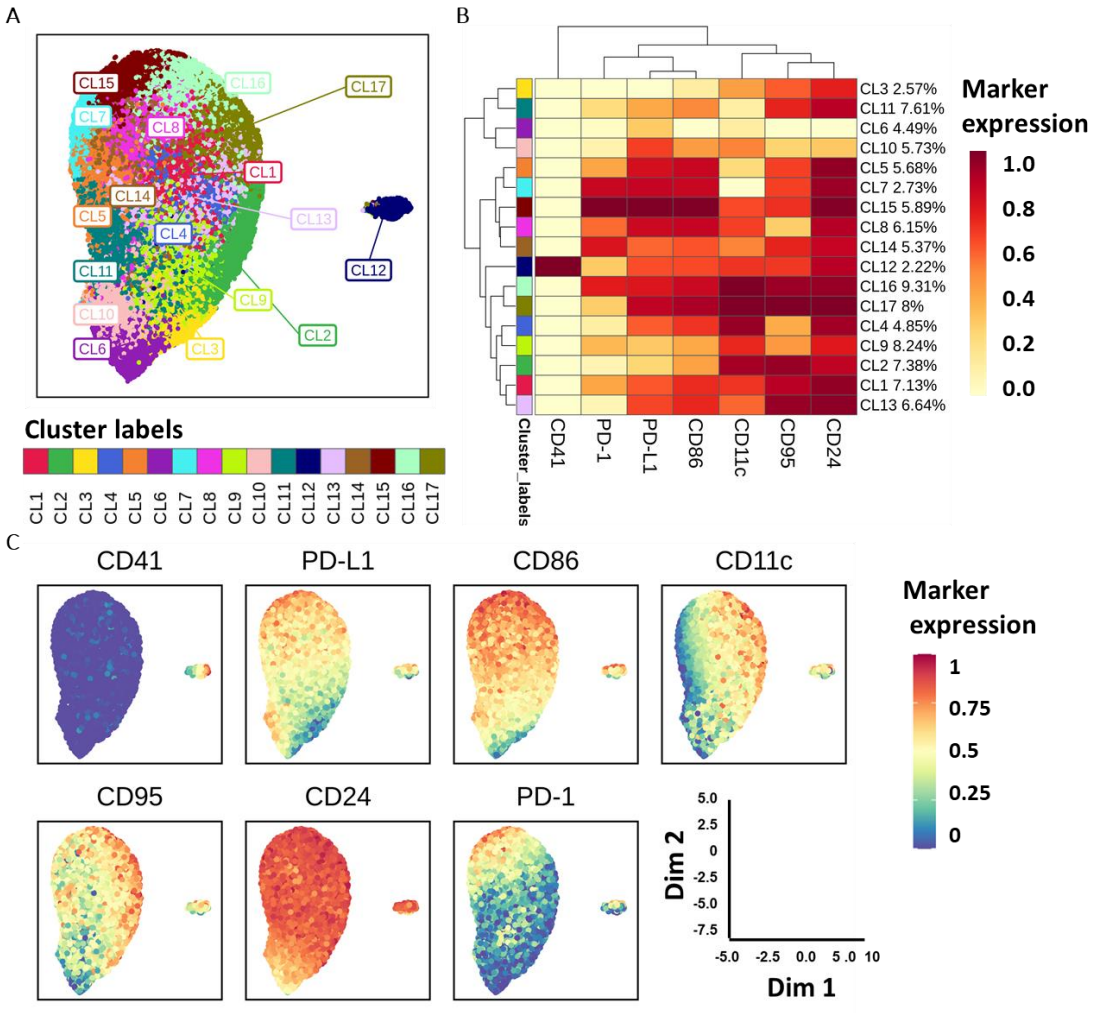

Figure 51 PhenoGraph clustering for the granulocyte compartment

(A) PhenoGraph was built on aggregated file and identified 17 clusters that are represented by UMAP and colored according to the cluster names. UMAP was built using the aggregated file and clustering markers. (B) Heatmap representing median intensities for clustering markers across the 17 PhenoGraph clusters, shown in A. The color intensity in the heatmap represents the median of the arcsinh, 0-1 transformed marker expression of the cells included in the cluster using the aggregated file. The colors assigned to the clusters correspond to the cluster colors shown in panel A, and are the same through all the figures corresponding to granulocyte analysis. The dendrogram represents the hierarchical clustering using Euclidian distance and average linkage. (C) Cells are represented as in A but colored according to the expression level of the clustering markers, the expression is 0 – 1 normalized. 50,000 randomly selected cells are used for the visualization

8.2.5 Differential analysis based on granulocytes

Same as for PBMC (sections 8.2.3), in a first approach we explored the differences in the relative frequency and expression of functional markers of the different granulocyte clusters in relation to the diagnosis. The exploratory analysis using UMAP and density plots showed evident differences in the cell distribution across different diseases (Figure 52A). Differences in

the MSI of several functional markers were also observed, and some of them are represented in Figure 52B.

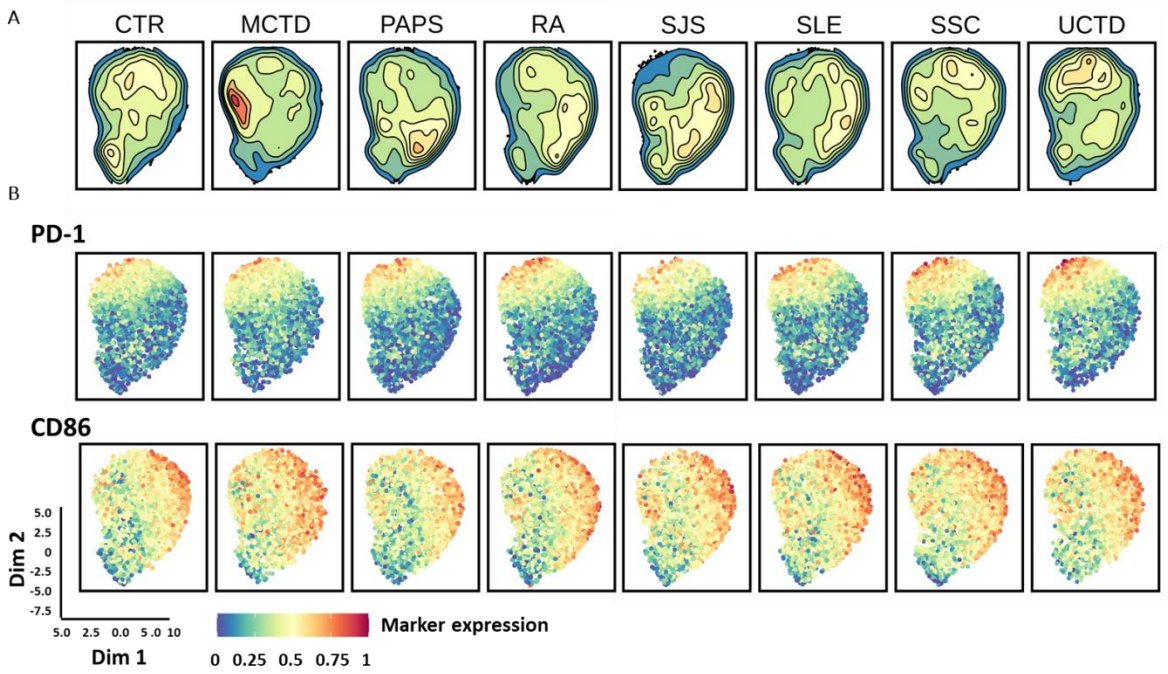

Figure 52 Cell frequency and MSI exploration in granulocytes.

UMAP was generated as described above and represented across different groups of patients using density plots (A) or dot plots (B). For the density plot equal number of randomly selected cells (1,000 per diagnosis) from each disease are represented and for the dot plot 50,000 cells are drawn. (A) Data are represented as in Figure 47A. (B) The diagnosis labels are represented as in A. Cells are colored according to the expression level of the functional makers PD-1 or CD86, and represented as in Figure 47B.

To get a deeper look into the differences between patient groups we performed a K-W analysis followed by a Dunn *post-hoc* test for both cluster frequencies (Figure 53) and MSI features, (Figure 54).

In total, 9 clusters were differentially expressed between some pairs of groups of patients, and 7 showed statistically significant differences in the *post-hoc* analysis. In CL2, SJS patients had higher cell frequencies compared to controls, the same was observed for CL3 and CL15, and, additionally, SJS patients had higher cell frequency in CL3 and lower in CL15 when compared to SSC and UCTD. Lower CL8 frequency compared to CTR was observed for SJS, SLE and SSC, and for SSC and UCTD for CL10. Higher frequency of CL16 was observed for SSC and UCTD patients when compared to SJS, although no statistical significance was detected between patients and CTR.

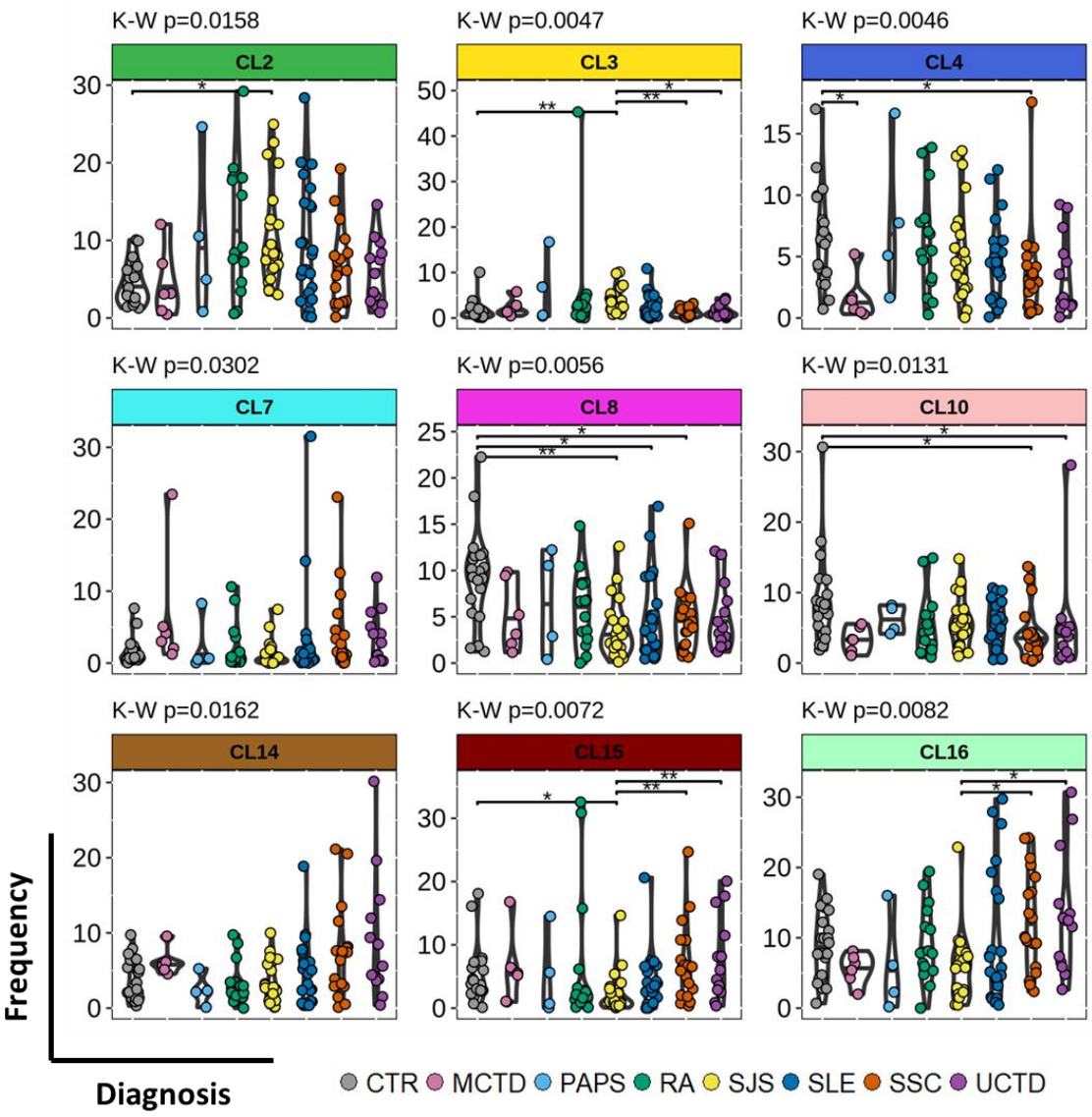

Figure 53 Differential analysis based on granulocyte cluster frequencies.

Cell frequencies were quantified for each cluster as described in methods. Differential analysis was performed using K-W followed by Dunn test. Data are represented as in Figure 48. Each plot is colored by cluster and each dot in the plot represents an individual, colored by the diagnosis. *p < 0.05, **p < 0.01, ***p < 0.001 in Dunn test.

The expression of three markers (CD86, CD95 and CD38) in specific clusters was statistically different between the groups. Among them a decrease in CD86 expression was observed for UCTD, SSC, SLE and SJS patients compared to CTR. Additionally UCTD patients had lower CD86 expression compared to PAPS. The UCTD group had also lower CD86 expression in CL7 compared to CTR. CD95 increased expression in patients was observed in CL3, CL5, CL7 and CL15 compared to CTR, however no difference was observed between any group of patients. The expression of CD38 was decreased in RA, SLE and UCTD when compared to MCTD, additionally MCTD has higher CD38 level than CTR.

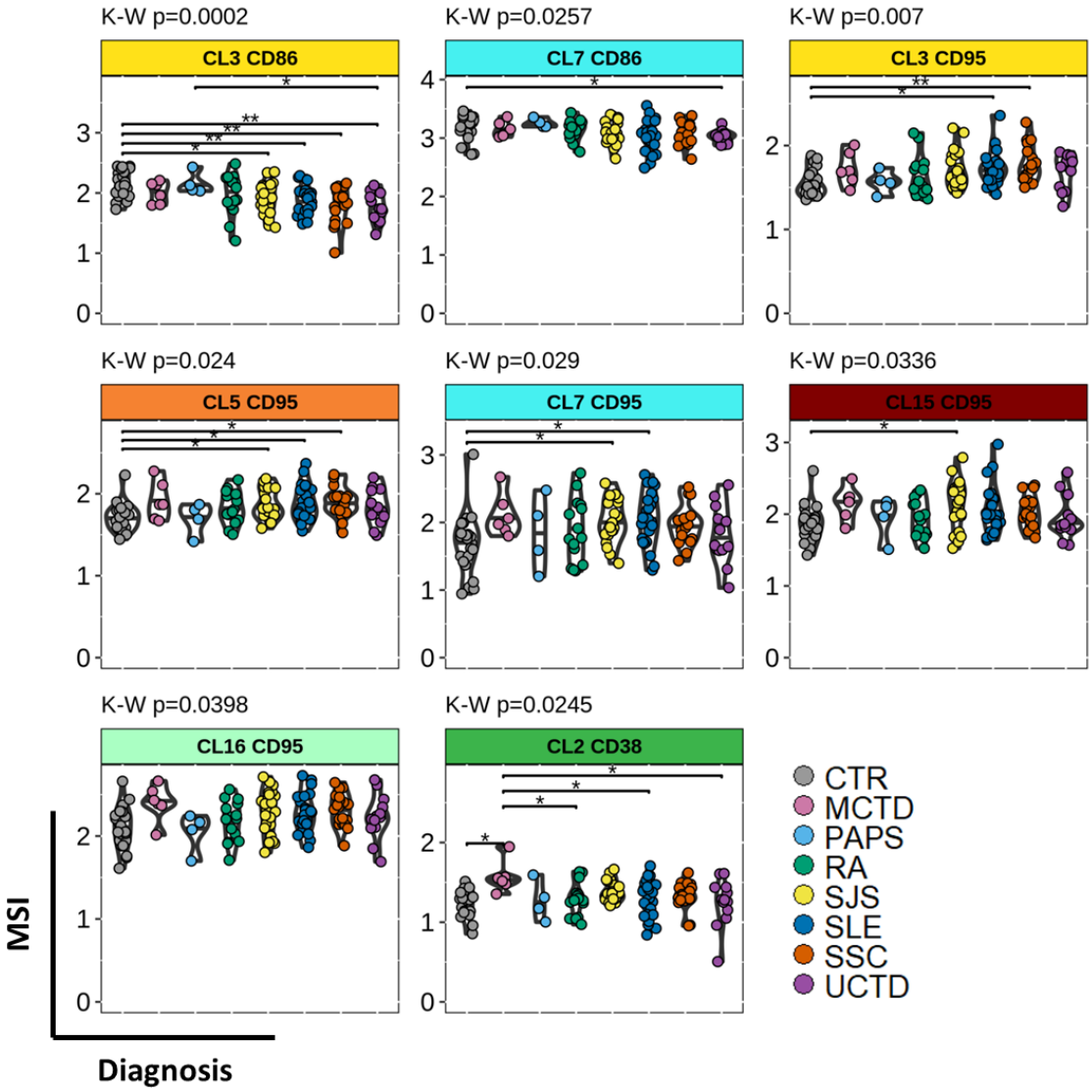

Figure 54 Differential analysis based on MSI of functional markers for granulocytes.

MSI of functional markers were quantified for each cluster and the data are represented as in Figure 48

The hierarchical clustering analysis showed 3 main groups of diseases using differentially expressed features detected by K-W test (Figure 55). Group 1 contained highly similar SSC and UCTD patients as observed in the PBMC compartment, and additionally these two groups were grouped together with MCTD patients. This group was characterized by high frequency of CL16, CL7, CL14 and CL15 but low frequency of CL2 and CL3 cells. They were also characterized by increased CD95 expression. Group 2 contained SJS and SLE patients, which were also grouped together in PBMC analysis. This group was characterized by high CD95 expression as Group 1, but was opposite in clusters representing cell frequency. In Group 2 although CTR and

PAPS were grouped together as in the PBMC analysis, higher similarity of PAPS to RA patients than to CTR was observed. This group had lower CD95 and CD38 expression than Group 1 and 2, but higher expression of CD86 marker and frequency of CL8, CL4 and CL10 cells.

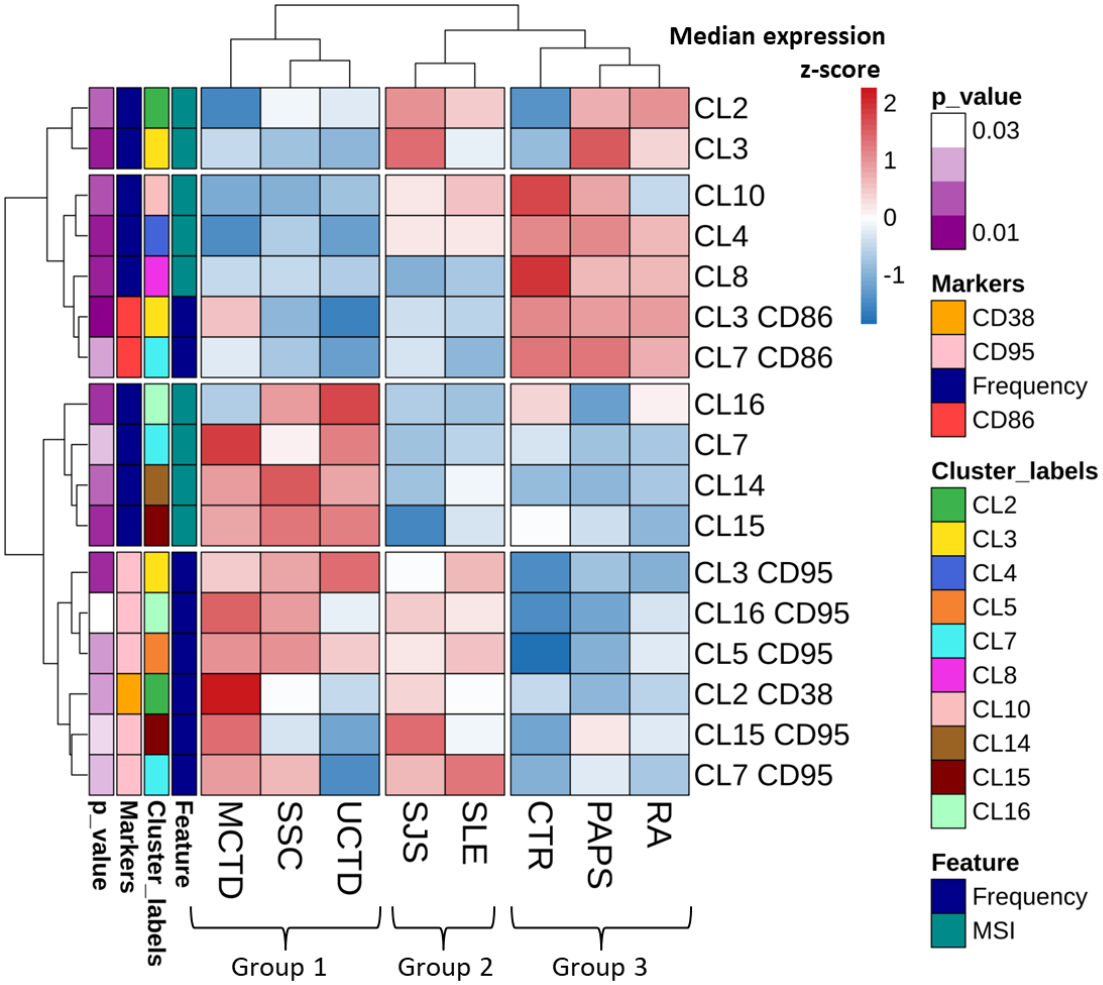

Figure 55 Hierarchical clustering of SADs based on K-W selected granulocyte features.

Features with significant differential values in K-W analysis (shown in Figure 53 and Figure 54) were selected for clustering analysis. The median for each feature and disease category was calculated. Data are represented as in Figure 50.

8.2.6 Feature selection for reclassification analysis

As mentioned in the introduction, although SADs have different diagnostic labels and clinical manifestations, they can be characterized by similar molecular and cellular mechanisms that could be used for their reclassification.

In order to verify if patient clusters can be obtained based on this deep-phenotyping study, we first selected features that were SADs-specific, that is, that differentiated the patients

form the healthy controls. To do this, we joined all metaclusters and clusters from PBMC and granulocyte respectively, together with MSI of functional markers, and we performed the M-W analysis as described in the methods section.

The volcano plot represents the cell features that differ between SADs and CTR (Figure 56). Thirty two differentially expressed features were selected. Among them cluster and metacluster frequencies were mostly at lower level in SADs compared to CTR, and markers of cell activation and ability for induced-cell death, represented by CD38 and CD95 markers, respectively, were at higher levels in SADs as compared to CTR.

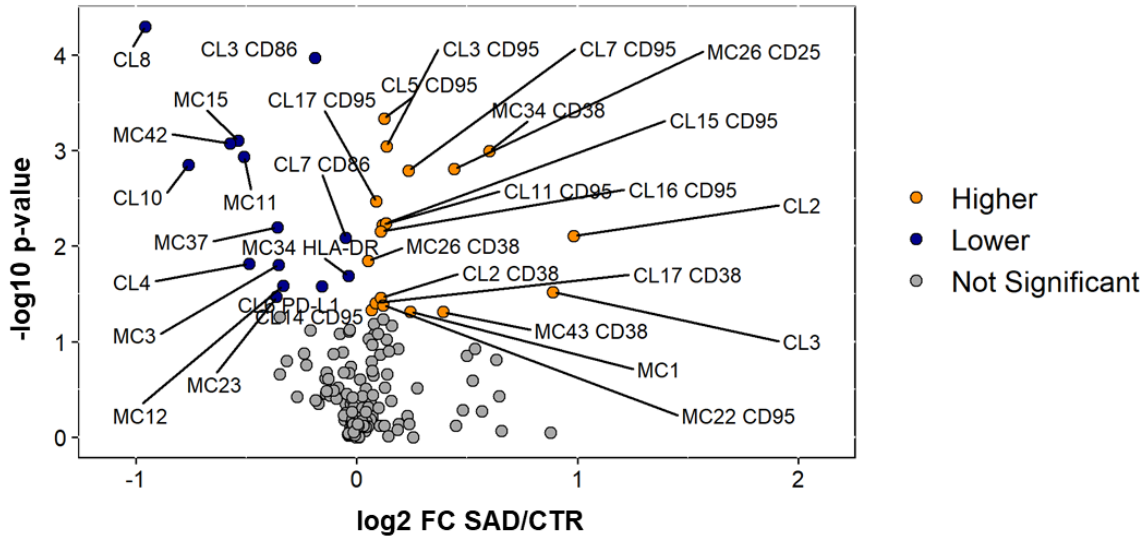

Figure 56 Feature selection for SADs reclassification study.

Volcano plot represents features being differentially expressed between SADs (autoimmune disease, n = 104) and CTR (control individuals, n = 22). The M-W test was used. On the y-axis are the –log10 transformed p-values, and on the x-axis the log2 fold change (FC) between SADs and CTR. The blue and orange points represent features with lower or higher values in SADs than in CTR respectively, which are statistically significant (p-value ≤ 0.05). The grey points represent features that are not-differentially expressed. Features labeled only with MC or CL number represent frequency features, and those with MC or CL number and marker represents MSI.

We next verified how these features were affected by the three most abundant treatments used in our cohort: antimalarials, immunosuppressants and steroids. We compared treated (Tx) and non-treated (NTx) groups, but also tracked the changes when compared to the CTR group (Table 13).

Some changes were observed associated with antimalarials and steroids when compared Tx with NTx groups, and mostly affected the PBMC compartment. In antimalarial treated patients, the frequency of MC1 ($CD14^{hi}$ Monocytes) was affected, and patients receiving treatment had

increased levels of these cells were compared to the NTx and CTR groups. On the other hand, a decrease in MC15 (pDCs) frequency was observed when comparing treated patients to both NTx and CTR groups. The expression of HLA-DR in MC34 ($CD4^{+}$ CM T cells, Tregs) was also affected by treatment, and Tx patients had lower HLA-DR expression when compared to NTx and CTR groups. The frequency of granulocytes in CL10 was also affected by the drug, but this time treated patients had higher and lower cell frequencies when compared to NTx and CTR, respectively.

Steroid treatment affected the frequency of MC1 ($CD14^{hi}$ monocytes), and treated patients had higher number of these cells compared to NTx group. In MC11 ($CD56^{mid}$ NK cells), MC15 and MC42 (γδ T cells) a decrease was observed in patients receiving the drug as compared to NTx and CTR. An increased expression of CD25 and CD38 markers in MC26 (basophils) was observed when compared Tx vs NTx and this effect was stronger for the CD38 marker. No differences between Tx and NTx groups were observed for immunosuppressant treatment.

Table 13 Treatment influence on cell frequencies and MSI

CL/MC	Median [IQR]			Mann-Whitney (FDR)		
	CTR	Tx	NTx	CTR-NTx	CTR-Tx	NTx-Tx
Antimalarial CTR (N = 22); Tx (N = 20), NTx (N = 84)						
CL10	7.61 [4.72 - 9.51]	5.54 [2.83 - 7.96]	3.8 [2.04 - 5.43]	***	*	*
CL11 CD95	1.71 [1.6 - 1.88]	1.89 [1.73 - 2.08]	1.88 [1.7 - 1.97]	*	*	ns
CL14 CD95	1.91 [1.75 - 1.98]	2.01 [1.88 - 2.13]	1.95 [1.82 - 2.09]	ns	ns	ns
CL15 CD95	1.85 [1.7 - 1.95]	2 [1.87 - 2.28]	1.98 [1.79 - 2.21]	*	**	ns
CL16 CD95	2.09 [1.95 - 2.24]	2.3 [2.18 - 2.47]	2.23 [2.08 - 2.42]	ns	**	ns
CL17 CD38	1.45 [1.37 - 1.52]	1.51 [1.34 - 1.62]	1.56 [1.43 - 1.65]	*	ns	ns
CL17 CD95	2.18 [2.09 - 2.29]	2.33 [2.25 - 2.5]	2.31 [2.17 - 2.41]	*	**	ns
CL2	3.48 [2.16 - 5.95]	7.86 [3.5 - 14.77]	6.93 [2.93 - 9.7]	ns	**	ns
CL2 CD38	1.28 [1.11 - 1.35]	1.32 [1.19 - 1.43]	1.36 [1.26 - 1.48]	ns	ns	ns
CL3	1.06 [0.47 - 1.97]	2.19 [0.84 - 4.19]	1.68 [0.76 - 3.14]	ns	ns	ns
CL3 CD86	2.12 [1.96 - 2.34]	1.83 [1.67 - 2.07]	1.94 [1.75 - 2.11]	***	***	ns
CL3 CD95	1.51 [1.44 - 1.64]	1.73 [1.57 - 1.88]	1.66 [1.55 - 1.75]	**	**	ns
CL4	6.36 [3.8 - 7.93]	4.42 [1.55 - 5.62]	3.59 [1.68 - 6.65]	*	*	ns
CL5 CD95	1.69 [1.59 - 1.79]	1.85 [1.75 - 2.07]	1.82 [1.73 - 1.96]	**	***	ns
CL6 PD-L1	1.59 [1.46 - 1.75]	1.35 [1.15 - 1.64]	1.41 [1.2 - 1.63]	ns	*	ns
CL7 CD86	3.23 [3.12 - 3.36]	3.05 [2.93 - 3.22]	3.11 [3.01 - 3.24]	*	*	ns
CL7 CD95	1.73 [1.44 - 1.83]	1.99 [1.71 - 2.37]	1.93 [1.7 - 2.1]	**	**	ns
CL8	9.65 [7.21 - 11.5]	3.22 [1.75 - 6.79]	4.49 [2.23 - 6.96]	***	***	ns
MC1	16.76 [12.88 - 19.18]	20.49 [16.48 - 24.4]	17.25 [13.68 - 19.73]	ns	**	**
MC11	3.71 [2.51 - 4.2]	2.64 [1.49 - 3.22]	2.09 [1.35 - 2.85]	***	*	ns
MC12	2.92 [2.24 - 3.97]	2.12 [1.42 - 2.96]	2.48 [1.69 - 3.26]	ns	*	ns
MC15	0.33 [0.25 - 0.5]	0.2 [0.15 - 0.3]	0.27 [0.2 - 0.35]	*	***	*
MC22 CD95	1.55 [1.39 - 1.72]	1.78 [1.45 - 1.99]	1.71 [1.43 - 1.92]	ns	ns	ns
MC23	0.07 [0.05 - 0.08]	0.06 [0.04 - 0.09]	0.04 [0.03 - 0.07]	*	ns	ns
MC26 CD25	1.16 [0.92 - 1.48]	1.75 [1.47 - 2.12]	1.5 [1.15 - 2]	*	***	ns
MC26 CD38	3.62 [3.45 - 3.69]	3.84 [3.53 - 3.99]	3.76 [3.52 - 3.89]	*	*	ns
MC3	0.04 [0.03 - 0.05]	0.03 [0.02 - 0.05]	0.03 [0.02 - 0.04]	ns	ns	ns

MC34 CD38	0.93 [0.63 - 1.46]	1.88 [1.44 - 2.16]	1.68 [0.81 - 2.17]	*	***	ns
MC34 HLA-DR	4.23 [4.13 - 4.33]	4.03 [3.84 - 4.18]	4.15 [4.08 - 4.4]	ns	***	***
MC37	4.94 [4.04 - 6.47]	3.16 [1.51 - 5.48]	3.22 [1.98 - 4.74]	*	*	ns
MC42	1.59 [1.19 - 2.28]	1.06 [0.66 - 1.68]	0.83 [0.46 - 1.61]	**	*	ns
MC43 CD38	1.21 [0.83 - 1.99]	2.11 [0.86 - 2.76]	1.66 [1.13 - 2.36]	ns	ns	ns
Immunosuppressant CTR (N = 22); Tx (N = 46), NTx (N = 58)						
CL10	7.61 [4.72 - 9.51]	5.31 [2.59 - 6.07]	4.27 [2.19 - 6.56]	**	*	ns
CL11 CD95	1.71 [1.6 - 1.88]	1.87 [1.68 - 1.99]	1.89 [1.73 - 2.03]	*	ns	ns
CL14 CD95	1.91 [1.75 - 1.98]	1.9 [1.74 - 2.05]	2 [1.89 - 2.11]	ns	ns	ns
CL15 CD95	1.85 [1.7 - 1.95]	2.04 [1.76 - 2.26]	1.99 [1.84 - 2.22]	*	ns	ns
CL16 CD95	2.09 [1.95 - 2.24]	2.26 [2.07 - 2.43]	2.25 [2.14 - 2.45]	*	ns	ns
CL17 CD38	1.45 [1.37 - 1.52]	1.61 [1.43 - 1.72]	1.53 [1.36 - 1.63]	ns	*	ns
CL17 CD95	2.18 [2.09 - 2.29]	2.28 [2.18 - 2.4]	2.32 [2.2 - 2.46]	**	ns	ns
CL2	3.48 [2.16 - 5.95]	8.75 [4.25 - 17.83]	6.66 [3.03 - 10.47]	*	*	ns
CL2 CD38	1.28 [1.11 - 1.35]	1.35 [1.27 - 1.56]	1.34 [1.24 - 1.44]	ns	ns	ns
CL3	1.06 [0.47 - 1.97]	1.92 [0.84 - 3.22]	1.91 [0.74 - 3.57]	ns	ns	ns
CL3 CD86	2.12 [1.96 - 2.34]	1.94 [1.8 - 2.22]	1.9 [1.68 - 2.06]	***	ns	ns
CL3 CD95	1.51 [1.44 - 1.64]	1.58 [1.5 - 1.75]	1.7 [1.59 - 1.82]	***	ns	ns
CL4	6.36 [3.8 - 7.93]	5 [2.17 - 8.05]	3.92 [1.42 - 5.69]	*	ns	ns
CL5 CD95	1.69 [1.59 - 1.79]	1.85 [1.75 - 2.01]	1.83 [1.73 - 2.01]	**	**	ns
CL6 PD-L1	1.59 [1.46 - 1.75]	1.34 [1.18 - 1.59]	1.42 [1.16 - 1.63]	ns	ns	ns
CL7 CD86	3.23 [3.12 - 3.36]	3.13 [3.05 - 3.26]	3.07 [2.95 - 3.22]	*	ns	ns
CL7 CD95	1.73 [1.44 - 1.83]	1.92 [1.66 - 2.14]	1.97 [1.71 - 2.27]	**	ns	ns
CL8	9.65 [7.21 - 11.5]	4.35 [2.01 - 7.23]	3.68 [1.91 - 6.78]	***	**	ns
MC1	16.76 [12.88 - 19.18]	18.68 [16.2 - 22.32]	18.63 [14.32 - 21.62]	ns	ns	ns
MC11	3.71 [2.51 - 4.2]	1.88 [1.29 - 2.48]	2.51 [1.48 - 3.17]	**	**	ns
MC12	2.92 [2.24 - 3.97]	1.94 [1.38 - 2.33]	2.47 [1.66 - 3.23]	ns	*	ns
MC15	0.33 [0.25 - 0.5]	0.2 [0.15 - 0.25]	0.27 [0.18 - 0.34]	**	***	ns
MC22 CD95	1.55 [1.39 - 1.72]	1.89 [1.55 - 2.03]	1.73 [1.43 - 1.93]	ns	ns	ns
MC23	0.07 [0.05 - 0.08]	0.04 [0.03 - 0.07]	0.05 [0.03 - 0.08]	ns	ns	ns
MC26 CD25	1.16 [0.92 - 1.48]	1.71 [1.18 - 1.98]	1.62 [1.27 - 2.06]	**	*	ns
MC26 CD38	3.62 [3.45 - 3.69]	3.63 [3.45 - 3.81]	3.8 [3.56 - 3.96]	*	ns	ns
MC3	0.04 [0.03 - 0.05]	0.03 [0.02 - 0.05]	0.03 [0.02 - 0.04]	*	ns	ns
MC34 CD38	0.93 [0.63 - 1.46]	1.68 [1.02 - 2.15]	1.73 [1.15 - 2.16]	**	*	ns
MC34 HLA-DR	4.23 [4.13 - 4.33]	4.17 [4.05 - 4.36]	4.1 [3.95 - 4.25]	*	ns	ns
MC37	4.94 [4.04 - 6.47]	2.6 [1.92 - 3.81]	3.22 [1.95 - 5.2]	*	**	ns
MC42	1.59 [1.19 - 2.28]	0.89 [0.44 - 1.36]	0.96 [0.56 - 1.69]	**	**	ns
MC43 CD38	1.21 [0.83 - 1.99]	1.47 [0.69 - 2.51]	1.98 [1.16 - 2.6]	ns	ns	ns
Steroids CTR (N = 22); Tx (N = 39), NTx (N = 65)						
CL10	7.61 [4.72 - 9.51]	4.3 [2.54 - 6.69]	4.5 [2.28 - 6.33]	**	**	ns
CL11 CD95	1.71 [1.6 - 1.88]	1.89 [1.71 - 2.12]	1.89 [1.72 - 1.97]	*	*	ns
CL14 CD95	1.91 [1.75 - 1.98]	1.97 [1.84 - 2.12]	2 [1.89 - 2.09]	ns	ns	ns
CL15 CD95	1.85 [1.7 - 1.95]	1.99 [1.83 - 2.26]	1.99 [1.82 - 2.23]	*	*	ns
CL16 CD95	2.09 [1.95 - 2.24]	2.33 [2.16 - 2.46]	2.24 [2.1 - 2.42]	*	*	ns
CL17 CD38	1.45 [1.37 - 1.52]	1.57 [1.37 - 1.76]	1.53 [1.38 - 1.64]	ns	ns	ns
CL17 CD95	2.18 [2.09 - 2.29]	2.34 [2.21 - 2.51]	2.31 [2.18 - 2.4]	*	**	ns
CL2	3.48 [2.16 - 5.95]	8.4 [2.92 - 15.45]	6.14 [3.16 - 9.76]	*	*	ns
CL2 CD38	1.28 [1.11 - 1.35]	1.35 [1.25 - 1.48]	1.32 [1.24 - 1.44]	ns	ns	ns
CL3	1.06 [0.47 - 1.97]	2.41 [1.01 - 3.62]	1.67 [0.74 - 3.2]	ns	ns	ns
CL3 CD86	2.12 [1.96 - 2.34]	1.85 [1.72 - 2.1]	1.93 [1.7 - 2.09]	***	***	ns
CL3 CD95	1.51 [1.44 - 1.64]	1.7 [1.57 - 1.83]	1.68 [1.55 - 1.79]	**	**	ns
CL4	6.36 [3.8 - 7.93]	3.91 [1.16 - 5.61]	4.08 [1.68 - 6.31]	*	*	ns
CL5 CD95	1.69 [1.59 - 1.79]	1.87 [1.72 - 2.05]	1.83 [1.74 - 1.96]	**	**	ns
CL6 PD-L1	1.59 [1.46 - 1.75]	1.33 [1.17 - 1.57]	1.43 [1.19 - 1.66]	ns	ns	ns
CL7 CD86	3.23 [3.12 - 3.36]	3.12 [2.9 - 3.24]	3.08 [3 - 3.2]	*	*	ns
CL7 CD95	1.73 [1.44 - 1.83]	2 [1.66 - 2.26]	1.97 [1.72 - 2.18]	**	**	ns
CL8	9.65 [7.21 - 11.5]	3.5 [1.59 - 6.72]	3.79 [1.99 - 7.17]	***	****	ns
MC1	16.76 [12.88 - 19.18]	20.14 [17.27 - 25.57]	16.79 [13.68 - 20.02]	ns	**	**

MC11	3.71 [2.51 - 4.2]	1.92 [1.15 - 2.78]	2.62 [1.68 - 3.28]	**	**	*
MC12	2.92 [2.24 - 3.97]	2.41 [1.9 - 3.04]	2.13 [1.46 - 3.11]	ns	ns	ns
MC15	0.33 [0.25 - 0.5]	0.22 [0.15 - 0.28]	0.28 [0.18 - 0.36]	*	****	*
MC22 CD95	1.55 [1.39 - 1.72]	1.81 [1.54 - 1.97]	1.68 [1.39 - 1.91]	ns	*	ns
MC23	0.07 [0.05 - 0.08]	0.04 [0.03 - 0.07]	0.06 [0.04 - 0.08]	ns	*	ns
MC26 CD25	1.16 [0.92 - 1.48]	1.82 [1.39 - 2.2]	1.54 [1.18 - 1.98]	*	***	*
MC26 CD38	3.62 [3.45 - 3.69]	3.91 [3.76 - 4.11]	3.67 [3.49 - 3.87]	ns	***	***
MC3	0.04 [0.03 - 0.05]	0.03 [0.02 - 0.04]	0.03 [0.02 - 0.05]	ns	*	ns
MC34 CD38	0.93 [0.63 - 1.46]	1.55 [1.09 - 2.13]	1.89 [1.14 - 2.17]	**	*	ns
MC34 HLA-DR	4.23 [4.13 - 4.33]	4.15 [3.97 - 4.33]	4.1 [3.96 - 4.23]	*	ns	ns
MC37	4.94 [4.04 - 6.47]	3.22 [1.51 - 5.06]	3.21 [1.99 - 5.11]	*	*	ns
MC42	1.59 [1.19 - 2.28]	0.7 [0.43 - 1.15]	1.03 [0.63 - 2.04]	*	****	*
MC43 CD38	1.21 [0.83 - 1.99]	1.65 [0.93 - 2.46]	1.89 [1.11 - 2.65]	ns	ns	ns

ns p > 0.05, *p < 0.05, **p < 0.01, ***p < 0.001
CTR – healthy control, Tx – treated, NTx – non-treated

8.2.7 Patient reclassification

K-means clustering, performed as described in the methods section, identified 4 main clusters, annotated as C1, C2, C3 and C4, as shown in Figure 57A. These clusters grouped the patients independently of their diagnosis, as mixtures of different diseases can be observed in different clusters (Figure 57A and C). Additionally 4 groups of features could be also identified. One group contained mostly frequencies extracted from the PBMC compartment, a second group contained the MSI signals from CD38, CD25 and HLA-DR also from PBMC metaclusters, and two groups from granulocyte-derived features had the frequency of CL and features expressing CD86, PD-L1 and CD95 in CL3, in addition to MSI features containing both CD95 and CD38 expressing CLs.

C1 contained 24 samples exclusively coming from patients, as shown by pink color in the column annotation, named “Diagnosis_SAD_CTR” (Figure 57A). This cluster was mostly characterized by high CD95 and CD38 expression in multiple granulocyte features, besides low CD95 expression in CL3. The low expression of CD86 and PD-L1 in CL and low frequencies of some granulocyte-derived features was also observed. On the other hand, higher frequency of metaclusters derived from the PBMC compartment was noticed, and markers like CD38 and CD95 were elevated in MC22 (unknown) and MC26 (basophils), respectively. On the other hand, lower expression of activation markers like CD38 in MC34 ($CD4^+$ CM T cells) and MC43 ($CD8^+$ CM T cells), CD25 together with HLA-DR in MC25 ($CD8^+$ TEMRA T cells) and MC26 (basophils), was observed. C2 contained 32 individuals, of which 14 samples (44%) were CTRs (Figure 57A). The C2 cluster was exactly opposite to C1, hence it was characterized by lower CD95 expression and CD38 expression in the granulocyte compartment, besides high CD95

expression in CL3. C3 included 43 individuals which were mostly patients, as only 3 CTRs could be found (7%). This cluster was unclassifiable, as a mixture of different feature levels could be found. C4 with 27 individuals, including 5 CTRs (19%) was an intermediate cluster between C1 and C2. The patients in this group were characterized by moderate levels of CD95 and CD38 in granulocyte populations, although the expression of CD95 in CL3 and CD86 is more related to C2 than to C1. On the other hand, the levels of CD95 and CD38 in MC22 and MC26 were similar to C1. It should be noted that a Spearman's correlation of the features used for clustering showed some blocks of highly ($r_s \geq 0.8$) and moderately ($r_s < 0.8$ and ≥ 0.5) correlated (positively and negatively) features. CD95 expression showed high and moderate positive correlations with other CL in various granulocyte subsets, and showed moderate inverse correlation with CD86 expression in granulocyte compartments. An inverse correlation was also observed for CL4 and CL8 frequencies. Low positive correlation was noticed between clusters with CD95 expression and activation marker expression (CD38, CD25, HLA-DR) in the PBMC compartment. Low correlations were detected for features derived from the PBMC compartment.

When exploring disease composition of the clusters, excluding CTRs (Figure 57C), it can be appreciated that the different diseases were distributed across the clusters. However, diagnosis-specific increments could also be observed: SLE patients were evenly distributed across the clusters, however the majority of RA patients could be found in C2 and SSC were mostly located in C3 and C4. SJS patients were enriched in C1 and C3. MCTD could not be found in the C3 group. In relation to the treatment, it could be observed that patients with immunosuppressive treatment were equally distributed across the clusters. However some enrichment of antimalarial and steroid drugs could be observed in C1. The age of the patients did not show any differences and some differences in the disease duration could be seen across the clusters, although *post-hoc* Dunn analysis did not detect significant changes.

We next measured the level of cytokines/chemokines expressed in each cluster, Figure 58. To do this we tested 45 proteins (as described in methods insert) and detected 5 differentially expressed cytokines across 4 clusters. GROα was highly expressed in clusters C1, C2, C3 but not C4, and CTR had moderate expression of this cytokine. IL-10 and TNFα expression was high in C1 and C4 and there was a statistical difference between these clusters and C2. The highest expression of IP-10 was observed in C1. Furthermore, there was a statistical significance compared to C2 and C3. On the other hand, the level of TGFα was the lowest in C1 and the highest in C2 and C3. It was interesting to notice that the CTR group used here as a reference

had similar cytokine levels compared to C2 except for GROα, for which C2 had higher expression than observed in CTRs. Besides TNFα, cytokine production was not affected by the treatment, Table 14. However, some differences could be observed for the cell frequency and MSI in antimalarial and steroid treatment (see Table 13), thus this could affect the patients clustering especially in C1. Nevertheless, it should be pointed out that while the treated group differed from non-treated patients, there were still important differences from CTRs, suggesting that the C1 group enriched in treated patients was associated with higher severity than the rest of the individuals. It is to be noted that the treatment presented here had a larger impact on the PBMC compartment and almost none on granulocytes, despite its clear dysregulation in some groups of patients.

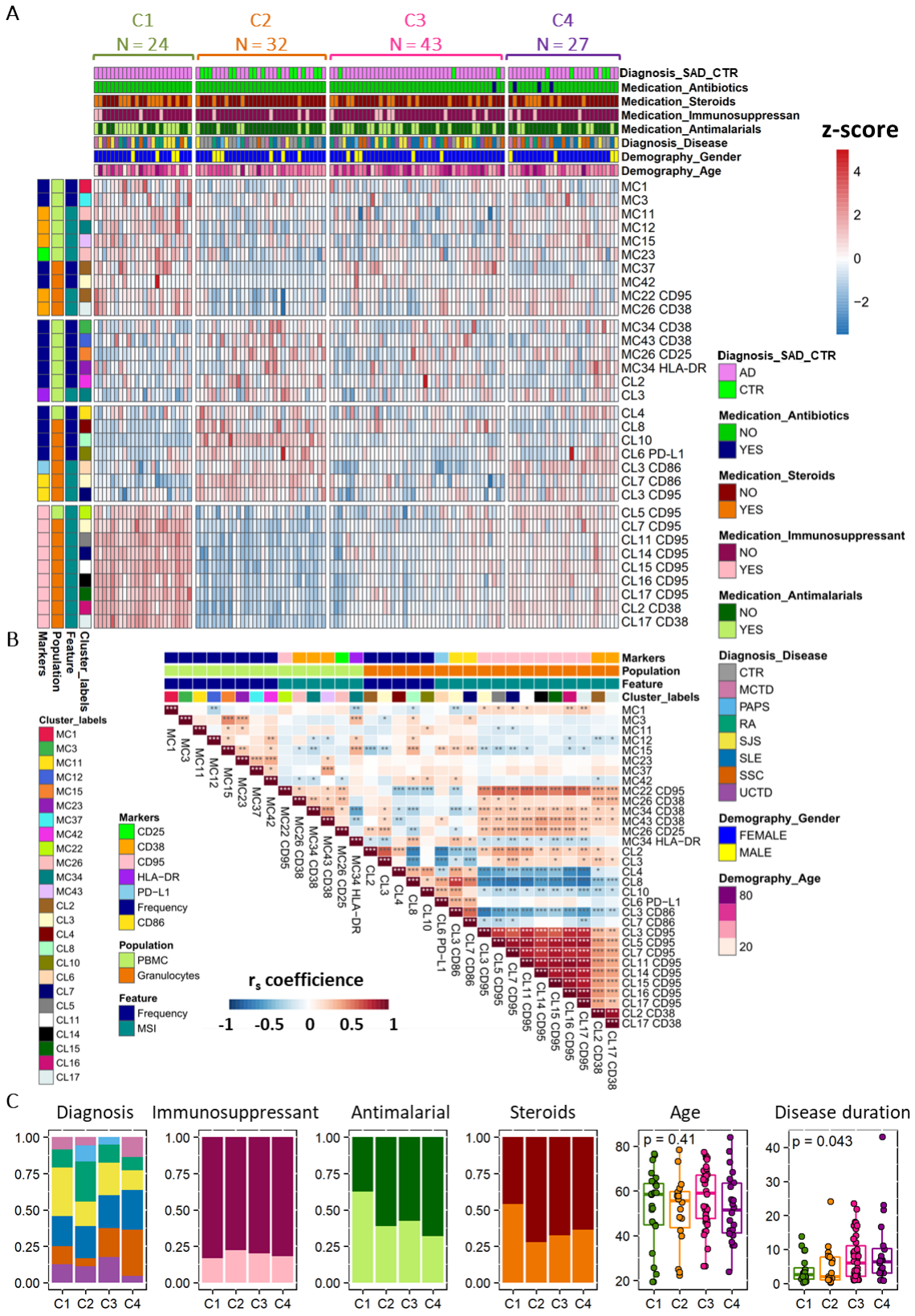

Figure 57 Patient reclassification.

(A) The heatmap represents scaled values (z-scores) for each selected feature across all individuals. In rows, features selected as in Figure 56 are shown together with the annotation on the left. The annotation colors show the manual label of each PBMC metacluster, and whether or not they represent frequency or MSI feature from PBMC or granulocytes (see legend in panel B for details). In the columns, each individual is plotted together with

color-coded clinical and experimental information shown at the top of the heatmap and in the legend on the right. Four clusters were identified (C1 – green, C2 – orange, C3 – pink, C4 - purple) by k-means clustering. (B) Heatmap representing Spearman's correlation coefficients, positive (red) and negative (blue) for the features selected as described above. Color intensity is proportional to the strength of the correlation. The column annotation is represented as row annotation in A and the significance is indicated by asterisks. (C) Distribution of different clinical parameters in the clusters identified in A and represented on the x-axis. The y-axis represents the total number of patients for each cluster or for the boxplots on the right, for age and disease duration. Colors are represented as in legend from A and B, besides age and disease duration that have cluster-specific colors, as shown in panel A . *p < 0.05, **p < 0.01, ***p < 0.001 in Spearman test

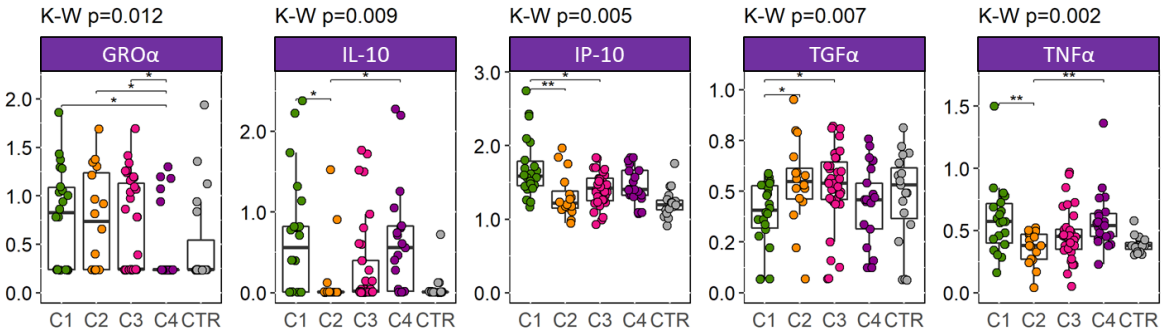

Figure 58 Cytokine expression between clusters.

Cytokines were quantified in the diluted plasma of UNS blood samples as described in the methods section, and their levels were measured across identified clusters. Data are represented by the boxplot where the x-axis shows cluster labels together with CTR group and the y-axis represents log transformed values for cytokine expression. Each dot represents one individual and is colored by the cluster colors as in Figure 57. Differential analysis was performed using K-W followed by the Dunn test. The K-W p-values can be found above each plot and for the Dunn test statistical intervals are shown on the plots. The p-values for the Dunn test were adjusted using false discovery rate (FDR) method to account for multiple comparisons. CTR were not included in the statistical tests, and are shown for reference purposes. Only cytokines with p-values ≤ 0.05 for K-W are shown. *p < 0.05, **p < 0.01, ***p < 0.001 in Dunn test.

Table 14 Treatment influence on cytokine production

Cytokines	Median [IQR]			Mann-Whitney (FDR)		
	CTR	Tx	NTx	CTR-NTx	CTR-Tx	NTx-Tx
Immunosuppressant (N = 19); T (N = 19), NT (N = 75)						
GROα	0.24 [0.24 - 0.54]	0.87 [0.24 - 1.07]	0.24 [0.24 - 1.09]	ns	ns	ns
IL-10	0.01 [0.01 - 0.02]	0.15 [0.01 - 0.71]	0.05 [0.01 - 0.79]	*	*	ns
IP-10	1.2 [1.13 - 1.26]	1.38 [1.27 - 1.69]	1.45 [1.24 - 1.66]	***	***	ns
TGFα	0.53 [0.36 - 0.61]	0.51 [0.42 - 0.58]	0.49 [0.35 - 0.59]	ns	ns	ns
TNFα	0.38 [0.35 - 0.4]	0.5 [0.38 - 0.64]	0.46 [0.38 - 0.59]	*	*	ns
Antimalarial (N = 19); Tx (N = 43), NTx (N = 51)						
GROα	0.24 [0.24 - 0.54]	0.78 [0.24 - 1.23]	0.24 [0.24 - 0.94]	ns	ns	ns
IL-10	0.01 [0.01 - 0.02]	0.28 [0.01 - 0.87]	0.01 [0.01 - 0.61]	ns	**	ns
IP-10	1.2 [1.13 - 1.26]	1.42 [1.22 - 1.67]	1.44 [1.28 - 1.66]	***	**	ns
TGFα	0.53 [0.36 - 0.61]	0.49 [0.36 - 0.59]	0.51 [0.43 - 0.59]	ns	ns	ns
TNFα	0.38 [0.35 - 0.4]	0.51 [0.39 - 0.71]	0.45 [0.38 - 0.53]	*	**	*
Steroids CTR (N = 19); Tx (N = 37), NTx (N = 57)						
GROα	0.24 [0.24 - 0.54]	0.39 [0.24 - 1.07]	0.24 [0.24 - 1.1]	ns	ns	ns

IL-10	0.01 [0.01 - 0.02]	0.02 [0.01 - 0.82]	0.05 [0.01 - 0.71]	*	*	ns
IP-10	1.2 [1.13 - 1.26]	1.51 [1.32 - 1.7]	1.39 [1.22 - 1.56]	**	****	ns
TGFα	0.53 [0.36 - 0.61]	0.53 [0.4 - 0.65]	0.49 [0.36 - 0.56]	ns	ns	ns
TNFα	0.38 [0.35 - 0.4]	0.46 [0.38 - 0.62]	0.47 [0.38 - 0.57]	*	*	ns
ns p > 0.05, *p < 0.05, **p < 0.01, ***p < 0.001 CTR – healthy control, Tx – treated, NTx – non-treated						

8.3 Disscusion

Here we performed a deep-phenotyping study using mass cytometry to compare and reclassify the SADs. Using cell frequencies and levels of expression of functional markers we noticed poor feature discrimination capacity between the different diseases when using a differential analysis approach. Hence no disease-specific biomarker could be identified. However, the analysis of autoimmune-specific features together with unsupervised clustering analysis identified 4 clusters of the diseases that differed in the cell frequencies and their activation status. Importantly these clusters grouped different diagnoses showing high patient heterogeneity within the clinical labels. Our data thus supports the hypothesis that SADs are heterogeneous and have overlapping cellular phenotypes across different diagnoses. These overlapping patterns can be captured by high content fine immune phenotyping using mass cytometry

In this study we used FlowSOM and PhenoGraph to extract features from PBMC and granulocytes, respectively. In PBMC analysis we used canonical markers to identify known cell populations and we observed that FlowSOM was a good tool to do this, based on high scores for purity and F-measure. The number of metaclusters was established by the visual inspection of the known cells and took into consideration the metacluster purities, and thus is biased towards known cell populations. As a future direction, unsupervised analysis using all the clusters could be explored, giving the possibility to compare rare or undescribed cell populations between SADs. Nevertheless, in this study a higher combination of markers could be analyzed in a single tube, in contrast to some flow cytometry studies where multiple panels were used[9]. Therefore, our setting provides a greater number of different populations in a single tube, and the possibility to discover novel cell phenotypes and their cellular state.

PBMCs comprise a heterogeneous and well-studied group of cells. Cell types can be usually distinguished based on bimodal distribution of known markers. On the other hand, granulocytes are usually depleted from the samples after ficoll isolation of PBMC, have a low activation threshold, and important cell death upon preservation. For this reason they are less

studied and therefore markers defining clear-cut subgroups are not well defined. Because of this, to extract granulocyte-related features we used PhenoGraph, an unsupervised clustering algorithm, as described before[28]. This method identified 17 different clusters using 7 markers that showed a different expression gradient across cells. For instance, we found cells that differ in CD11c and CD24 expression. These markers can distinguish neutrophils freshly released from the bone marrow ($CD11c^{low}$ $CD24^{low}$) from aged neutrophils ($CD11c^{hi}$ $CD24^{hi}$)[30,31], although these markers are not canonical. As described before, the aged neutrophils were more activated and had altered pathways for migration and cell death[31]. This is in agreement with the higher CD86 (activation marker) and CD95 expression (Fas, cell death marker) observed in our study. We also found a substantial number of neutrophils expressing the PD-L1 receptor, an immunoregulatory molecule that delivers inhibitory signals to target cells like activated B or T cells. This expression was already described and was associated with the development of diseases like sepsis[32] and tuberculosis[33]. More interestingly it was shown that neutrophils form active tuberculosis patients not only have higher PD-L1 expression[33] but also display a type I IFN signature, which can further upregulate its expression[34]. Moreover, we identified $PD\text{-}1^{+}$ neutrophils, whose high expression was reported to be associated with extreme phenotypes in sepsis[35]. Because CD16 expression cannot be relied due to the fixation of the blood samples, we did not separate the neutrophils from eosinophils, thus these cells are analyzed together. Therefore, the interpretation of $CD11c^{-}$ clusters .that could potentially contain eosinophils should be taken carefully.

In total we detected 62 distinct cell populations (45 metaclusters in PBCM and 17 clusters in granulocytes). Additionally, due to our experimental setting that took special care of experimental variability (e.g. frozen antibody cocktail, barcoding), batch effect tracking, and correction (reference sample), we could also analyze the MSI for functional markers. These gave us another layer of information that was missing in previous studies[6,8,9,36]. The markers CD28, CD69, and PD-L1 could not be analyzed in PBMC due to inefficient correction at normalization, but could be included in the analysis of the granulocyte compartment. The cell-type specific batch effect was previously described[37].

The knowledge about dysregulated immune cell populations in SADs usually comes from differential studies where patients with one concrete disease is compared to CTRs. From these reports we know that SJS patients had lower level of SWME B cells and pDCs in the blood compared to controls[8,38] or RA had lower level of γδ T cells[39], as confirmed in this study. However, it is not known if the same populations are downregulated in other SADs or if they

are disease-specific. In the literature there is also a bias towards studies regarding RA and SLE treated as a model of SADs. However, less is known about MCTD, SSC or UCTD or PAPS. That is why we first performed differential analysis for PBMC and granulocytes comparing 7 different SADs and controls. Although some differences were detected in both frequency and MSI markers we could not report any disease-specific biomarker that could differentiate between patients and controls, thus suggesting their poor diagnostic value. This conclusion was also drawn from other MC study where 3 different SADs (SJS, SLE, SSC) were studied[6]. Nevertheless, the clustering analysis using median expression of either cell frequencies and MSI calculated for each disease showed common patterns between some SADs. Three blocks of related diseases could be observed in the clustering analysis using both PBMC and granulocyte-related features.

Using the data derived from PBMC analysis, SJS and SLE patients grouped together showing their high similarity. Their resemblance was mainly due to CD38 up-regulation in various immune cells and low expression of HLA-DR marker in the myeloid compartment. Thus it seems that SLE and SJS patients could benefit from the same lines of treatment involving CD38 and/or HLA-DR molecules. The activation marker CD38 is dysregulated in various immune cell populations like $CD4^+$ and $CD8^+$ T cells, NK $CD56^{mid}$ cells, DCs and B cells[40,41] in SLE patients. Although here we did not observe any significant differences between SLE and CTR we saw an increased expression of this molecule mostly in MCTD, SLE and SJS patients, moderate level in CTR, SSC and UCTD and a clear down regulation in RA and PAPS that reached statistically significant differences between RA and SLE, MCTD and SJS in multiple populations. It was shown that CD38 expression can be upregulated by TNFα[42], IFNγ[43] or IFNα[44], and its upregulation in T cells was correlated with TNFα and IFNγ production[41]. All these cytokines are known to be involved in SADs pathogenesis and participate in the acceleration of the inflammatory response. It was also reported that virus-activated pDCs producing IFNα are sufficient for CD38 upregulation in both $CD4^+$ and $CD8^+$ T cells[45], suggesting that patients with a high molecular IFN signature can also have elevated CD38 expression. Thus, the CD38 molecule seems to be a good candidate for the treatment of some SADs patients. Interestingly, TNFα and type I IFNs synergistically regulate CD38 expression in human airway smooth muscle cells, making these cells refractory to the anti-inflammatory action of steroids[46]. Daratumumab, an anti-CD38 drug, was successfully used to treat refractory SLE in a case report study[47]. Based on our results, it seems that it could be also applied to other SADs like MCTD and SJS, having a broad spectrum of action on the immune system. However, according

to our results, CD38 expression seems to well differentiate some group of SADs like MCTD-SLE-SJS from RA, but it does not differentiate patients from the healthy controls. Thus, this marker could be used for further substratification of patients who are already classified as having a systemic autoimmune disease.

In contrast to CD38 expression HLA-DR was reduced in several populations, mostly in SLE patients when compared to CTR and RA or SSC patients. This suggests less activation of $CD14^{hi}$ monocytes, $CD1c^{+}$ cDC and $CD4^{+}$ CM T cells, especially in SLE patients but also in SJS in the case of T cells. The down-regulation of HLA-DR on classical monocytes was shown to convert them into immunosuppressive cells[48]. However, as reported in psoriatic patients, these cells induce Treg with decreased suppressive functionality compared to cells from healthy controls[49]. The reduced expression of HLA-DR on DC was already reported for SLE[50] and was attributed to the higher infection rate observed in these patients[51]. Closer analysis of MC34 represented by $CD4^{+}$ CM T cells shows their low and high expression of CD127 and CD25 respectively, suggesting their regulatory phenotype. The HLA-DR expression was shown to be present in mature regulatory T cells[52], and these cells were reported to have higher suppressive function[53]. Additionally high levels of HLA-DR were positively correlated with Treg suppressive activity, and their low expression of HLA-DR was shown to contribute to transplant rejection[54]. This may suggest that the lower expression of HLA-DR detected in SLE and SJS could indicate their lower capacity to suppress other cell functions compared to controls and to RA and SSC.

CTLA-4 is an inhibitory molecule that competes with CD86 and CD80 for interaction with the CD28 activation marker, hence blocking T cell activation[55]. It is interesting to note that its surface expression is upregulated in MC45 ($CD8^{+}$ naïve T cells) in UCTD and SJS patients compared to CTR, MCTD and RA and SLE (only for UCTD). Abatacept is a fusion protein that consists Fc region of the IgG1 immunoglobulin fused to extracellular domain of human CTLA-4. The extracellular domain is pharmacologically active, binds to CD80/CD86 on antigen-presenting cells and thereby prevents CD28 interaction[56]. Therefore, patients with lower expression of CD28 could be eligible for the abatacept treatment. Some RA patients were already treated with this drug[57] and it seems that due to their lower level of CTLA-4 expression, they are good candidates for this treatment. Additionally, from our data, patients with MCTD and SSC could also be considered for this line of therapy. In this context it would be also interesting to compare the CD28 expression, but due to batch effect issue we could not perform the analysis of this marker on PBMC, as commented before.

In the granulocyte compartment, 7 clusters were identified in *post hoc* analysis and 6 of them were able to discriminate SADs from CTRs. Four of these clusters (CL2, CL4, CL8, and CL15) were characterized by $CD11c^{hi}$ expression, suggesting more mature and activated state of these cells and 3 of them were significantly decreased in blood of SSC (CL4, CL8,); SJS (CL8, CL15); SLE (CL8) compared to CTR. On the other hand, CL2 was elevated in all SADs and significantly different between SJS and CTR, although being also high in RA and SLE patients. The difference between CL2 and CL4, CL8 and CL10 lies in CD95 expression, CL2 opposite to the rest of the CLs has higher Fas expression. It was described that aged $CD95^{+}$ neutrophils have higher migratory capacity to the tissue under inflammatory condition[58]. Thus, it can be that the lower frequency of these cells in the circulation of some SADs is due to their migration to the inflamed tissue. On the other hand, aged neutrophils expressing high level of CD95 are elevated in SADs, and could be more prone to cell death, in agreement with the increased frequency of apoptotic neutrophils already reported in the circulation of SADs patients[59,60]. Alternatively, CD95-CD95L interaction can promote neutrophil migration to the inflamed tissue[61,62]. Surprisingly the highest frequencies of $CD95^{hi}$ neutrophils were observed in SJS, suggesting that more research should be performed for neutrophil pathogenesis in SJS, as so far not much is known. Very recently, elevated levels of aged neutrophils were reported in patients with psoriasis both in circulation and skin[63]. Their pathological function was attributed to the NETs formation and T cell activation functions. It is therefore unclear whether the lower level of these cells observed here could have some protective role, or if their diminished presence is a reflection of their migration to the tissue. This question should be addressed in future studies. It should be noticed that in both studies different markers were used to distinguish immature from aged neutrophils. Here we used CD11c and CD24 expression, however markers like CD62L[31] and CD10[64] should also be introduced to better characterize the maturation state of neutrophils. Most of the knowledge regarding neutrophils comes from mouse studies, hence a better characterization of these cells in patients, is also needed. CL3 and CL10 were characterized by lower expression of CD11c and CD24, thus could be considered as less mature. CL3 was characterized by high CD95 and low PD-L1 expression in contrast to CL10. The frequency of this cluster was again higher in SJS compared to CTR but also compared to SSC and UCTD. The level of the activation marker CD86 on this cluster was significantly decreased comparing SJS and other SADs to CTR, suggesting an even less mature phenotype of these cells in SADs. Additionally, patients had higher expression of CD95 compared to CTR showing that these less mature cells were also more prone to apoptosis. The

elevated expression of CD95 in SADs compared to CTR was confirmed for multiple clusters, mostly in cells characterized by low CD11c expression. Thus, it can support the hypothesis that aged neutrophils migrate to the tissue and are constantly replaced by fresh neutrophils, which are less activated and more prone to death. On the other hand, the CL10 frequency was low in SSC and UCTD. An immunosuppressive neutrophil subpopulation was described and its interaction with T cells through PD-L1 receptors was demonstrated[65]. It was shown that neutrophils could reduce $CD4^+$ T cell proliferation and IFNγ production and this inhibition was mediated by PD-L1[66]. Thus, it is possible that this immunosuppressive function is reduced in SSC and UCTD patients.

SJS and SLE patients were grouped together in the analysis of the granulocyte compartment as well. They were characterized by higher CD95 expression in both mature and immature clusters of granulocytes, suggesting increased apoptosis or migration to the tissue together with lower activation of $CD11c^{low}$ neutrophils measured by CD86, suggesting their even less mature state. Similarity between SLE and SJS immune phenotypes was already reported for PBMC compartment[36] and their combined enrichment in reclassification studies was also shown[67].

Interestingly, in the PBMC compartment MCTD grouped with SLE and SJS patients mostly due to the high CD38 expression, although some discrepancies were seen for HLA-DR. Nevertheless, these patients did not align together using granulocyte-derived features, event though they had similar levels of CD95. Due to differences in cell frequencies they were grouped together with SSC and UCTD patients instead. UCTD and SSC patients clustered together in both the PBMC and granulocyte compartments, however their PBMC compartment was more similar to RA than to MCTD. The term Undifferentiated Connective Tissue Disease at risk for Systemic Sclerosis (UCTD-risk-SSc) was created for the undiagnosed patients that are characterized by Raynaud's phenomena, representing 30-50% of UCTD as initial manifestation, and are more prone to develop full symptoms of SSC[68]. Therefore, it can be that the UCTD patients are similar to SSC at the immune cell level as well. PAPS and CTR were grouped together in both the PBMC and granulocyte analysis, suggesting a more physiological phenotype in these patients. Nevertheless, care needs to be taken regarding PAPS conclusions as only 4 patients were recruited and thus the study was severely underpowered.

Our results showed that we could compare and group patients based on the similar cellular phenotypes using differential analysis, but no disease-specific biomarkers could be selected, underlining the common mechanisms shared by different SADs. Additionally, the comparison

of medians is limited, as it does not fully explore individuals on the extremes of the distribution, thus omitting an important information that could be used when studying disease mechanisms. Hence, it seems that patient reclassification involving unsupervised clustering can give another layer of information and find relevant groups of patients as in Barturen et al 2021. For the reclassification analysis we chose features that were differentially expressed in SADS patients compared with CTR, regardless of their clinical diagnosis, hence they were SADs-specific. Features from both granulocytes and PBMC were selected, showing their important role in patient discrimination and grouped patients into four clusters. Cluster C1 was characterized by increased levels of circulating cells specifically from PBMC compartment, and in general lower activation in the T cell compartment including T regulatory cells and $CD8^+$ T cells, but also in basophils. It presented lower frequency in multiple granulocyte populations and the highest expression of CD95 and CD38 molecule in some granulocyte subsets, especially in $CD11c^{hi}$ cells. Clusters C1 and C2 were exactly opposite to each other, cluster C4 was characterized by intermediate features between C1 and C2 and cluster C4 could be considered as undifferentiated, mixed group. The different diagnoses are distributed across the clusters, however higher percentages of SJS and SLE patients were found in C1, emphasizing the similarity between these two groups of patients. The lack of controls and the high association with antimalarial and steroid treatments in this cluster suggest that these patients could be the most active. Although no disease scores are available at this point we observed higher levels of TNFα, IL-10 and IP-10 in the supernatant of unstimulated blood from C1 compared to C2. These cytokines were shown to be increased in RA[69,70], SLE[71–73] and SJS[74] patients and correlated with the symptoms of severity in SLE[8,73,75–78], RA[79–81], SJS[72,82]. Elevated levels of TNFα and IP-10 were also found in the reclassification study performed by Barturen et, al 2020[83], and was associated with the interferon cluster, characterized by higher disease activity in SLE and SJS patients. The finding of more than 40% of CTR in C2 suggests that it is the most physiological cluster and patients with less severe symptoms are probably placed here. A cluster with high enrichment in CTR was also observed in Barturen et al, 2020 and was clearly correlated with lower severity scores[83]. In our study this is confirmed by lower levels of TNFα, IL-10 and IP-10. More interestingly these cytokines reached the levels of the CTR group, emphasizing their physiological level. The difference in the production of GROα (neutrophil chemoattractant) in C2 and CTR marked the difference between SADS patients and healthy individuals. It is interesting to notice that higher production of TGFα is observed in C2 compared to C1. TGFα has not been well studied in the context of SADs. It is a member of

epidermal growth factor (EGF) family and is a ligand for EGF receptor (R)[84], which acts through the mammalian target of rapamycin (mTOR) signaling pathway[85]. The involvement in the pathogenesis and beneficial blockade of the mTOR signaling pathway was reported in SLE[86] and RA[87], the patients that are mostly represented in this cluster. Thus, this study opens a new possible role for TGFα and also shows that some group of patients could benefit from the treatment involving mTOR inhibition, as suggested in[88].

It is worth to mention that the cytokine levels were not related with the treatment, besides TNFα and antimalarial treatment. However, some differences could be observed for the cell frequency and MSI in patients treated with antimalarials and steroids, thus this could affect the patient clustering especially in C1. Nevertheless, it should be pointed out that while the treated group differed from non-treated patients, they were still highly different from the CTRs, suggesting again that the C1 group is enriched in treated patients, who could have a more severe disease than the rest of the individuals. It is calling the attention that the treatments presented here had a larger impact on PBMC, and almost none on granulocytes despite clear neutrophil dysregulation in some groups of patients. Thus, this suggests that granulocyte-focused treatments should also be considered in the future. Not only neutrophil activation, but also basophils participated in the patients clustering. Basophil involvement in the pathogenesis of MCTD was recently described[89] and they are also known to be involved in SLE[90,91].

Here we showed that using mass cytometry we cannot only compare the SADs patients at multiple cellular levels, but also find groups of patients that share similar immune landscapes, and thus could benefit from the same line of treatment. Mass cytometry is not used in the clinic nowadays, hence the translation of our results to the patients' treatment and diagnosis is not straight forward. FC is currently being used in the clinical practice. Therefore, due to their similar nature, these techniques should be used interchangeably. For this we should reduce our panel to the most relevant markers allowing the extraction of informative features and verify their utility using FC techniques. The high correlation observed within some of the features suggests the possibility of decreasing the number of cellular markers. This step will be undertaken as a future direction for this project. Due to limitations in sample number per diagnosis we could not replicate our results, hence as another future direction we see data replication as a necessary step. Although for the first time we have analyzed both common and rare SADs using MC, we are aware that the groups with the limited number of samples (especially PAPS and MCTD) should be interpreted with caution and the number of patients

should be increased in a replication cohort. Additionally, we emphasize the importance of studying whole blood samples, as multiple cellular compartments seem to play a role in differentiating patients. Both cellular frequency and the levels of functional marker expression are important sources of information and in our opinion, should be used when this type of study is performed. Cytokines play an important role in SADs and multiple lines of treatment include them as targets. Thus, we believe that the analysis of cytokines that so far was omitted in this thesis will give another layer of information in patient reclassification. This step is an undergoing future direction of this project.

Conclusiones and conclusions

Conclusiones

1. Hemos demostrado que los estudios de inmunofenotipado de superficie y de medida de citoquinas intracelulares se pueden realizar con éxito utilizando pequeñas cantidades de sangre fijada / congelada. Hemos observado un mejor rendimiento usando Proteomic Stabilizer siendo, por tanto, la elección para nuestro estudio.
2. Las muestras de sangre fijadas y congeladas se pueden almacenar durante más de un año, por lo que son elegibles para estudios retrospectivos, multicéntricos y a gran escala.
3. Hemos establecido un protocolo de preparación y tinción de muestras de sangre total que permite realizar estudios de inmunofenotipado a gran escala usando CyTOF. El protocolo incluye estabilización de la sangre, lotes congelados de cócteles de anticuerpos, uso de códigos de barras, uso de una muestra de referencia y adquisición de múltiples lotes.
4. Hemos creado un flujo de análisis de datos basado en R que permite realizar el preprocesamiento y control de calidad de los datos adquiridos. Lo más importante, permite alinear múltiples lotes de adquisición, lo que permite el análisis tanto de frecuencias como de MSI en marcadores funcionales a partir de estudios de múltiples lotes y a gran escala.
5. Hemos realizado un estudio de fenotipado profundo mediante citometría de masas utilizando 39 sondas en un solo tubo, involucrando a 126 pacientes con EAS, recolectados en dos centros diferentes. La comparación de EAS reveló poblaciones de células expresadas diferencialmente y MSI específica de células, sin embargo, ninguno de ellos permitió distinguir entre EAS.
6. Seleccionamos características específicas de EAS, incluyendo frecuencias celulares y MSI de marcadores funcionales, tanto en PBMC como en granulocitos. El estudio de reclasificación utilizando estas características identificó 4 grupos de pacientes compuestos por individuos con diferentes etiquetas de diagnóstico, mostrando sus similitudes inmunopatológicas internas a pesar de su diagnóstico heterogéneo.

Conclusions

1. We demonstrated that surface immunophenotyping and intracellular cytokine response studies can be successfully performed with small amounts of fixed/frozen blood. We reported better performance of the Proteomic Stabilizer buffer, being therefore, the choice of our study.
2. The fixed and frozen blood samples can be stored for more than one year, thus, they are eligible for retrospective, multicenter, and large-scale studies.
3. We have established a whole blood sample preparation and staining protocol that allows to perform large-scale immunophenotyping studies. This involves blood stabilization, frozen batches of antibody cocktails, barcoding, use of a reference sample and multi-batch acquisition on CyTOF.
4. We created an R-based data analysis pipeline that allows to perform preprocessing and quality control of the acquired data. Most importantly, it allows to align multiple acquisition batches, thus enabling the analysis of both frequencies and MSI of functional markers from multi-batch and large-scale studies.
5. We performed a deep-phenotyping, mass cytometry study using 39 probes in one single tube, involving 126 SADs patients, collected in two different centers. The SADs comparison revealed differentially expressed cell populations and cell-specific MSI, however none of them allowed to distinguish between SADs.
6. We selected SADs-specific features, that contained cell frequencies and MSI of functional markers from both PBMC and granulocyte compartments. The reclassification study using these features identified 4 clusters composed of patients with different diagnostic labels, showing their internal immunopathological similarities despite their different diagnosis.

References

References

1. Wang, L., Wang, F.-S. & Gershwin, M. E. Human autoimmune diseases: a comprehensive update. Journal of Internal Medicine 278, 369–395 (2015).
2. Theofilopoulos, A. N. et al. Sensors of the innate immune system: their link to rheumatic diseases. Nat Rev Rheumatol 6, 146–156 (2010).
3. Goldblatt, F. & O'Neill, S. G. Clinical aspects of autoimmune rheumatic diseases. The Lancet 382, 797–808 (2013).
4. Ramos-Casals, M. et al. Google-driven search for big data in autoimmune geoepidemiology: analysis of 394,827 patients with systemic autoimmune diseases. Autoimmun Rev 14, 670–679 (2015).
5. Lim, S. S. et al. The incidence and prevalence of systemic lupus erythematosus, 2002-2004: The Georgia Lupus Registry. Arthritis Rheumatol 66, 357–368 (2014).
6. Patel, R. & Shahane, A. The epidemiology of Sjögren's syndrome. Clin Epidemiol 6, 247–255 (2014).
7. Pons-Estel, G. J., Alarcón, G. S., Scofield, L., Reinlib, L. & Cooper, G. S. Understanding the epidemiology and progression of systemic lupus erythematosus. Semin Arthritis Rheum 39, 257–268 (2010).
8. Crowson, C. S. et al. The lifetime risk of adult-onset rheumatoid arthritis and other inflammatory autoimmune rheumatic diseases. Arthritis Rheum 63, 633–639 (2011).
9. Peoples, C., Medsger, T. A., Lucas, M., Rosario, B. L. & Feghali-Bostwick, C. A. Gender differences in systemic sclerosis: relationship to clinical features, serologic status and outcomes. J Scleroderma Relat Disord 1, 177–240 (2016).
10. Alamanos, Y., Voulgari, P. V. & Drosos, A. A. Incidence and prevalence of rheumatoid arthritis, based on the 1987 American College of Rheumatology criteria: a systematic review. Semin Arthritis Rheum 36, 182–188 (2006).
11. R, C., Mc, B., Ma, K. & Gr, H. The Euro-Phospholipid project: epidemiology of the antiphospholipid syndrome in Europe. Lupus vol. 18 https://pubmed.ncbi.nlm.nih.gov/19671788/ (2009).
12. Duarte-García, A. et al. The Epidemiology of Antiphospholipid Syndrome. A Population-Based Study. Arthritis & rheumatology (Hoboken, N.J.) 71, 1545 (2019).
13. Kaul, A. et al. Systemic lupus erythematosus. Nat Rev Dis Primers 2, 16039 (2016).
14. Somers, E. C. et al. Population-Based Incidence and Prevalence of Systemic Lupus Erythematosus. Arthritis Rheumatol 66, 369–378 (2014).
15. Laustrup, H., Voss, A., Green, A. & Junker, P. Occurrence of systemic lupus erythematosus in a Danish community: an 8-year prospective study. Scandinavian Journal of Rheumatology 38, 128–132 (2009).
16. Rees, F. et al. The incidence and prevalence of systemic lupus erythematosus in the UK, 1999-2012. Ann Rheum Dis 75, 136–141 (2016).
17. Tobón, G. J., Youinou, P. & Saraux, A. The environment, geo-epidemiology, and autoimmune disease: Rheumatoid arthritis. J Autoimmun 35, 10–14 (2010).
18. Ungprasert, P. et al. Epidemiology of Mixed Connective Tissue Disease 1985-2014: A Population Based Study. Arthritis Care Res (Hoboken) 68, 1843–1848 (2016).
19. Steen, V., Domsic, R. T., Lucas, M., Fertig, N. & Medsger, T. A. A CLINICAL AND SEROLOGIC COMPARISON OF AFRICAN-AMERICAN AND CAUCASIAN PATIENTS WITH SYSTEMIC SCLEROSIS. Arthritis Rheum 64, 2986–2994 (2012).
20. Chifflot, H., Fautrel, B., Sordet, C., Chatelus, E. & Sibilia, J. Incidence and prevalence of systemic sclerosis: a systematic literature review. Semin Arthritis Rheum 37, 223–235 (2008).
21. Suurmond, J. & Diamond, B. Autoantibodies in systemic autoimmune diseases: specificity and pathogenicity. J Clin Invest 125, 2194–2202 (2015).

22. Tan, E. M. et al. Range of antinuclear antibodies in 'healthy' individuals. Arthritis Rheum 40, 1601–1611 (1997).

23. Ruffatti, A. et al. Anti-double-stranded DNA antibodies in the healthy elderly: prevalence and characteristics. J Clin Immunol 10, 300–303 (1990).

24. Alves, M. R. & Isenberg, D. A. "Mixed connective tissue disease": a condition in search of an identity. Clin Exp Med 20, 159–166 (2020).

25. Bizzaro, N., Villalta, D., Giavarina, D. & Tozzoli, R. Are anti-nucleosome antibodies a better diagnostic marker than anti-dsDNA antibodies for systemic lupus erythematosus? A systematic review and a study of metanalysis. Autoimmun Rev 12, 97–106 (2012).

26. Amoura, Z. et al. Presence of antinucleosome autoantibodies in a restricted set of connective tissue diseases: antinucleosome antibodies of the IgG3 subclass are markers of renal pathogenicity in systemic lupus erythematosus. Arthritis Rheum 43, 76–84 (2000).

27. Bruns, A., Bläss, S., Hausdorf, G., Burmester, G. R. & Hiepe, F. Nucleosomes are major T and B cell autoantigens in systemic lupus erythematosus. Arthritis Rheum 43, 2307–2315 (2000).

28. Sun, X.-Y., Shi, J., Han, L., Su, Y. & Li, Z.-G. Anti-histones antibodies in systemic lupus erythematosus: prevalence and frequency in neuropsychiatric lupus. J Clin Lab Anal 22, 271–277 (2008).

29. Solhjoo, M., Bansal, P., Goyal, A. & Chauhan, K. Drug-Induced Lupus Erythematosus. in StatPearls (StatPearls Publishing, 2020).

30. Muller, S. & Radic, M. Citrullinated Autoantigens: From Diagnostic Markers to Pathogenetic Mechanisms. Clin Rev Allergy Immunol 49, 232–239 (2015).

31. Laustriat, G. et al. Anti-citrullinated peptides antibodies in systemic sclerosis: Meta-analysis of frequency and meaning. Joint Bone Spine 85, 147–153 (2018).

32. Payet, J. et al. Anticyclic citrullinated peptide antibodies in rheumatoid and nonrheumatoid rheumatic disorders: experience with 1162 patients. J Rheumatol 41, 2395–2402 (2014).

33. Mond, C. B., Peterson, M. G. E. & Rothfield, N. F. Correlation of anti-Ro antibody with photosensitivity rash in systemic lupus erythematosus patients. Arthritis & Rheumatism 32, 202–204 (1989).

34. Kurien, B. T., Newland, J., Paczkowski, C., Moore, K. L. & Scofield, R. H. Association of neutropenia in systemic lupus erythematosus (SLE) with anti-Ro and binding of an immunologically cross-reactive neutrophil membrane antigen. Clin Exp Immunol 120, 209–217 (2000).

35. Bournia, V.-K. & Vlachoyiannopoulos, P. G. Subgroups of Sjögren syndrome patients according to serological profiles. J Autoimmun 39, 15–26 (2012).

36. Salomonsson, S. & Strandberg, L. Autoantibodies Associated with Congenital Heart Block. Scandinavian Journal of Immunology 72, 185–188 (2010).

37. Mierau, R. et al. Frequency of disease-associated and other nuclear autoantibodies in patients of the German network for systemic scleroderma: correlation with characteristic clinical features. Arthritis Res Ther 13, R172 (2011).

38. Ihn, H. et al. Distribution and antigen specificity of anti-U1RNP antibodies in patients with systemic sclerosis. Clin Exp Immunol 117, 383–387 (1999).

39. Anderton, H., Wicks, I. P. & Silke, J. Cell death in chronic inflammation: breaking the cycle to treat rheumatic disease. Nature Reviews Rheumatology 16, 496–513 (2020).

40. Frisoni, L. et al. Nuclear Autoantigen Translocation and Autoantibody Opsonization Lead to Increased Dendritic Cell Phagocytosis and Presentation of Nuclear Antigens: A Novel Pathogenic Pathway for Autoimmunity? The Journal of Immunology 175, 2692–2701 (2005).

41. Xu, J. et al. Extracellular histones are major mediators of death in sepsis. Nat Med 15, 1318–1321 (2009).

42. Dieker, J. W. et al. Apoptosis-induced acetylation of histones is pathogenic in systemic lupus erythematosus. Arthritis Rheum 56, 1921–1933 (2007).

43. van Bavel, C. C. et al. Apoptosis-associated acetylation on histone H2B is an epitope for lupus autoantibodies. Mol Immunol 47, 511–516 (2009).

44. van Bavel, C. C. et al. Apoptosis-induced histone H3 methylation is targeted by autoantibodies in systemic lupus erythematosus. Ann Rheum Dis 70, 201–207 (2011).

45. Brinkmann, V. et al. Neutrophil Extracellular Traps Kill Bacteria. Science 303, 1532–1535 (2004).

46. Knight, J. S., Carmona-Rivera, C. & Kaplan, M. J. Proteins derived from neutrophil extracellular traps may serve as self-antigens and mediate organ damage in autoimmune diseases. Front Immunol 3, 380 (2012).

47. Pisetsky, D. S. Anti-DNA antibodies--quintessential biomarkers of SLE. Nat Rev Rheumatol 12, 102–110 (2016).

48. Villanueva, E. et al. Netting neutrophils induce endothelial damage, infiltrate tissues, and expose immunostimulatory molecules in systemic lupus erythematosus. J Immunol 187, 538–552 (2011).

49. Yalavarthi, S. et al. Release of Neutrophil Extracellular Traps by Neutrophils Stimulated With Antiphospholipid Antibodies: A Newly Identified Mechanism of Thrombosis in the Antiphospholipid Syndrome. Arthritis & Rheumatology 67, 2990–3003 (2015).

50. Pieterse, E. et al. Acetylated histones contribute to the immunostimulatory potential of neutrophil extracellular traps in systemic lupus erythematosus. Clin Exp Immunol 179, 68–74 (2015).

51. Khandpur, R. et al. NETs are a source of citrullinated autoantigens and stimulate inflammatory responses in rheumatoid arthritis. Sci Transl Med 5, 178ra40 (2013).

52. Lande, R. et al. Plasmacytoid dendritic cells sense self-DNA coupled with antimicrobial peptide. Nature 449, 564–569 (2007).

53. Honda, K. et al. Spatiotemporal regulation of MyD88–IRF-7 signalling for robust type-I interferon induction. Nature 434, 1035–1040 (2005).

54. Liu, G. & Zhao*, Y. Toll-like receptors and immune regulation: their direct and indirect modulation on regulatory CD4+ CD25+ T cells. Immunology 122, 149–156 (2007).

55. Takeda, K. & Akira, S. TLR signaling pathways. Semin Immunol 16, 3–9 (2004).

56. Akira, S. & Hemmi, H. Recognition of pathogen-associated molecular patterns by TLR family. Immunol Lett 85, 85–95 (2003).

57. Kanzler, H., Barrat, F. J., Hessel, E. M. & Coffman, R. L. Therapeutic targeting of innate immunity with Toll-like receptor agonists and antagonists. Nat Med 13, 552–559 (2007).

58. Farrugia, M. & Baron, B. The Role of Toll-Like Receptors in Autoimmune Diseases through Failure of the Self-Recognition Mechanism. Int J Inflam 2017, (2017).

59. Fanouriakis, A. et al. 2019 update of the EULAR recommendations for the management of systemic lupus erythematosus. Annals of the Rheumatic Diseases 78, 736–745 (2019).

60. Smolen, J. S. et al. EULAR recommendations for the management of rheumatoid arthritis with synthetic and biological disease-modifying antirheumatic drugs: 2016 update. Annals of the Rheumatic Diseases 76, 960–977 (2017).

61. Tektonidou, M. G. et al. EULAR recommendations for the management of antiphospholipid syndrome in adults. Annals of the Rheumatic Diseases 78, 1296–1304 (2019).

62. Schrezenmeier, E. & Dörner, T. Mechanisms of action of hydroxychloroquine and chloroquine: implications for rheumatology. Nat Rev Rheumatol 16, 155–166 (2020).

63. Ohkuma, S. & Poole, B. Fluorescence probe measurement of the intralysosomal pH in living cells and the perturbation of pH by various agents. Proc Natl Acad Sci U S A 75, 3327–3331 (1978).

64. Häcker, H. et al. CpG-DNA-specific activation of antigen-presenting cells requires stress kinase activity and is preceded by non-specific endocytosis and endosomal maturation. EMBO J 17, 6230–6240 (1998).

65. Vollmer, J. et al. Immune stimulation mediated by autoantigen binding sites within small nuclear RNAs involves Toll-like receptors 7 and 8. J Exp Med 202, 1575–1585 (2005).

66. Lau, C. M. et al. RNA-associated autoantigens activate B cells by combined B cell antigen receptor/Toll-like receptor 7 engagement. J Exp Med 202, 1171–1177 (2005).

67. van den Borne, B. E., Dijkmans, B. A., de Rooij, H. H., le Cessie, S. & Verweij, C. L. Chloroquine and hydroxychloroquine equally affect tumor necrosis factor-alpha, interleukin 6, and interferon-gamma production by peripheral blood mononuclear cells. J Rheumatol 24, 55–60 (1997).

68. Sacre, K., Criswell, L. A. & McCune, J. M. Hydroxychloroquine is associated with impaired interferon-alpha and tumor necrosis factor-alpha production by plasmacytoid dendritic cells in systemic lupus erythematosus. Arthritis Res Ther 14, R155 (2012).

69. Hjorton, K. et al. Cytokine production by activated plasmacytoid dendritic cells and natural killer cells is suppressed by an IRAK4 inhibitor. Arthritis Res Ther 20, (2018).

70. Willis, R. et al. Effect of hydroxychloroquine treatment on pro-inflammatory cytokines and disease activity in SLE patients: data from LUMINA (LXXV), a multiethnic US cohort. Lupus 21, 830–835 (2012).

71. Torigoe, M. et al. Hydroxychloroquine efficiently suppresses inflammatory responses of human class-switched memory B cells via Toll-like receptor 9 inhibition. Clin Immunol 195, 1–7 (2018).

72. Wiese, M. D., Manning-Bennett, A. T. & Abuhelwa, A. Y. Investigational IRAK-4 inhibitors for the treatment of rheumatoid arthritis. Expert Opinion on Investigational Drugs 29, 475–482 (2020).

73. Monnet, E. et al. Efficacy and safety of NI-0101, an anti-toll-like receptor 4 monoclonal antibody, in patients with rheumatoid arthritis after inadequate response to methotrexate: a phase II study. Ann Rheum Dis 79, 316–323 (2020).

74. Muskardin, T. L. W. & Niewold, T. B. Type I interferon in rheumatic diseases. Nature Reviews Rheumatology 14, 214–228 (2018).

75. Lövgren, T., Eloranta, M.-L., Båve, U., Alm, G. V. & Rönnblom, L. Induction of interferon-alpha production in plasmacytoid dendritic cells by immune complexes containing nucleic acid released by necrotic or late apoptotic cells and lupus IgG. Arthritis Rheum 50, 1861–1872 (2004).

76. Fitzgerald-Bocarsly, P., Dai, J. & Singh, S. Plasmacytoid dendritic cells and type I IFN: 50 years of convergent history. Cytokine Growth Factor Rev 19, 3–19 (2008).

77. Swiecki, M. & Colonna, M. Type I interferons: diversity of sources, production pathways and effects on immune responses. Curr Opin Virol 1, 463–475 (2011).

78. Tucci, M. et al. Glomerular accumulation of plasmacytoid dendritic cells in active lupus nephritis: role of interleukin-18. Arthritis Rheum 58, 251–262 (2008).

79. Vogelsang, P. et al. Levels of plasmacytoid dendritic cells and type-2 myeloid dendritic cells are reduced in peripheral blood of patients with primary Sjogren's syndrome. Ann Rheum Dis 69, 1235–1238 (2010).

80. Psarras, A. et al. Functionally impaired plasmacytoid dendritic cells and non-haematopoietic sources of type I interferon characterize human autoimmunity. Nature Communications 11, 6149 (2020).

81. Hervas-Stubbs, S. et al. Direct Effects of Type I Interferons on Cells of the Immune System. Clin Cancer Res 17, 2619–2627 (2011).

82. Werth, V. et al. Op0193 Biib059, a Humanized Monoclonal Antibody Targeting Bdca2 on Plasmacytoid Dendritic Cells (pdc), Shows Dose-Related Efficacy in the Phase 2 Lilac Study in Patients (pts) with Active Cutaneous Lupus Erythematosus (cle). Annals of the Rheumatic Diseases 79, 120–121 (2020).

83. Gardet, A. et al. Effect of in vivo Hydroxychloroquine and ex vivo Anti-BDCA2 mAb Treatment on pDC IFNα Production From Patients Affected With Cutaneous Lupus Erythematosus. Front Immunol 10, 275 (2019).

84. Crow, M. K., Olferiev, M. & Kirou, K. A. Type I Interferons in Autoimmune Disease. Annual Review of Pathology: Mechanisms of Disease 14, 369–393 (2019).

85. Ghodke-Puranik, Y. & Niewold, T. B. Genetics of the type I interferon pathway in systemic lupus erythematosus. Int J Clin Rheumtol 8, (2013).

86. Kariuki, S. N. et al. Cutting edge: autoimmune disease risk variant of STAT4 confers increased sensitivity to IFN-alpha in lupus patients in vivo. J Immunol 182, 34–38 (2009).

87. Robinson, T. et al. Autoimmune disease risk variant of IFIH1 is associated with increased sensitivity to IFN-α and serologic autoimmunity in lupus patients. J Immunol 187, 1298–1303 (2011).

88. Graham, R. R. et al. Three functional variants of IFN regulatory factor 5 (IRF5) define risk and protective haplotypes for human lupus. Proc Natl Acad Sci U S A 104, 6758–6763 (2007).

89. International Consortium for Systemic Lupus Erythematosus Genetics (SLEGEN) et al. Genome-wide association scan in women with systemic lupus erythematosus identifies susceptibility variants in ITGAM, PXK, KIAA1542 and other loci. Nat Genet 40, 204–210 (2008).

90. Lessard, C. J. et al. Variants at multiple loci implicated in both innate and adaptive immune responses are associated with Sjögren's syndrome. Nat Genet 45, 1284–1292 (2013).

91. Dieguez-Gonzalez, R. et al. Association of interferon regulatory factor 5 haplotypes, similar to that found in systemic lupus erythematosus, in a large subgroup of patients with rheumatoid arthritis. Arthritis Rheum 58, 1264–1274 (2008).

92. Mahoney, J. M. et al. Systems level analysis of systemic sclerosis shows a network of immune and profibrotic pathways connected with genetic polymorphisms. PLoS Comput Biol 11, e1004005 (2015).

93. Fu, Q. et al. Association of a functional IRF7 variant with systemic lupus erythematosus. Arthritis Rheum 63, 749–754 (2011).

94. Gorlova, O. et al. Identification of novel genetic markers associated with clinical phenotypes of systemic sclerosis through a genome-wide association strategy. PLoS Genet 7, e1002178 (2011).

95. Lessard, C. J. et al. Identification of IRF8, TMEM39A, and IKZF3-ZPBP2 as susceptibility loci for systemic lupus erythematosus in a large-scale multiracial replication study. Am J Hum Genet 90, 648–660 (2012).

96. Niewold, T. B. et al. Association of the IRF5 risk haplotype with high serum interferon-alpha activity in systemic lupus erythematosus patients. Arthritis Rheum 58, 2481–2487 (2008).

97. Cherian, T. S. et al. IRF5 SLE-Risk Haplotype is Associated with Asymptomatic Serologic Autoimmunity and Progression to Clinical Autoimmunity in Neonatal Lupus Mothers. Arthritis Rheum 64, 3383–3387 (2012).

98. Radstake, T. R. D. J. et al. Genome-wide association study of systemic sclerosis identifies CD247 as a new susceptibility locus. Nat Genet 42, 426–429 (2010).

99. Remmers, E. F. et al. STAT4 and the risk of rheumatoid arthritis and systemic lupus erythematosus. N Engl J Med 357, 977–986 (2007).

100. Lee, Y. H. et al. The PTPN22 C1858T functional polymorphism and autoimmune diseases—a meta-analysis. Rheumatology 46, 49–56 (2007).

101. Kariuki, S. N. et al. Genetic analysis of the pathogenic molecular sub-phenotype interferon-alpha identifies multiple novel loci involved in systemic lupus erythematosus. Genes Immun 16, 15–23 (2015).

102. Wuttge, D. M. et al. Increased serum type I interferon activity in early systemic sclerosis patients is associated with antibodies against Sjögren's syndrome antigens and nuclear ribonucleoprotein antigens. Scand J Rheumatol 42, 235–240 (2013).

103. Emamian, E. S. et al. Peripheral blood gene expression profiling in Sjögren's syndrome. Genes Immun 10, 285–296 (2009).

104. Kalunian, K. C. et al. A Phase II study of the efficacy and safety of rontalizumab (rhuMAb interferon-α) in patients with systemic lupus erythematosus (ROSE). Ann Rheum Dis 75, 196–202 (2016).

105. Khamashta, M. et al. Sifalimumab, an anti-interferon-α monoclonal antibody, in moderate to severe systemic lupus erythematosus: a randomised, double-blind, placebo-controlled study. Ann Rheum Dis 75, 1909–1916 (2016).

106. Furie, R. et al. Anifrolumab, an Anti-Interferon-α Receptor Monoclonal Antibody, in Moderate-to-Severe Systemic Lupus Erythematosus. Arthritis Rheumatol 69, 376–386 (2017).

107. Furie, R. A. et al. Type I interferon inhibitor anifrolumab in active systemic lupus erythematosus (TULIP-1): a randomised, controlled, phase 3 trial. The Lancet Rheumatology 1, e208–e219 (2019).

108. Morand, E. F. et al. Trial of Anifrolumab in Active Systemic Lupus Erythematosus. New England Journal of Medicine (2019) doi:10.1056/NEJMoa1912196.

109. Guo, X. et al. Suppression of T Cell Activation and Collagen Accumulation by an Anti-IFNAR1 mAb, Anifrolumab, in Adult Patients with Systemic Sclerosis. J Invest Dermatol 135, 2402–2409 (2015).

110. Fragoulis, G. E., McInnes, I. B. & Siebert, S. JAK-inhibitors. New players in the field of immune-mediated diseases, beyond rheumatoid arthritis. Rheumatology (Oxford) 58, i43–i54 (2019).

111. Wallace, D. J. et al. Baricitinib for systemic lupus erythematosus: a double-blind, randomised, placebo-controlled, phase 2 trial. The Lancet 392, 222–231 (2018).

112. Chen, X. & Oppenheim, J. J. Paradoxical effects of targeting TNF signalling in the treatment of autoimmunity. Nature Reviews Rheumatology 12, 625–626 (2016).

113. Rath, P. C. & Aggarwal, B. B. TNF-Induced Signaling in Apoptosis. J Clin Immunol 19, 350–364 (1999).

114. Liu, H. et al. TNF-alpha-induced apoptosis of macrophages following inhibition of NF-kappa B: a central role for disruption of mitochondria. J Immunol 172, 1907–1915 (2004).

115. Wei, S.-T., Sun, Y.-H., Zong, S.-H. & Xiang, Y.-B. Serum Levels of IL-6 and TNF-α May Correlate with Activity and Severity of Rheumatoid Arthritis. Med Sci Monit 21, 4030–4038 (2015).

116. Sikorska, D., Kawka, E., Rutkowski, R., Samborski, W. & Witowski, J. The intensity of joint pain in relation to changes in serum TNFα during therapy with anti-TNFα inhibitors. Inflammopharmacol 27, 679–683 (2019).

117. Nguyen, D. X. & Ehrenstein, M. R. Anti-TNF drives regulatory T cell expansion by paradoxically promoting membrane TNF-TNF-RII binding in rheumatoid arthritis. J Exp Med 213, 1241–1253 (2016).

118. Ehrenstein, M. R. et al. Compromised Function of Regulatory T Cells in Rheumatoid Arthritis and Reversal by Anti-TNFα Therapy. J Exp Med 200, 277–285 (2004).

119. Kemanetzoglou, E. & Andreadou, E. CNS Demyelination with TNF-α Blockers. Current Neurology and Neuroscience Reports 17, (2017).

120. Shakoor, N., Michalska, M., Harris, C. A. & Block, J. A. Drug-induced systemic lupus erythematosus associated with etanercept therapy. Lancet 359, 579–580 (2002).

121. Dörner, T. et al. Enhanced membrane expression of the 52 kDa Ro(SS-A) and La(SS-B) antigens by human keratinocytes induced by TNF alpha. Ann Rheum Dis 54, 904–909 (1995).

122. Yamamura, Y. et al. TNF-α inhibits aquaporin 5 expression in human salivary gland acinar cells via suppression of histone H4 acetylation. J Cell Mol Med 16, 1766–1775 (2012).

123. Gabay, C. et al. Circulating levels of tumor necrosis factor soluble receptors in systemic lupus erythematosus are significantly higher than in other rheumatic diseases and correlate with disease activity. J Rheumatol 24, 303–308 (1997).

124. Sabry, A. et al. Proinflammatory cytokines (TNF-alpha and IL-6) in Egyptian patients with SLE: its correlation with disease activity. Cytokine 35, 148–153 (2006).

125. Weckerle, C. E. et al. Brief Report: Large-scale analysis of tumor necrosis factor α levels in systemic lupus erythematosus. Arthritis & Rheumatism 64, 2947–2952 (2012).

126. Aringer, M. et al. Adverse events and efficacy of TNF-alpha blockade with infliximab in patients with systemic lupus erythematosus: long-term follow-up of 13 patients. Rheumatology (Oxford) 48, 1451–1454 (2009).

127. Alijotas-Reig, J., Esteve-Valverde, E., Llurba, E. & Gris, J. M. Treatment of refractory poor aPL-related obstetric outcomes with TNF-alpha blockers: Maternal-fetal outcomes in a series of 18 cases. Seminars in Arthritis and Rheumatism 49, 314–318 (2019).

128. Denton, C. P. et al. An open-label pilot study of infliximab therapy in diffuse cutaneous systemic sclerosis. Ann Rheum Dis 68, 1433–1439 (2009).

129. Phumethum, V., Jamal, S. & Johnson, S. R. Biologic therapy for systemic sclerosis: a systematic review. J Rheumatol 38, 289–296 (2011).

130. Mariette, X. et al. Inefficacy of infliximab in primary Sjögren's syndrome: Results of the randomized, controlled trial of remicade in primary Sjögren's syndrome (TRIPSS). Arthritis & Rheumatism 50, 1270–1276 (2004).

131. Sankar, V. et al. Etanercept in Sjögren's syndrome: A twelve-week randomized, double-blind, placebo-controlled pilot clinical trial. Arthritis & Rheumatism 50, 2240–2245 (2004).

132. Biggioggero, M., Crotti, C., Becciolini, A. & Favalli, E. G. Tocilizumab in the treatment of rheumatoid arthritis: an evidence-based review and patient selection. Drug Des Devel Ther 13, 57–70 (2018).

133. Yoshimoto, K. et al. BAFF induces IL-6 production by monocytes through a BAFF receptor and promotes IgG production by B cells in patients with primary Sjögren's syndrome. (CCR3P.210). The Journal of Immunology 192, 115.7-115.7 (2014).

134. Linker-Israeli, M. et al. Elevated levels of endogenous IL-6 in systemic lupus erythematosus. A putative role in pathogenesis. J Immunol 147, 117–123 (1991).

135. Acosta-Rodriguez, E. V., Napolitani, G., Lanzavecchia, A. & Sallusto, F. Interleukins 1beta and 6 but not transforming growth factor-beta are essential for the differentiation of interleukin 17-producing human T helper cells. Nat Immunol 8, 942–949 (2007).

136. Gong, T., Liu, L., Jiang, W. & Zhou, R. DAMP-sensing receptors in sterile inflammation and inflammatory diseases. Nat Rev Immunol 20, 95–112 (2020).

137. Ding, J. et al. Serum interleukin-6 level is correlated with the disease activity of systemic lupus erythematosus: a meta-analysis. Clinics (Sao Paulo) 75, (2020).

138. Matsumoto, T., Tsurumoto, T. & Shindo, H. Interleukin-6 levels in synovial fluids of patients with rheumatoid arthritis correlated with the infiltration of inflammatory cells in synovial membrane. Rheumatol Int 26, 1096–1100 (2006).

139. Madhok, R., Crilly, A., Watson, J. & Capell, H. A. Serum interleukin 6 levels in rheumatoid arthritis: correlations with clinical and laboratory indices of disease activity. Ann Rheum Dis 52, 232–234 (1993).

140. Abdel-Magied, R. A. et al. Serum interleukin-6 in systemic sclerosis and its correlation with disease parameters and cardiopulmonary involvement. Sarcoidosis Vasc Diffuse Lung Dis 33, 321–330 (2016).

141. Tanaka, T., Hishitani, Y. & Ogata, A. Monoclonal antibodies in rheumatoid arthritis: comparative effectiveness of tocilizumab with tumor necrosis factor inhibitors. Biologics 8, 141–153 (2014).

142. Illei, G. G. et al. Tocilizumab in systemic lupus erythematosus: data on safety, preliminary efficacy, and impact on circulating plasma cells from an open-label phase I dosage-escalation study. Arthritis Rheum 62, 542–552 (2010).

143. Shirota, Y. et al. Impact of anti-interleukin-6 receptor blockade on circulating T and B cell subsets in patients with systemic lupus erythematosus. Annals of the Rheumatic Diseases 72, 118–128 (2013).

144. Khanna, D. et al. Safety and efficacy of subcutaneous tocilizumab in systemic sclerosis: results from the open-label period of a phase II randomised controlled trial (faSScinate). Annals of the Rheumatic Diseases 77, 212–220 (2018).

145. Felten, R. et al. Interleukin 6 receptor inhibition in primary Sjögren syndrome: a multicentre double-blind randomised placebo-controlled trial. Annals of the Rheumatic Diseases 80, 329–338 (2021).

146. Ghoreschi, K., Balato, A., Enerbäck, C. & Sabat, R. Therapeutics targeting the IL-23 and IL-17 pathway in psoriasis. The Lancet 397, 754–766 (2021).

147. Oppmann, B. et al. Novel p19 protein engages IL-12p40 to form a cytokine, IL-23, with biological activities similar as well as distinct from IL-12. Immunity 13, 715–725 (2000).

148. Hunter, C. A. New IL-12-family members: IL-23 and IL-27, cytokines with divergent functions. Nat Rev Immunol 5, 521–531 (2005).

149. Li, H. et al. IL-23 promotes TCR-mediated negative selection of thymocytes through the upregulation of IL-23 receptor and RORγt. Nature Communications 5, 4259 (2014).

150. Kannan, A. K. et al. IL-23 induces regulatory T cell plasticity with implications for inflammatory skin diseases. Scientific Reports 9, 17675 (2019).

151. Miossec, P. & Kolls, J. K. Targeting IL-17 and T H 17 cells in chronic inflammation. Nature Reviews Drug Discovery 11, 763–776 (2012).

152. Beringer, A. & Miossec, P. Systemic effects of IL-17 in inflammatory arthritis. Nature Reviews Rheumatology 15, 491–501 (2019).

153. Pisitkun, P. et al. Interleukin-17 Cytokines Are Critical in Development of Fatal Lupus Glomerulonephritis. Immunity 37, 1104–1115 (2012).

154. Mitsdoerffer, M. et al. Proinflammatory T helper type 17 cells are effective B-cell helpers. Proc Natl Acad Sci U S A 107, 14292–14297 (2010).

155. Yang, X., Yang, J., Xing, X., Wan, L. & Li, M. Increased frequency of Th17 cells in systemic sclerosis is related to disease activity and collagen overproduction. Arthritis Res Ther 16, R4 (2014).

156. Verstappen, G. M., Corneth, O. B. J., Bootsma, H. & Kroese, F. G. M. Th17 cells in primary Sjögren's syndrome: Pathogenicity and plasticity. Journal of Autoimmunity 87, 16–25 (2018).

157. Robak, E., Gerlicz-Kowalczuk, Z., Dziankowska-Bartkowiak, B., Wozniacka, A. & Bogaczewicz, J. Serum concentrations of IL-17A, IL-17B, IL-17E and IL-17F in patients with systemic sclerosis. Arch Med Sci 15, 706–712 (2019).

158. Vukelic, M., Laloo, A. & Kyttaris, V. C. Interleukin 23 is elevated in the serum of patients with SLE. Lupus 29, 1943–1947 (2020).

159. Du, J. et al. The association between genetic polymorphisms of interleukin 23 receptor gene and the risk of rheumatoid arthritis: An updated meta-analysis. Clinical Immunology 210, 108250 (2020).

160. Manolova, I. et al. Impact of IL12B Polymorphisms on Genetic Susceptibility and IL-12p40 and IL-23 Serum Levels in Rheumatoid Arthritis. Immunological Investigations 49, 1–14 (2020).

161. Rafael-Vidal, C., Pérez, N., Altabás, I., Garcia, S. & Pego-Reigosa, J. M. Blocking IL-17: A Promising Strategy in the Treatment of Systemic Rheumatic Diseases. Int J Mol Sci 21, (2020).

162. Taams, L. S. Interleukin-17 in rheumatoid arthritis: Trials and tribulations. J Exp Med 217, (2020).

163. Vollenhoven, R. F. van et al. Efficacy and safety of ustekinumab, an IL-12 and IL-23 inhibitor, in patients with active systemic lupus erythematosus: results of a multicentre, double-blind, phase 2, randomised, controlled study. The Lancet 392, 1330–1339 (2018).

164. Barturen, G., Beretta, L., Cervera, R., Van Vollenhoven, R. & Alarcón-Riquelme, M. E. Moving towards a molecular taxonomy of autoimmune rheumatic diseases. Nat Rev Rheumatol 14, 75–93 (2018).

165. Segura, E. et al. Human Inflammatory Dendritic Cells Induce Th17 Cell Differentiation. Immunity 38, 336–348 (2013).

166. Rossato, M. et al. Association of MicroRNA-618 Expression With Altered Frequency and Activation of Plasmacytoid Dendritic Cells in Patients With Systemic Sclerosis. Arthritis Rheumatol 69, 1891–1902 (2017).

167. van den Hoogen, L. L. et al. microRNA downregulation in plasmacytoid dendritic cells in interferon-positive systemic lupus erythematosus and antiphospholipid syndrome. Rheumatology (Oxford) 57, 1669–1674 (2018).

168. van der Kroef, M. et al. Cytometry by time of flight identifies distinct signatures in patients with systemic sclerosis, systemic lupus erythematosus and Sjögrens syndrome. Eur J Immunol 50, 119–129 (2020).

169. Kalled, S. L., Ambrose, C. & Hsu, Y.-M. The Biochemistry and Biology of BAFF, APRIL and Their Receptors. B Cell Trophic Factors and B Cell Antagonism in Autoimmune Disease 8, 206–242 (2005).

170. Migita, K. et al. Reduced blood BDCA-2+ (lymphoid) and CD11c+ (myeloid) dendritic cells in systemic lupus erythematosus. Clin Exp Immunol 142, 84–91 (2005).

171. Jongbloed, S. L. et al. Enumeration and phenotypical analysis of distinct dendritic cell subsets in psoriatic arthritis and rheumatoid arthritis. Arthritis Res Ther 8, R15 (2006).

172. Ohl, L. et al. CCR7 governs skin dendritic cell migration under inflammatory and steady-state conditions. Immunity 21, 279–288 (2004).

173. Wakim, L. M., Waithman, J., van Rooijen, N., Heath, W. R. & Carbone, F. R. Dendritic cell-induced memory T cell activation in nonlymphoid tissues. Science 319, 198–202 (2008).

174. Humby, F. et al. Ectopic Lymphoid Structures Support Ongoing Production of Class-Switched Autoantibodies in Rheumatoid Synovium. PLOS Medicine 6, e1 (2009).

175. Medzhitov, R. Toll-like receptors and innate immunity. Nature Reviews Immunology 1, 135–145 (2001).

176. Ghebrehiwet, B., Hosszu, K., Valentino, A. & Peerschke, E. I. B. The C1q Family of Proteins: Insights into the Emerging Non-Traditional Functions. Front. Immunol. 3, (2012).

177. Jansen, D. T. S. L. et al. Genetic variants of C1q are a risk for rheumatoid arthritis. Annals of the Rheumatic Diseases 71, A54–A54 (2012).

178. Walport, M. J., Davies, K. A. & Botto, M. C1q and Systemic Lupus Erythematosus. Immunobiology 199, 265–285 (1998).

179. Martin, M. & Blom, A. M. Complement in removal of the dead – balancing inflammation. Immunological Reviews 274, 218–232 (2016).

180. Merah-Mourah, F., Cohen, S. O., Charron, D., Mooney, N. & Haziot, A. Identification of Novel Human Monocyte Subsets and Evidence for Phenotypic Groups Defined by Interindividual Variations of Expression of Adhesion Molecules. Scientific Reports 10, 1–16 (2020).

181. Ruiz-Limon, P. et al. Molecular Characterization of Monocyte Subsets Reveals Specific and Distinctive Molecular Signatures Associated With Cardiovascular Disease in Rheumatoid Arthritis. Front. Immunol. 10, (2019).

182. Rossol, M., Kraus, S., Pierer, M., Baerwald, C. & Wagner, U. The CD14(bright) CD16+ monocyte subset is expanded in rheumatoid arthritis and promotes expansion of the Th17 cell population. Arthritis Rheum 64, 671–677 (2012).

183. Chara, L. et al. The number of circulating monocytes as biomarkers of the clinical response to methotrexate in untreated patients with rheumatoid arthritis. J Transl Med 13, 2 (2015).

184. Lescoat, A. et al. CD16-positive circulating monocytes and fibrotic manifestations of systemic sclerosis. Clin Rheumatol 36, 1649–1654 (2017).

185. Katsiari, C. G. et al. Aberrant Expression of the Costimulatory Molecule CD40 Ligand on Monocytes from Patients with Systemic Lupus Erythematosus. Clinical Immunology 103, 54–62 (2002).

186. Harigai, M. et al. Responsiveness of peripheral blood B cells to recombinant CD40 ligand in patients with systemic lupus erythematosus. Lupus 8, 227–233 (1999).

187. Decker, P., Kötter, I., Klein, R., Berner, B. & Rammensee, H.-G. Monocyte-derived dendritic cells over-express CD86 in patients with systemic lupus erythematosus. Rheumatology 45, 1087–1095 (2006).

188. Rubin, S. J. S., Bloom, M. S. & Robinson, W. H. B cell checkpoints in autoimmune rheumatic diseases. Nature Reviews Rheumatology 15, 303–315 (2019).

189. Hansen, A. et al. Abnormalities in peripheral B cell memory of patients with primary Sjögren's syndrome. Arthritis Rheum 50, 1897–1908 (2004).

190. Roberts, M. E. P. et al. Primary Sjögren's syndrome is characterized by distinct phenotypic and transcriptional profiles of IgD+ unswitched memory B cells. Arthritis Rheumatol 66, 2558–2569 (2014).

191. Corneth, O. B. J. et al. Enhanced Bruton's Tyrosine Kinase Activity in Peripheral Blood B Lymphocytes From Patients With Autoimmune Disease. Arthritis & Rheumatology 69, 1313–1324 (2017).

192. Simon, D. et al. Reduced non-switched memory B cell subsets cause imbalance in B cell repertoire in systemic sclerosis. Clin Exp Rheumatol 34 Suppl 100, 30–36 (2016).

193. Odendahl, M. et al. Disturbed peripheral B lymphocyte homeostasis in systemic lupus erythematosus. J Immunol 165, 5970–5979 (2000).

194. Yap, D. Y. H. & Chan, T. M. B Cell Abnormalities in Systemic Lupus Erythematosus and Lupus Nephritis—Role in Pathogenesis and Effect of Immunosuppressive Treatments. Int J Mol Sci 20, (2019).

195. Iwata, S. & Tanaka, Y. B-cell subsets, signaling and their roles in secretion of autoantibodies. Lupus 25, 850–856 (2016).

196. Nimmerjahn, F. & Ravetch, J. V. Fc-receptors as regulators of immunity. Adv Immunol 96, 179–204 (2007).

197. Murphy, G. & Isenberg, D. A. New therapies for systemic lupus erythematosus — past imperfect, future tense. Nature Reviews Rheumatology 15, 403–412 (2019).

198. Wei, C. et al. A New Population of Cells Lacking Expression of CD27 Represents a Notable Component of the B Cell Memory Compartment in Systemic Lupus Erythematosus. The Journal of Immunology 178, 6624–6633 (2007).

199. You, X. et al. Double Negative B Cell Is Associated With Renal Impairment in Systemic Lupus Erythematosus and Acts as a Marker for Nephritis Remission. Front. Med. 7, (2020).

200. Jenks, S. A. et al. Distinct Effector B Cells Induced by Unregulated Toll-like Receptor 7 Contribute to Pathogenic Responses in Systemic Lupus Erythematosus. Immunity 49, 725-739.e6 (2018).

201. Hansen, A. et al. Diminished peripheral blood memory B cells and accumulation of memory B cells in the salivary glands of patients with Sjögren's syndrome. Arthritis Rheum 46, 2160–2171 (2002).

202. Mingueneau, M. et al. Cytometry by time-of-flight immunophenotyping identifies a blood Sjögren's signature correlating with disease activity and glandular inflammation. J. Allergy Clin. Immunol. 137, 1809-1821.e12 (2016).

203. Lugar, P. L., Love, C., Grammer, A. C., Dave, S. S. & Lipsky, P. E. Molecular Characterization of Circulating Plasma Cells in Patients with Active Systemic Lupus Erythematosus. PLOS ONE 7, e44362 (2012).

204. Hisada, R. et al. Circulating plasmablasts contribute to antiphospholipid antibody production, associated with type I interferon upregulation. J Thromb Haemost 17, 1134–1143 (2019).

205. Halliley, J. L. et al. Long-lived Plasma Cells Are Contained Within the CD19−CD38hiCD138+ Subset in Human Bone Marrow. Immunity 43, 132–145 (2015).

206. Sanges, S. et al. Role of B cells in the pathogenesis of systemic sclerosis. Rev Med Interne 38, 113–124 (2017).

207. Sato, S., Hasegawa, M., Fujimoto, M., Tedder, T. F. & Takehara, K. Quantitative Genetic Variation in CD19 Expression Correlates with Autoimmunity. The Journal of Immunology 165, 6635–6643 (2000).

208. Karrar, S. & Cunninghame Graham, D. S. Abnormal B Cell Development in Systemic Lupus Erythematosus. Arthritis Rheumatol 70, 496–507 (2018).

209. Looney, R. J. et al. B cell depletion as a novel treatment for systemic lupus erythematosus: a phase I/II dose-escalation trial of rituximab. Arthritis Rheum 50, 2580–2589 (2004).

210. Gunnarsson, I. et al. Histopathologic and clinical outcome of rituximab treatment in patients with cyclophosphamide-resistant proliferative lupus nephritis. Arthritis Rheum 56, 1263–1272 (2007).

211. Dass, S. et al. Reduction of fatigue in Sjögren syndrome with rituximab: results of a randomised, double-blind, placebo-controlled pilot study. Ann Rheum Dis 67, 1541–1544 (2008).

212. Meijer, J. M. et al. Effectiveness of rituximab treatment in primary Sjögren's syndrome: a randomized, double-blind, placebo-controlled trial. Arthritis Rheum 62, 960–968 (2010).

213. Devauchelle-Pensec, V. et al. Treatment of primary Sjögren syndrome with rituximab: a randomized trial. Ann Intern Med 160, 233–242 (2014).

214. Bowman, S. J. et al. Randomized Controlled Trial of Rituximab and Cost-Effectiveness Analysis in Treating Fatigue and Oral Dryness in Primary Sjögren's Syndrome. Arthritis Rheumatol 69, 1440–1450 (2017).

215. Rovin, B. H. et al. Efficacy and safety of rituximab in patients with active proliferative lupus nephritis: The lupus nephritis assessment with rituximab study. Arthritis & Rheumatism 64, 1215–1226 (2012).

216. Merrill, J. et al. Assessment of flares in lupus patients enrolled in a phase II/III study of rituximab (EXPLORER). Lupus 20, 709–716 (2011).

217. Lazarus, M. N., Turner-Stokes, T., Chavele, K.-M., Isenberg, D. A. & Ehrenstein, M. R. B-cell numbers and phenotype at clinical relapse following rituximab therapy differ in SLE patients according to anti-dsDNA antibody levels. Rheumatology (Oxford) 51, 1208–1215 (2012).

218. Rydén-Aulin, M. et al. Off-label use of rituximab for systemic lupus erythematosus in Europe. Lupus Sci Med 3, e000163 (2016).

219. Bootsma, H., Kroese, F. G. M. & Vissink, A. Editorial: Rituximab in the Treatment of Sjögren's Syndrome: Is It the Right or Wrong Drug? Arthritis & Rheumatology 69, 1346–1349 (2017).

220. Mei, H. E. et al. A unique population of IgG-expressing plasma cells lacking CD19 is enriched in human bone marrow. Blood 125, 1739–1748 (2015).

221. Zhao, Q. Bispecific Antibodies for Autoimmune and Inflammatory Diseases: Clinical Progress to Date. BioDrugs 34, 111–119 (2020).

222. Eilertsen, G. Ø., Van Ghelue, M., Strand, H. & Nossent, J. C. Increased levels of BAFF in patients with systemic lupus erythematosus are associated with acute-phase reactants, independent of BAFF genetics: a case-control study. Rheumatology (Oxford) 50, 2197–2205 (2011).

223. Groom, J. et al. Association of BAFF/BLyS overexpression and altered B cell differentiation with Sjögren's syndrome. J Clin Invest 109, 59–68 (2002).

224. Bosello, S. et al. Concentrations of BAFF correlate with autoantibody levels, clinical disease activity, and response to treatment in early rheumatoid arthritis. J Rheumatol 35, 1256–1264 (2008).

225. Carter, E. E., Barr, S. G. & Clarke, A. E. The global burden of SLE: prevalence, health disparities and socioeconomic impact. Nature Reviews Rheumatology 12, 605–620 (2016).

226. Cambridge, G. et al. B cell depletion therapy in systemic lupus erythematosus: relationships among serum B lymphocyte stimulator levels, autoantibody profile and clinical response. Ann Rheum Dis 67, 1011–1016 (2008).

227. Dörner, T. et al. Treatment of primary Sjögren's syndrome with ianalumab (VAY736) targeting B cells by BAFF receptor blockade coupled with enhanced, antibody-dependent cellular cytotoxicity. Ann Rheum Dis 78, 641–647 (2019).

228. Chamberlain, C. et al. Repeated administration of dapirolizumab pegol in a randomised phase I study is well tolerated and accompanied by improvements in several composite measures of systemic lupus erythematosus disease activity and changes in whole blood transcriptomic profiles. Ann Rheum Dis 76, 1837–1844 (2017).

229. Farag, A. et al. Novel Anti-CD40 Monoclonal Antibody CFZ533 in Patients with Primary Sjogren Syndrome: A Phase Iia Double-Blind, Placebo–Controlled Randomized Trial. Oral Surgery, Oral Medicine, Oral Pathology and Oral Radiology 126, e203–e204 (2018).

230. Cheng, Y., Wong, M. T., Maaten, L. van der & Newell, E. W. Categorical Analysis of Human T Cell Heterogeneity with One-Dimensional Soli-Expression by Nonlinear Stochastic Embedding. The Journal of Immunology 196, 924–932 (2016).

231. Boumpas, D. T. et al. A short course of BG9588 (anti-CD40 ligand antibody) improves serologic activity and decreases hematuria in patients with proliferative lupus glomerulonephritis. Arthritis Rheum 48, 719–727 (2003).

232. Kalunian, K. C. et al. Treatment of systemic lupus erythematosus by inhibition of T cell costimulation with anti-CD154: a randomized, double-blind, placebo-controlled trial. Arthritis Rheum 46, 3251–3258 (2002).

233. O'Reilly, S., Hügle, T. & van Laar, J. M. T cells in systemic sclerosis: a reappraisal. Rheumatology (Oxford) 51, 1540–1549 (2012).

234. Zhou, H., Yang, J., Tian, J. & Wang, S. CD8+ T Lymphocytes: Crucial Players in Sjögren's Syndrome. Front. Immunol. 11, (2021).

235. Piantoni, S. et al. Effector T-cells are expanded in systemic lupus erythematosus patients with high disease activity and damage indexes. Lupus 27, 143–149 (2018).

236. Vilá, L. M. et al. Systemic lupus erythematosus in a multiethnic US cohort, XXXVII: Association of lymphopenia with clinical manifestations, serologic abnormalities, disease activity, and damage accrual. Arthritis Care & Research 55, 799–806 (2006).

237. Schmidt, D., Goronzy, J. J. & Weyand, C. M. CD4+ CD7- CD28- T cells are expanded in rheumatoid arthritis and are characterized by autoreactivity. J Clin Invest 97, 2027–2037 (1996).

238. Fasth, A. E. et al. Skewed distribution of proinflammatory CD4+CD28null T cells in rheumatoid arthritis. Arthritis Res Ther 9, R87 (2007).

239. Fox, D. A. et al. Lymphocyte subset abnormalities in early diffuse cutaneous systemic sclerosis. Arthritis Research & Therapy 23, 10 (2021).

240. Pieper, J. et al. Peripheral and site-specific CD4+CD28null T cells from Rheumatoid Arthritis patients show distinct characteristics. Scand J Immunol 79, 149–155 (2014).

241. Chemin, K., Gerstner, C. & Malmström, V. Effector Functions of CD4+ T Cells at the Site of Local Autoimmune Inflammation—Lessons From Rheumatoid Arthritis. Front. Immunol. 10, (2019).

242. Sudzius, G. et al. Activity of T-helper cells in patients with primary Sjogren's syndrome. In Vivo 27, 263–268 (2013).

243. Kang, E. H., Lee, Y. J., Hyon, J. Y., Yun, P. Y. & Song, Y. W. Salivary cytokine profiles in primary Sjögren's syndrome differ from those in non-Sjögren sicca in terms of TNF-α levels and Th-1/Th-2 ratios. Clin Exp Rheumatol 29, 970–976 (2011).

244. Brown, M. & O'Reilly, S. The immunopathogenesis of fibrosis in systemic sclerosis. Clinical & Experimental Immunology 195, 310–321 (2019).

245. Maehara, T. et al. Selective localization of T helper subsets in labial salivary glands from primary Sjögren's syndrome patients. Clin Exp Immunol 169, 89–99 (2012).

246. Muhammad Yusoff, F., Wong, K. K. & Mohd Redzwan, N. Th1, Th2, and Th17 cytokines in systemic lupus erythematosus. Autoimmunity 53, 8–20 (2020).

247. Sakai, A., Sugawara, Y., Kuroishi, T., Sasano, T. & Sugawara, S. Identification of IL-18 and Th17 cells in salivary glands of patients with Sjögren's syndrome, and amplification of IL-17-mediated secretion of inflammatory cytokines from salivary gland cells by IL-18. J Immunol 181, 2898–2906 (2008).

248. Chizzolini, C., Dufour, A. M. & Brembilla, N. C. Is there a role for IL-17 in the pathogenesis of systemic sclerosis? Immunol Lett 195, 61–67 (2018).

249. Pène, J. et al. Chronically Inflamed Human Tissues Are Infiltrated by Highly Differentiated Th17 Lymphocytes. The Journal of Immunology 180, 7423–7430 (2008).

250. Ohl, K. & Tenbrock, K. Regulatory T cells in systemic lupus erythematosus. European Journal of Immunology 45, 344–355 (2015).

251. Lyssuk, E. Y., Torgashina, A. V., Soloviev, S. K., Nassonov, E. L. & Bykovskaia, S. N. Reduced number and function of CD4+CD25highFoxP3+ regulatory T cells in patients with systemic lupus erythematosus. Adv Exp Med Biol 601, 113–119 (2007).

252. Lin, S.-C. et al. The quantitative analysis of peripheral blood FOXP3-expressing T cells in systemic lupus erythematosus and rheumatoid arthritis patients. Eur J Clin Invest 37, 987–996 (2007).

253. Vargas-Rojas, M. I., Crispín, J. C., Richaud-Patin, Y. & Alcocer-Varela, J. Quantitative and qualitative normal regulatory T cells are not capable of inducing suppression in SLE patients due to T-cell resistance. Lupus 17, 289–294 (2008).

254. Samson, M. et al. Brief Report: Inhibition of interleukin-6 function corrects Th17/Treg cell imbalance in patients with rheumatoid arthritis. Arthritis & Rheumatism 64, 2499–2503 (2012).

255. Valencia, X. et al. TNF downmodulates the function of human CD4+CD25hi T-regulatory cells. Blood 108, 253–261 (2006).

256. Amelsfort, J. M. R. van, Jacobs, K. M. G., Bijlsma, J. W. J., Lafeber, F. P. J. G. & Taams, L. S. CD4+CD25+ regulatory T cells in rheumatoid arthritis: Differences in the presence, phenotype, and function between peripheral blood and synovial fluid. Arthritis & Rheumatism 50, 2775–2785 (2004).

257. Cao, D. et al. Isolation and functional characterization of regulatory CD25brightCD4+ T cells from the target organ of patients with rheumatoid arthritis. European Journal of Immunology 33, 215–223 (2003).

258. Herrath, J. et al. The inflammatory milieu in the rheumatic joint reduces regulatory T-cell function. European Journal of Immunology 41, 2279–2290 (2011).

259. Krasimirova, E. et al. Treg/Th17 cell balance and phytohaemagglutinin activation of T lymphocytes in peripheral blood of systemic sclerosis patients. World J Exp Med 7, 84–96 (2017).

260. Maria, N. I. et al. Association of Increased Treg Cell Levels With Elevated Indoleamine 2,3-Dioxygenase Activity and an Imbalanced Kynurenine Pathway in Interferon-Positive Primary Sjögren's Syndrome. Arthritis Rheumatol 68, 1688–1699 (2016).

261. Klein, S. et al. Reduction of regulatory T cells in skin lesions but not in peripheral blood of patients with systemic scleroderma. Ann Rheum Dis 70, 1475–1481 (2011).

262. Fenoglio, D. et al. Alteration of Th17 and Treg cell subpopulations co-exist in patients affected with systemic sclerosis. Clin Immunol 139, 249–257 (2011).

263. Fuschiotti, P., Medsger, T. A. & Morel, P. A. Effector CD8+ T cells in systemic sclerosis patients produce abnormally high levels of interleukin-13 associated with increased skin fibrosis. Arthritis Rheum 60, 1119–1128 (2009).

264. Maldonado, A. et al. Decreased effector memory CD45RA+ CD62L- CD8+ T cells and increased central memory CD45RA- CD62L+ CD8+ T cells in peripheral blood of rheumatoid arthritis patients. Arthritis Res Ther 5, R91-96 (2003).

265. Cho, B.-A. et al. Characterization of effector memory CD8+ T cells in the synovial fluid of rheumatoid arthritis. J Clin Immunol 32, 709–720 (2012).

266. Carvalheiro, H., Duarte, C., Silva-Cardoso, S., Silva, J. A. P. da & Souto-Carneiro, M. M. CD8+ T Cell Profiles in Patients With Rheumatoid Arthritis and Their Relationship to Disease Activity. Arthritis & Rheumatology 67, 363–371 (2015).

267. Valenzuela, H. F. & Effros, R. B. Divergent telomerase and CD28 expression patterns in human CD4 and CD8 T cells following repeated encounters with the same antigenic stimulus. Clin Immunol 105, 117–125 (2002).

268. Żabińska, M., Krajewska, M., Kościelska-Kasprzak, K. & Klinger, M. CD3+CD8+CD28− T Lymphocytes in Patients with Lupus Nephritis. J Immunol Res 2016, (2016).

269. Thompson, C., Davies, R., Williams, A., Jones, G. & Choy, E. H. S. CD28− Cells Are Increased in Early Rheumatoid Arthritis and Are Linked With Cytomegalovirus Status. Front Med (Lausanne) 7, (2020).

270. Fujihara, T. et al. Preferential Localization of CD8+ αEβ7+ T Cells Around Acinar Epithelial Cells with Apoptosis in Patients with Sjögren's Syndrome. The Journal of Immunology 163, 2226–2235 (1999).

271. Jung, J. H. et al. Synovial fluid CD69+CD8+ T cells with tissue-resident phenotype mediate perforin-dependent citrullination in rheumatoid arthritis. Clin Transl Immunology 9, (2020).

272. Rodríguez-Rodríguez, N. et al. Programmed Cell Death 1 and Helios Distinguish TCR-αβ+ Double-Negative (CD4−CD8−) T Cells That Derive from Self-Reactive CD8 T Cells. The Journal of Immunology 194, 4207–4214 (2015).

273. Bristeau-Leprince, A. et al. Human TCR α/β+ CD4−CD8− Double-Negative T Cells in Patients with Autoimmune Lymphoproliferative Syndrome Express Restricted Vβ TCR Diversity and Are Clonally Related to CD8+ T Cells. The Journal of Immunology 181, 440–448 (2008).

274. Li, H. et al. Systemic lupus erythematosus favors the generation of IL-17 producing double negative T cells. Nature Communications 11, 2859 (2020).

275. Ford, M. S., Zhang, Z.-X., Chen, W. & Zhang, L. Double-Negative T Regulatory Cells Can Develop Outside the Thymus and Do Not Mature from CD8+ T Cell Precursors. The Journal of Immunology 177, 2803–2809 (2006).

276. Crispín, J. C. et al. Expanded Double Negative T Cells in Patients with Systemic Lupus Erythematosus Produce IL-17 and Infiltrate the Kidneys. J Immunol 181, 8761–8766 (2008).

277. Alunno, A. et al. IL-17-producing double-negative T cells are expanded in the peripheral blood, infiltrate the salivary gland and are partially resistant to corticosteroid therapy in patients with Sjögren's syndrome. Reumatismo 65, 192–198 (2013).

278. Shivakumar, S., Tsokos, G. C. & Datta, S. K. T cell receptor alpha/beta expressing double-negative (CD4-/CD8-) and CD4+ T helper cells in humans augment the production of pathogenic anti-DNA autoantibodies associated with lupus nephritis. J Immunol 143, 103–112 (1989).

279. Crispín, J. C. & Tsokos, G. C. Interleukin-17-producing T cells in lupus. Curr Opin Rheumatol 22, 499–503 (2010).

280. Roberts, S. & Girardi, M. Conventional and Unconventional T Cells. in Clinical and Basic Immunodermatology (eds. Gaspari, A. A. & Tyring, S. K.) 85–104 (Springer, 2008). doi:10.1007/978-1-84800-165-7_6.

281. Nielsen, M. M., Witherden, D. A. & Havran, W. L. γδ T cells in homeostasis and host defence of epithelial barrier tissues. Nature Reviews Immunology 17, 733–745 (2017).

282. Wu, M., Yang, J., Li, X. & Chen, J. The Role of γδ T Cells in Systemic Lupus Erythematosus. Journal of Immunology Research 2016, e2932531 (2016).

283. Eberl, M. Antigen recognition by human γδ T cells: one step closer to knowing. Immunology & Cell Biology 98, 351–354 (2020).

284. Wang, L., Das, H., Kamath, A. & Bukowski, J. F. Human Vγ2Vδ2 T Cells Produce IFN-γ and TNF-α with an On/Off/On Cycling Pattern in Response to Live Bacterial Products. The Journal of Immunology 167, 6195–6201 (2001).

285. Glatzel, A. et al. Patterns of Chemokine Receptor Expression on Peripheral Blood γδ T Lymphocytes: Strong Expression of CCR5 Is a Selective Feature of Vδ2/Vγ9 γδ T Cells. The Journal of Immunology 168, 4920–4929 (2002).

286. Casetti, R. et al. Cutting Edge: TGF-β1 and IL-15 Induce FOXP3+ γδ Regulatory T Cells in the Presence of Antigen Stimulation. The Journal of Immunology 183, 3574–3577 (2009).

287. Huang, Y. et al. The Influence of IgE-Enhancing and IgE-Suppressive γδ T Cells Changes with Exposure to Inhaled Ovalbumin. The Journal of Immunology 183, 849–855 (2009).

288. Wang, L. et al. Downregulation of CD94/NKG2A inhibitory receptor on decreased γδ T cells in patients with systemic lupus erythematosus. Scand J Immunol 76, 62–69 (2012).

289. Lu, Z. et al. Elevated Apoptosis and Impaired Proliferation Contribute to Downregulated Peripheral γδ T Cells in Patients with Systemic Lupus Erythematosus. Clinical and Developmental Immunology 2013, e405395 (2013).

290. Holcombe, R. F., Baethge, B. A., Wolf, R. E., Betzing, K. W. & Stewart, R. M. Natural killer cells and gamma delta T cells in scleroderma: relationship to disease duration and anti-Scl-70 antibodies. Annals of the Rheumatic Diseases 54, 69–72 (1995).

291. Giacomelli, R. et al. Circulating Vdelta1+ T cells are activated and accumulate in the skin of systemic sclerosis patients. Arthritis Rheum 41, 327–334 (1998).

292. Lamour, A. et al. Analysis of T cell receptors in rheumatoid arthritis: the increased expression of HLA-DR antigen on circulating gamma delta+ T cells is correlated with disease activity. Clin Exp Immunol 89, 217–222 (1992).

293. Liu, M.-F. et al. Distribution of Double-Negative (CD4−CD8−, DN) T Subsets in Blood and Synovial Fluid from Patients with Rheumatoid Arthritis. Clin Rheumatol 18, 227–231 (1999).

294. Abuzakouk, M. et al. Increased HLA-DR and CD44 antigen expression in the gut: evidence of extraarticular immunological activity in rheumatoid arthritis. J Rheumatol 26, 1869–1876 (1999).

295. Bodman-smith, M. D., Anand, A., Durand, V., Youinou, P. Y. & Lydyard, P. M. Decreased expression of FcγRIII (CD16) by γδ T cells in patients withrheumatoid arthritis. Immunology 99, 498–503 (2000).

296. Jacobs, M. R. & Haynes, B. F. Increase in TCRγδ T lymphocytes in synovia from rheumatoid arthritis patients with active synovitis. J Clin Immunol 12, 130–138 (1992).

297. Ichikawa, Y., Shimizu, H., Yoshida, M., Takaya, M. & Arimori, S. T cells bearing gamma/delta T cell receptor and their expression of activation antigen in peripheral blood from patients with Sjögren's syndrome. Clin Exp Rheumatol 9, 603–609 (1991).

298. Ceeraz, S., Nowak, E. C., Burns, C. M. & Noelle, R. J. Immune checkpoint receptors in regulating immune reactivity in rheumatic disease. Arthritis Research & Therapy 16, 469 (2014).

299. Chiossone, L., Dumas, P.-Y., Vienne, M. & Vivier, E. Natural killer cells and other innate lymphoid cells in cancer. Nature Reviews Immunology 18, 671–688 (2018).

300. Crinier, A. et al. High-Dimensional Single-Cell Analysis Identifies Organ-Specific Signatures and Conserved NK Cell Subsets in Humans and Mice. Immunity 49, 971-986.e5 (2018).

301. Peritt, D. et al. Differentiation of human NK cells into NK1 and NK2 subsets. J Immunol 161, 5821–5824 (1998).

302. Jacobs, R. et al. CD56bright cells differ in their KIR repertoire and cytotoxic features from CD56dim NK cells. Eur J Immunol 31, 3121–3127 (2001).

303. Poli, A. et al. CD56bright natural killer (NK) cells: an important NK cell subset. Immunology 126, 458–465 (2009).

304. Fauriat, C., Long, E. O., Ljunggren, H.-G. & Bryceson, Y. T. Regulation of human NK-cell cytokine and chemokine production by target cell recognition. Blood 115, 2167–2176 (2010).

305. Ming, B. et al. The Increased Ratio of Blood CD56bright NK to CD56dim NK Is a Distinguishing Feature of Primary Sjögren's Syndrome. J Immunol Res 2020, (2020).

306. Hervier, B. et al. Phenotype and function of natural killer cells in systemic lupus erythematosus: excess interferon-γ production in patients with active disease. Arthritis Rheum 63, 1698–1706 (2011).

307. Park, Y.-W. et al. Impaired differentiation and cytotoxicity of natural killer cells in systemic lupus erythematosus. Arthritis Rheum 60, 1753–1763 (2009).

308. Almeida, I. et al. T and NK Cell Phenotypic Abnormalities in Systemic Sclerosis: a Cohort Study and a Comprehensive Literature Review. Clin Rev Allergy Immunol 49, 347–369 (2015).

309. Henriques, A. et al. NK cells dysfunction in systemic lupus erythematosus: relation to disease activity. Clin Rheumatol 32, 805–813 (2013).

310. Schepis, D. et al. Increased proportion of CD56bright natural killer cells in active and inactive systemic lupus erythematosus. Immunology 126, 140–146 (2009).

311. Lin, S.-J. et al. Phenotypic and functional characterization of natural killer cells in rheumatoid arthritis-regulation with interleukin-15. Sci Rep 10, 5858 (2020).

312. Horikawa, M. et al. Abnormal natural killer cell function in systemic sclerosis: altered cytokine production and defective killing activity. J Invest Dermatol 125, 731–737 (2005).

313. Arazi, A. et al. The immune cell landscape in kidneys of patients with lupus nephritis. Nat Immunol 20, 902–914 (2019).

314. Hudspeth, K. et al. Natural killer cell expression of Ki67 is associated with elevated serum IL-15, disease activity and nephritis in systemic lupus erythematosus. Clin Exp Immunol 196, 226–236 (2019).

315. Segerberg, F. et al. Autoantibodies to Killer Cell Immunoglobulin-Like Receptors in Patients With Systemic Lupus Erythematosus Induce Natural Killer Cell Hyporesponsiveness. Front Immunol 10, 2164 (2019).

316. de Matos, C. T. et al. Activating and inhibitory receptors on synovial fluid natural killer cells of arthritis patients: role of CD94/NKG2A in control of cytokine secretion. Immunology 122, 291–301 (2007).

317. Dalbeth, N. et al. CD56bright NK cells are enriched at inflammatory sites and can engage with monocytes in a reciprocal program of activation. J Immunol 173, 6418–6426 (2004).

318. Carli, L., Tani, C., Vagnani, S., Signorini, V. & Mosca, M. Leukopenia, lymphopenia, and neutropenia in systemic lupus erythematosus: Prevalence and clinical impact--A systematic literature review. Semin Arthritis Rheum 45, 190–194 (2015).

319. Brito-Zerón, P. et al. Prevalence and clinical relevance of autoimmune neutropenia in patients with primary Sjögren's syndrome. Semin Arthritis Rheum 38, 389–395 (2009).

320. Donnelly, S. et al. Impaired recognition of apoptotic neutrophils by the C1q/calreticulin and CD91 pathway in systemic lupus erythematosus. Arthritis & Rheumatism 54, 1543–1556 (2006).

321. Perazzio, S. F., Salomão, R., Silva, N. P. & Andrade, L. E. C. Increased neutrophil oxidative burst metabolism in systemic lupus erythematosus. Lupus 21, 1543–1551 (2012).

322. Bengtsson, A. A. et al. Low production of reactive oxygen species in granulocytes is associated with organ damage in systemic lupus erythematosus. Arthritis Research & Therapy 16, R120 (2014).

323. Denny, M. F. et al. A Distinct Subset of Proinflammatory Neutrophils Isolated from Patients with Systemic Lupus Erythematosus Induces Vascular Damage and Synthesizes Type I IFNs. The Journal of Immunology 184, 3284–3297 (2010).

324. Rahman, S. et al. Low-density granulocytes activate T cells and demonstrate a non-suppressive role in systemic lupus erythematosus. Annals of the Rheumatic Diseases 78, 957–966 (2019).

325. Hoogen, L. L. van den, Fritsch-Stork, R. D. E., Roon, J. A. G. van & Radstake, T. R. D. J. Low-Density Granulocytes Are Increased in Antiphospholipid Syndrome and Are Associated With Anti–β2-Glycoprotein I Antibodies: Comment on the Article by Yalavarthi et al. Arthritis & Rheumatology 68, 1320–1321 (2016).

326. Wright, H. L., Makki, F. A., Moots, R. J. & Edwards, S. W. Low-density granulocytes: functionally distinct, immature neutrophils in rheumatoid arthritis with altered properties and defective TNF signalling. Journal of Leukocyte Biology 101, 599–611 (2017).

327. Midgley, A. & Beresford, M. W. Increased expression of low density granulocytes in juvenile-onset systemic lupus erythematosus patients correlates with disease activity. Lupus 25, 407–411 (2016).

328. Morell, M., Varela, N. & Marañón, C. Myeloid Populations in Systemic Autoimmune Diseases. Clin Rev Allergy Immunol 53, 198–218 (2017).

329. Eggleton, P., Wang, L., Penhallow, J., Crawford, N. & Brown, K. A. Differences in oxidative response of subpopulations of neutrophils from healthy subjects and patients with rheumatoid arthritis. Ann Rheum Dis 54, 916–923 (1995).

330. Cross, A., Barnes, T., Bucknall, R. C., Edwards, S. W. & Moots, R. J. Neutrophil apoptosis in rheumatoid arthritis is regulated by local oxygen tensions within joints. Journal of Leukocyte Biology 80, 521–528 (2006).

331. Cross, A., Bucknall, R. C., Cassatella, M. A., Edwards, S. W. & Moots, R. J. Synovial fluid neutrophils transcribe and express class II major histocompatibility complex molecules in rheumatoid arthritis. Arthritis & Rheumatism 48, 2796–2806 (2003).

332. Talbot, J. et al. CCR2 Expression in Neutrophils Plays a Critical Role in Their Migration Into the Joints in Rheumatoid Arthritis. Arthritis & Rheumatology 67, 1751–1759 (2015).

333. Brennan, F. M. et al. Detection of interleukin 8 biological activity in synovial fluids from patients with rheumatoid arthritis and production of interleukin 8 mRNA by isolated synovial cells. European Journal of Immunology 20, 2141–2144 (1990).

334. de Siqueira, M. B. P., da Mota, L. M. H., Pereira Couto, S. C. & Muniz-Junqueira, M. I. Enhanced neutrophil phagocytic capacity in rheumatoid arthritis related to the autoantibodies rheumatoid factor and anti-cyclic citrullinated peptides. BMC Musculoskeletal Disorders 16, 159 (2015).

335. Robinson, J. J., Watson, F., Bucknall, R. C. & Edwards, S. W. Stimulation of neutrophils by insoluble immunoglobulin aggregates from synovial fluid of patients with rheumatoid arthritis. Eur J Clin Invest 22, 314–318 (1992).

336. Wright, H. L., Moots, R. J. & Edwards, S. W. The multifactorial role of neutrophils in rheumatoid arthritis. Nature Reviews Rheumatology 10, 593–601 (2014).

337. Derouet, M. et al. Sodium salicylate promotes neutrophil apoptosis by stimulating caspase-dependent turnover of Mcl-1. J Immunol 176, 957–965 (2006).

338. Weinmann, P. et al. Delayed neutrophil apoptosis in very early rheumatoid arthritis patients is abrogated by methotrexate therapy. Clin Exp Rheumatol 25, 885–887 (2007).

339. Kraan, M. C. et al. Inhibition of neutrophil migration soon after initiation of treatment with leflunomide or methotrexate in patients with rheumatoid arthritis: findings in a prospective, randomized, double-blind clinical trial in fifteen patients. Arthritis Rheum 43, 1488–1495 (2000).

340. Tani, C. et al. Rhupus syndrome: assessment of its prevalence and its clinical and instrumental characteristics in a prospective cohort of 103 SLE patients. Autoimmun Rev 12, 537–541 (2013).

341. Alarcón-Segovia, D. & Cardiel, M. H. Comparison between 3 diagnostic criteria for mixed connective tissue disease. Study of 593 patients. J Rheumatol 16, 328–334 (1989).

342. Sharp, G. C., Irvin, W. S., Tan, E. M., Gould, R. G. & Holman, H. R. Mixed connective tissue disease--an apparently distinct rheumatic disease syndrome associated with a specific antibody to an extractable nuclear antigen (ENA). Am J Med 52, 148–159 (1972).

343. Skopouli, F. N., Drosos, A. A., Papaioannou, T. & Moutsopoulos, H. M. Preliminary diagnostic criteria for Sjögren's syndrome. Scand J Rheumatol Suppl 61, 22–25 (1986).

344. Wilson, W. A. et al. International consensus statement on preliminary classification criteria for definite antiphospholipid syndrome: report of an international workshop. Arthritis Rheum 42, 1309–1311 (1999).

345. Barturen, G. et al. Integrative Analysis Reveals a Molecular Stratification of Systemic Autoimmune Diseases. Arthritis & Rheumatology n/a,.

346. Ingegnoli, F., Castelli, R. & Gualtierotti, R. Rheumatoid Factors: Clinical Applications. Dis Markers 35, 727–734 (2013).

347. Aringer, M. et al. 2019 European League Against Rheumatism/American College of Rheumatology Classification Criteria for Systemic Lupus Erythematosus. Arthritis Rheumatol 71, 1400–1412 (2019).

348. van den Hoogen, F. et al. 2013 classification criteria for systemic sclerosis: an American College of Rheumatology/European League against Rheumatism collaborative initiative. Arthritis Rheum 65, 2737–2747 (2013).

349. McKinney, E. F. et al. A CD8+ T cell transcription signature predicts prognosis in autoimmune disease. Nat Med 16, 586–591, 1p following 591 (2010).

350. Banchereau, R. et al. Personalized Immunomonitoring Uncovers Molecular Networks that Stratify Lupus Patients. Cell 165, 551–565 (2016).

351. Toro-Domínguez, D. et al. Stratification of Systemic Lupus Erythematosus Patients Into Three Groups of Disease Activity Progression According to Longitudinal Gene Expression. Arthritis Rheumatol 70, 2025–2035 (2018).

352. Robinson, G. A. et al. Disease-associated and patient-specific immune cell signatures in juvenile-onset systemic lupus erythematosus: patient stratification using a machine-learning approach. The Lancet Rheumatology 2, e485–e496 (2020).

353. van der Pouw Kraan, T. C. T. M. et al. Discovery of distinctive gene expression profiles in rheumatoid synovium using cDNA microarray technology: evidence for the existence of multiple pathways of tissue destruction and repair. Genes Immun 4, 187–196 (2003).

354. Humby, F. et al. Rituximab versus tocilizumab in anti-TNF inadequate responder patients with rheumatoid arthritis (R4RA): 16-week outcomes of a stratified, biopsy-driven, multicentre, open-label, phase 4 randomised controlled trial. The Lancet 397, 305–317 (2021).

355. Bader, L. et al. Candidate Markers for Stratification and Classification in Rheumatoid Arthritis. Front Immunol 10, (2019).

356. Milano, A. et al. Molecular Subsets in the Gene Expression Signatures of Scleroderma Skin. PLoS One 3, (2008).

357. Altorok, N., Tsou, P.-S., Coit, P., Khanna, D. & Sawalha, A. H. Genome-wide DNA methylation analysis in dermal fibroblasts from patients with diffuse and limited systemic sclerosis reveals common and subset-specific DNA methylation aberrancies. Ann Rheum Dis 74, 1612–1620 (2015).

358. Assassi, S. et al. Dissecting the heterogeneity of skin gene expression patterns in systemic sclerosis. Arthritis Rheumatol 67, 3016–3026 (2015).

359. Liu, X. et al. Correlation of interferon-inducible chemokine plasma levels with disease severity in systemic sclerosis. Arthritis & Rheumatism 65, 226–235 (2013).

360. Brkic, Z. et al. The interferon type I signature is present in systemic sclerosis before overt fibrosis and might contribute to its pathogenesis through high BAFF gene expression and high collagen synthesis. Ann Rheum Dis 75, 1567–1573 (2016).

361. Maas, K. et al. Cutting Edge: Molecular Portrait of Human Autoimmune Disease. The Journal of Immunology 169, 5–9 (2002).

362. Olsen, N. et al. A gene expression signature for recent onset rheumatoid arthritis in peripheral blood mononuclear cells. Annals of the Rheumatic Diseases 63, 1387–1392 (2004).

363. Toro-Domínguez, D., Carmona-Sáez, P. & Alarcón-Riquelme, M. E. Shared signatures between rheumatoid arthritis, systemic lupus erythematosus and Sjögren's syndrome uncovered through gene expression meta-analysis. Arthritis Res Ther 16, (2014).

364. Simon, Q. et al. A cytokine network profile delineates a common Th1/Be1 pro-inflammatory group of patients in four systemic autoimmune diseases. Arthritis Rheumatol (2021) doi:10.1002/art.41697.

365. Martin-Gutierrez, L. et al. Two shared immune cell signatures stratify patients with Sjögren's syndrome and systemic lupus erythematosus with potential therapeutic implications. Arthritis Rheumatol (2021) doi:10.1002/art.41708.

366. Cheung, P., Khatri, P., Utz, P. J. & Kuo, A. J. Single-cell technologies — studying rheumatic diseases one cell at a time. Nature Reviews Rheumatology 15, 340–354 (2019).

367. Mair, F. & Prlic, M. OMIP-044: 28-color immunophenotyping of the human dendritic cell compartment. Cytometry Part A 93, 402–405 (2018).

368. Hartmann, F. J. et al. High-dimensional single-cell analysis reveals the immune signature of narcolepsy. Journal of Experimental Medicine 213, 2621–2633 (2016).

369. O'Gorman, W. E. et al. Single-cell systems-level analysis of human Toll-like receptor activation defines a chemokine signature in patients with systemic lupus erythematosus. J. Allergy Clin. Immunol. 136, 1326–1336 (2015).

370. O'Gorman, W. E. et al. Mass cytometry identifies a distinct monocyte cytokine signature shared by clinically heterogeneous pediatric SLE patients. J Autoimmun (2017) doi:10.1016/j.jaut.2017.03.010.

371. Behbehani, G. K., Bendall, S. C., Clutter, M. R., Fantl, W. J. & Nolan, G. P. Single Cell Mass Cytometry Adapted to Measurements of the Cell Cycle. Cytometry A 81, 552–566 (2012).

372. Frei, A. P. et al. Highly multiplexed simultaneous detection of RNAs and proteins in single cells. Nat Methods 13, 269–275 (2016).

373. Cossarizza, A. et al. Guidelines for the use of flow cytometry and cell sorting in immunological studies. European Journal of Immunology 47, 1584–1797 (2017).

374. Stern, A. D., Rahman, A. H. & Birtwistle, M. R. Cell size assays for mass cytometry. Cytometry A 91, 14–24 (2017).

375. Jun, Y. W., Kim, H. R., Reo, Y. J., Dai, M. & Ahn, K. H. Addressing the autofluorescence issue in deep tissue imaging by two-photon microscopy: the significance of far-red emitting dyes. Chem. Sci. 8, 7696–7704 (2017).

376. Rahman, A. H., Lavin, Y., Kobayashi, S., Leader, A. & Merad, M. High-Dimensional Single Cell Mapping of Cerium Distribution in the Lung Immune Microenvironment of an Active Smoker. Cytometry B Clin Cytom 94, 941–945 (2018).

377. Keller, B. C., Presti, R. M., Byers, D. E. & Atkinson, J. J. Significant Interference in Mass Cytometry from Medicinal Iodine in Human Lung. Am J Respir Cell Mol Biol 55, 150–151 (2016).

378. Han, G., Spitzer, M. H., Bendall, S. C., Fantl, W. J. & Nolan, G. P. Metal-isotope-tagged monoclonal antibodies for high-dimensional mass cytometry. Nature Protocols 13, 2121–2148 (2018).

379. Takahashi, C. et al. Mass cytometry panel optimization through the designed distribution of signal interference. Cytometry Part A 91, 39–47 (2017).

380. Guidelines for the use of flow cytometry and cell sorting in immunological studies (second edition) - Cossarizza - 2019 - European Journal of Immunology - Wiley Online Library. https://onlinelibrary.wiley.com/doi/full/10.1002/eji.201970107.

381. Perfetto, S. P. & Roederer, M. Increased immunofluorescence sensitivity using 532 nm laser excitation. Cytometry A 71, 73–79 (2007).

382. Giesecke, C. et al. Determination of background, signal-to-noise, and dynamic range of a flow cytometer: A novel practical method for instrument characterization and standardization. Cytometry Part A 91, 1104–1114 (2017).

383. Leipold, M. D., Newell, E. W. & Maecker, H. T. Multiparameter Phenotyping of Human PBMCs Using Mass Cytometry. Methods Mol. Biol. 1343, 81–95 (2015).

384. Jamin, C. et al. Multi-center harmonization of flow cytometers in the context of the European "PRECISESADS" project. Autoimmunity Reviews 15, 1038–1045 (2016).

385. Leipold, M. D. et al. Comparison of CyTOF assays across sites: Results of a six-center pilot study. Journal of Immunological Methods 453, 37–43 (2018).

386. Hartmann, F. J. & Bendall, S. C. Immune monitoring using mass cytometry and related high-dimensional imaging approaches. Nature Reviews Rheumatology 16, 87–99 (2020).

387. Duffy, D. et al. Functional Analysis via Standardized Whole-Blood Stimulation Systems Defines the Boundaries of a Healthy Immune Response to Complex Stimuli. Immunity 40, 436–450 (2014).

388. Duffy, D. et al. Standardized whole blood stimulation improves immunomonitoring of induced immune responses in multi-center study. Clinical Immunology 183, 325–335 (2017).

389. Mikes, J., Olin, A., Lakshmikanth, T., Chen, Y. & Brodin, P. Automated Cell Processing for Mass Cytometry Experiments. Methods Mol. Biol. 1989, 111–123 (2019).

390. Lu, Y., Ahmed, S., Harari, F. & Vahter, M. Impact of Ficoll density gradient centrifugation on major and trace element concentrations in erythrocytes and blood plasma. J Trace Elem Med Biol 29, 249–254 (2015).

391. Sumatoh, H. R., Teng, K. W. W., Cheng, Y. & Newell, E. W. Optimization of mass cytometry sample cryopreservation after staining. Cytometry Part A 91, 48–61 (2017).

392. Fernandez, R. & Maecker, H. Cytokine-Stimulated Phosphoflow of Whole Blood Using CyTOF Mass Cytometry. Bio Protoc 5, (2015).

393. Amir, E. D. et al. Development of a Comprehensive Antibody Staining Database Using a Standardized Analytics Pipeline. Front. Immunol. 10, (2019).

394. Sakkestad, S. T., Skavland, J. & Hanevik, K. Whole blood preservation methods alter chemokine receptor detection in mass cytometry experiments. Journal of Immunological Methods 112673 (2019) doi:10.1016/j.jim.2019.112673.

395. Yan, L. et al. OSAT: a tool for sample-to-batch allocations in genomics experiments. BMC Genomics 13, 689 (2012).

396. Lai, L., Ong, R., Li, J. & Albani, S. A CD45-based barcoding approach to multiplex mass-cytometry (CyTOF). Cytometry Part A 87, 369–374 (2015).

397. Hartmann, F. J., Simonds, E. F. & Bendall, S. C. A Universal Live Cell Barcoding-Platform for Multiplexed Human Single Cell Analysis. Sci Rep 8, (2018).

398. Schulz, A. R. & Mei, H. E. Surface Barcoding of Live PBMC for Multiplexed Mass Cytometry. Methods Mol. Biol. 1989, 93–108 (2019).

399. Pitoiset, F. et al. Deep phenotyping of immune cell populations by optimized and standardized flow cytometry analyses. Cytometry Part A 93, 793–802 (2018).

400. Schulz, A. R. et al. Stabilizing Antibody Cocktails for Mass Cytometry. Cytometry Part A 95, 910–916 (2019).

401. Kleinsteuber, K. et al. Standardization and quality control for high-dimensional mass cytometry studies of human samples. Cytometry A 89, 903–913 (2016).

402. Ryherd, M. et al. Improved panels for clinical immune phenotyping: Utilization of the violet laser. Cytometry Part B: Clinical Cytometry 94, 827–835 (2018).

403. Finak, G. et al. Standardizing Flow Cytometry Immunophenotyping Analysis from the Human ImmunoPhenotyping Consortium. Sci Rep 6, (2016).

404. Qiu, P. et al. Extracting a Cellular Hierarchy from High-dimensional Cytometry Data with SPADE. Nat Biotechnol 29, 886–891 (2011).

405. Amir, E. D., Guo, X. V., Mayovska, O. & Rahman, A. H. Average Overlap Frequency: A simple metric to evaluate staining quality and community identification in high dimensional mass cytometry experiments. Journal of Immunological Methods 453, 20–29 (2018).

406. Mair, F. & Tyznik, A. J. High-Dimensional Immunophenotyping with Fluorescence-Based Cytometry: A Practical Guidebook. Methods Mol. Biol. 2032, 1–29 (2019).

407. Brodie, T. M., Tosevski, V. & Medová, M. OMIP-045: Characterizing human head and neck tumors and cancer cell lines with mass cytometry. Cytometry Part A 93, 406–410 (2018).

408. Brummelman, J. et al. Development, application and computational analysis of high-dimensional fluorescent antibody panels for single-cell flow cytometry. Nat Protoc 14, 1946–1969 (2019).

409. Kalina, T. Reproducibility of Flow Cytometry Through Standardization: Opportunities and Challenges. Cytometry 97, 137–147 (2020).

410. Bendall, S. C., Nolan, G. P., Roederer, M. & Chattopadhyay, P. K. A deep profiler's guide to cytometry. Trends in Immunology 33, 323–332 (2012).

411. Nowicka, M. et al. CyTOF workflow: differential discovery in high-throughput high-dimensional cytometry datasets. F1000Res 6, 748 (2019).

412. Mair, F. et al. The end of gating? An introduction to automated analysis of high dimensional cytometry data. Eur. J. Immunol. 46, 34–43 (2016).

413. Weber, L. M., Nowicka, M., Soneson, C. & Robinson, M. D. diffcyt: Differential discovery in high-dimensional cytometry via high-resolution clustering. Commun Biol 2, 1–11 (2019).

414. Bendall, S. C. et al. Single-cell mass cytometry of differential immune and drug responses across a human hematopoietic continuum. Science 332, 687–696 (2011).

415. Wang, S. & Brinkman, R. R. Data-Driven Flow Cytometry Analysis. Methods Mol. Biol. 1989, 245–265 (2019).

416. Monaco, G. et al. flowAI: automatic and interactive anomaly discerning tools for flow cytometry data. Bioinformatics 32, 2473–2480 (2016).

417. Meskas, J. & Wang, S. Precise and Accurate Automated Removal of Outlier Events and Flagging of Files Based on Time Versus Fluorescence Analysis. Github Repository: https://github.com/jmeskas/flowCut (2019).

418. Fletez-Brant, K., Špidlen, J., Brinkman, R. R., Roederer, M. & Chattopadhyay, P. K. flowClean: Automated identification and removal of fluorescence anomalies in flow cytometry data. Cytometry A 89, 461–471 (2016).

419. Zunder, E. R. et al. Palladium-based mass tag cell barcoding with a doublet-filtering scheme and single-cell deconvolution algorithm. Nat Protoc 10, 316–333 (2015).

420. Finck, R. et al. Normalization of mass cytometry data with bead standards. Cytometry A 83, 483–494 (2013).

421. Chevrier, S. et al. Compensation of Signal Spillover in Suspension and Imaging Mass Cytometry. cels 6, 612-620.e5 (2018).

422. Olsen, L. R., Leipold, M. D., Pedersen, C. B. & Maecker, H. T. The anatomy of single cell mass cytometry data. Cytometry Part A 95, 156–172 (2019).

423. Lee, B. H. & Rahman, A. H. Acquisition, Processing, and Quality Control of Mass Cytometry Data. in Mass Cytometry: Methods and Protocols (eds. McGuire, H. M. & Ashhurst, T. M.) 13–31 (Springer New York, 2019). doi:10.1007/978-1-4939-9454-0_2.

424. Bagwell, C. B. et al. Automated Data Cleanup for Mass Cytometry. Cytometry A (2019) doi:10.1002/cyto.a.23926.

425. Finak, G. & Jiang, M. flowWorkspace: Infrastructure for representing and interacting with gated and ungated cytometry data sets. (Bioconductor version: Release (3.9), 2019). doi:10.18129/B9.bioc.flowWorkspace.

426. Lux, M. et al. flowLearn: fast and precise identification and quality checking of cell populations in flow cytometry. Bioinformatics 34, 2245–2253 (2018).

427. Hahne, F., Gopalakrishnan, N., Khodabakhshi, A. H., Wong, C.-J. & Lee, K. flowStats: Statistical methods for the analysis of flow cytometry data. (Bioconductor version: Release (3.9), 2019). doi:10.18129/B9.bioc.flowStats.

428. Malek, M. et al. flowDensity: reproducing manual gating of flow cytometry data by automated density-based cell population identification. Bioinformatics 31, 606–607 (2015).

429. Mertens, B. J. A. Transformation, Normalization, and Batch Effect in the Analysis of Mass Spectrometry Data for Omics Studies. in Statistical Analysis of Proteomics, Metabolomics, and Lipidomics Data Using Mass Spectrometry (eds. Datta, S. & Mertens, B. J. A.) 1–21 (Springer International Publishing, 2017). doi:10.1007/978-3-319-45809-0_1.

430. Hahne, F. et al. Per-channel basis normalization methods for flow cytometry data. Cytometry Part A 77A, 121–131 (2010).

431. Finak, G. et al. High Throughput Flow Cytometry Data Normalization for Clinical Trials. Cytometry A 85, 277–286 (2014).

432. Shaham, U. et al. Removal of batch effects using distribution-matching residual networks. Bioinformatics 33, 2539–2546 (2017).

433. Van Gassen, S., Gaudilliere, B., Angst, M., Saeys, Y. & Aghaeepour, N. CytoNorm: A Normalization Algorithm for Cytometry Data. Github Repository: https://github.com/saeyslab/CytoNorm/ (2019).

434. Schuyler, R. P. et al. Minimizing Batch Effects in Mass Cytometry Data. Front. Immunol. 10, (2019).

435. Van Gassen, S. et al. FlowSOM: Using self-organizing maps for visualization and interpretation of cytometry data. Cytometry A 87, 636–645 (2015).

436. Saeys, Y., Gassen, S. V. & Lambrecht, B. N. Computational flow cytometry: helping to make sense of high-dimensional immunology data. Nature Reviews Immunology 16, 449–462 (2016).

437. Lever, J., Krzywinski, M. & Altman, N. Principal component analysis. Nat Methods 14, 641–642 (2017).

438. Hotelling, H. Analysis of a complex of statistical variables into principal components. Journal of Educational Psychology 24, 417–441 (1933).

439. Maaten, L. van der & Hinton, G. Visualizing Data using t-SNE. Journal of Machine Learning Research 9, 2579–2605 (2008).

440. Unen, V. van et al. Visual analysis of mass cytometry data by hierarchical stochastic neighbour embedding reveals rare cell types. Nat Commun 8, 1–10 (2017).

441. Linderman, G. C., Rachh, M., Hoskins, J. G., Steinerberger, S. & Kluger, Y. Fast interpolation-based t-SNE for improved visualization of single-cell RNA-seq data. Nat Methods 16, 243–245 (2019).

442. Belkina, A. C. et al. Automated optimized parameters for T-distributed stochastic neighbor embedding improve visualization and analysis of large datasets. Nature Communications 10, 1–12 (2019).

443. McInnes, L., Healy, J., Saul, N. & Großberger, L. UMAP: Uniform Manifold Approximation and Projection. Journal of Open Source Software https://joss.theoj.org (2018) doi:10.21105/joss.00861.

444. Tenenbaum, J. B. A Global Geometric Framework for Nonlinear Dimensionality Reduction. Science 290, 2319–2323 (2000).

445. Becher, B. et al. High-dimensional analysis of the murine myeloid cell system. Nature Immunology 15, 1181–1189 (2014).

446. Coifman, R. R. & Lafon, S. Diffusion maps. Applied and Computational Harmonic Analysis 21, 5–30 (2006).

447. Amir, E. D. et al. viSNE enables visualization of high dimensional single-cell data and reveals phenotypic heterogeneity of leukemia. Nat Biotechnol 31, 545–552 (2013).

448. Konstorum, A., Jekel, N., Vidal, E. & Laubenbacher, R. Comparative Analysis of Linear and Nonlinear Dimension Reduction Techniques on Mass Cytometry Data. bioRxiv 273862 (2018) doi:10.1101/273862.

449. Costa, E. S. et al. Automated pattern-guided principal component analysis vs expert-based immunophenotypic classification of B-cell chronic lymphoproliferative disorders: a step forward in the standardization of clinical immunophenotyping. Leukemia 24, 1927–1933 (2010).

450. Jansen, J. J. et al. FLOOD: FLow cytometric Orthogonal Orientation for Diagnosis. Chemometrics and Intelligent Laboratory Systems 151, 126–135 (2016).

451. Tinnevelt, G. H. et al. Novel data analysis method for multicolour flow cytometry links variability of multiple markers on single cells to a clinical phenotype. Scientific Reports 7, 1–11 (2017).

452. Maaten, L. van der. Accelerating t-SNE using Tree-Based Algorithms. Journal of Machine Learning Research 15, 3221–3245 (2014).

453. Olin, A. et al. Stereotypic Immune System Development in Newborn Children. Cell 174, 1277-1292.e14 (2018).

454. Becht, E. et al. Dimensionality reduction for visualizing single-cell data using UMAP. Nature Biotechnology 37, 38–44 (2019).

455. Wong, M. T. et al. A High-Dimensional Atlas of Human T Cell Diversity Reveals Tissue-Specific Trafficking and Cytokine Signatures. Immunity 45, 442–456 (2016).

456. Haghverdi, L., Buettner, F. & Theis, F. J. Diffusion maps for high-dimensional single-cell analysis of differentiation data. Bioinformatics 31, 2989–2998 (2015).

457. Chen, Y. et al. Continuous Immune Cell Differentiation Inferred From Single-Cell Measurements Following Allogeneic Stem Cell Transplantation. Front. Mol. Biosci. 5, (2018).

458. Angerer, P. et al. destiny: diffusion maps for large-scale single-cell data in R. Bioinformatics 32, 1241–1243 (2016).

459. Saelens, W., Cannoodt, R., Todorov, H. & Saeys, Y. A comparison of single-cell trajectory inference methods. Nat Biotechnol 37, 547–554 (2019).

460. Guilliams, M. et al. Unsupervised High-Dimensional Analysis Aligns Dendritic Cells across Tissues and Species. Immunity 45, 669–684 (2016).

461. Weber, L. M. & Robinson, M. D. Comparison of clustering methods for high-dimensional single-cell flow and mass cytometry data. Cytometry A 89, 1084–1096 (2016).

462. Krieg, C. et al. High-dimensional single-cell analysis predicts response to anti-PD-1 immunotherapy. Nat Med 24, 144–153 (2018).

463. Emmaneel, A. et al. A Computational Pipeline for the Diagnosis of CVID Patients. Front. Immunol. 10, (2019).

464. Platon, L. et al. A computational approach for phenotypic comparisons of cell populations in high-dimensional cytometry data. Methods 132, 66–75 (2018).

465. Melchiotti, R., Gracio, F., Kordasti, S., Todd, A. K. & de Rinaldis, E. Cluster stability in the analysis of mass cytometry data. Cytometry A 91, 73–84 (2017).

466. Kratochvíl, M. et al. Rapid single-cell cytometry data visualization with EmbedSOM. bioRxiv 496869 (2018) doi:10.1101/496869.

467. Kimball, A. K. et al. A Beginner's Guide To Analyzing and Visualizing Mass Cytometry Data. J Immunol 200, 3–22 (2018).

468. Levine, J. H. et al. Data-Driven Phenotypic Dissection of AML Reveals Progenitor-like Cells that Correlate with Prognosis. Cell 162, 184–197 (2015).

469. Samusik, N., Good, Z., Spitzer, M. H., Davis, K. L. & Nolan, G. P. Automated Mapping of Phenotype Space with Single-Cell Data. Nat Methods 13, 493–496 (2016).

470. Liu, X. et al. A comparison framework and guideline of clustering methods for mass cytometry data. Genome Biology 20, 297 (2019).

471. Shekhar, K., Brodin, P., Davis, M. M. & Chakraborty, A. K. Automatic Classification of Cellular Expression by Nonlinear Stochastic Embedding (ACCENSE). Proc. Natl. Acad. Sci. U.S.A. 111, 202–207 (2014).

472. Brodin, P. & Davis, M. M. Human immune system variation. Nat Rev Immunol 17, 21–29 (2017).

473. Nowicki, T. S. et al. A Pilot Trial of the Combination of Transgenic NY-ESO-1–reactive Adoptive Cellular Therapy with Dendritic Cell Vaccination with or without Ipilimumab. Clin Cancer Res 25, 2096–2108 (2019).

474. Gaudilliere, B. et al. Clinical recovery from surgery correlates with single-cell immune signatures. Science Translational Medicine 6, 255ra131-255ra131 (2014).

475. Böttcher, C. et al. Multi-parameter immune profiling of peripheral blood mononuclear cells by multiplexed single-cell mass cytometry in patients with early multiple sclerosis. Scientific Reports 9, 1–14 (2019).

476. Barcenilla, H., Åkerman, L., Pihl, M., Ludvigsson, J. & Casas, R. Mass Cytometry Identifies Distinct Subsets of Regulatory T Cells and Natural Killer Cells Associated With High Risk for Type 1 Diabetes. Front. Immunol. 10, (2019).

477. Gadalla, R. et al. Validation of CyTOF Against Flow Cytometry for Immunological Studies and Monitoring of Human Cancer Clinical Trials. Front Oncol 9, (2019).

478. Nicholas, K. J. et al. Multiparameter analysis of stimulated human peripheral blood mononuclear cells: a comparison of mass and fluorescence cytometry. Cytometry A 89, 271–280 (2016).

479. Mallone, R. et al. Isolation and preservation of peripheral blood mononuclear cells for analysis of islet antigen-reactive T cell responses: position statement of the T-Cell Workshop Committee of the Immunology of Diabetes Society. Clinical & Experimental Immunology 163, 33–49 (2011).

480. Brodin, P., Duffy, D. & Quintana-Murci, L. A Call for Blood—In Human Immunology. Immunity 50, 1335–1336 (2019).

481. Teng, T.-S., Ji, A., Ji, X.-Y. & Li, Y.-Z. Neutrophils and Immunity: From Bactericidal Action to Being Conquered. Journal of Immunology Research vol. 2017 e9671604 https://www.hindawi.com/journals/jir/2017/9671604/ (2017).

482. Mukherjee, M., Lacy, P. & Ueki, S. Eosinophil Extracellular Traps and Inflammatory Pathologies—Untangling the Web! Front. Immunol. 9, (2018).

483. Miyake, K. & Karasuyama, H. Emerging roles of basophils in allergic inflammation. Allergology International 66, 382–391 (2017).

484. Naumenko, V., Turk, M., Jenne, C. N. & Kim, S.-J. Neutrophils in viral infection. Cell Tissue Res 371, 505–516 (2018).

485. Wang, X., Qiu, L., Li, Z., Wang, X.-Y. & Yi, H. Understanding the Multifaceted Role of Neutrophils in Cancer and Autoimmune Diseases. Front. Immunol. 9, (2018).

486. Granger, V., Peyneau, M., Chollet-Martin, S. & de Chaisemartin, L. Neutrophil Extracellular Traps in Autoimmunity and Allergy: Immune Complexes at Work. Front Immunol 10, 2824 (2019).

487. Damsgaard, C. T., Lauritzen, L., Calder, P. C., Kjær, T. M. R. & Frøkiær, H. Whole-blood culture is a valid low-cost method to measure monocytic cytokines — A comparison of cytokine production in cultures of human whole-blood, mononuclear cells and monocytes. Journal of Immunological Methods 340, 95–101 (2009).

488. Appay, V. et al. New Generation Vaccine Induces Effective Melanoma-Specific CD8+ T Cells in the Circulation but Not in the Tumor Site. The Journal of Immunology 177, 1670–1678 (2006).

489. O'Gorman, W. E. et al. Mass Cytometry Identifies a Distinct Monocyte Cytokine Signature Shared by Clinically Heterogeneous Pediatric SLE Patients. J Autoimmun (2017) doi:10.1016/j.jaut.2017.03.010.

490. Nemes, E. et al. Differential leukocyte counting and immunophenotyping in cryopreserved ex vivo whole blood: Cell Count in Cryopreserved Whole Blood. Cytometry 87, 157–165 (2015).

491. Kagina, B. M. et al. Qualification of a whole blood intracellular cytokine staining assay to measure mycobacteria-specific CD4 and CD8 T cell immunity by flow cytometry. Journal of Immunological Methods 417, 22–33 (2015).

492. Rybakowska, P. et al. Stabilization of Human Whole Blood Samples for Multicenter and Retrospective Immunophenotyping Studies. Cytometry Part A n/a,.

493. Jang, J. S. et al. Single-cell mass cytometry on peripheral blood identifies immune cell subsets associated with primary biliary cholangitis. Scientific Reports 10, 12584 (2020).

494. Rybakowska, P., Alarcón-Riquelme, M. E. & Marañón, C. Key steps and methods in the experimental design and data analysis of highly multi-parametric flow and mass cytometry. Computational and Structural Biotechnology Journal 18, 874–886 (2020).

495. Warth, S. & Kunkel, D. Setting Up Mass Cytometry in a Shared Resource Lab Environment. Methods Mol. Biol. 1989, 3–11 (2019).

496. Gassen, S. V. et al. FlowSOM: Using self-organizing maps for visualization and interpretation of cytometry data. Cytometry Part A 87, 636–645 (2015).

497. Beyrend, G., Stam, K., Höllt, T., Ossendorp, F. & Arens, R. Cytofast: A workflow for visual and quantitative analysis of flow and mass cytometry data to discover immune signatures and correlations. Comput Struct Biotechnol J 16, 435–442 (2018).

498. Chen, H. et al. Cytofkit: A Bioconductor Package for an Integrated Mass Cytometry Data Analysis Pipeline. PLoS Comput Biol 12, (2016).

499. Bodolay, E. et al. Five-year follow-up of 665 Hungarian patients with undifferentiated connective tissue disease (UCTD). Clin Exp Rheumatol 21, 313–320 (2003).

500. Rahmouni, S. et al. Mixed connective tissue disease: Not always an obvious diagnosis. Clin Case Rep 8, 1979–1983 (2020).

501. Aringer, M., Steiner, G. & Smolen, J. S. Does mixed connective tissue disease exist? Yes. Rheum Dis Clin North Am 31, 411–420, v (2005).

502. Morris, D. L. et al. MHC associations with clinical and autoantibody manifestations in European SLE. Genes Immun 15, 210–217 (2014).

503. Kroef, M. van der et al. Cytometry by time of flight identifies distinct signatures in patients with systemic sclerosis, systemic lupus erythematosus and Sjögrens syndrome. European Journal of Immunology 50, 119–129 (2020).

504. Jacobi, A. M. et al. Correlation between circulating CD27high plasma cells and disease activity in patients with systemic lupus erythematosus. Arthritis Rheum 48, 1332–1342 (2003).

505. Spidlen, J., Breuer, K. & Brinkman, R. Preparing a Minimum Information about a Flow Cytometry Experiment (MIFlowCyt) Compliant Manuscript Using the International Society for Advancement of Cytometry (ISAC) FCS File Repository (FlowRepository.org). Current Protocols in Cytometry 61, 10.18.1-10.18.26 (2012).

506. Meskas, J., Wang, S. & Brinkman, R. flowCut — An R package for precise and accurate automated removal of outlier events and flagging of files based on time versus fluorescence analysis. bioRxiv 2020.04.23.058545 (2020) doi:10.1101/2020.04.23.058545.

507. Rahman, A. H., Tordesillas, L. & Berin, M. C. Heparin Reduces Nonspecific Eosinophil Staining Artifacts in Mass Cytometry Experiments. Cytometry A 89, 601–607 (2016).

508. Ruiter, K. de et al. A field-applicable method for flow cytometric analysis of granulocyte activation: Cryopreservation of fixed granulocytes. Cytometry Part A 93, 540–547 (2018).

509. Selliah, N. et al. Flow Cytometry Method Validation Protocols. Current Protocols in Cytometry 87, e53 (2019).

510. Abdelaal, T. et al. CyTOFmerge: integrating mass cytometry data across multiple panels. Bioinformatics 35, 4063–4071 (2019).

511. Vicetti Miguel, R. D., Maryak, S. A. & Cherpes, T. L. Brefeldin A, but not monensin, enables flow cytometric detection of interleukin-4 within peripheral T cells responding to ex vivo stimulation with Chlamydia trachomatis. J. Immunol. Methods 384, 191–195 (2012).

512. Gassen, S. V., Gaudilliere, B., Angst, M. S., Saeys, Y. & Aghaeepour, N. CytoNorm: A Normalization Algorithm for Cytometry Data. Cytometry Part A 97, 268–278 (2020).

513. Ji, W.-J. et al. The influence of different anticoagulants and time-delayed sample processing and measurements on human monocyte subset and monocyte-platelet aggregate analyses. Cytometry Part B: Clinical Cytometry 92, 371–379 (2017).

514. Ibeagha-Awemu, E. M., Ibeagha, A. E. & Zhao, X. The influence of different anticoagulants and sample preparation methods on measurement of mCD14 on bovine monocytes and polymorphonuclear neutrophil leukocytes. BMC Res Notes 5, 93 (2012).

515. Hoffmeister, B., Bunde, T., Rudawsky, I. M., Volk, H.-D. & Kern, F. Detection of antigen-specific T cells by cytokine flow cytometry: the use of whole blood may underestimate frequencies. European Journal of Immunology 33, 3484–3492 (2003).

516. Crowell, H. L., Zanotelli, V. R. T., Chevrier, S., Robinson, M. D. & Bodenmiller, B. CATALYST: Cytometry dATa anALYSis Tools. (Bioconductor version: Release (3.11), 2020). doi:10.18129/B9.bioc.CATALYST.

517. Wickham, H. et al. ggplot2: Create Elegant Data Visualisations Using the Grammar of Graphics. (2020).

518. Finak, G., Jiang, W. & Gottardo, R. CytoML for cross-platform cytometry data sharing. Cytometry Part A 93, 1189–1196 (2018).

519. Finak, G. et al. OpenCyto: An Open Source Infrastructure for Scalable, Robust, Reproducible, and Automated, End-to-End Flow Cytometry Data Analysis. PLOS Computational Biology 10, e1003806 (2014).

520. Thrash, E. M. et al. High-Throughput Mass Cytometry Staining for Immunophenotyping Clinical Samples. STAR Protocols 100055 (2020) doi:10.1016/j.xpro.2020.100055.

521. McCarthy, R. L., Mak, D. H., Burks, J. K. & Barton, M. C. Rapid monoisotopic cisplatin based barcoding for multiplexed mass cytometry. Scientific Reports 7, 3779 (2017).

522. Mei, H. E., Leipold, M. D., Schulz, A. R., Chester, C. & Maecker, H. T. Barcoding of live human PBMC for multiplexed mass cytometry. J Immunol 194, 2022–2031 (2015).

523. Finck, R. et al. Normalization of mass cytometry data with bead standards. Cytometry A 83, 483–494 (2013).

524. Le Lann, L., Jouve, P.-E., Alarcón-Riquelme, M., Jamin, C. & Pers, J.-O. Standardization procedure for flow cytometry data harmonization in prospective multicenter studies. Scientific Reports 10, 11567 (2020).

525. Pontikos, N. flowBeads: flowBeads: Analysis of flow bead data. (Bioconductor version: Release (3.12), 2021). doi:10.18129/B9.bioc.flowBeads.

526. Dendrou, C. A. et al. Fluorescence Intensity Normalisation: Correcting for Time Effects in Large-Scale Flow Cytometric Analysis. Adv Bioinformatics 2009, (2009).

527. Giudice, V., Fantoni, G. & Biancotto, A. Fluorescent Cell Barcoding for Immunophenotyping. Methods Mol. Biol. 2032, 53–68 (2019).

528. Majonis, D., Ornatsky, O., Kinach, R. & Winnik, M. A. Curious results with palladium- and platinum-carrying polymers in mass cytometry bioassays and an unexpected application as a dead cell stain. Biomacromolecules 12, 3997–4010 (2011).

529. Bagwell, C. B. et al. Automated Data Cleanup for Mass Cytometry. Cytometry Part A 97, 184–198 (2020).

530. Lee, B. H. et al. A Modified Injector and Sample Acquisition Protocol Can Improve Data Quality and Reduce Inter-Instrument Variability of the Helios Mass Cytometer. Cytometry Part A 95, 1019–1030 (2019).

531. Rein, I. D., Notø, H. Ø., Bostad, M., Huse, K. & Stokke, T. Cell Cycle Analysis and Relevance for Single-Cell Gating in Mass Cytometry. Cytometry Part A 97, 832–844 (2020).

532. Gassen, S. V., Vens, C., Dhaene, T., Lambrecht, B. N. & Saeys, Y. FloReMi: Flow density survival regression using minimal feature redundancy. Cytometry Part A 89, 22–29 (2016).

533. Saeys, Y., Van Gassen, S. & Lambrecht, B. N. Computational flow cytometry: helping to make sense of high-dimensional immunology data. Nat. Rev. Immunol. 16, 449–462 (2016).

534. Höllt, T. et al. Cytosplore: Interactive Immune Cell Phenotyping for Large Single-Cell Datasets. Computer Graphics Forum 35, 171–180 (2016).